**Untersuchung von atmosphärischem CO und $CH_4$ anhand von Isotopenmessungen** Die Analyse von Isotophenverhältnissen ist ein weit verbreitetes Mittel zur Erforschung von atmosphärischen Spurengasen. Wir haben sowohl das Verhältnis der stabilen Isotope $\delta^{13}C$ und $\delta D$ an atmosphärischem $CH_4$, als auch $\delta^{13}C$, $\delta^{18}O$ und die Konzentration von $^{14}CO$ an atmosphärischem CO an der Station Izaña, Tenerife, von 1996 bis 1999 gemessen. Die Genauigkeit der $\delta D$ Messungen erlaubte zum ersten mal einen Jahresgang von $\delta D$ nachzuweisen. Die ausgeprägten Jahresgänge in den Isotopensignalen von $CH_4$ und CO ermöglichte Rückschlüsse auf ihre Quellen und Senken. Starke Abweichungen mancher Proben von den mittleren Jahresgängen konnten den wichtigen Quell-Regionen Nord Amerika und Europa, bzw sauberen Luftmasen aus Afrika und dem Nordatlantik zugeordnet werden. Weiterhin haben wir $\delta^{13}C$ ($CH_4$) und $\delta D$ ($CH_4$) an Firnluft Proben von zwei Antarktischen Stationen gemessen. Mit Hilfe eines Firnluft-Diffusionsmodells konnten die $\delta^{13}C$ und $\delta D$ Signale von atmosphärischem $CH_4$ der letzten fünfzig Jahre rekonstruiert werden. Parallel zu den steigenden $CH_4$ Konzentrationen der letzten Jahrzehnte wurde ein positiver $\delta^{13}C$ Trend nachgewiesen, welcher den wachsenden Beitrag der anthropogenen $CH_4$ Quellen widerspiegelt. $\delta D$ zeigt ein ausgeprägtes Minimum um 1975, verursacht durch das Ungleichgewicht zwischen den Quellen und Senken von $CH_4$. Dieser Effekt konnte somit zum ersten mal auch für $\delta D$ nachgewiesen werden.

**Study of atmospheric CO and $CH_4$ using isotopic analysis** The analysis of isotope ratios is widely used for the investigation of atmospheric trace gases. We measured the stable isotopes $\delta^{13}C$ and $\delta D$ of atmospheric $CH_4$ as well as $\delta^{13}C$, $\delta^{18}O$ and the $^{14}CO$ concentrations of atmospheric CO at Izaña, Tenerife, from 1996 to 1999. We report the first directly measured $\delta D$ seasonality for atmospheric background $CH_4$. The large seasonal cycles in mixing and isotopic ratios of $CH_4$ and CO enable inferences about the underlying source and sink processes. The large synoptic scale variations occurring for these trace gases at Izaña made it possible to study source regions such as North America, Europe, as well as background conditions over the North Atlantic and Africa. We also measured $\delta^{13}C$ and $\delta D$ on firn air samples from two Antarctic sites. From these measurements the atmospheric trends of $\delta^{13}C$ and $\delta D$ of $CH_4$ over the past fifty years have been reconstructed with the help of a firn air diffusion model. We find that parallel to increasing $CH_4$ mixing ratios $\delta^{13}C$ increases, which is evidence for a growing contribution of the heavier anthropogenic $CH_4$ sources. For $\delta D$ we find a period of decline previous to 1975, followed by a gradual increase. This $\delta D$ minimum is due to the non-equilibrium state between $CH_4$ and its sources and sinks and has for the first time been detected for $\delta D$.

# Contents

# List of acronyms

| | | |
|---|---|---|
| AEROCE | : | Atmospheric/Ocean Chemistry Experiment (Trajectory Archive) |
| AMS | : | Accelerator Mass Spectrometry |
| AVHRR | : | Advanced Very High Resolution Radiometer measurements [Dywer & Gregoire, 1998] |
| BERLIOZ | : | BERlin-Ozone Experiment |
| BMBF | : | Bundesministerium für Bildung und Forschung |
| BOSCAGE-8 | : | 8-BOx $SF_6$ CAlibrated Global Euler transport model [Marik, 1998] |
| CIR | : | Centre for Isotope Research |
| ECD | : | Electron Capture Detector |
| EDGARV2.0 | : | Emission Database for Global Atmospheric Research Version 2.0 [Olivier et al., 1999] |
| FID | : | Flame Ionization Detector |
| FIRETRACC | : | Firn Record of Trace Gases Relevant to Atmospheric Chemical Change Over 100 Years |
| FFT | : | Fast Fourier Transformation |
| GAW | : | Global Atmospheric Watch station |
| GEIA | : | Global Emissions Inventory Activity [Guenther et al., 1995] |
| GC | : | Gas Chromatography |
| GWP | : | Global Warming Potential |
| HYSPLIT | : | HYbrid Single-Particle Lagrangian Integrated Trajectory program |
| IRMS | : | Isotope Ratio Mass Spectrometry |
| K | : | Kelvin |
| KIE | : | Kinetic Isotope Effect |

| | | |
|---|---|---|
| MFC | : | Mass Flow Controller |
| MG | : | Messer-Griesheim |
| MIF | : | Mass independent fractionation |
| MISOS | : | Methane Isotopomer Spectrometer |
| MPI | : | Max Planck Institute Mainz |
| NH | : | Northern Hemisphere |
| NILU | : | Norwegian Institute for Air Research |
| NIWA | : | National Institute of Water and Atmospheric Research |
| NMHC | : | Nonmethane-Hydrocarbons |
| NOAA/CMDL | : | National Oceanic and Atmospheric Administration Climate Monitoring and Diagnostics Laboratory |
| pmC | : | percent modern Carbon |
| SH | : | Southern Hemisphere |
| STE | : | Stratosphere-Troposphere Exchange |
| STP | : | Standard Temperature and Pressure |
| TC1 | : | Chemistry Module [Hein et al., 1997] |
| TDL | : | Tunable Diode Laser |
| TFS | : | Troposphären Forschungsschwerpunkt |
| UBA | : | Umwelt Bundesamt |
| VERA | : | Vienna Environmental Research Accelerator |
| V-PDB | : | Vienna PeDeBelimnite |
| V-SMOW | : | Vienna Standard Mean Ocean Water |

# Chapter 1

# Review of atmospheric $CH_4$ and CO

Methane ($CH_4$) and carbon monoxide (CO) are two important atmospheric trace gases because of their large influence on atmospheric chemistry and, in the case of $CH_4$, its significant impact on the earth's radiative budget. The cycles of these two trace gases are closely linked via their common sink, the reaction with hydroxyl (OH) radicals, and also because $CH_4$ oxidation is an important source for CO.

For tropospheric background chemistry the increasing emissions and atmospheric concentrations of $CH_4$ and CO are of special importance. They lead to changes in the concentrations of tropospheric ozone ($O_3$), an important greenhouse gas, and in the highly reactive OH radicals, which are responsible for the oxidation of several trace gases. Thus large efforts are made to understand the cycles of CO and $CH_4$ and to improve their budget calculations. For this purpose concentration measurements are done on a global scale. Additional valuable information about the global $CH_4$ and CO cycles can be gained through measurements of their isotopic composition.

## 1.1 Atmospheric $CH_4$ and CO

Atmospheric methane is, after carbon dioxide, the second most important greenhouse gas. The absorbtion properties of methane were first measured by John Tyndall in 1859, who discovered that water vapor, carbon dioxide and methane were trapping infrared (terrestrial) radiation, while the most abundant atmospheric gases, nitrogen and oxygen, were not. Meanwhile methane is responsible for nearly 20 % of the current anthropogenic greenhouse forcing. Its direct contribution is estimated to be 0.44 $Wm^{-2}$, plus an additional 0.13 $Wm^{-2}$ due to indirect, chemically induced effects [Lelieveld et al., 1998]. On a per molecule basis $CH_4$ has a much greater

Global Warming Potential (GWP) than $CO_2$ (GWP of $\sim 56$ for the next 20 years [IPCC, 1996]).

$CH_4$ plays a central role in tropospheric and stratospheric chemistry. In the troposphere about 90 % of $CH_4$ destruction occurs via OH radicals, providing a major sink for OH. Thus, $CH_4$ has a significant influence on the oxidizing capacity of the atmosphere and hence on the lifetime of several other trace gases, such as CO, non-methane hydrocarbons (NMHCs) and hydrochlorofluocarbons (HCFCs) [Crutzen & Zimmermann, 1991], [Logan et al. 1981], [Prather, 1996], [Thompson, 1992]. The oxidation of $CH_4$ by OH leads to the formation of formaldehyde ($CH_2O$) and CO. In environments with sufficient $NO_x$ it can also result in $O_3$ (see Figure 1.1).

In the stratosphere $CH_4$ acts as a sink for chlorine atoms and is therefore important in stratospheric ozone chemistry. Methane oxidation by OH is also a major source of water vapor in the stratosphere. This influences the formation of polar stratospheric clouds, which are involved in the formation of the arctic and antarctic ozone hole.

Carbon monoxide is an important atmospheric trace gas and a major pollutant in

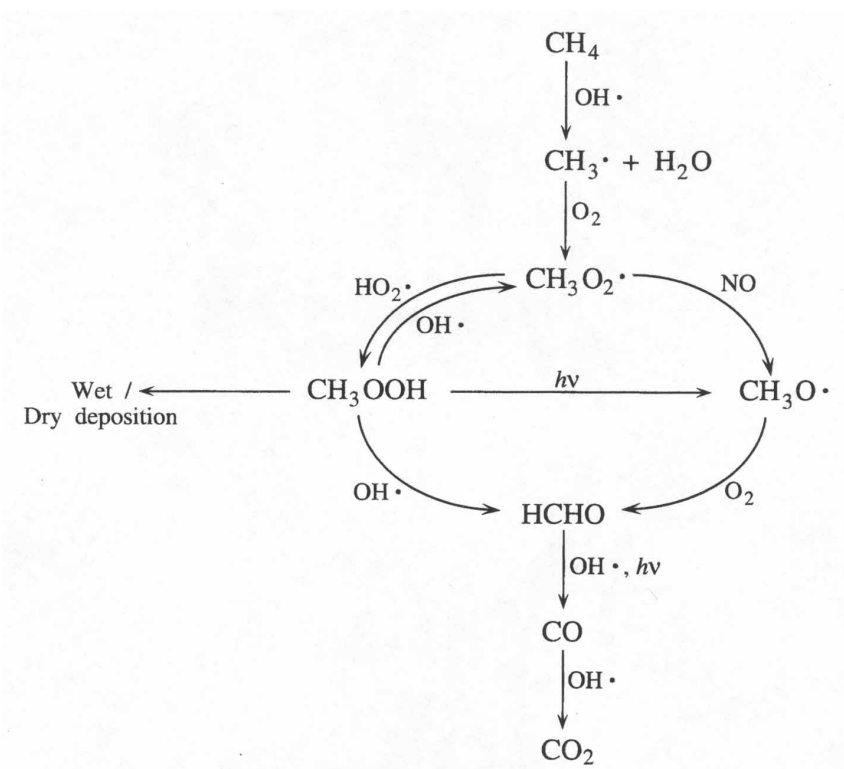


**Figure 1.1:** Atmospheric methane oxidation chain [Seinfeld & Pandis, 1998].

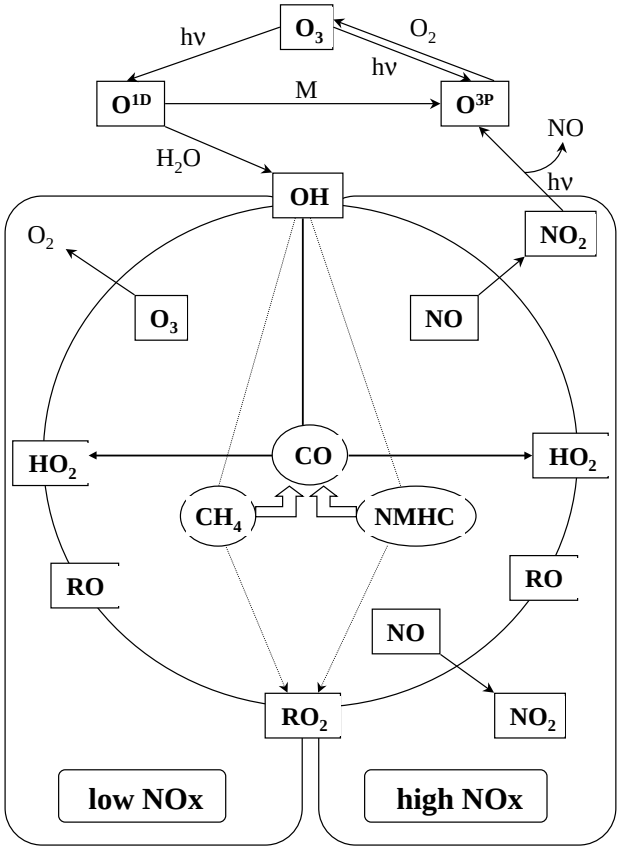


**Figure 1.2:** Atmospheric CO oxidation chain.

industrialized areas. Although not a significant greenhouse gas, CO plays a central role in tropospheric chemistry via its reaction with the OH radical. In the background troposphere about 60% of the OH radicals react with CO, and most of the rest with $CH_4$ and its different oxidation products. Thus increasing CO and $CH_4$ concentrations could influence the tropospheric concentrations of OH and thus the lifetime of several other trace gases that are removed by reaction with OH. Nevertheless, the reactions with CO and $CH_4$ do not necessarily lead to the removal of OH. For instance, in the presence of sufficiently large amounts of nitric oxide, the oxidation of CO will lead to the formation of $O_3$, without loss of the catalysts OH, $HO_2$, NO and $NO_2$. The catalytic reaction chain is shown in Figure 1.1, the net reaction is:

$$CO + 2O_2 \rightarrow CO_2 + O_3 \tag{1.1}$$

In contrast, in NO-poor (typically maritime) environments the oxidation of CO to $CO_2$ leads to ozone destruction, likewise without loss of OH and $HO_2$ radicals (see

also Figure 1.1). The net reaction being:

$$CO + O_3 \rightarrow CO_2 + O_2 \tag{1.2}$$

## 1.2 The global $CH_4$ budget

Estimating the contribution of individual $CH_4$ sources to the global budget often relies on extrapolation of local flux measurements to the global scale, resulting in significant (20-75% [Crutzen, 1995]) uncertainties in the individual source terms. Recent estimates of the global methane budget are shown in Table 1.2 together with their isotopic source signatures. The anthropogenic contribution to $CH_4$ sources ($\sim$410 Tg yr$^{-1}$) is more than twice the contribution of natural sources ($\sim$160 Tg yr$^{-1}$), i.e. $\sim$70% [Lelieveld et al., 1998]. The most important natural $CH_4$ sources are wetlands in the tropics and at northern latitudes. Important anthropogenic sources are coal mining, natural gas losses and landfills. Large amounts of $CH_4$ are also released by biomass burning.

$CH_4$ sources can be further distinguished by their different production processes. Nearly 70% of total $CH_4$ sources is due to biogenic $CH_4$ production by acetate fermentation (e.g. the digestive tracs of cattles or termites) or $CO_2$ reduction in strictly anaerobic environments such as swamps, rice paddies, tundera and also landfills. Another $\sim$20% of total $CH_4$ sources results from thermogenic production at high temperatures by which most of the natural gas has been formed. Finally $\sim$10% of total $CH_4$ sources is formed by incomplete combustion of biomass or fossil fuels.

The global source strength is currently estimated at $\sim$600 Tg yr$^{-1}$ [Lelieveld et al., 1998], derived from the atmospheric burden and estimates of the $CH_4$ sink. The largest $CH_4$ sink is OH oxidation, while stratospheric removal accounts for less than 10%. The small soil sink ($\sim$30 Tg yr$^{-1}$) is due to the consumption of $CH_4$ by methanotrophic bacteria in soils (see Table 1.2).

## 1.3 $CH_4$ measurements

In 1948 the first measurements of atmospheric $CH_4$ were published by Migenotte [Migeotte, 1948] showing concentrations of about 2 µmol/mol. In 1951 Glueckauf regarded $CH_4$ as a 'non-variable component of atmospheric air' and until the 1970s methane was believed to be a stable gas in the Earth's atmosphere.

| Sources | $Tg\,yr^{-1}$ [a] | $\delta^{13}C$ [b] [‰]V-PDB | $\delta D$ [c] [‰]V-SMOW |
|---|---|---|---|
| coal mining and combustion | 45±15 | | |
| oil and gas related emissions | 65±30 | | |
| total fossil fuel related | 110±45 | $-40 \pm 7$ | $-175 \pm 10$ |
| methane hydrates | 10±5 | | |
| total $^{14}CH_4$-free | 120±40 | | |
| wetlands | 145±30 | $-60 \pm 5$ | $-322 \pm 30$ |
| termites | 20±20 | | |
| oceans | 10±5 | | |
| wild ruminants | 5±5 | | |
| freshwaters | 5±5 | | |
| $CH_4$ from sediments | 5±5 | | |
| total natural | 190±70 | | |
| landfills | 40±20 | $-50 \pm 2$ | $-293 \pm 20$ |
| biomass burning | 40±30 | $-24 \pm 3$ | $-30 \pm 20$[d] |
| | | | $-210 \pm 16$[e] |
| domestic ruminants | 80±20 | $-60 \pm 5$ | $-305 \pm 9$ |
| animal waste | 30±10 | | |
| rice paddies | 80±50 | $-63.5 \pm 5$ | $-323 \pm 18$ |
| total agricultural | 230±115 | | |
| total sources | 580±80 | $-53.5 \pm 2.6$ | $-283 \pm 13$ |

[a] [Lelieveld et al., 1998]

[b] [Stevens & Engelkemeir, 1988], [Rust, 1981], [Tyler et al., 1988], [Quay et al., 1991], [Levin et al., 1993], [Stevens, 1993], [Wahlen, 1993], [Tyler et al., 1994], [Wahlen et al., 1989], [Kuhlmann et al., 1998], [Zimov et al., 1997] [Chanton et al., 1997], [Bergamaschi, 1997], [Quay et al., 1988]

[c] [Wassmann et al., 1992], [Burke et al., 1988], [Levin et al., 1993],[Wahlen et al., 1989], [Bergamaschi, 1997], [Bergamaschi et al. 1998b], [Liptay et al., 1998],[Kuhlmann et al., 1998], [Rice & Claypool, 1981], [Zimov et al., 1997],[Bergamaschi & Harris, 1995], [Bönisch, 1997]

[d] Wahlen, pers. communic. cited in [Bergamaschi et al., 1998a]

[e] [Snover et al., 1999]

**Table 1.1:** The budget of $CH_4$, with source strengths and the isotopic composition of $CH_4$ sources. For the total source the $\delta$ values of the mean atmospheric source are given (bottom-up calculation, see equation 1.9).

| Sinks | $Tg\,yr^{-1}$ | KIE($\delta^{13}C$) | KIE($\delta D$) |
|---|---|---|---|
| reaction with OH | 510±50 | 1.0039±0.0004[f] | 1.294±0.018[e] |
| in the troposphere | | 1.0054±0.0009[a] | |
| bacterial oxidation in soils | 30±15 | 1.021±0.005[c] | 1.066[g] |
| | | | 1.25±0.07[b] |
| | | | 1.16±0.04[f] |
| reaction with OH, Cl and $O^1D$ | 40±10 | 1.012[d] | 1.19±0.02[h] |
| in the stratosphere | | | 1.161[g] |
| total sink | 580±80 | | |
| mean average source | | $-52.0 \pm 0.8$ | $-274 \pm 10$ |

[a][Cantrell et al., 1990]
[b][Gierczak et al., 1997]
[c][King et al., 1989]
[d][Brenninkmeijer et al., 1995]
[e][Saueressig, 1999]
[f][Snover & Quay, 1999]
[g][Wahlen, 1993]
[h][Irion et al., 1996]

**Table 1.2:** Estimated sink strengths [Lelieveld et al., 1998] and kinetic isotope effects. The derived $\delta$ value of the mean sources are given (top-down calculation, see equation 1.10).

### 1.3.1 Atmospheric Trends

First hints for the rapid increase of $CH_4$ concentrations in the atmosphere came from the improvement of $CH_4$ gas chromatographic measurements in the 1960s and 1970s [Rasmussen & Khalil, 1981], from first global $CH_4$ budget estimations [Ehhalt & Volz, 1974] and from the first $CH_4$ measurements of air extracted from polar ice in 1973 [Robbins et al., 1973]. However, only in the 1980s direct atmospheric observations established a significant increase of $CH_4$ mixing ratios [Dlugokencky et al., 1994c]. In addition, ice core measurement established that atmospheric $CH_4$ mixing ratios have more than doubled since pre-industrial times [Chappellaz et al., 1990], [Etheridge et al., 1992]. During the early 1990s the slowing down and temporary cessation of growth rates has induced a wide scientific discussion about possible reasons [Bekki et al., 1994], [Dlugokencky et al., 1994a], [Dlugokencky et al., 1994b], [Hogan & Harriss, 1994], [Rudolph, 1994]. However, recent measurements clearly indicate that atmospheric $CH_4$ mixing ratios have not yet stabilized.

The causes of the large increase from the pre-industrial 730 nmol/mol to the present 1720 nmol/mol shown in Figure 1.3 are not known in detail. Increasing anthropogenic methane emissions from the industrial (e.g. fossil fuel sources and landfills) and agricultural sectors (e.g. rice paddies, ruminant animals and biomass burning) are probably the main factors. In addition, the main sink for methane,

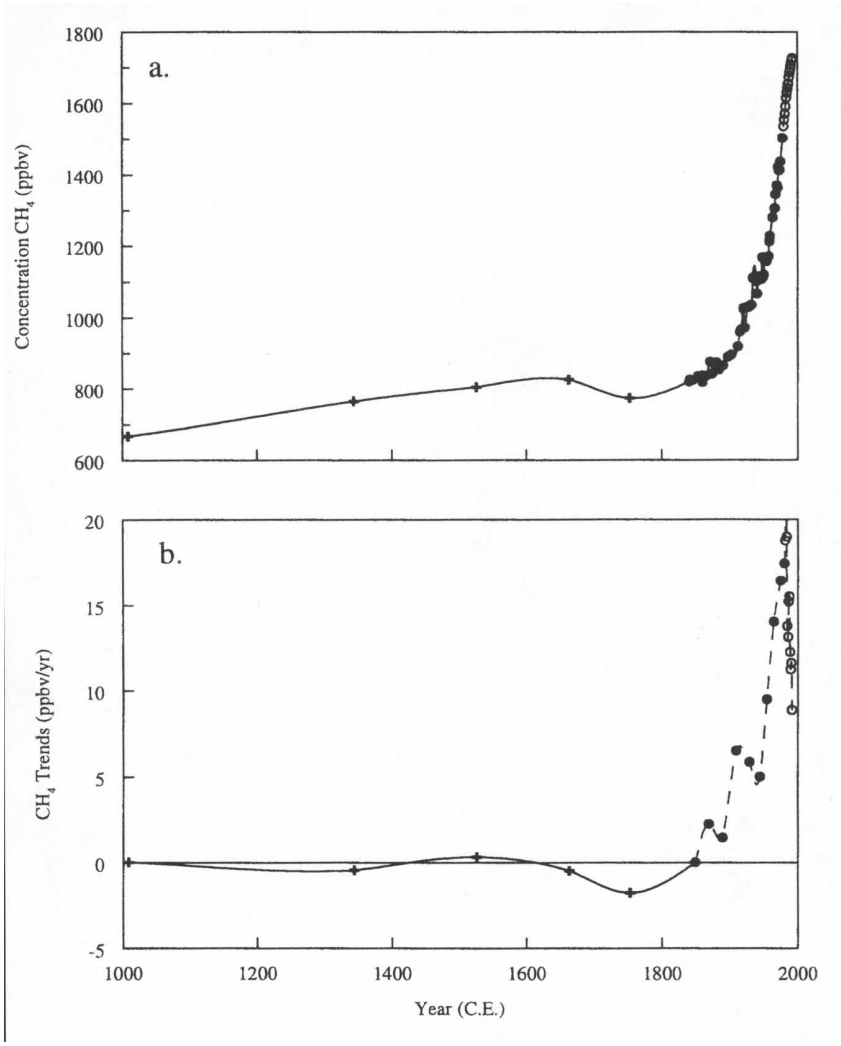


**Figure 1.3:** (a) Concentrations and (b) trends of methane over the last 1000 years. ppbv stands for nmol/mol. Data of Rasmussen and Khalil [1984](+) and Etheridge et al. [1992](•) are from ice core samples. NOAA/CMDL atmospheric data (∘)[Khalil, 2000].

i.e. the reaction with OH, may have simultaneously decreased [Thompson, 1992 and references therein].

Measurements made on the Vostoc ice core allowed the reconstruction of $CH_4$ and $CO_2$ concentrations over the last 420.000 years [Petit et al., 1999]. From this time record it is obvious that the mixing ratios of these two greenhouse gases are positively correlated with atmospheric temperature.

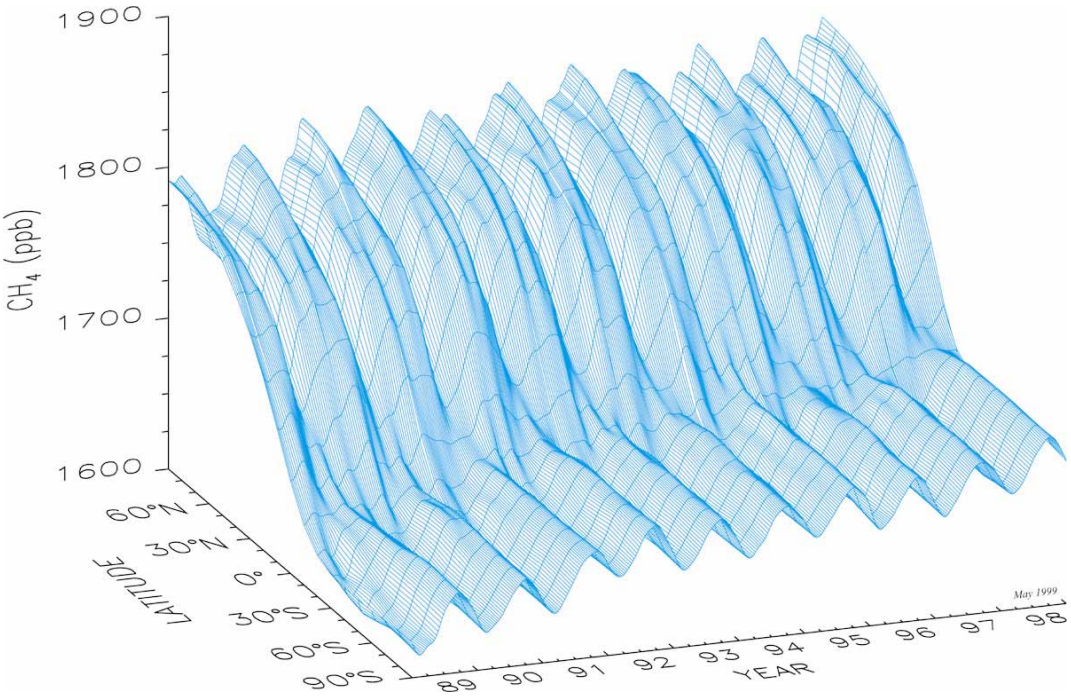


**Figure 1.4:** Three-dimensional representation of the global distribution of atmospheric $CH_4$ [Dlugokencky et al., 1994b].

### 1.3.2 Global distribution

The annual pattern of surface $CH_4$ concentrations shows a large seasonality and pronounced interhemispheric differences. In Figure 1.4 the global distribution of atmospheric $CH_4$ is plotted. The surface represents data from the National Oceanic and Atmospheric Administration Climate Monitoring and Diagnostics Laboratory (NOAA/CMDL) monitoring network that have been smoothed over time and latitude.

$CH_4$ sources and the atmospheric OH sink are generally more active during the summer months. However, the net effect is that the lowest concentrations are observed during the summer and the largest concentrations in winter. This effect causes the observed six months phase difference in the seasonal cycles of the Northern and Southern Hemisphere. The overall mixing ratios and amplitudes of the seasonal cycle are larger in the Northern Hemisphere, where emissions are more important.

## 1.4 Isotope studies

Elements can have different stable and radioactive isotopes which only differ by the number of neutrons in the nucleus. The relative abundance of the isotopes of a

| Element | Isotope | rel. amount [% ] | Standard Isotopic Material |
|---|---|---|---|
| Hydrogen | H | 99.985 | V-SMOW |
| | D | 0.015 | |
| Carbon | $^{12}$C | 98.90 | V-PDB |
| | $^{13}$C | 1.10 | |
| Oxygen | $^{16}$O | 99.762 | V-SMOW |
| | $^{17}$O | 0.038 | |
| | $^{18}$O | 0.200 | |

**Table 1.3:** Terrestrial abundance of Standard Isotopic Materials [Kaye, 1987].

trace gas can be measured with the help of mass spectometry and optical techniques (sections 2.6 and 2.7). Isotopic substitution into a molecules leads to changes in the reaction speed which affect both the atmospheric sink and the production pathways. From observed variations in the isotope ratios of a trace gas information of the relative strength of different sources and sinks can be inferred, as well as transport processes influencing its distribution [Kaye, 1987]. Trace gases emitted from a certain source tend to carry a distinct isotopic composition that is representative for the source. The isotopic composition of a source is often referred to as its isotopic fingerprint.

### 1.4.1 $\delta$-notation

As isotopic variations are usually small, only relative deviations are measured and reported in the $\delta$-notation. The $\delta$ value is defined as the relative deviation of an isotope ratio from an international standard ratio in ‰,

$$\delta = [\frac{R_{sample}}{R_{std}} - 1] \cdot 1000\,‰ \tag{1.3}$$

where $R_{sample}$ and $R_{std}$ denote the isotope ratio of a sample and the corresponding standard respectively [Coplen, 1994]. For example, for $\delta^{13}$C the $R$ stands for $^{13}$C/$^{12}$C. $\delta^{13}$C measurements are usually reported relative to the international standard V-PDB, which stands for 'Vienna Pee Dee Belemnite' [Craig, 1957], [Gonfiantini, 1978]. Isotopic ratios of $\delta^{18}$O and $\delta$D are expressed relative to V-SMOW, which stands for Vienna Standard Mean Ocean Water [Gonfiantini, 1978]. In Table 1.4.1 the isotope ratios of these reference materials are listed.

### 1.4.2 Kinetic Isotope Effect (KIE)

The first work on isotope fractionation processes was done by Bigeleisen et al. [1947], Biegeleisen [1949] and Urey [1947]. During the formation and destruction of $CH_4$ the

original balance of its isotopes is disturbed by fractionation effects. These kinetic isotope effects (KIE) arise because isotopes have different energy levels (vibrational and rotational) leading to differences in bond strength.

In the methane oxidation KIEs of both primary and secondary form occur. In the primary isotope effect the deuterium atom is directly involved in the reaction

$$OH + CH_4 \rightarrow H_2O + CH_3 \tag{1.4}$$

$$OH + CH_3D \rightarrow H_2O + CH_2D \tag{1.5}$$

The fractionation of the sink process in equations 1.4 and 1.5 is given by the factor $\alpha$ or KIE and is the ratio of the inverse lifetime $k$ of the heavy isotopomer to that of the light (rare) isotopomer:

$$\alpha_D = KIE^D_{OH} = k_{CH_4}/k_{CH_3D} \tag{1.6}$$

The reaction of the deuterated form is about 30% slower than the normal form (due to stronger, e.g. less reactive, C-D bonds compared to the C-H bonds). This results in a $KIE_{OH}$ of 1.29 [Saueressig, 1999].

In the case of the secondary isotope effects, the isotopically labeled atoms are remote from the reaction site and exert an effect only through the dependence of the overall energy levels on mass. In this case, the isotopic effects are much smaller (~0.5%).

$$OH +^{12} CH_4 \rightarrow H_2O +^{12} CH_3 \tag{1.7}$$

$$OH +^{13} CH_4 \rightarrow H_2O +^{13} CH_4 \tag{1.8}$$

The rate coefficients of the wide range of observed isotope effects can be calculated [Bigeleisen & Mayer, 1947]. However, this is difficult, even at a 10% level, due to difficulties in defining the exact energies of the transition state and effects of quantum mechanical tunneling [Gellene, 1993].

## 1.5 Isotope variations in $CH_4$

The isotopic composition of atmospheric methane can be used to better constrain the large uncertainties in present $CH_4$ budget estimations. Individual source types have typical $\delta^{13}C$ and $\delta D$ isotopic signatures as illustrated in Figure 1.5, that reflect different methane production processes. $CH_4$ from biogenic (bacterial) methane formation is highly depleted in $\delta^{13}C$. For $CH_4$ from thermogenic formation fractionation processes are important, whilst they are less important during incomplete combustion

of biomass or fossil fuels. The methane sinks also affect the isotopic composition by inducing significant changes via isotopic fractionation in the reaction with OH, with $O^1D$ and Cl in the stratosphere [Saueressig, 1999] and the oxidation in soil. As a result $\delta^{13}C$ and $\delta D$ reflect changing source and sink contributions to the $CH_4$ budget.

The fractionation of the sinks and the $\delta^{13}C$ and $\delta D$ measurements on atmospheric methane can be used to determine the isotopic composition of the mean source [Cantrell et al., 1990]:

$$\delta_{source} = \sum_{i=1}^{n} \frac{Q_i}{Q}\delta_i \qquad \text{(bottom-up calculation)} \tag{1.9}$$

$$= \delta_{atm} + [f_{OH}(\frac{1}{KIE_{OH}} - 1) + f_{soil}(\frac{1}{KIE_{soil}} - 1) + f_{stra}(\frac{1}{KIE^*_{stra}} - 1)]$$

$$\times(1 + \frac{\delta_{atmos}}{1000}) \times 1000 \qquad \text{(top-down calculation)} \tag{1.10}$$

$\delta_{source}$: $\delta^{13}C$ or $\delta D$ of the mean source
$\delta_i$: $\delta^{13}C$ or $\delta D$ of the source $i$
$\delta_{atm}$: $\delta^{13}C$ or $\delta D$ value of the mean atmosphere
$Q_i$: global source strength of source $i$
$Q$: global source strength of all methane sources
$f$: fraction of the global sink (of the sink OH, soil oxidation or net transport into the stratosphere)

Table 1.2 lists the mean $\delta^{13}C$ and $\delta D$ sources which have been derived with equation 1.9 (bottom-up calculation) from the corresponding source strengths and source signatures of the individual sources. Equation 1.10 (top-down calculation) is only valid for an atmosphere at equilibrium. In Table 1.2 the mean sources from the top-down calculations are given.

The $^{13}C/^{12}C$ content of atmospheric $CH_4$ has been used to examine the budget of atmospheric $CH_4$ on both regional [Thom et al., 1993], [Lassey et al., 1993], [Bergamaschi et al., 1998a] and global scales [Stevens & Engelkemeir, 1988], [Quay et al., 1999], [Fung et al., 1991],[Hein et al., 1997]. The D/H content of $CH_4$ is a potential useful tracer for the atmospheric $CH_4$ budget but is less well developed than $^{13}C/^{12}C$ [Bergamaschi et al., 1998a], [Quay et al., 1999], [Marik, 1998]. There are fewer determinations of the $\delta D$ composition of $CH_4$, the hydrogen KIEs associated with the $CH_4$ sinks and the $\delta D$ composition of the $CH_4$ sources.

With equation 1.6 the expected average isotope fractionation in the troposphere $KIE_{avg}$ can be calculated:

$$KIE_{avg} = f_{OH}KIE_{OH} + f_{soil}KIE_{soil} \tag{1.11}$$

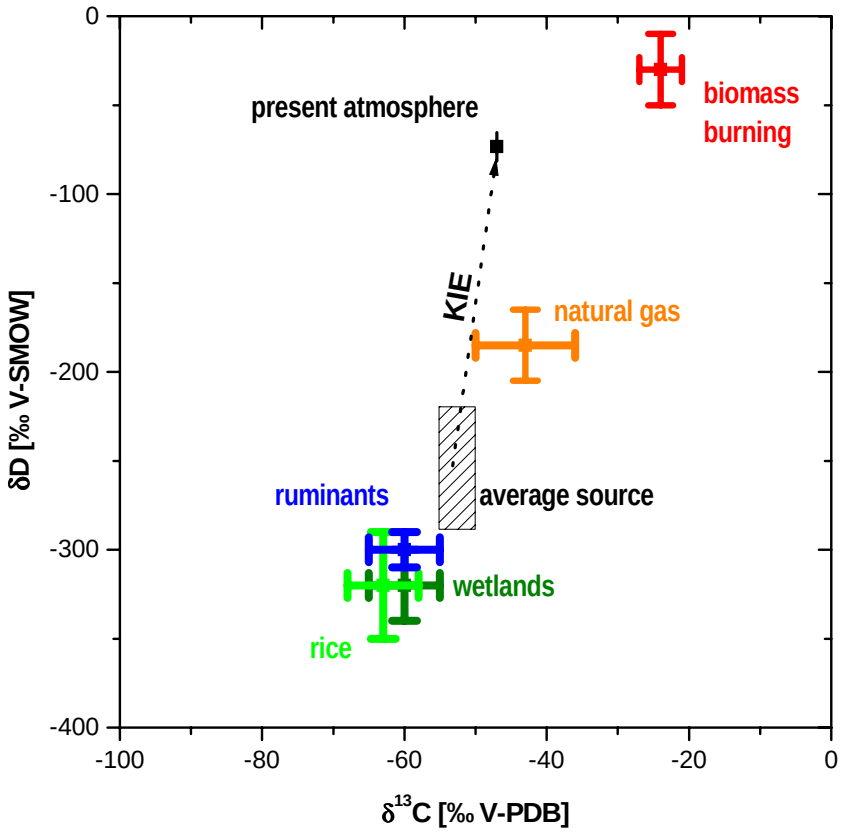


**Figure 1.5:** δD versus $\delta^{13}$C is plotted for different methane source signatures (see Table 1.2) and the mean atmospheric methane values are shown together with the mean source. The sink fractionation is indicated by the solid line.

with $f_{OH}$ and $f_{soil}$ representing the fractional contribution of the OH sink and soil sink respectively ($f_{OH}+f_{soil} = 1$).

### 1.5.1 Atmospheric $CH_4$ isotope data

Additional constraint on the global $CH_4$ cycle have been obtained by isotope measurements ($^{14}$C, $^{13}$C, D), utilizing the fact that the individual sources bear typical isotopic signatures (Figure 1.5). $^{14}$C measurements were mainly used to estimate the fraction of fossil $CH_4$ sources, such as losses during exploration and distribution of natural gas or from coal mining [Lowe et al., 1988], [Quay et al., 1991], [Wahlen et al., 1989], while $\delta^{13}$C measurements have been reported for a small number of global observational sites [Lowe et al., 1997], [Marik, 1998], [Quay et al., 1999]. Precise δD measurements have so far been hampered by difficulties in sample preparation required prior to isotope ratio mass spectrometry (IRMS) analysis [Marik, 1998]. As a princi-

pal alternative to IRMS, an optical technique has been developed by Bergamaschi et al. [1994], allowing direct measurements on $CH_4$ without conversion into $H_2$. This technique, originally used for studies of $CH_4$ sources and sinks, has been further refined and now allows the investigation of the small variations expected in atmospheric background $CH_4$ (see section 3.2).

## 1.6 The global CO budget

CO is released at the surface by incomplete combustion associated with fossil fuels and biomass burning. CO is also produced by the oxidation of $CH_4$ and other hydrocarbons such as isoprene. Sources of less importance include emission by vegetation and microorganisms on the continents and by photochemical oxidation of dissolved organic matter in the oceans. In Table 1.4 the global CO budget is given. The average atmospheric residence time of about 2 months, combined with an concentration of the order of 100 nmol/mol, correspond to an annual global turnover of approximatively 3000 Tg. However, the global budget of CO is not well defined, mainly due to the wide variety of natural and anthropogenic sources. About 50% to 60% of the CO emissions result from human activities, part of which is biomass burning, that comprises perhaps a third of total sources. The amount of CO from non-methane hydrocarbons is nearly as important as from $CH_4$ oxidation and a major part of both is also indirectly attributed to the anthropogenic source. The dominant sink for atmospheric CO is the oxidation by OH (90%), while the uptake by soils accounts for the remaining 10%. The problem of constructing a reliable budget is further aggravated by the relatively short atmospheric lifetime of CO of about 2 months, which results in large concentration gradients and variations.

## 1.7 CO measurements

The first atmospheric CO measurements were made by Mignotte in 1949 in the Swiss Alps. He assigned absorption lines in the 4.7 $\mu$m region of the solar spectrum to atmospheric CO. In the 1960s gas chromatographic methods allowed to study the first global distribution of CO [Robinson & Robins, 1970]. Since, measurements of CO in the troposphere have been made at various locations around the world [Seiler, 1974], [Seiler et al., 1984], [Brunke et al., 1990], [Khalil & Rasmussen, 1988] and monitoring networks have been developed, the most extensive one being managed since 1988 by NOAA/CMDL [Novelli et al., 1998a]. The first CO measurements from space were done in 1981 aboard the spaces shuttle [Reichle et al., 1986]. Satellite

| Sources | $Tg\,yr^{-1}$ | $\delta^{13}C$ [‰] V-PDB | $\delta^{18}O$ [‰] V-SMOW | $^{14}CO$ [pmC] | $\Delta^{17}O$[‰] |
|---|---|---|---|---|---|
| Fossil fuel combustion | 300-550 | $-27.5^{a}$ | $23.5^{a,b,m}$ | 0.0 | $0.0^{l}$ |
| Biomass burning | 300-700 | $-21.3^{c}$ | $\sim 16.3^{b,n}$ | $\sim 115$ | $0.0^{l}$ |
| | | $-24.5^{d}$ | $\sim 18^{e}$ | | |
| $CH_4$ oxidation | 400-1000 | $-52.6^{f}$ | $\sim 0^{b,g}$ | $\sim 125$ | 0? |
| | | | $\sim 15^{e}$ | | |
| NMHC oxidation | 200-600 | $-32.2^{e}$ | $\sim 0^{b,g}$ | $\sim 110$ | 0.0? |
| | | | $14.9^{e}$ | | |
| Ozonolysis | | | $80\text{-}100^{h}$ | | $25\text{-}40^{l}$ |
| Biogenic | 60-160 | | | $\sim 110$ | 0.0 |
| Oceans | 20-200 | $-13.5^{i}$ | | $\sim 110$ | |
| Total sources | 1800-2700 | | | | |

| Sinks | $Tg\,yr^{-1}$ | KIE($\delta^{13}C$) | KIE($\delta^{18}O$) | KIE($^{14}CO$) | KIE($\Delta^{17}O$) |
|---|---|---|---|---|---|
| CO + OH | 1400-2600 | $1.006^{j,o}$ | $0.990^{j,o}$ | $1.010^{k}$ | $1.004^{o}$ |
| Soil uptake | 250-640 | | | | |
| Loss to stratosphere | $\sim 100$ | | | | |
| Total sinks | 2100-3000 | | | | |

[a] [Stevens & Krout, 1972]
[b] [Brenninkmeijer, 1993]
[c] [Conny et al., 1997]
[d] [Conny, 1998]
[e] [Stevens & Wagner, 1989]
[f] [Quay et al., 1991]
Value based on $CH_4$ $\delta^{13}C$ of $-47.2$ ‰
and the fractionation in $CH_4$ + OH of 5.4 ‰
[g] [Brenninkmeijer & Röckmann, 1997]
[h] [Röckmann et al., 1998]
[i] [Manning et al., 1997]
[j] At atmospheric pressure
[k] Inferred from the value for $\delta^{13}C$, assuming mass dependent behavior.
[l] [Röckmann & Brenninkmeijer, 1998b]
[m] [Kato et al., 1999a]
[n] [Kato et al., 1999b]
[o] [Röckmann et al., 1998c]

**Table 1.4:** The tropospheric budget of CO, with source strengths and respective isotopic composition and with the sink fractionation constants.

measurements of CO promise true global scale coverage of its distribution.

### 1.7.1 Global distribution

Figure 1.6 shows the large seasonality and pronounced interhemispheric differences of CO mixing ratios which have been derived from the NOAA/CMDL data. As for $CH_4$ mixing ratios a phase shift of 6 months is observed for the seasonal cycles of the Northern and Southern Hemisphere. The highest mixing ratios are observed in the northern winter ($\sim$ 210 nmol/mol) and the lowest ones in the southern summer ($\sim$ 40 nmol/mol). The interhemispheric gradient exhibits a strong seasonality with maximum differences between the high latitudes of the northern and southern hemispheres in February and March ($\sim$ 170 nmol/mol) and a minimum in July and August (10 to 20 nmol/mol).

In areas of regional scale pollution, mixing ratios range from near background levels to more than 500 nmol/mol. In urban environments or areas of biomass burning CO levels may reach several µmol/mol.

### 1.7.2 Atmospheric trends

Ice core measurements from Greenland [Haan et al., 1996] indicate a significant increase of CO mixing ratios in the Northern Hemisphere during the last 200 years. The observed increase is attributed to anthropogenic activities, mainly combustion of fossil fuel. In contrast, CO mixing ratio derived from an Antarctic ice core for the high Southern Hemisphere, revealed only small variations during the last 2000 years [Haan & Raynaud, 1998].

For central Europe comparison of spectroscopic measurements of CO between the early 1950s to mid-1980s suggest an average increase of $\sim$1 nmol/mol $yr^{-1}$. After the eruption of Mount Pinatubo in June 1991 a significant anomaly was observed for CO mixing ratios [Khalil & Rasmussen, 1994], [Novelli et al., 1994]. For the period from 1990 through 1995 a decrease of CO mixing ratios of approximately 2 nmol/mol $yr^{-1}$ is reported by Novelli et al. [1998a].

## 1.8 Isotope variations in CO

For the isotopical analysis of CO four rare isotopes are available, $^{13}C$, $^{14}C$, $^{17}O$ and $^{18}O$. The major atmospheric sources exhibit clearly different $^{13}C/^{12}C$ and $^{18}O/^{16}O$ isotope ratios [Stevens & Krout, 1972], [Stevens & Wagner, 1989], [Brenninkmeijer, 1993]. In Figure 1.7 the $\delta^{13}C$ and $\delta^{18}O$ signatures of CO sources are plotted.

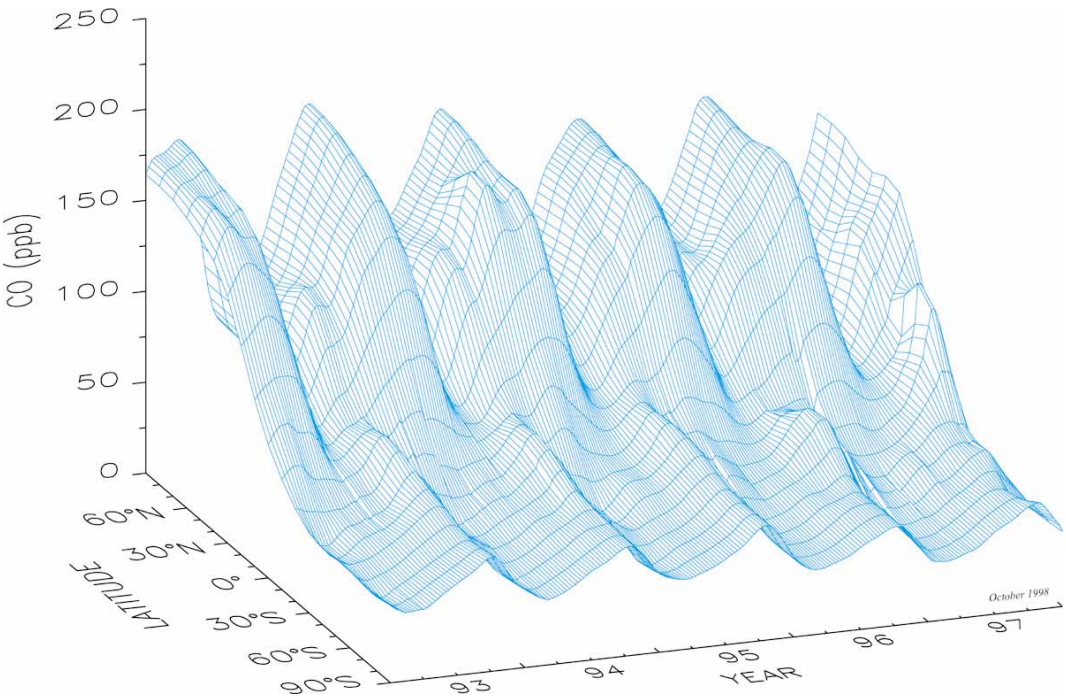


**Figure 1.6:** Three-dimensional representation of the global distribution of atmospheric CO [Novelli et al., 1998a].

The $\delta^{13}C$ balance in atmospheric CO is largely influenced by CO from $CH_4$ oxidation, which represents by far the most depleted source. Atmospheric $CH_4$ is already quite depleted, with an average $\delta^{13}C$ of around $-47$‰ and the kinetic isotope effect in the reaction of $CH_4$ with OH of $3.9 \pm 0.4$‰ [Saueressig, 1999] further reduces the $\delta^{13}C$ of the resulting CO to values below $-50$‰. In contrast, all the remaining major sources are in the $\delta^{13}C$ range between $-32$ and $-12$‰ (see Table 1.4 for references). Technological sources have typical $\delta^{13}C$ values around $-27.5$‰, reflecting the $\delta^{13}C$ of combusted fuel, as usually no significant isotope fractionation occurs in high-temperature combustion processes. Similarly, CO from biomass burning is thought to have $\delta^{13}C$ values close to the $\delta^{13}C$ of burnt plant matter. Slightly depleted compared to these sources is CO originating from the oxidation of natural non-methane hydrocarbons.

The $\delta^{18}O$ signatures are clearly not correlated with $\delta^{13}C$, thus providing a further independent tracer. CO from technological sources has the most enriched $\delta^{18}O$, close to $\delta^{18}O$ of atmospheric oxygen of 23.5‰. Measurements in plumes from large cities showed a remarkably low $\delta^{18}O$ variability [Brenninkmeijer & Röckmann, 1997], [Stevens & Wagner, 1989], while $\delta^{18}O$ values from individual automobiles show a much wider spread (11 to 29‰) [Huff & Thiemens, 1998], [Kato et al., 1999a], the

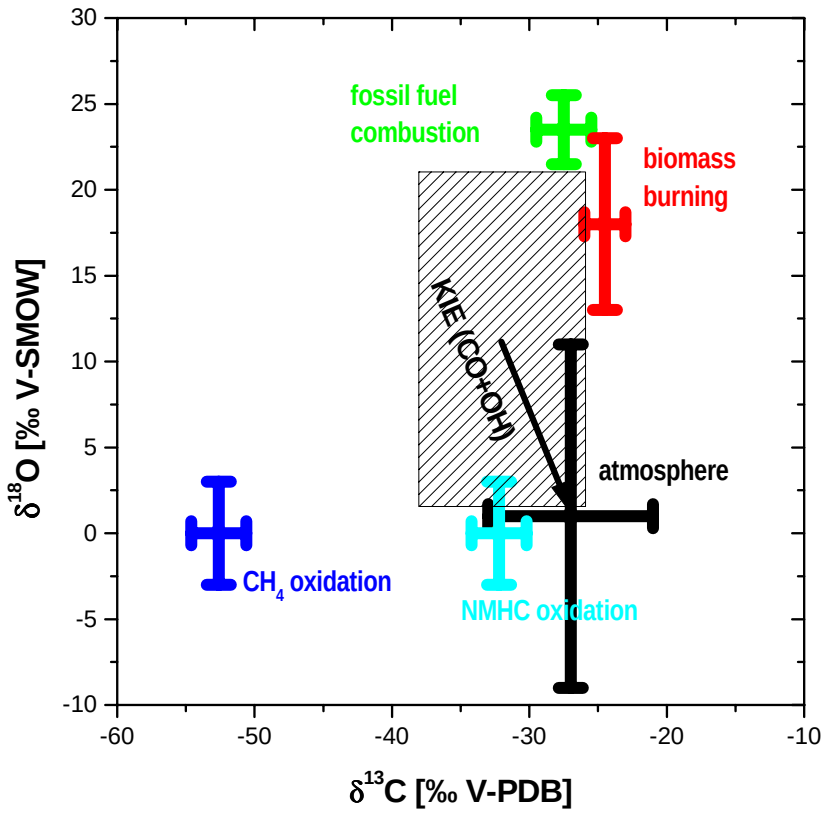


**Figure 1.7:** $\delta^{18}$O versus $\delta^{13}$C is plotted for different CO source signatures (see Table 1.4 for error bars) together with the range of atmospheric CO data. The kinetic isotope effect of the sink process is also indicated.

most common being again 23.5 ‰. For biomass burning, $\delta^{18}$O values of 18±1 ‰ are reported by [Stevens & Wagner, 1989], while $\delta^{18}$O values varied from 10 to 26 ‰ during flaming and smoldering of plants [Kato et al., 1999b]. No direct measurements are available for $\delta^{18}$O from the oxidation of NMHCs and $CH_4$. Stevens and Wagner [1989] inferred a value of 14.9 ‰ for oxidation of natural NMHCs, based on observed CO - $\delta^{18}$O correlations at a rural site in Illinois. On the basis of atmospheric observations and simple budget considerations for CO and $\delta^{18}$O in the Southern Hemisphere, Brenninkmeijer and Röckmann [1997] estimated the $\delta^{18}$O of both $CH_4$ and NMHC oxidation to be near 0 ‰.

Over the last years atmospheric observations of CO isotopes from several stations have been reported, e.g. from Scott Base (Antarctica) and Bearing Head (New Zealand) [Brenninkmeijer, 1993], from Montauk Point (Long Island) [Mak & Kra, 1999], Alert and Spitsbergen [Röckmann, 1998a], Happo (Japan) [Kato et al., 2000]

and Sonnblick (Austrian Alps) [Gros et al., 2000]. These measurements reveal pronounced seasonal cycles both in $\delta^{13}C$ and $\delta^{18}O$ at all stations and a large, seasonally varying, latitudinal gradient.

### 1.8.1 Kinetic Isotope Effect

In order to relate atmospheric observations to the isotopic signatures of the individual sources, the kinetic isotope effect (KIE) of the sinks has to be taken into account. The KIE is defined as the ratio of reaction rate constants i.e., KIE($\delta^{13}C$) = k($^{12}CO$)/k($^{13}CO$), and KIE($\delta^{18}O$)=k($C^{16}O$)/k($C^{18}O$), respectively (see also section 1.4.2).

Fig. 1

Measurements of the fractionation factor KIE for $\delta^{13}C$ have been made by Stevens et al. [1980], Smit et al. [1982] and Röckmann et al. [1998]. A modest fractionation exists which declines with decreasing temperature. Already below 400 hPa the isotopic effect reverses into an inverse effect, where $^{13}CO$ reacts faster with OH than $^{12}CO$. The overall fractionation in the troposphere is $\sim 3$ ‰. Measurements for $\delta^{18}O$ have also been made by Stevens et al. [1980] and Röckmann et al. [1998] and

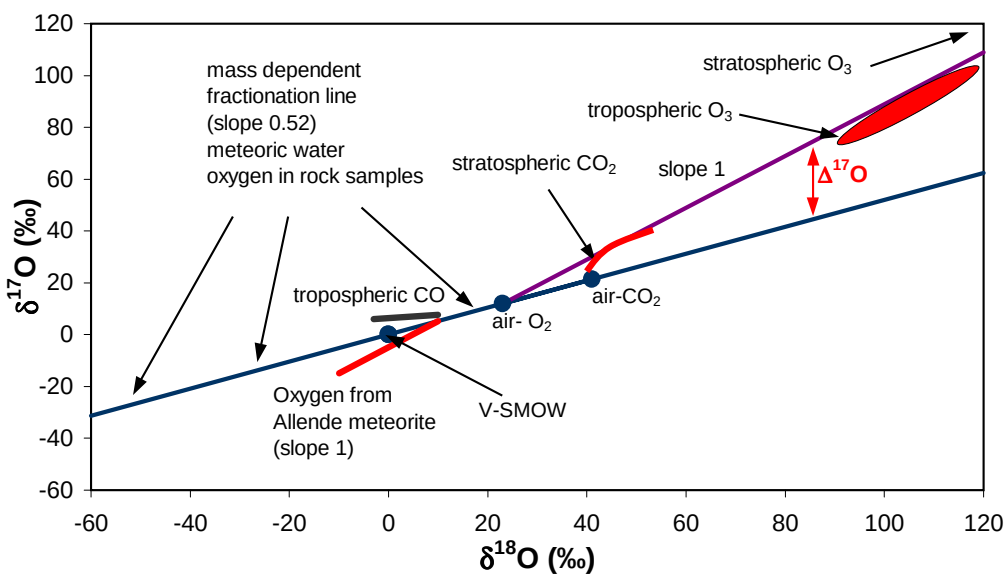


**Figure 1.8:** A three isotope diagram illustrating the concept of mass independent fractionation and the distribution of the oxygen isotopes in different oxygen bearing compounds. Most compounds on earth define the terrestrial mass dependent fractionation line with slope $\sim$ 0.52. A MIF process causes a deviation from this line [Röckmann & Brenninkmeijer, 1998b]

.

show an inverse slight pressure dependent effect. A KIE value of ~0.990 is representative for most of the troposphere. For the soil sink, KIE($\delta^{13}$C )=1.0060±0.0009 and KIE($\delta^{18}$O )=1.014±0.002 have been determined [Bergamaschi et al., 2000c] (personal communication C. Stevens therein).

Most fractionation processes depend on mass and therefore scale with the relative mass differences of the different isotopes (see section 1.4.2). In the case of oxygen this leads to $^{17}O/^{16}O$ variations matching approximately half of the accompanying $^{18}O/^{16}O$ variations, i.e.

$$\delta^{17}O = 0.52 \cdot \delta^{18}O \tag{1.12}$$

Almost all oxygen bearing substances (e.g. minerals, water, atmospheric oxygen and tropospheric $CO_2$) show $\delta^{17}$O and $\delta^{18}$O variations that define a line with slope ≈0.52 (see Figure 1.8). Any deviation from this mass dependent fractionation line is a clear indicator for mass-independent isotope fractionation (MIF). Significant MIF had first been detected for meteoritic material. In the atmosphere MIF has been found for $O_3$ [Mauersberger, 1987], stratospheric $CO_2$ [Thiemens et al., 1995], and $N_2O$ [Cliff & Thiemens, 1997]. $\delta^{17}$O(CO) measurements also established a mass-independent isotope fractionation in atmospheric CO [Hodder et al., 1994]. For tropospheric CO, two different mechanism cause MIF. The reaction of $O_3$ with unsaturated hydrocarbons produces CO that inherits the relative strong MIF in $O_3$ [Röckmann et al., 1998]. But the major source of MIF in atmospheric CO is the fractionation in the removal reaction CO + OH = $CO_2$ + H [Röckmann et al., 1998c]. At high northern latitudes an $^{17}$O excess of up to 7.5 ‰ was observed during summer.

In Figure 1.9 we have used a simple 1-box model to simulate the isotopic changes of atmospheric CO during the CO + OH sink reaction. Air representative of the mid latitude Northern hemisphere at 150 nmol/mol ($\delta^{13}$C =−27 ‰, $\delta^{18}$O =10 ‰) has been used in these examples. The changes with and without the $CH_4$ oxidation source and an added fossil source are shown. CO mixing ratios take several months before they approach the equilibrium (average OH levels of $10^6$ molec./cm$^3$). This illustrates the difficulty of interpreting isotope data without modeling. The typical meridional transport times in the troposphere and seasonal changes in OH are comparable to its chemical lifetime and the time of isotopic change.

### 1.8.2 Atmospheric $^{14}$CO

$^{14}$CO is a natural atmospheric tracer occurring at concentration levels of 5 to 30 molec./cm$^3$. The main source 1of atmospheric $^{14}$CO is the nuclear reaction [Libby,

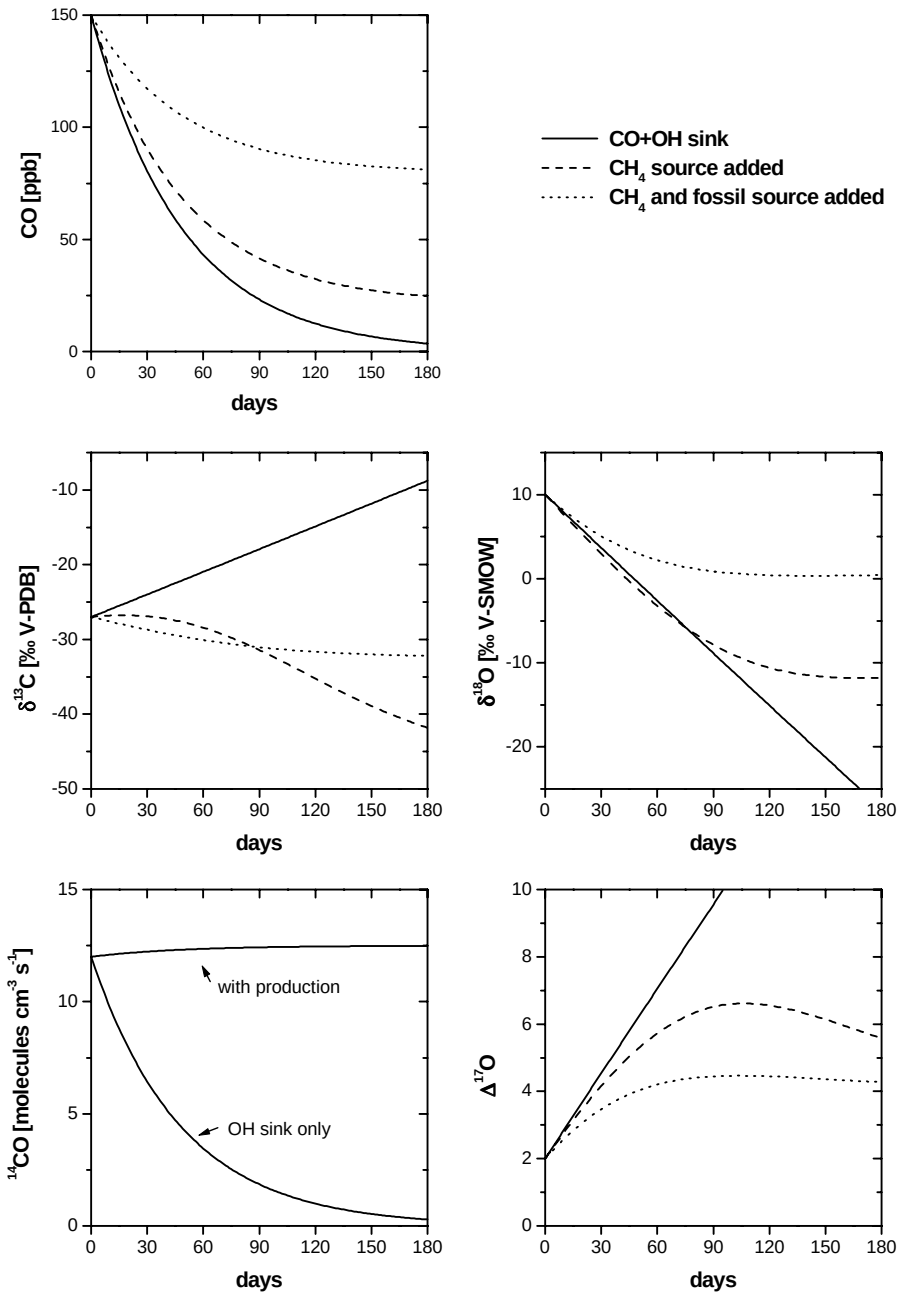


**Figure 1.9:** The changes in concentration and isotopic composition for CO in a given air mass due to the effect of OH. Scenarios are shown without sources, including the methane oxidation source (assuming $10^6$ OH $cm^{-3}$ and 1780 nmol/mol $CH_4$) and an additional constant fossil source (of 1.2 nmol/mol per day, $\delta^{13}C = -27$ ‰, $\delta^{18}O = 15$ ‰) respectively. For $^{14}CO$ scenario two scenarios are shown (OH sink only, additional constant source of $3 \cdot 10^{-6}$ molecules $s^{-1}$ $cm^{-3}$).

1946]:

$$^{14}N + n \rightarrow ^{14}C + p \tag{1.13}$$

$$^{14}C + O_2 \rightarrow ^{14}CO + O \tag{1.14}$$

followed by the subsequent oxidation of the exited radiocarbon atom to $^{14}$CO (yield about 95%) [McKay et al., 1963], [Pandow et al., 1960].

More than 75% of atmospheric $^{14}$CO is from the cosmogenic source. The cosmogenic production rate increases with increasing altitude up to about 16 km and then decreases. The cosmogenic source is modulated by the solar wind plasma with a cycle time of 11 years, while the Earth magnetic field provides a shielding and focusing to the magnetic poles. These effects lead to an atmospheric source distribution with a maximum production rate in the lowermost stratosphere and a varying total source strength of ±25% within 11 years [Lingenfelter & Flamm, 1963].

The smaller biogenic fraction of $\sim 25\%$ is recycled $^{14}$CO from biomass, released into the atmosphere by $CH_4$ oxidation, NMHC oxidation and biomass burning. The relative contribution from these sources containing recycled $^{14}$CO can be estimated, because they all have similar $^{14}C/^{12}C$ ratios of about $1.4 \cdot 10^{-12}$, or 120% modern carbon (pmC). Uncertainties in the magnitude of these sources are mitigated since the $^{14}C/^{12}C$ ratio in atmospheric CO is generally between 400 and 900 pmC.

Apart from a small soil sink (about 10%), $^{14}$CO is removed from the atmosphere via oxidation by OH. Thus atmospheric $^{14}$CO and CO share the same sinks, but have very different sources. The abundance of OH is highest in the tropics year-round and shows a strong seasonal cycle in the middle and high latitudes. Given the distinct source and sink distribution and the relatively fast rate constant for the CO+OH reaction, $^{14}$CO measurements provide a unique tracer of OH abundance.

Weinstock et al. [1969] used the $^{14}$C data from McKay et al. [1963] to estimate the atmospheric lifetime of CO. Volz et al. [1981] measured the first annual $^{14}$CO cycle for the mid northern latitudes and showed that it agreed with the existing OH distribution and seasonality. For this purpose they processed samples of 20.000 l to extract enough $^{14}$CO as $^{14}CO_2$ for applying proportional beta counting. The development of accelerator mass spectrometry for $^{14}$C (see section 2.8) enabled Brenninkmeijer et al. [1992] to make routine $^{14}$C measurements in the southern hemisphere, using 1 $m^3$ air samples. They published $^{14}$CO measurements from New Zealand and Germany exposing a large $^{14}$CO abundance difference, while also inferring a rather small southern hemispheric latitudinal gradient. Various mechanisms, like differences in production due to changes in solar activity, latitudinal gradients, troposphere stratosphere exchange, and biogenic $^{14}$CO were not considered adequate

to explain the large difference. They suggested higher southern hemisphere OH levels as a possible explanation.

## 1.9 Scope of this thesis

In this study the stable isotope ratios $^{13}C/^{12}C$ and D/H of atmospheric $CH_4$ were measured as well as the $^{13}C/^{12}C$, $^{18}O/^{16}O$ ratios and $^{14}CO$ concentrations of atmospheric CO. In chapter 2 the further improvements of these measurements are documented. This mainly involved changes of the $CH_4$ extraction procedure, necessary for the subsequent analysis of $\delta^{13}C$ by mass spectrometry and $\delta D$ by tunable diode laser.

A major part of this thesis was the measurement of a three year record of the isotopic composition of atmospheric $CH_4$ (chapter 3) and CO (chapter 4) at the background station Izaña, Tenerife. The large seasonal cycles in mixing and isotopic ratios of $CH_4$ and CO allowed to infer the impact of source and sink processes on these trace gases. Thus the average kinetic isotope effect in the sink processes of atmospheric methane could be deduced from the $\delta^{13}C$ and $\delta D$ records. The measured $\delta D$ seasonality is the first ever reported for atmospheric background $CH_4$. The comparison of the $\delta^{13}C$ and $\delta D$ records with results from an inverse $CH_4$ model study in which the isotope records of Izaña were included, allowed the quantification of the different source contributions. Similarly the Izaña records for $\delta^{13}C$ and $\delta^{18}O$ of CO were compared to an inverse CO model study from which the seasonal pattern of the source and sink processes could be quantified for Izaña. Finally, the large synoptic scale variations occurring at Izaña made it possible to study source regions such as North America, Europe and partly Africa, as well as maritime background conditions of the North Atlantic.

Finally we compare the Izaña records to CO isotope measurements done at a number of other stations, i.e Spitsbergen, a remote station at high northern latitude, Schauinsland (Germany) and Sonnblick (Austria), which are representative for continental stations at mid latitudes. In contrast more polluted air masses have been encountered at Kollumerwaard, The Netherlands, and during the BERLIOZ campaign in summer 1998, for which CO, $\delta^{13}C$ , $\delta^{18}O$ and $^{14}CO$ have been investigated.

In chapter 5 we present the measurement and interpretation of two Antarctic firn air records, which have been analyzed for methane and its stable isotopes. With the help of a firn air diffusion model the atmospheric trends of $\delta^{13}C$ and $\delta D$ of atmospheric $CH_4$ since the mid-20th century were reconstructed. In step with increasing $CH_4$ mixing ratios a positive $\delta^{13}C$ trend was inferred reflecting a shift in

atmospheric source strength towards the heavier anthropogenic sources. For $\delta$D a period of decline was observed previous to 1975, followed by a gradual increase also towards the heavier anthropogenic sources. This is the first time the non-equilibrium state between $CH_4$ and its sources and sinks has not only been observed for $\delta^{13}$C but also for $\delta$D.

# Chapter 2

# Sampling and Measurement

The sampling, extraction and subsequent analysis of CO and $CH_4$ and their isotopic composition require a high degree of accuracy in order to establish seasonal variations and long-term trends. To measure the isotopic composition of atmospheric CO and $CH_4$ those gases have to be extracted from atmospheric air samples prior to their analysis by mass spectrometry or by tunable diode laser spectroscopy. As this is a very time consuming task it can only be done for selected samples. The ongoing progress with continuous flow GC-MS measurements will change this for selected stable isotopes in the future, but cannot at present compete with our precision in $\delta$D for example. Neither can GC-MS be used for $^{14}$CO measurements.

In this chapter we describe how ambient air samples are collected in high pressure cylinders with a high purity compressor (see section 2.1.1 and 2.1.2) at various stations for long-term observation and during short-term field campaigns (section 4.7 and 5). At the MPI a complete analysis of the air samples consists in a first step of the measurement of $CH_4$, $CO_2$, $N_2O$ and $SF_6$ mixing ratios by gas chromatography (GC) (section 2.2). Subsequently the isotopic composition of $CO_2$, CO and $CH_4$ are determined by mass spectrometry (section 2.3 and 2.6). Only $\delta$D of $CH_4$ is measured by tunable diode laser spectroscopy (section 2.7). For the analysis of $^{14}$CO we send the samples to accelerator mass spectrometry facilities (section 2.8).

The process used for the measurement of CO mixing ratios and isotopic compositions has been previously documented in [Brenninkmeijer, 1993] and [Röckmann, 1998]. The measurement procedure for $CH_4$ and its isotopes, $\delta^{13}$C and $\delta$D, including improvements that have been made during this thesis, are described here for the first time.

## 2.1 Air sampling

Air samples of 500 to 1100 L (STP) are taken on a regular basis at several world-wide stations (see Table 3.1) and the air samples are sent to the MPI for analysis. There air samples are stored and shipped in high pressure cylinders. While atmospheric $CH_4$ can be sampled and stored in appropriate cylinders without significant contamination [Marik, 1998] this is more difficult for CO. Cylinders and compressors are known to easily produce CO which contaminates the air samples. To ensure high quality air sampling we use a modified compressor system and high pressure aluminum cylinders which will be described in the next subsections.

### 2.1.1 The compressor system

The compressor used is an oil-free three-stage-compressor (Rix Industries, Oakland, CA, USA) which has been modified according to Mak and Brenninkmeijer [1994]. The aim of these modifications is to suppress possible sources of CO contamination, either due to leakage or the formation of CO during operation. Further modifications consisted of the introduction of a drying unit (Drierite, anhydrous $CaSO_4$, Hammond, Ohio) to trap $H_2O$ both at the inlet and on the high pressure side of the compressor system. Separate tests have shown that the drying agent neither affects CO and $CH_4$ mixing ratios nor their isotopic composition.

Before sampling the compressor is flushed by opening an additional vent valve mounted on the high pressure side. Thereafter, the high pressure sample cylinder is filled twice to ~5 bar and drained again. Thus contamination from remaining air of previous air samples is reduced to less than 0.1%. Finally, cylinders are filled to 120 bar at typical flow rates of 15 $\mathrm{l\,min^{-1}}$.

The modified RIX compressors have been shown to produce less than 1 nmol/mol CO in the sampled air [Mak & Brenninkmeijer, 1994a]. They are used at the different sampling stations and need little maintenance apart from regular exchange of the Drierite. Nevertheless, after several years of regular air sampling some problems may occur. Corrosion processes can be significant at sampling stations with high humidity and this can affect the valves. Also the sealing of the pistons gets less effective due to wear and air on the high pressure side is lost. This results in longer filling times and may also lead to leakage into the first stage piston. To prevent these problems, compressors are send to Mainz every 1 to 2 years for maintenance.

Another problem has been the air sampling at low temperatures. These problems were encountered during winter at the stations Mount Sonnblick, Austria, and Happo, Japan. The compressors failed to start unless they were warmed before

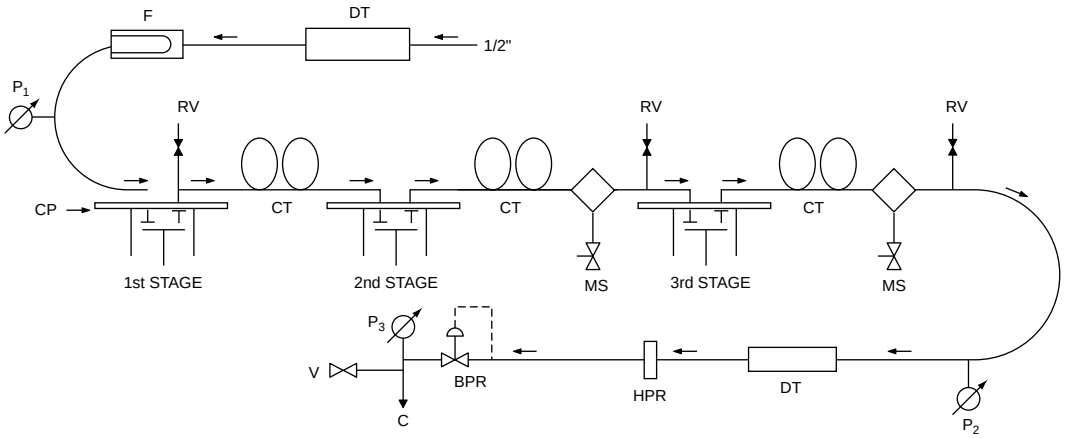


**Figure 2.1:** The modified three-stage RIX compressor. 1/2 inch: teflon inlet; BPR: Back pressure regulator; C: Sample cylinder; CP: Cooling plates; CT: Cooling tubings; DT: Drying trap; F: Glass fibre filter; HPR: High pressure filter; MS: Moisture separator; $P_{1-3}$: Pressure gauges (fluid dampened); RV: Pressure relief valve; V: Vent valve. [Röckmann, 1998a]

use. The compressor system used for the firn air sampling in Antarctica was further modified (see Figure 5.2 in section 5.1).

### 2.1.2 High pressure sample cylinders

We use high pressure aluminum cylinders (4.7 liter: BOC Gases, UK; 5 and 10 liter: Scott Marrin Inc., Riverside, CA, USA). Tests have shown that the cylinders only insignificantly increase the CO mixing ratios of air samples (below 2ppb in two months [Mak & Brenninkmeijer, 1994a]). Nevertheless single cylinders may still exhibit a strong CO increase in mixing ratios accompanied with significant changes in the isotopic CO signal. This happened with one of the BOC cylinders filled twice in Izaña in 1996, which has not been used afterwards. In this case CO mixing ratios increased by ~20 nmol/mol and $\delta^{18}O$ and $\delta^{13}C$ values of CO were enhanced by ~5 ‰ and 1 ‰ to 2 ‰ respectively. The more than 80 remaining cylinders have not exhibited such problems. Measurements of a large number (>60) of duplicate samples have never shown significant differences in the CO mixing ratios and isotopic composition (see section 4.1). $CH_4$ is much less sensitive to storage in cylinders and air samples can be stored over several years without changes in the mixing ratio and isotopic signal [Francey et al., 1999].

### 2.1.3 Spot air sampling

The compressor is usually kept in a laboratory or storage room at the sampling stations. The air is pumped through a 1/2 inch PFA tube with the inlet mounted on a sampling tower. To collect spot samples we pump air through the air inlet line directly into high pressure cylinders. These air samples are representative for air masses encountered during the 0.5 to 1 hour filling time. In general spot samples are taken biweekly at the stations listed in Table 3.1.

### 2.1.4 Continuous air sampling

Due to important synoptic scale variations occuring at Izaña, we decided to collect 2-week time-integrated samples in addition to the biweekly spot samples. This continuous sampling makes it possible to define seasonal background signals representative for the sampling station. The system for the continuous sampling at Izaña has been set up by T. Röckmann and P. Bergamaschi in 1996 [Röckmann, 1998a].

The continuous sampling proceeds as follows. A diaphragm compressor (KNF Neuberger, Freiburg, Germany) is used to continuously pump air at a flow rate of $\sim 3$ l min$^{-1}$ and a pressure of $\sim 3$ bar through a drier (Perma Pure Inc, Toms River, NJ, USA). The first part of the Perma Pure drier is heated to about 40 °C to prevent condensation and to improve the drying efficiency (achieved dew point: $<$ -20 °C). Only a small fraction of the air coming out of the drier is used for the samples while the rest is redirected into the drier as counter-current purge gas (after expansion to ambient pressure).

To monitor the quality of the sample storage process a sample fraction of 2x100 cm$^3$min$^{-1}$ were directed via two mass flow controllers into two separate $\sim$ 500 L polyethylene coated aluminium bags. These sampling bags are suited for storage of air and did not exhibit any significant CO increase during tests. Nevertheless, CO mixing ratios from continuous samples during summer 1998 were significantly higher than those from spot samples over the same period, suggesting contamination problems. This will be further discussed in section 4 together with the data. Both sampling bags are continuously filled for one week and then replaced with two new bags. Finally the air from two consecutive weeks is transferred via the compressor into a high pressure cylinder (final filling pressure is usually about 120 bar). This is done for the two separate sets of sampling bags. We therefore end up with duplicate air samples for every two week period.

## 2.2 GC measurements

Measurements of mixing ratios of different gases were made using a HP 6890 GC equipped with a flame ionization detector (FID) and an electron capture detector (ECD). The FID channel allows the measurement of $CH_4$ and also $CO_2$ after methanization. The ECD channel is used for measurements of $N_2O$ and $SF_6$. The sample inlet is through an 8-port valve, allowing the fully automated measurement of up to 8 cylinders, controlled via HP Chemstation software.

Working reference gases are calibrated for $CH_4$ (as well as for $CO_2$ and $N_2O$) versus two calibration gases (NOAA-1 and NOAA-2) from the National Oceanic and Atmospheric Administration Climate Monitoring and Diagnostics Laboratory (NOAA/CMDL). In Table 2.1 their reported mixing ratios are given together with their confidence intervals. The results of the regular intercalibration between our working reference gases MPI-1 to MPI-4 and these two calibration gases since December 1996 are also listed in Table 2.1 and are shown in more detail in Figures 2.2 and 2.3 for $CH_4$ and $CO_2$ respectively.

With measurements of mixing ratios extending over several years at our sampling stations (see section 3 to 5), the long time stability of our GC reference gases is of high importance. Without this long term trends in the atmospheric mixing ratios

| | $CH_4$ [nmol/mol] | $CO_2$ [mmol/mol] | $N_2O$ [nmol/mol] | $SF_6$ [pmol/mol] | n |
|---|---|---|---|---|---|
| NOAA-1 | $1781 \pm 18$ | $365.50 \pm 0.4$ | $312.4 \pm 3$ | $3.595 \pm 0.02$ | |
| NOAA-2 | $1815 \pm 3$ | $362.95 \pm 0.06$ | $312.6 \pm 3.1$ | $4.042 \pm 0.02$ | |
| MPI-1 (Feb 97-Jul 98) | $1961.1 \pm 2.5$ | $382.85 \pm 0.52$ | $315.19 \pm 0.32$ | $4.817 \pm 0.001$ | 13 |
| MPI-2 (Jul 98-Mar 00) | $1974.6 \pm 1.1$ | $376.02 \pm 0.29$ | $310.32 \pm 0.29$ | $5.968 \pm 0.132$ | 23 |
| MPI-3 | $1776.5 \pm 0.5$ | $347.77 \pm 0.10$ | $305.53 \pm 0.39$ | $4.363 \pm 0.024$ | 21 |
| MPI-4 (since Apr 98) | $1846.0 \pm 0.5$ | $373.29 \pm 0.08$ | $320.25 \pm 0.38$ | $4.203 \pm 0.000$ | 19 |
| duplicates | $\pm 0.78$ | $\pm 0.50$ | $\pm 0.26$ | $\pm 0.009$ | 55 |

**Table 2.1:** NOAA/CMDL calibration standards, GC working reference gases and mean deviation of duplicate continuous samples. The time periods during which the MPI standards were used as working reference gases are given and $n$ is the number of calibrations performed against NOAA-2.

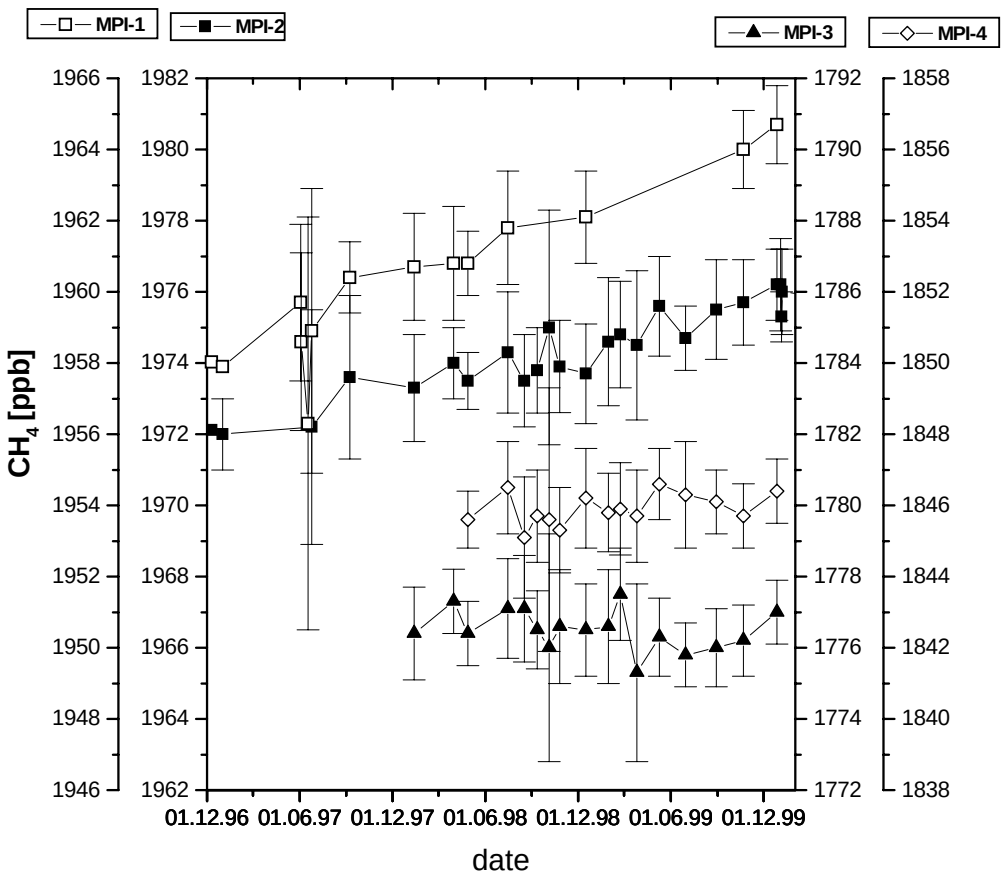


**Figure 2.2:** $CH_4$ working reference gas MPI-1 to MPI-4 versus NOAA-2.

cannot be established. Figures 2.2 and 2.3 show the $CH_4$ and $CO_2$ mixing ratios of our working reference gases MPI-1 to 4 against the NOAA/CMDL standard NOAA-2 over the last 4 years. An obvious, but weak temporal trend can be detected for MPI-1 and 2 from Dec 96 to Dec 99 in $CH_4$ mixing ratios of 8 and 4 nmol/mol respectively. A strong decrease in $CO_2$ for MPI-1 and MPI-2 of $\sim 3\,\mu$mol/mol was observed between Dec 96 and Jan 98.

The high precision of our $SF_6$ GC-measurements of 0.01 pmol/mol is gained by reprocessing the ECD chromatographs for selected samples. The calibration of our $SF_6$ measurements is made against a set of standards prepared at the University of Heidelberg [Maiss et al., 1996]. In addition, most of the continuous samples were also analyzed for $SF_6$ at the Institut für Umweltphysik, Heidelberg, using a cryo-trapping GC/ECD system [Maiss et al., 1996], with a precision of $\pm 0.02$ pmol/mol.

The $N_2O$ GC-measurements suffer from the nonlinearity of the ECD detector [Bräunlich, 1996]. Dilution tests starting from $N_2O$ mixing ratios close to atmo-

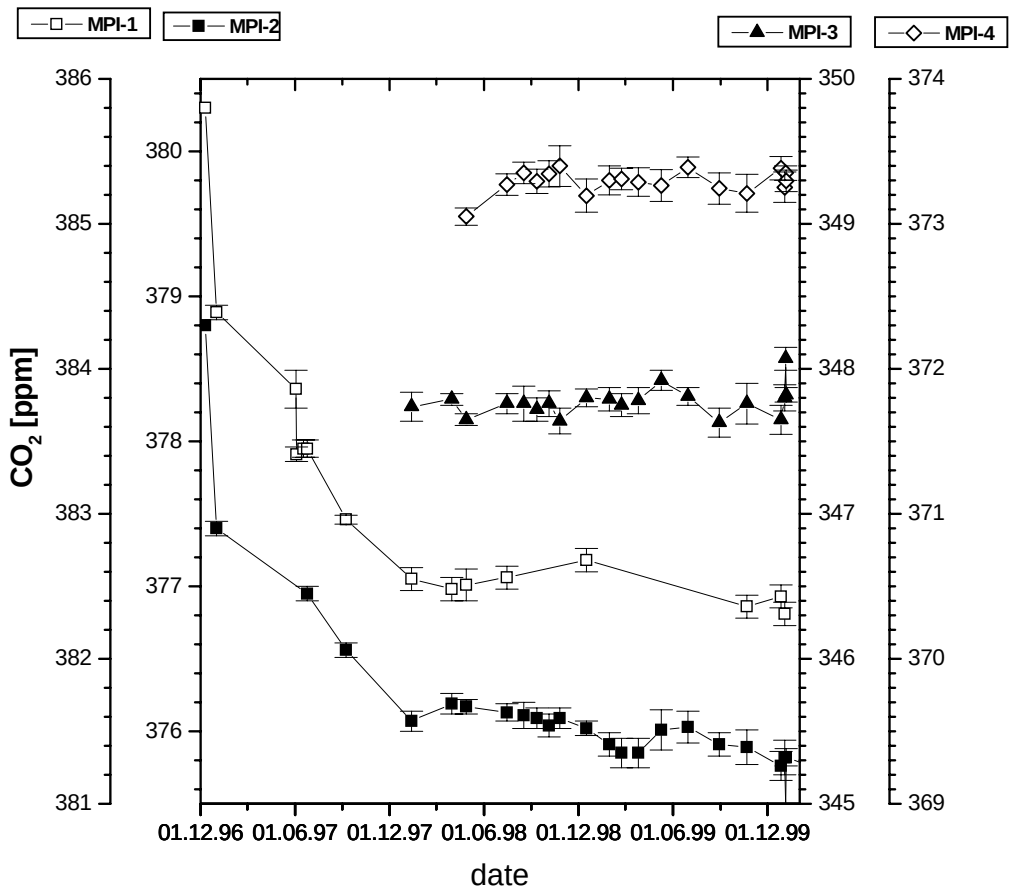


**Figure 2.3:** $CO_2$ working reference gas MPI-1 to MPI-4 versus NOAA-2.

spheric values down to 10 nmol/mol established a correction factor for the GC in Mainz of 20% of the difference between sample and standard. However, problems with the ECD in 1998 make further correction of our $N_2O$ data necessary before detailed studies of atmospheric trends can be done.

For the final reporting of the GC trace gas measurements we correct all mixing ratios of air samples relative to the NOAA/CMDL calibration gas NOAA-2. Each air samples is measured against our MPI working gas. We then use the mean of working gas values measured against NOAA-2 previous and subsequent to the GC analysis to calculate the final mixing ratio of the sample.

The precision of the GC system (for a single measurement series consisting of about 10 injections) is approximately $\pm 1$ nmol/mol for $CH_4$, $\pm 0.2$ µmol/mol for $CO_2$, $\pm 0.4$ nmol/mol for $N_2O$ and $\pm 0.04$ pmol/mol for $SF_6$. The mean deviation between the average values (usually from at least two different measurement se-

ries on different days) from 55 duplicate continuous samples was ±0.8 nmol/mol for $CH_4$, ±0.5 µmol/mol for $CO_2$, ±0.3 nmol/mol for $N_2O$ and ±0.009 pmol/mol for $SF_6$. These values reflect the overall precision that is obtained during sampling, storing and subsequent GC-analysis.

## 2.3 The extraction system

In 1996 a new sample preparation system was set up, which allows the successive extraction of $CO_2$, CO and $CH_4$ for isotope analysis [Bergamaschi et al., 1998a]. During the research for this thesis, nearly 400 air samples have been processed on this system. Improvements of the $CH_4$ extraction and combustion system increased the accuracy of stable isotope measurements of atmospheric $CH_4$ (see section 2.3.3). Figures 2.4 to 2.6 show the three parts of the extraction system, the CO and $CO_2$ extraction section, the $CH_4$ extraction section and the $CH_4$ combustion section respectively.

The CO section of the system is similar to that described in Brenninkmeijer [1993] and Brenninkmeijer et al. [2000] and is based on the extraction technique developed by Stevens and Krout [1972]. The main idea is to remove $CO_2$ before oxidizing CO to $CO_2$ which is subsequently collected and analyzed by mass spectrometry. The volumetric measurement of the collected $CO_2$ also allows an absolute and very precise measurement of the CO mixing ratio.

The $CH_4$ extraction system has been designed to enable the pre-concentration of the methane samples necessary for the direct δD analysis by tunable diode laser spectroscopy [Bergamaschi et al., 1994](see section 2.7). In the $CH_4$ combustion system $CH_4$ is combusted to $CO_2$ with the help of a platinum catalyst. The derived $CO_2$ is then measured by mass spectrometry to infer the $\delta^{13}C$ value of $CH_4$.

### 2.3.1 The CO and $CO_2$ extraction system

The air sample is introduced into the glass line at a flow rate of 1.5 to 5 $l\,min^{-1}$ (STP) controlled by a thermal mass flow controller (MFC, Hastings type HFC-202F). A safety pressure relief valve designed by Brenninkmeijer and Bergamaschi [1998d] is installed at the outlet of the MFC to protect the glass line from any unwanted build-up of high pressure. Condensable compounds such as $H_2O$, $CO_2$, $N_2O$ and NMHCs are removed from the air stream by cryogenic trapping. For this purpose two ultra-efficient metal Russian Doll traps (RDT) with a yield of more than 99.95% per RDT for the removal of $CO_2$ and $N_2O$ (overall yield >99.999) [Brenninkmeijer, 1991] are connected in series with an U-tube between them. The RDT are stainless steel cylin-

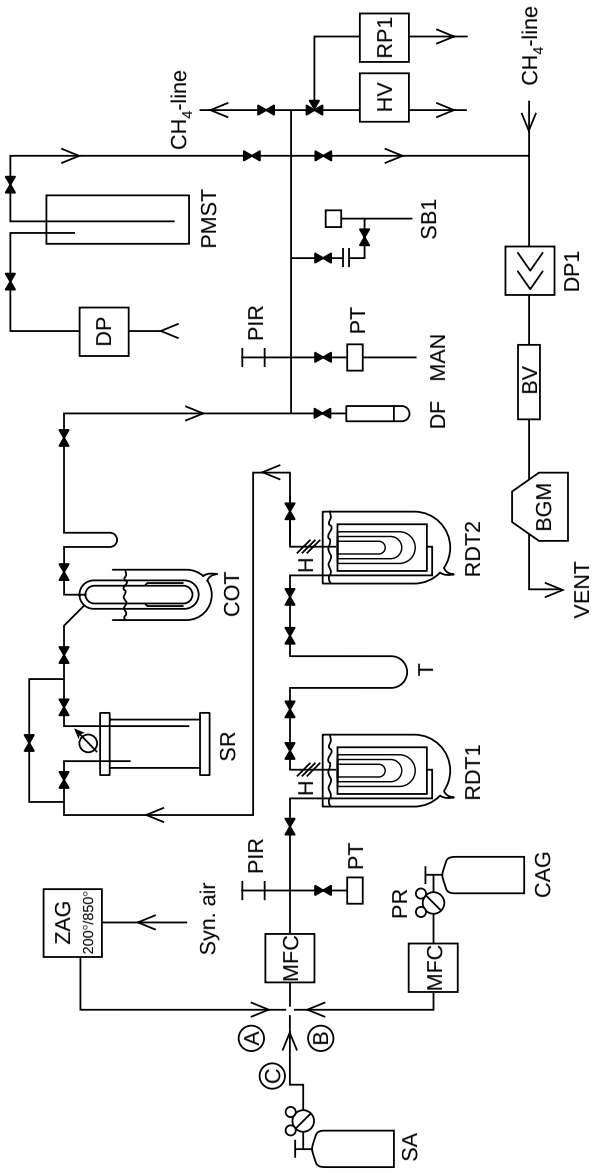


**Figure 2.4:** The CO and $CO_2$ extraction system. A, B and C indicate the inlets of zero-air, calibration gas (CAG) and air sample respectively. BGM: Bellow gas meter; BV: Buffer volume; COT: Collection trap (glass RDT); DF: Drying finger containing $P_2O_5$; MAN: Manometer; DP and DP1: Diaphragm pump; HV: High vacuum pump; MFC: Thermal sensor mass flow controller with integrator; PIR: Pirani vacuum gauge; PMST: Purge molecular sieve trap; PT: piezoresistive absolute pressure transducer; RDT: Cryogenic metal Russian Doll trap with thermocouple based heater elements (H); RP1: Rotary pump; SA: Air sample cylinder with pressure regulator (PR); SB1: Sample bottle; SR: Schütze reactor; T: U-tube; ZAG: Generator of zero air (Pt catalyst heated to 200 °C (850 °C) for CO ($CH_4$) free air).

ders incorporating three concentric borosilicate glass fiber thimbles and metal bellow tubes (Cajon) as inlet and outlet. When submerged in liquid nitrogen, sheathed thermocouples, which are wrapped around the outlet bellows, are used as heater elements, to prevent excessive cooling of the outlet valves. The U-tube makes it possible to recover the trapped $CO_2$ (and $N_2O$) quantitatively from the first RDT.

Subsequently the sample air passes through a Schütze reactor (stainless steel reactor of 1 l volume filled with 0.8 l of Schütze reagent) in which the important oxidation step from CO to $CO_2$ takes place. Schütze reagent is $I_2O_5$ acidified with sulfiric acid on a silica gel support [Schütze, 1949] and allows the quantitative conversion of CO into $CO_2$. It is prepared according to [Smiley, 1965] by loading dry silicagel with an aqueous solution of $I_2O_5$ (Merck). After drying, the white material is impregnated with concentrated $H_2SO_4$ and finally activated by driving out the water under a flow of synthetic air (MG, 5.0) at a temperature of near 220 °C. Accurate temperature control is essential during the activation. The oxidation has shown to be most efficient when the final reagent is of a bright yellow color. The exact oxidation mechanism is not known, but various iodic acids are assumed to be active. It is imperative to keep the material dry because hydrolysis is rapid. The Schütze reactor is sealed-off with underpressure ($\sim 10^{-2}$ hPa) when not in use. The reagent granules rest on a glass fiber disc supported by a perforated stainless steel disc. Glass wool at the inlet and outlet prevent the contamination of the extraction line with dust from the reagent. The reactor is kept at room temperature.

The small quantity of CO derived $CO_2$ is trapped at liquid nitrogen temperature in a succeeding glass collection trap (COT) [Brenninkmeijer & Röckmann, 1996]. The $CO_2$ glass collection trap differs in design from the metal traps and has only two concentric glass fiber thimbles. This number has shown to be the optimum for efficient trapping and realizing of µmol quantities of $CO_2$. It also has a heat exchange section which reduces the consumption of liquid nitrogen and a subsequent U-tube which facilitates the quantitative transfer of the $CO_2$ from the trap. From here, the air passes either through the diaphragm pump DP1 and the gasmeter when $CH_4$ isotopes are not analyzed, or is pumped through the methane extraction section. Pressure is held below 200 hPa within the entire system to prevent liquefaction of $O_2$.

After processing of the air sample, first the CO derived $CO_2$ is transferred from the glass COT through the U-tube into a drying finger (containing $P_2O_5$). This drying agent is very effective and does not lead to isotopic exchange of the oxygen of the $CO_2$, which is important for the isotopic analysis. The quantity of $CO_2$ formed is measured volumetrically. The manometer consists of a volume isolated

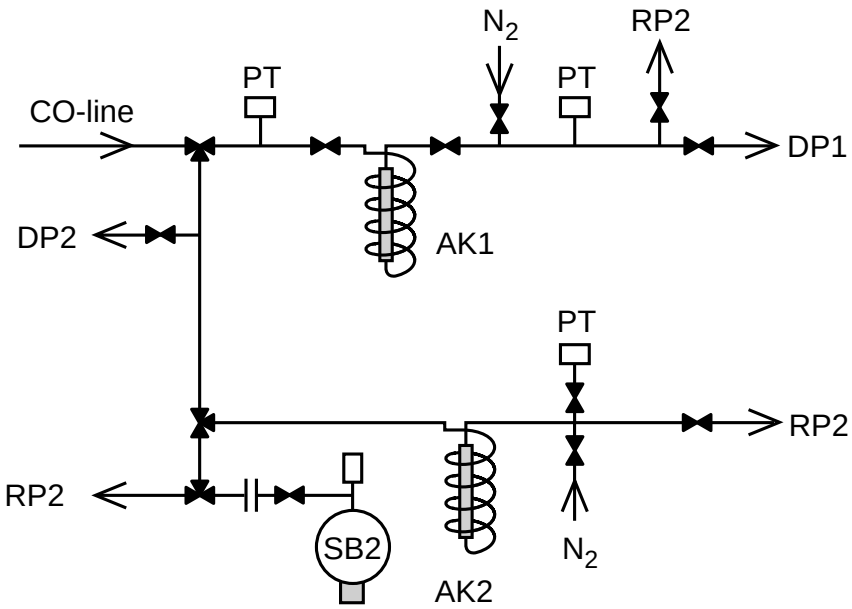


**Figure 2.5:** The extraction system for $CH_4$. AK(1&2): Activated charcoals; DP(1&2): Diaphragm pumps; $N_2$: Nitrogen inlet; PT: Piezoresistive absolute pressure transducer; RP2: Rotary pump; SB2: Sample bottle with septum.

glass valve [Brenninkmeijer & Louwers, 1985] and is equipped with a small piezo-resistive absolute semiconductor pressure transducer (IGNS, Model 9401). The small total volume of only 0.915 $cm^3$ improves the pressure level and therefore the obtained resolution. Finally the $CO_2$ is transferred into a small sample bottle (SB1). A high vacuum pump (HV, Pfeiffer molecular drag pump) is used together with a rotary pump (RP1) as a fore pump in order to reach pressure of less than 1 hPa prior to the transfer of the CO derived $CO_2$ sample.

### 2.3.2 The $CH_4$ extraction system

After extracting CO, $CH_4$ can be extracted by passing the air stream through the $CH_4$ extraction line (Figure 2.5). The main components of the $CH_4$ extraction system are two activated charcoal traps (AK1 and AK2), which allow the enrichment of $CH_4$ from air samples by a factor of 1000.

The first trap AK1, which is kept at liquid nitrogen temperature (77 K), contains 277 g of granular activated charcoal which quantitatively absorbs $CH_4$. Desorption of $CH_4$ from the activated charcoal trap is achieved by heating it to 100 °C. During the desorbtion process the gases are directed through a second small activated charcoal trap (AK2, 75 g) which is also kept at 77 K. Subsequent desorption of $CH_4$ from

this small trap occurs rapidly at room temperature (see section 2.4.4). By using this second charcoal trap a $CH_4$ pre-concentration to about 3000 nmol/mol is attained. The enriched $CH_4$ sample is transferred with a $N_2$ flow from the second charcoal trap into a sample bottle (SB2). This $CH_4$ sample bottle has a volume of $\sim$ 300 ml and is equipped with a septum that allows the extraction of some gas for $CH_4$ mixing ratio measurements. Special care has been taken to ensure safety on the methane extraction system. The Russian Doll Traps on the CO side as well as the activated charcoals are cooled with liquid nitrogen for more than an hour. In case of leakage this may lead to liquification of air, which will boil off rapidly when the liquid nitrogen is removed. A safety pressure relief valve (RV), similar to the one at the inlet of the CO line, has been installed at the outlet of the first activated charcoal. The second activated charcoal is connected to PVC tubes via Cajons, which would disconnect in case of high pressure.

### 2.3.3 The $CH_4$ combustion system

One third of the pre-concentrated $CH_4$ sample is introduced into a separate $CH_4$ combustion line (Figure 2.6) via a MFC. Oxygen is admixed via another MFC and the gas mixture is directed through a platinum catalyst heated to 800 °C (platinized quartz wool, Shimadzu Europe, Duisburg, Germany) for the quantitative conversion of $CH_4$ into $CO_2$:

$$CH_4 + 2O_2 \rightarrow CO_2 + 2H_2O \tag{2.1}$$

The resulting $H_2O$ and $CO_2$ are trapped in two subsequent glass RDTs, the first held at 195 K (ethanol cooled with liquid nitrogen) and the second at 77 K. The subsequent processing of the $CH_4$ derived $CO_2$ is the same as described above for the CO derived $CO_2$. In order to remove small amounts of CO arising from the activated charcoal an additional trap, consisting of Schütze reagent and Ascarite, was inserted into the inlet of the combustion line between the MFC and the catalyst. This modification was introduced in February 1998, and small $\delta^{13}C$ corrections are applied for all samples processed before this date (see section 2.6).

## 2.4 The extraction procedure

The extraction procedure for air samples depends on the trace gases that are analyzed. In this section we describe the full procedure to extract CO and $CH_4$ from the air sample. This procedure can also be used to extract $CO_2$ and $N_2O$ for subsequent analysis. In a first step samples are pumped through the CO and $CH_4$ extraction lines (section 2.4.1). After this the CO derived $CO_2$ (section 2.4.2) and also $CO_2$

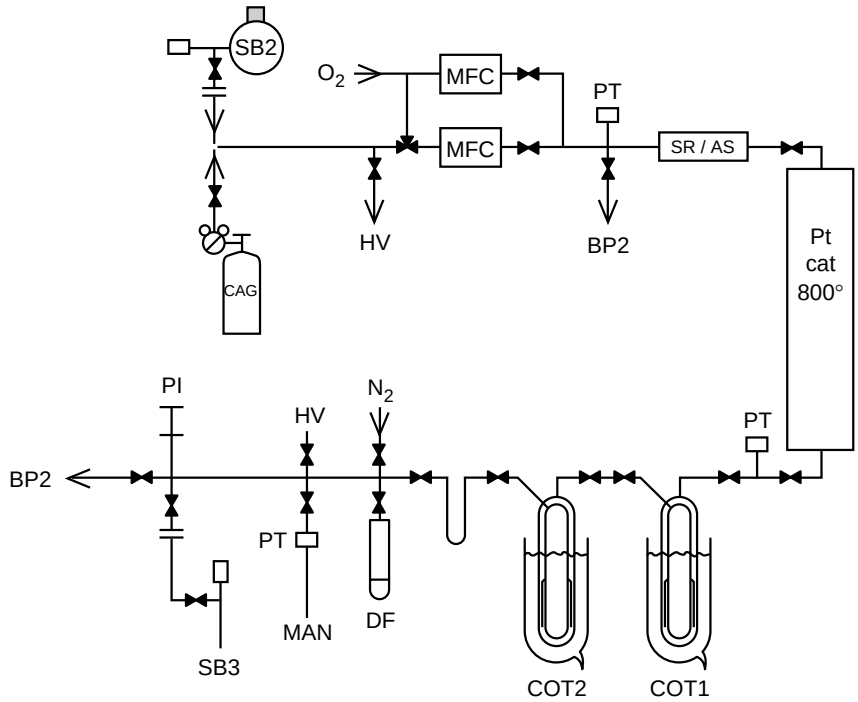


**Figure 2.6:** The combustion system for $CH_4$. CAG: Calibration gas; COT(1&2): Collection traps (glass RDT); DF: Drying finger containing $P_2O_5$; BP2: Diaphragm pump; HV: High vacuum pump; MAN: Manometer; MFC: Thermal mass flow controller; PI: Piezoresistive absolute pressure transducer; Pt cat: Platinum catalyst; SB2: Sample bottle with septum; SB3: Sample bottle; SR/AS: Schütze/ ascerite reagent.

and $N_2O$ (section 2.4.3) can be recovered and measured on the mass spectrometer. To measure the stable $CH_4$ isotopes, $\delta^{13}C$ and $\delta D$, two further steps are necessary, described in sections 2.4.4 and 2.4.5 respectively.

When not in use, the CO system is back-flushed with laboratory air that has been cleaned by pumping it through a large bed of purge molecular sieve trap (PMST). This back-flushing process removes the condensable compounds trapped in the Russian doll traps. The Schütze reagent is kept sealed-off at 100 hPa. The $CH_4$ extraction line is filled with $N_2$ and kept slightly overpressurized ($\sim$ 1100 hPa) in order to avoid the contamination of the activated charcoal. The $CH_4$ combustion system is kept evacuated with the Pt catalyst shut down and sealed-off.

### 2.4.1 Processing of the air sample

The sample cylinder is fitted with a pressure regulator which is flushed several times. The sample cylinder is then connected to the extraction line. Back-flushing is ter-

minated, the inlet valve closed and the CO line evacuated via the diaphragm pump (Vacubrand, type MZ4, several extra o-rings were used for improved sealing). At 10 (hPa) the line is sealed-off and the pressure is monitored to identify any leakage of the CO line before processing sample air. Then the first metal RDT is submerged in liquid nitrogen and 2 min later sample air is let into the line with an initial flow rate of 1.5 $\mathrm{Lmin}^{-1}$ and pumped away using the diaphragm pump again. The system pressure is close to 50 mbar under those conditions. Then the second RDT is cooled with liquid nitrogen and the system is flushed for 6 min. The appropriate trap heaters are switched on. Next, the air is shunted through the Schütze reactor and the bypass is then closed. The entire line is now flushed again for 10 min. This procedure consumes 30 l of the sample air. Subsequently the collection trap is cooled, and the heater activated. After one minute the glass fiber thimbles have reached low enough temperatures and the collection commences. At this point the integrator of the flow controller is initialized, and the gas meter readings are recorded.

If methane is processed, then the $CH_4$ extraction line (Figure 2.5) has previously been evacuated via the rotary pump (RP1). This is done after connecting a new sample bottle with a new septum. All 3-way valves are open during the evacuation process of the entire $CH_4$ line. After a minimum pumping time of 10 min the upper part of the $CH_4$ extraction line is sealed-off while the second activated charcoal and the sample bottle are still evacuated with the rotary pump. A leakage test is done by checking if pressure stays constant in the upper part. Subsequently the first activated charcoal is cooled with liquid nitrogen for 10 min before air processing through the $CH_4$ extraction line can start. After 2 min of collecting sample air on the CO line, the sample cylinder is closed again and the collection glass COT is sealed-off by closing the valve behind the Schütze reactor and the one for the diaphragm pump (DP1). The integrator of the flow controller and the gas meter readings are again recorded. The connection to the $CH_4$ extraction line is now opened and pressure drops when the air expands into the cooled activated charcoal (AK1). The valve behind the Schütze reactor and the sample cylinder is opened again and the re-established air stream increases the pressure in the line. Once it reaches 30 hPa the diaphragm pump (DP1) it starts pumping the air away from behind the activated charcoal.

The flow is increased to 5 $\mathrm{Lmin}^{-1}$ and all three heaters turned to maximum. The pressure in the system increases to 200 hPa in the CO line and is significantly lower (110 hPa) after the sample air has passed the activated charcoal. The pressure is kept as high as possible to maximize the residence time of CO molecules in the Schütze reactor, but has to be low enough to prevent freezing out oxygen. Still 10-20 l(STP) of air oxygen is trapped in the cooled activated charcoal under these conditions.

In general samples with 350 to 800 l of air are processed, which results in collecting times ranging from 1 to 3 h. During this time several readings of temperature, pressure, gas meter and integrator values are made and the liquid nitrogen of the different collection traps is refilled. The processing of sample air is stopped after a definite amount of air has been processed or the pressure in the sample cylinder falls below 5 hPA. The sample air flow is then reduced with the mass flow controller to 1.5 $\mathrm{l\,min^{-1}}$ and stopped altogether after another minute. Pumping is also terminated at that moment and all heaters are switched off. The CO line is separated from the $CH_4$ extraction line by closing the valve between both systems. On the $CH_4$ side the activated charcoal is now pumped with the rotary pump (RP2) that first has to be sealed from the lower part of the $CH_4$ extraction line, where it has up to now evacuated the second activated charcoal and the sample bottle.

### 2.4.2 Transfer of the CO derived $CO_2$ sample

On the CO side, the valve at the inlet of the collection trap is closed, the bypass opened and the Schütze reactor isolated. Next, the valve to the high vacuum pumping stage is opened and the collection trap evacuated until pressure gets below $10^{-3}$ hPa on the Pirani pressure sensor (for at least 8 min). Thereafter, the U-tube is submerged in liquid nitrogen, its outlet valve closed and the large dewar surrounding the collection trap removed. During 5 min the sample $CO_2$ is distilled into the U-tube. Next, the outlet valve is opened again and the U-tube evacuated for 8 min. During this procedure the trapped $CO_2$ on the two concentric glass fiber thimbles of the collection trap is completely released. From the U-tube, the CO derived $CO_2$ is distilled into a small finger containing some $P_2O_5$ that removes traces of water. From the drying tube the $CO_2$ is transferred into the manometer. After establishing pressure (typically 20 to 60 hPa) and temperature, the sample is trapped in a small sample bottle for transfer to the mass spectrometer.

### 2.4.3 Transfer of the $CO_2$ sample

For selected samples the $CO_2$ trapped in the first Russian Doll trap is recovered for isotopic analysis. This is done after the transfer of the CO derived $CO_2$ sample is finished and the high vacuum pump (HV) can be used for the evacuation of the whole CO extraction line. Due to the flow resistance of the collection traps, it takes up to 10 min for pressure to drop below 4 hPa at the outlet of the first RDT. Once the U-tube between the two RDTs is cooled with liquid nitrogen the Dewar is removed from the first trap. During 35 min the transfer of $CO_2$ and $N_2O$ can be observed by first rising and than falling pressure levels at the outlet of the warming RDT1. We

continue to pump with the high vacuum pump at the end of the CO line. Before $H_2O$ also starts to desorb, we seal-off the U-tube by closing the valves at the in and outlet. The trapped $CO_2$ and $N_2O$ can subsequently be used for isotopic analysis.

### 2.4.4 Transfer of the $CH_4$ sample

On the $CH_4$ extraction line (Figure 2.5) the methane sample is now transferred from the first activated charcoal AK1 to the second activated charcoal AK2. When the pressure over AK1 has dropped below 1 hPa we start the transfer procedure. Any leakage over AK2 and the sample bottle is checked by controlling the pressure in the sealed-off lower part of the extraction line. Next, AK2 is cooled with liquid nitrogen. The dewar is removed from AK1 and during exactly 4 min the released gases from the no longer cooled first activated charcoal are pumped away. This process increases the pre-concentration of the $CH_4$ sample once more.

Afterwards the outlet valve to the rotary pump (RP2) is closed and the two charcoals are now linked via the 3-way valve. At the same time the valve at the outlet of the second activated charcoal is opened so that the rotary pump is now pumping the trapped air from AK1 through AK2. For the quantitative desorption of the $CH_4$ AK1 is heated to 100 °C for 1 h. Temperature is critical during this time, as beyond 100 °C the activated charcoal produces $CO_2$. However, even at 100 °C the charcoal releases considerably amounts of CO (1 to 2 µmol/mol in the final $CH_4$ sample bottle, see section 2.6.2). After 1 h both activated charcoals are flushed for 10 min with $N_2$ (MG, 5.0) which is introduced from behind AK1 while the rotary pump at the outlet of AK2 is still pumping. This is done in order to transfer the remaining $CH_4$ from AK1 to AK2. Once the flushing with $N_2$ is stopped, the activated charcoals are evacuated until the pressure is below 1 hPa before pumping is stopped altogether. With the help of the lower 3-way valve we separate the upper part of the extraction line and connect AK2 with the still closed sample bottle (SB2).

Similar to the procedure for AK1 we pump for exactly 3 min at the outlet of AK2 once the liquid nitrogen is removed from AK2. The pumping time of 4 and 3 min for AK1 and AK2 respectively has been checked by taking small air samples from behind the activated charcoals during those pumping processes and analyzing their $CH_4$ content. The desorbtion of $CH_4$ only starts at least 30 sec after these pumping times. After 3 min the pumping is stopped and the sample bottle opened. During the following 10 min $CH_4$ desorbs from AK2 (which is heated with an water-bath at room-temperature) and expands into the 300 ml sample bottle. Subsequently a $N_2$ flow is used to transfer remaining gases from AK2 into the sample bottle and to store the sample sligthly overpressurized ($\sim$ 1100 hPa). Pressure and temperature

are recorded for yield calculation.

In order to desorb both activated charcoals completely before they are used for new samples, we heat them for 1 h at 200 °C while they are flushed with $N_2$. They cool down to room-temperature while still being flushed and are then put under overpressure.

### 2.4.5 $CH_4$ combustion

Most of the samples are now transferred to the $CH_4$ combustion line, where approximatively one third of the enriched $CH_4$ sample is used for $\delta^{13}C$ analysis. The remaining gas is used for $\delta D$ analysis by tunable diode laser spectroscopy (see section 2.7). In case of low $CH_4$ abundance this order is reversed, e.g. for the firn samples reported in chapter 5. In this case samples are first analyzed on the MISOS system, recovered after the measurement procedure and then processed on the $CH_4$ combustion line.

The platinum catalyst from the $CH_4$ combustion line is heated to 800 °C and evacuated with the high vacuum pump (HV) while the inlet valve of the reactor is still closed. Once pressure stabilizes at less than $10^{-4}$ hPa this part of the system is sealed-off. Now the first part of the combustion line, from the sample bottle to the closed inlet of the reactor, is evacuated with the HV pump. Mainly due to the Schütze/ascarite trap which needs low amounts of humidity on the ascarite side, pressure does not drop below $10^{-4}$ hPa. Once pressure stabilizes, we close the valve towards the HV pump and the valve at the outlet of the mass flow controller (MFC) and open the sample bottle. Temperature and pressure between sample bottle and MFC are again recorded. The valve at the inlet of the reactor is opened and the first collection trap (COT1) is cooled down to 195 K (ethanol-bath with added liquid nitrogen). We start with flushing the combustion line with $O_2$ (MG, 5.0) for 2 min. For this purpose the valve at the outlet of the MFC on the $O_2$-side is opened and the mass flow controller regulated to 100 sccm. The valve towards the diaphragm pump (DP2) is opened once the pressure in the system is above 20 hPa. Now the second collection trap (COT2) is cooled with liquid nitrogen and the system flushed for an additional 2 min in order to wait for the glass fiber thimbles on both collection traps COT1 and COT2 to be cool enough for the caption of $H_2O$ and $CO_2$.

The enriched methane sample is now added to the $O_2$-stream by opening the valve at the outlet of the corresponding MFC, which is also regulated to 100 sccm. Traces of CO and $CO_2$ are removed by the Schütze/ascarite trap (SR/AS) and only the $CH_4$ is quantitatively converted to $CO_2$ in the Pt-catalyst-reactor. The valve behind the MFC on the sample side is closed once sufficient $CH_4$ has been processed

(app. 300 ml $CO_2$). Pressure between sample bottle and MFC is again recorded (for subsequent volumetric calculation of the $CH_4$ mixing ratio of the original air sample and thus the corresponding extraction yield). The system continuous to be flushed for another 2 min with $O_2$. We switch from the diaphragm pump to the HV pump to evacuate the system below $10^{-3}$ hPa. The reactor is then sealed-off and the transfer of the $CH_4$ derived $CO_2$ from the second collection trap to the final sample bottle (SB3) is identical to the transfer of the CO derived $CO_2$ described above in section 2.3.1. As typical sample sizes range from 280 to 350 ml $CO_2$ the calibration volume is with 1.0898 ml not as small as the corresponding calibration volume on the CO side.

## 2.5 Determination of CO mixing ratios

The extraction of CO allows the calculation of the absolute CO mixing ratio of an air sample. This calculation is based on the volume of CO derived $CO_2$ that has been recovered in the manometer and the volume of dry air processed. In this section, we address both steps: the determination of the quantity of processed air and the volumetric determination of the CO derived $CO_2$. Finally we document the achieved CO yields from calibration runs.

### 2.5.1 Determination of the quantity of air

The quantity of processed air is measured at the inlet of the extraction line with the integrator of the mass flow controller and at the outlet of the diaphragm pump DP1 with the gas meter. The quantity of air measured by the gas meter is equal to the processed air,
(1) if there is no leak between the inlet of the line and the gas meter at the end of the line,
(2) if there is no loss of air apart from the extracted trace gases and
(3) if we can correct for the expansion of air due to temperature changes.
The absence of leaks can be checked by observing the gas meter readings while the diaphragm pump runs under vacuum. Concerning point (2), it turned out that 10 to 20 l of air are trapped in addition to $CH_4$ on the first activated charcoal when samples are processed through the whole extraction line. Because no systematic correction for the amount of trapped air could be established, we rely for those air samples on the integrating electronic mass flow controller. Calibration of the MFC against a gas burette led to a constant correction of +1%. In addition, the ratio between both air quantity measurements have been recorded for samples which have only been

processed on the CO line. It has remained constant at 1.004±0.004 (n=84) since measurements started in 1996, thus no further correction is applied for the readings of the MFC.

The integrating electronic mass flow controller directly gives air quantities normalized to STP, while gas meter readings are corrected afterwards for temperature and pressure. Concerning problem (3), this has been analyzed in great detail for another CO extraction line (ACO-line) which does not include a further $CH_4$ extraction part and is otherwise identical to the one used during this thesis. Results are documented in [Brenninkmeijer et al., 2000]. If the weight of the sample cylinders is taken with an electronic balance before and after processing air on the ACO-line, then the measurement of the amount of air processed is found to be linear and precise within an 0.1% range. Similar tests on the BCO line have shown that results from the integrating electronic mass flow controller and an electronic balance were within a 1% range.

### 2.5.2 Volumetric determination of $CO_2$

More difficult is the accurate determination of the small amount of the CO derived and recovered $CO_2$. For this the volume of the manometer, the pressure, and the temperature have to be known accurately.

In the range from 0 to 200 hPA the electronic pressure transducer has a resolution of 0.01 hPA (0.1 hPA in the atmospheric pressure range). The reading of the gauge is regularly compared to the reading of an extremely stable atmospheric pressure gauge (Paroscientific, Digiquartz 740) which has a resolution of 0.001 hPA. The standard deviation for the difference in pressure readings over a period of one year amounts to only 0.1 hPA and the linearity of the pressure sensor is better than 0.1%. The volume of the manometer was established using a calibrated volume to be $903.0 \pm 1$ $\mu$l. The largest random error is introduced by the temperature measurement, which is read from an thermometer attached not far from the manometer. We discuss in the next section how completely the small amount of CO derived $CO_2$ is recovered for the accurate determination of the CO content of the air sample.

### 2.5.3 CO yield calibration

CO calibration runs are done regularly (on average after every 4 samples), during which isotopically known CO is injected into a flow of zero air. The frequent calibration runs allow to establish the effect of the Schütze reagent on the oxygen isotopic composition of the $CO_2$ produced. The CO calibration results concerning $\delta^{13}C$ and

$\delta^{18}O$ will be discussed in detail in section 2.6.1. In addition to this isotopic information, the yield of a calibration run allows the quantification of the amount of recovered CO derived $CO_2$ relative to the processed air. By injecting not only isotopically known CO, but also a known amount of CO, we expect to recover the same amount as $CO_2$ at the end of the extraction process.

It is essential that the zero air used for calibration runs is free of CO (in section 2.6.2 the same applies to $CH_4$). The ultrapure zero air (Linde or Messer Griessheim) used was found to have blank CO mixing ratios of up to 20 nmol/mol. Since these quantities would add a significant contamination to the final gas mixture, the zero air was first directed through a heated reactor that contained Pt on aluminum-oxide catalyst (Merck), operated at 200 °C. This purification reduced the CO mixing ratios to levels below 0.1 nmol/mol for flow rates of 5 $\mathrm{l\,min^{-1}}$. When only purified zero air is processed, one still recovers small amounts of condensables, presumably $CO_2$ and $SO_2$. Those 0.5±0.3 $\mu$l of condensables are subtracted from the quantity obtained from a normal air sample. For air samples containing 50 to 200 nmol/mol CO, of which 400 l of air is processed, the uncertainty in the blank correction introduces an uncertainty of 0.5 % to 0.1 % respectively.

During calibration runs, CO is not injected as pure CO gas, but as a mixture of 269±3 $\mu$mol/mol CO in nitrogen gas. The use of a reference gas mixture with such high mixing ratio has the advantage that the ~0.25 l of CO stored in one cylinder is suitable for many sample preparations. On the other hand, it is of course crucial to test the line with gas mixtures which have a CO mixing ratio close to ambient air. Therefore, the reference gas mixture is diluted dynamically into a flow of zero air with the ratio of mass flows adjusted so that the final mixture entering the extraction line has a mixing ratio of about 200 nmol/mol. For this purpose an additional thermal mass flow controller (Hastings HFC-202A) is used on the reference gas side and calibrated from time to time against a gas burette.

Based on 30 calibration runs on the BCO line since August 1998 with this calibration mixture, the yield of the CO extraction system is 99.8±1.3 %. Before August 1998 the MFC for the reference gas has not been calibrated and yields were slightly lower (99.3±2.1 %). Calibration runs done with the first Schütze reagent until July 1997 had an average yield of only 95.2 ± 2.4 %. Air samples analyzed during this period were corrected by +5%.

In Figure 2.7 the long term distribution for calibration runs are shown. The near 100 % yield of the calibration runs proves independently that the quantity of CO can be determined with a precision of about 1 %.

The precision of our CO mixing ratios can also be inferred from measurements

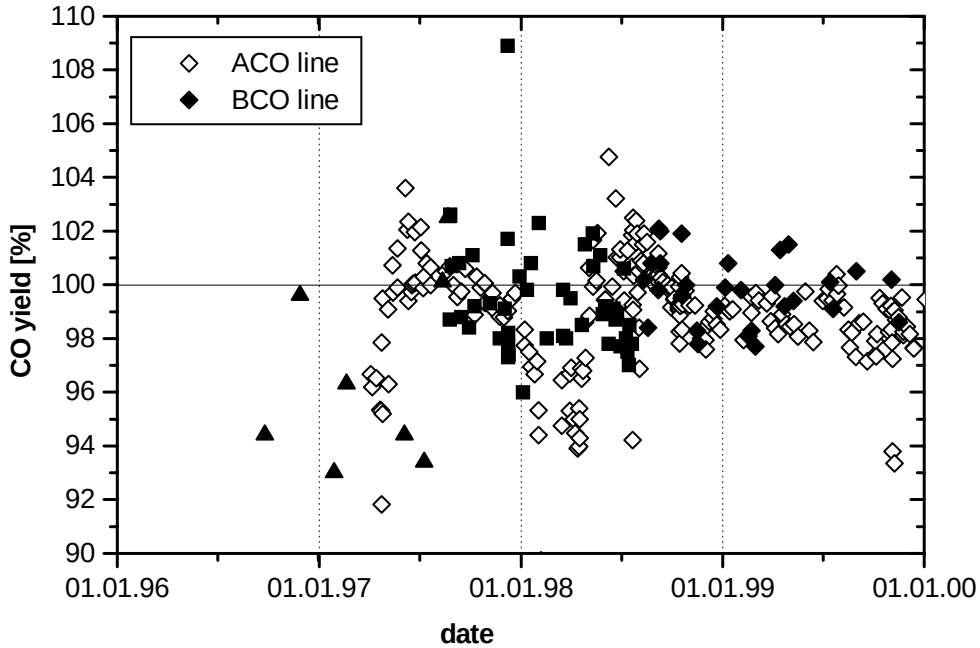


**Figure 2.7:** CO calibration runs of both CO extraction systems (ACO and BCO). For the BCO line we differentiate between three periods: the first Schütze reagent (solid triangle), the second Schütze reagent (solid square) and the new MFC calibration (solid diamonds).

done on duplicate samples (see section 2.1.4). They are a measure of the overall precision of our sampling, storage and analysis procedure. For 24 duplicates both sample cylinders have been measured on the BCO line and the standard deviation calculated for the duplicates was 2.3 nmol/mol. 15 duplicate samples were analyzed on both lines and for this subset of air samples the standard deviation for CO mixing ratios was also 2.3 nmol/mol (see Table 2.2).

## 2.6 Isotope ratio mass spectrometry (IRMS)

The measurements of the stable isotope composition of the CO and $CH_4$ derived $CO_2$ samples are performed on a dual inlet, eight collector, isotope ratio mass spectrometer (IRMS, Finnigan MAT 252). The $CO_2$ sample is analyzed for its masses 44, 45 and 46. Mass 45 includes $^{13}C^{16}O_2$ and $^{12}C^{17}O^{16}O$, for which the simultaneous determination of $^{12}C^{16}O^{16}O$ is used [Craig, 1957]. This is only possible for molecules with mass dependent fractionation. This is the case for the $CH_4$ derived $CO_2$ measurements. The isotopic composition of CO exhibits, however, mass independent fractionation with regard to $\delta^{18}O$ [Röckmann et al., 1998c] that also affects the $\delta^{13}C$

IRMS measurements [Röckmann & Brenninkmeijer, 1998b](see section 1.8.1). For the quantities of CO derived $CO_2$ (down to 20 $\mu$l) the MS is equipped with two microvolumes (for $CO_2$ and $O_2$). The $CH_4$ derived $CO_2$ samples of normally 200 to 500 $\mu$l are done by bellow measurements.

Our working standard (MG-$CO_2$, Messer Griesheim ultrapure $CO_2$) was calibrated against NBS-19 and assigned a $\delta^{13}C$ value of $-42.465$ ‰ V-PDB [Röckmann, 1998]. This value is close to the $\delta$ value of atmospheric methane ($\sim -47$ ‰), where precision has to be highest, and reasonably close to CO ($-26$ ‰ to $-32$ ‰). For $\delta^{18}O$ a value of $-29.058$ ‰ V-PDB has been assigned.

We regularly measured a separate aliquot of MG-$CO_2$ gas (stored in glass vessels) against the MG-$CO_2$ working standard in order to check the long-term stability of the MS measurements. This was usually done after filling the standard side with new reference gas and when $CH_4$ derived $CO_2$ samples were measured. Figure 2.8 shows that long-term drifts in $\delta^{13}C$ for this aliquot were less than 0.01 ‰ and the $1\sigma$ standard deviation over the whole 3-year measurement period was $\pm 0.02$ ‰ (n=140). For $\delta^{18}O$ the measurements exhibit a drift of less than 0.02 ‰ and the $1\sigma$ standard deviation has been $\pm 0.05$ ‰. Deviations of more than 0.05 ‰ and 0.15 ‰ have been measured for $\delta^{13}C$ and $\delta^{18}O$ respectively, when previous to the $CO_2$ measurements $O_2$ or $N_2O$ measurements had been performed. In Figure 2.8 these samples were labeled as outliers.

### 2.6.1 $\delta^{13}C$ and $\delta^{18}O$ calibration of CO

The calibration runs described in section 2.5.3 give information about the $^{13}C/^{12}C$ ratio, which for $\delta^{13}C$ of the formed $CO_2$ should match that of the CO injected. During the oxidation process from CO to $CO_2$ discussed in section 2.3.1, solely one oxygen atom is added to the CO molecule, while neither isotopic exchange occurs for CO, nor for the formed $CO_2$ [Stevens & Krout, 1972], [Brenninkmeijer, 1993], [Brenninkmeijer & Röckmann, 1997]. Thus, by using CO of known isotopic composition, the effect of the oxidation can be corrected for $\delta^{18}O$. Figures 2.9 and 2.10 show the long-term development of $\delta^{13}C$ and $\delta^{18}O$ for the reference gas which has been used on the two CO extraction systems ACO and BCO. In section 4 $\delta^{13}C$ and $\delta^{18}O$ measurements of atmospheric CO are presented that have been measured on both extraction lines. It is therefore essential that the final stable isotope CO data is reported relative to a coherent reference scale. In addition, atmospheric samples have also been divided for subsequent analysis on both lines. In the following two sections we document the applied $\delta^{13}C$ and $\delta^{18}O$ correction that allow the direct comparison of stable isotope CO measurements from both extraction lines.

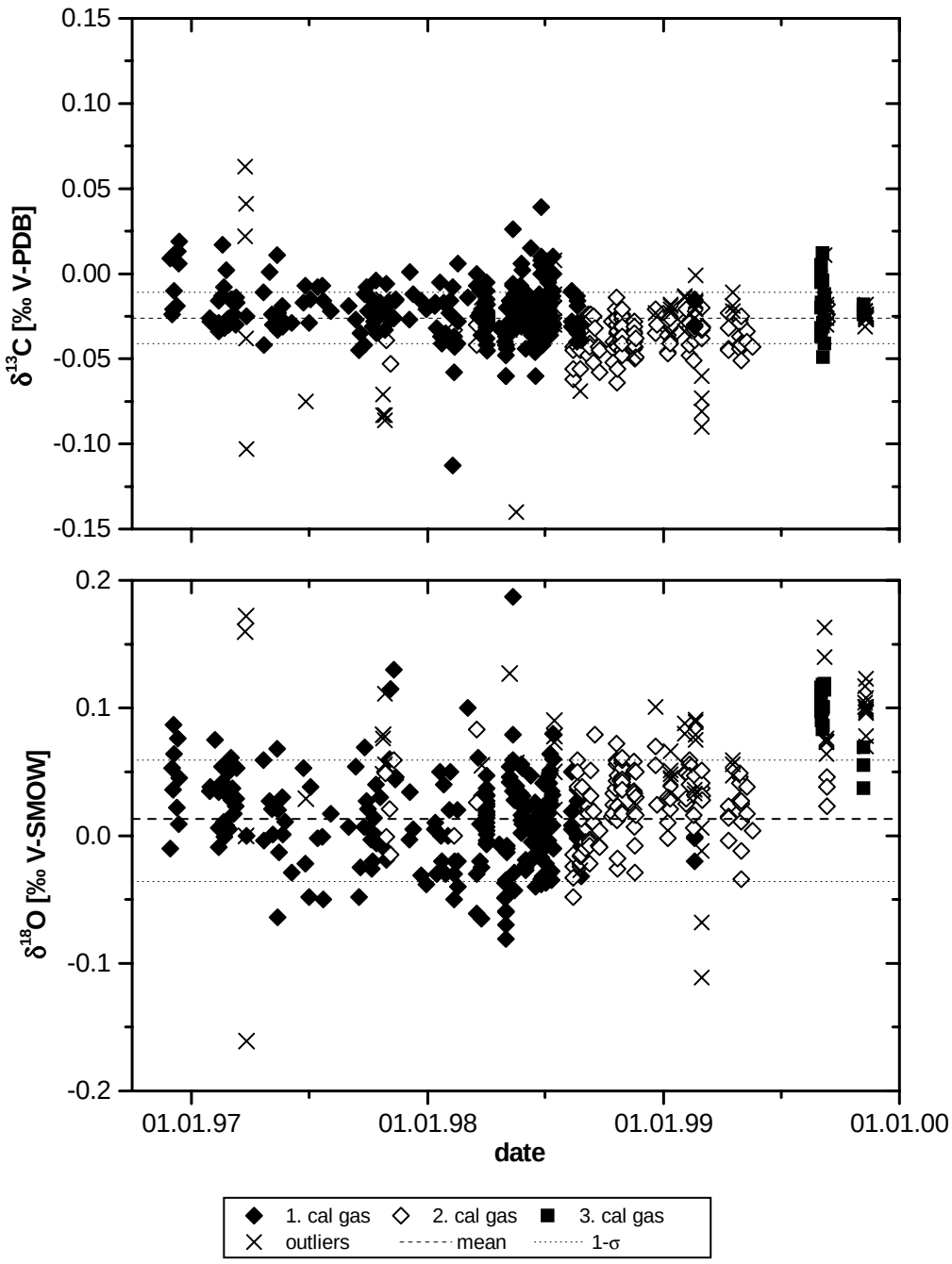


**Figure 2.8:** Measurements of (a) $\delta^{13}$C and (b) $\delta^{18}$O of a MG-$CO_2$ calibration gas aliquot versus the MS working standard MG-$CO_2$.

### Corrections for $\delta^{13}$C CO measurements

Over the considered 3.5 year period from July 1996 to December 1999 the $\delta^{13}$C CO calibration (Figure 2.9) have varied around $-43.99 \pm 0.19$ ‰ (n=84) and $-44.01 \pm$

0.22 ‰ (n=277) for the two CO extraction lines BCO and ACO respectively. Apart from two periods (Aug 1997 to Feb 1998 and May 1998 to Aug 1998) the $\delta^{13}$C calibration of both extraction lines agree well within their error specification.

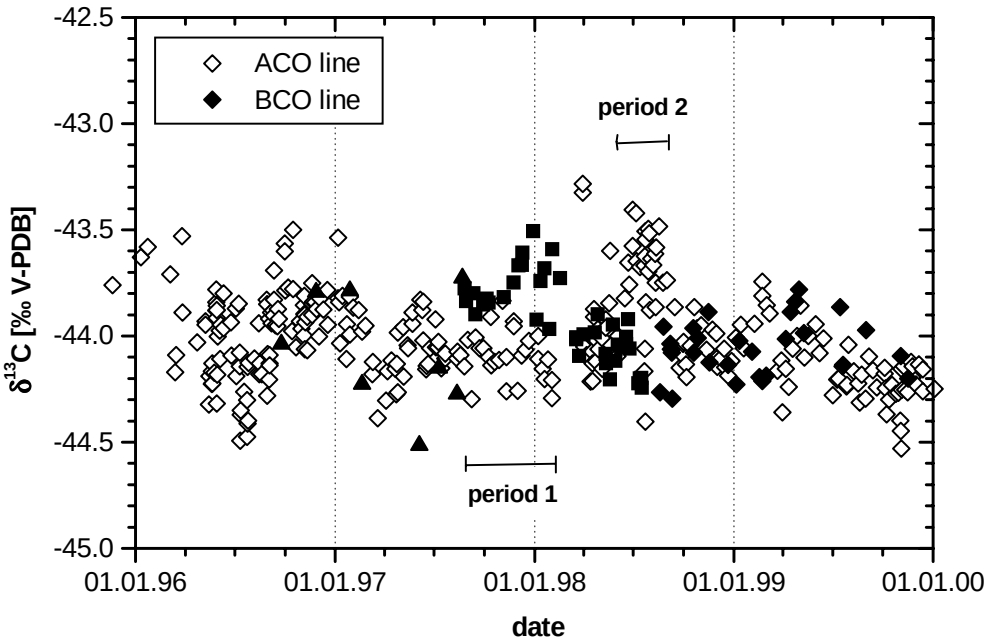


**Figure 2.9:** $\delta^{13}$C calibration runs of both CO extraction systems (ACO and BCO). For the BCO line we differentiate between: the first Schütze reagent (solid triangle), the second Schütze reagent (solid square) and the new MFC calibration (solid diamonds). Period 1 and 2 indicate the time periods for which samples are corrected in $\delta^{13}$C .

For the first period (period 1 in Figure 2.9) the CO measurements of the BCO line are considered to be 0.2 ‰ enriched compared to the average mean of −44 ‰. The final $\delta^{13}$C values of atmospheric air samples measured in this period on the BCO line are shifted by 0.2 ‰. For the ACO line a similar correction of 0.2 ‰ applies for atmospheric air samples measured between May and August 1998 (period 2 in Figure 2.9). $\delta^{13}$C calibration during this period have been too heavy compared to the average mean. To which extend a shift in $\delta^{13}$C from calibration runs can be directly translated to air samples is not clear. The calibration runs are more sensitive to contamination because of the differences of nearly 20 ‰ in the $\delta^{13}$C value.

Direct intercomparison between both extraction lines by measuring stable CO isotopes on the same cylinder have only been carried out in periods directly after those with differences in the calibration runs. In Table 2.2 they are listed (ACO+BCO) together with selected air samples from Izaña. This subset of 14 air samples consists of

| | CO [nmol/mol] | $\delta^{13}C$ [‰] | $\delta^{18}O$ [‰] | n |
|---|---|---|---|---|
| ACO + BCO | 4.0 | 0.26 | 0.59 | 3 |
| Duplicate ACO/BCO | 2.1 | 0.17 | 0.44 | 14 |
| Duplicate BCO/BCO | 2.3 | 0.23 | 0.40 | 24 |

**Table 2.2:** Direct intercomparison of both CO extraction systems, ACO and BCO. Standard deviations are given for duplicate samples and for samples analyzed on both lines.

duplicate continuous samples of which one has been measured on the BCO extraction system for the analysis of CO and $CH_4$ isotopes while the second has been analyzed on the ACO extraction system for CO isotopes only (duplicate ACO/BCO). With the applied correction factors from above those samples agree within 0.17‰. We compare the results from samples measured on both lines to duplicate samples only measured on the BCO line (duplicate BCO/BCO).

Important changes on the BCO system have been the replacement of the original Schütze reagent by a new batch in August 1997 and the readjustments of pumping times in the extraction procedure. Previous to August 1997, the pumping after the transfer from the collection trap to the U-tube was too short. Table 2.3 shows how the CO yield, as well as the standard deviation for a single $\delta^{13}C$ and $\delta^{18}O$ measurement have improved subsequently.

| | CO yield [%] | $\delta^{13}C$ [‰] | $\delta^{18}O$ [‰] | n |
|---|---|---|---|---|
| 1.Schütze (until Jul 97) | 95.2±2.4 | $-44.07 \pm 0.28$ | $-15.12 \pm 0.23$ | 8 |
| 2.Schütze (Aug 97 - Aug 98) | 99.3±2.1 | $-43.92 \pm 0.19$ | $-14.94 \pm 0.13$ | 46 |
| MFC cal. (since Aug 98) | 99.8±1.3 | $-44.06 \pm 0.13$ | $-14.86 \pm 0.19$ | 29 |

**Table 2.3:** CO calibration runs of the BCO line. CO yield, $\delta^{13}C$ and $\delta^{18}O$ values are given for the first Schütze, the second Schütze and for the additional calibration of the MFC.

### Corrections for $\delta^{18}O$ CO measurements

The isotopic analysis of air samples is performed on the CO derived $CO_2$. Thus regular $\delta^{18}O$ calibration runs are essential in order to retrieve the original oxygen isotopic composition of CO. With the help of the $\delta^{18}O$ value of the CO which is used in the calibration runs and the measured $\delta^{18}O$ of the CO derived $CO_2$, the $\delta^{18}O$ value of the Schütze reagent can be established. Subsequently the $\delta^{18}O$ value of air samples can be obtained by correcting for the added oxygen atom in the oxidation process (see equation 2.4). First the reaction

$$CO + I_2O_5 \rightarrow CO_2 \tag{2.2}$$

leads to an equation for the $\delta$ values [Brenninkmeijer, 1993]:

$$\delta_{CO} + \delta_{I_2O_5} = 2 * \delta_{CO_2} \tag{2.3}$$

with $\delta_{CO}$ : initial $\delta$ value of CO;

$\delta_{I_2O_5}$ : $\delta$ value of the Schütze reagent and

$\delta_{CO_2}$ : $\delta$ value of the CO derived $CO_2$.

By using equation 2.3 for sample and standard we can finally derive equation 2.4 which relates the initial $\delta^{18}O$ value of the CO sample to the $\delta^{18}O$ value of the corresponding calibration run:

$$^{SA}\delta_{CO} = 2 *^{SA} \delta_{CO_2} - (2 *^{CAL} \delta_{CO_2} -^{CAL} \delta_{CO}) \tag{2.4}$$

with $^{SA}\delta$ : $\delta$ value of the sample and

$^{CAL}\delta$ : $\delta$ value of the calibration gas.

The isotopic composition of the calibration gas ($^{CAL}\delta_{CO}$) has been established according to [Brenninkmeijer, 1993] and is given in Table 2.3. The $\delta^{18}O$ value has been confirmed by independent measurements using the conversion of known $CO_2$ to CO on activated charcoal [Röckmann, 1998a].

In Figure 2.10 the $\delta^{18}O$ calibration values for the two extraction lines are shown. The observed $\delta^{18}O$ variation of the calibration gas can be significant, because of changes in the isotopic composition of the Schütze reagent. Equation 2.4 not only allows the correction for direct intercomparison of $\delta^{18}O$ values for samples measured on different extraction systems but also for statistical variation as well as long term drifts of the two systems. For the $^{CAL}\delta_{CO_2}$ used in equation 2.4, the moving average over the previous and following 10 calibration runs is used in order to take into account the long term drift and the uncertainty of the single measurement.

On the ACO extraction system the Schütze reagent was changed in April 1997 because the CO yield dropped significantly (see Figure 2.7). After the exchange of

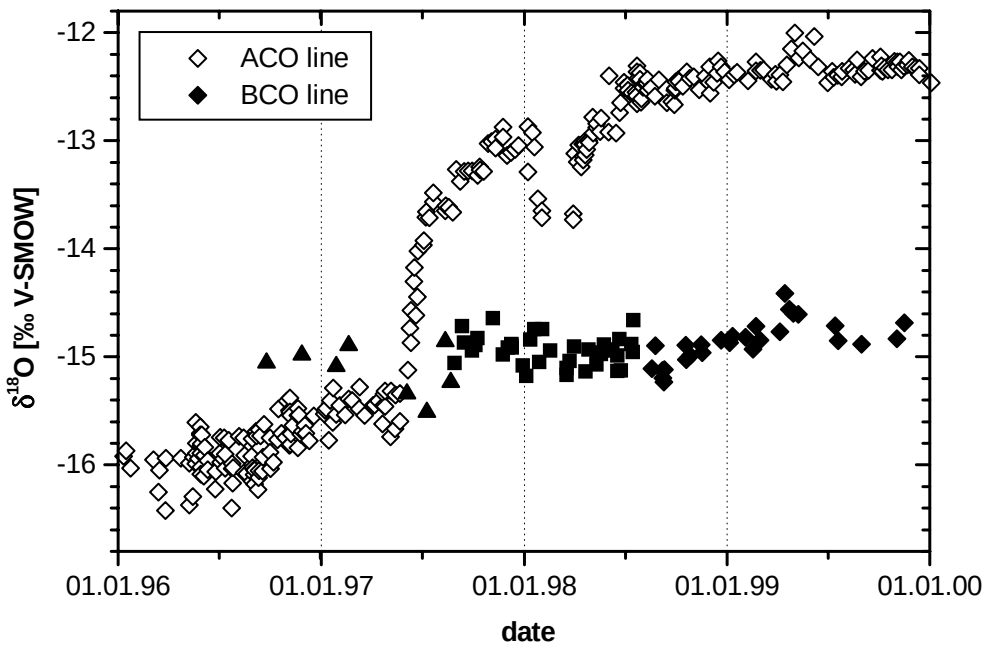


**Figure 2.10:** $\delta^{18}O$ calibration runs of both CO extraction systems (ACO and BCO). For the BCO line we differentiate between: the first Schütze reagent (solid triangle), the second Schütze reagent (solid square) and the new MFC calibration (solid diamonds).

the Schütze reagent the $\delta^{18}O$ displayed a large drift towards heavier values. The Schütze was therefore exchanged again in March 1998. The observed change in $\delta^{18}O$ shows that the isotopic composition of the Schütze reagent can vary from batch to batch. The $\delta^{18}O$ standard deviation calculated for duplicate samples processed on the two extraction systems, ACO and BCO, is 0.44 ‰ (Table 2.2).

### 2.6.2 $\delta^{13}C$ calibration of $CH_4$

The performance of the $CH_4$ extraction line was checked using the $CH_4$ reference gases EG-95 [Marik, 1998] and EG-96. Several dilutions of these gases in ultrapure $N_2$ were produced, resulting in final $CH_4$ mixing ratios of ~1000 to 4000 $\mu$mol/mol (see Table 2.4).

The use of these high concentration reference gas mixtures has the advantage, that the amount of $CH_4$ stored in one individual cylinder is suitable for numerous (~100) sample preparations. It is, however, crucial to test the line with gas mixtures which have a $CH_4$ concentration close to ambient air. Similar to the procedure with the CO calibration runs (2.6.1) the reference gas mixture is diluted dynamically into a

| | EG95-V2 | EG95-V3 | EG96-V1 |
|---|---|---|---|
| $CH_4$ [nmol/mol] | 834 | 1157 | 1171 |
| $\delta^{13}C$ [‰]: direct combustion (without Schütze) | $-50.55 \pm 0.05$ (n=33) | $-50.48 \pm 0.10$ (n=6) | $-51.17 \pm 0.02$ (n=30) |
| $\delta^{13}C$ [‰]: direct combustion (with Schütze) | $-50.60 \pm 0.01$ (n=8) | $-50.58 \pm 0.02$ (n=60) | |
| $\delta^{13}C$ [‰]: complete extraction (without Schütze) | $-50.42 \pm 0.05$ (n=12) | | |
| $\delta^{13}C$ [‰]: complete extraction (with Schütze) | $-50.7 \pm 0.05$ (n=6) | $-50.54 \pm 0.03$ (n=12) | $-51.11 \pm 0.02$ (n=11) |
| $\delta D$ [‰]: complete extraction | $-205.5 \pm 1.5$ (n=11) | $-204.7 \pm 1.7$ (n=9) | $-206.2 \pm 1.1$ (n=9) |
| $\delta D$ [‰]: direct TDL | | | $-205.7 \pm 0.9$ (n=3) |

**Table 2.4:** $\delta^{13}C$ and $\delta D$ calibration runs for different $CH_4$ reference gases with standard deviations and the number of calibration runs (n).

flow of zero air with the ratio of mass flows adjusted so that the final mixture entering the extraction line has a mixing ratio of about 2 µmol/mol. Again, the ultrapure zero air (Linde, Messer Griessheim) used was found to have blank $CH_4$ mixing ratios of, typically, several nmol/mol. Since these quantities added a significant contamination to the final gas mixture, the zero air was first directed through the Pt catalyst reactor, that operated at 850 °C for $CH_4$ calibration. This purification reduced the $CH_4$ mixing ratios to levels well below 1 nmol/mol, i.e. resulting in a final contamination of less than 0.05 %. In addition to these 'whole extractions' of the dynamically diluted calibration gas mixtures, also direct injections of the EG95/96-Vx mixtures into the combustion line were regularly performed ('direct combustion').

One important improvement in the $\delta^{13}C$ measurements of methane has been the introduction of a Schütze/Ascarite trap in the combustion line (section 2.3.2) in August 98. Prior to this a significant $\delta^{13}C$ offset between direct combustion runs and whole extractions for $\delta^{13}C$ of 0.12±0.07 ‰ was observed (see Table 2.4 and Figure

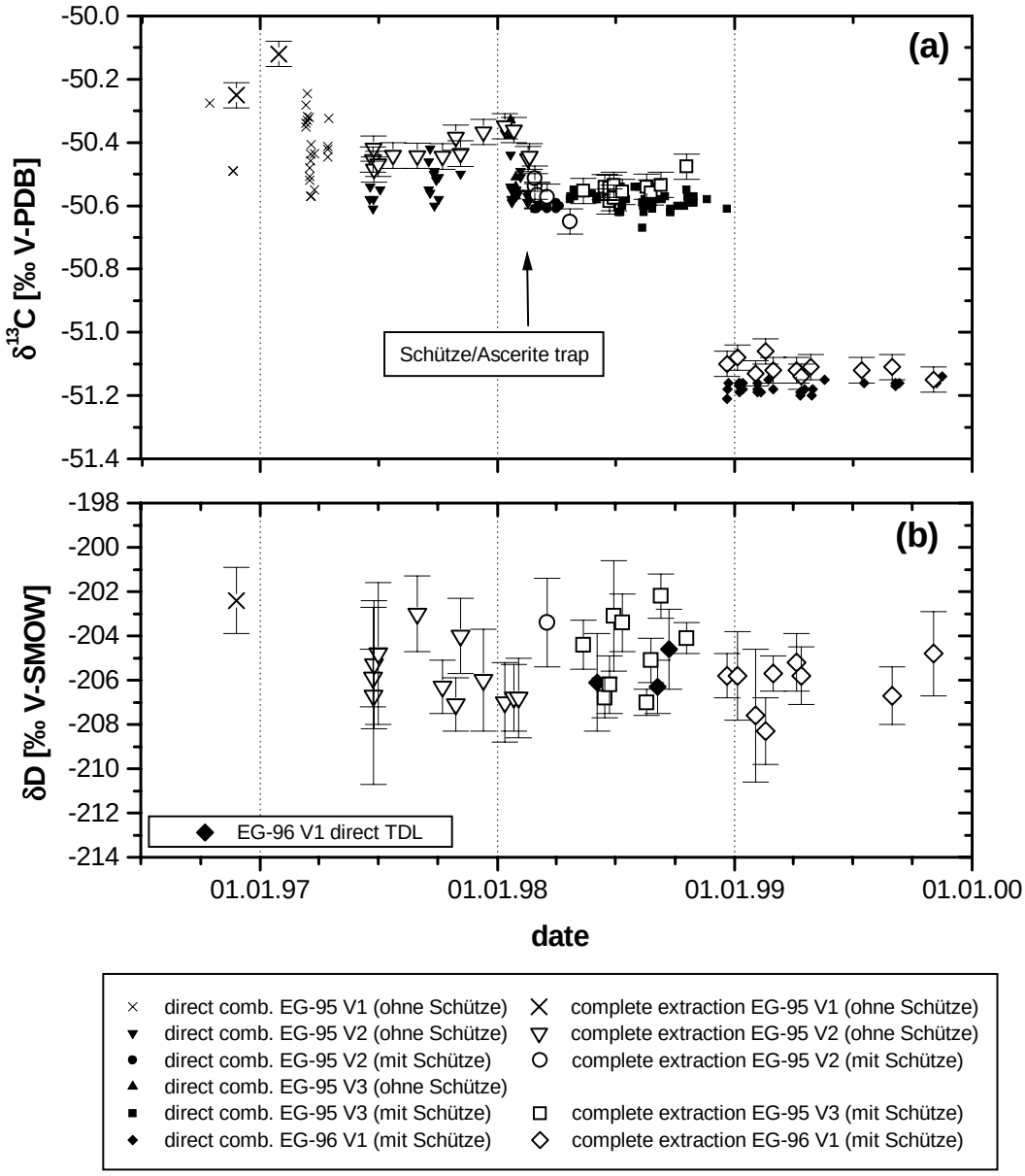


**Figure 2.11:** $\delta^{13}$C and δD calibration runs for $CH_4$ reference gases (as listed in Table 2.4).

2.11). This offset was attributed to a small amount of CO produced in the activated charcoal. Since the amount of contamination was obviously relatively constant, the complete extractions showed nevertheless a rather good reproducibility (EG95-V2: $-50.41 \pm 0.04$ ‰). After inserting the Schütze/ascarite trap, this offset became significantly smaller (0.03 - 0.04 ‰). Also the $\delta^{13}$C results for the direct combustion runs shifted slightly and their precision significantly improved, a behavior which is not fully understood. The difference in $\delta^{13}$C of the whole extraction calibration was applied to correct all $\delta^{13}$C data of samples processed without the trap. Although

the precision of the whole extraction calibration runs does not show a significant difference prior and after inserting the trap, we assume a larger uncertainty for all samples processed prior to this modification. We assign $\delta^{13}$C uncertainties of ±0.08 ‰ and ± 0.04 ‰ for the samples prior and after inserting the trap respectively. The mean deviation between measurements of duplicate continuous samples changed from ±0.041 ‰ to ±0.026 ‰ after the trap has been inserted.

## 2.7 Methane Isotopomer Spectrometer (MISOS)

Tunable diode laser spectroscopy is usually employed in atmospheric sciences as a highly selective and sensitive technique for in situ measurement of trace gases [Reid & Labrie, 1978]. A new tunable diode laser based Methane ISOtopomer Spectrometer (MISOS) has been developed by Bergamaschi et al. [1994], which allows δD measurements of atmospheric methane. The instrument makes use of the difference in the rotational-vibrational transitions and the corresponding infrared spectra for the different $CH_4$ isotopomers.

Many small molecules in the atmosphere, such as methane, have sharp absorption lines from rotational-vibrational transitions. At low pressure, the linewidth is limited by the Doppler shift of the individual molecules and the lines do not overlap. By adjusting the diode laser temperature via its current, the laser output can be produced at a single frequency, which can be scanned continuously over bandwidths of several $cm^{-1}$ in the mid infrared region. Multipass absorption cells allow absorption paths of $\sim$ 100 m.

The development of the MISOS system and its application to δD measurements of $CH_4$ have been extensively documented in [Bergamaschi et al., 1994] and [Saueressig, 1999]. In the following section we only briefly summarize the main steps of δD $CH_4$ measurements. In section 2.7.2 the calibration of our reference gases for atmospheric $CH_4$ measurements reported in this thesis is documented.

### 2.7.1 Methane δD measurements

For the measurement of δD the absorption lines for $^{12}CH_4$ and $^{12}CH_3D$ must have approximately the same intensity. To compensate for the ratio of mixing ratios $^{12}CH_3D/^{12}CH_4$ that is close to $6 * 10^{-4}$ the intensity of the $^{12}CH_3D$ line has to be up to $\sim$ 1500 times higher than that of the $^{12}CH_4$ line. Therefore the line pair chosen for δD measurements is at 3044.289 $cm^{-1}$ and 3044.170 $cm^{-1}$ for $^{12}CH_3D$ and $^{12}CH_4$ respectively.

The tunable diode laser is scanned over the spectral region of interest and the ab-

sorption spectra are recorded simultaneously for the sample and a working reference gas. The low variation in the ratio of the isotopomers can only be separated when the absorbtion of each species is high enough. Therefore the sample gas is introduced into an evacuated multipass reflection cell (White cell, volume 6.8 liter, base length 1 m [Roths, 1992]), while the working reference gas is in a 1 m reference cell. Optical path length of up to 126 m can be achieved and thus the minimum mixing ratio of the pre-concentrated $CH_4$ samples has to be $\sim 1500\,\mu$mol. The reference cell is put directly on top of the White cell, and both enclosed in a common, thermally insulated housing. Measurements are made at 30 hPa total pressure and room temperature. Multiple linear regression procedures are carried out online, comparing the $^{12}CH_3D$ and the $^{12}CH_4$ absorptions in the two optical channels. The precision of individual δD measurements with the MISOS instrument may vary slightly and individual errors are calculated for each measurement, considering the stability of the instrument during the actual measurement series.

### 2.7.2 δD calibration of $CH_4$

The working reference gas, CAL-3, was produced as a mixture of our reference gas REF (99.995 % $CH_4$, δD = −164.4 ‰ V-SMOW) with pure (∼99 %) $CH_3D$, resulting in a final δD value of −84.5 ‰ V-SMOW. In order to scale δD deviations of samples from the CAL-3 gas correctly, also the REF gas is measured within each measurement series.

Since the δD of the CAL-3 gas is very close to the atmospheric samples, the potential error in the scaling factor is almost negligible. The δD precision of the MISOS instrument is ±0.5 − ±1 ‰, and the overall accuracy including sample preparation is estimated to be around ±1 ‰. The mean deviation between duplicate continuous samples is ±0.9 ‰. Note, however, that no international standards so far exist for δD in $CH_4$. Our δD scale is based on measurements of our standards REF, and CAL-1 at the Bundesanstalt für Geowissenschaften und Rohstoffe, Hannover, using $CH_4$ combustion to $CO_2$ and $H_2O$, followed by reduction of $H_2O$ to $H_2$ and subsequent IRMS analysis on $H_2$ [Bergamaschi et al., 1994] [Dumke et al., 1989]. The calibration was against the IAEA water standards V-SMOW and V-SLAP. Since this common procedure only calibrates the δD measurement on $H_2O$ and since in particular the conversion of $CH_4$ into $H_2O$ may be subject to some $H_2O$ contamination, significant differences in the δD-$CH_4$ scale among different IRMS laboratories may arise [Marik, 1998]. Thus some uncertainty remains about the absolute δD-$CH_4$ scale, but the δD scale used for our MISOS measurements (including our previous studies on $CH_4$ sources and sinks) is considered to be internally consistent.

## 2.8 Accelerator Mass Spectrometry (AMS)

Accelerator Mass Spectrometry (AMS) is widely used for radiocarbon dating but can also be used for the determination of the ultra-rare atmospheric trace gas $^{14}CO$. Part of the European Project CO-OH-EUROPA has been the collaboration of three AMS facilities for the regular analysis of atmospheric $^{14}CO$ at several sampling stations (see Table 3.1).

- Centre for Isotope Research (CIR), University of Groningen, Netherlands
- Vienna Environmental Research Accelerator (VERA), University of Vienna, Austria
- University of Uppsala, Sweden

In addition some of the $^{14}CO$ data shown in section 4 have been analyzed at AMS facilities in Lower Hut, New Zealand and in Kiel (Leibniz Laboratory), Germany.

Following the conversion and extraction process, the CO derived $CO_2$ sample is recovered from the IRMS after the stable isotopic analysis. The samples are diluted with $^{14}C$-free $CO_2$ to increase the sample size to about 1 mg $CO_2$ and subsequently reduced to graphite. The graphite targets are then processed on the AMS. The dilution of the samples is carried out at the MPI in Mainz, while the graphitization is part of the $^{14}CO$ measurement procedure of the AMS facilities. A short description of the dilution procedure is given in the next section. Section 2.8.2 describes the main features of the AMS facilities. Finally in section 2.8.3 we describe in detail how we convert the pmC values of the different AMS facilities into a consistent $^{14}CO$ data set reported in molecules $cm^{-3}$ air at STP.

### 2.8.1 Dilution

The specific activity of atmospheric $^{14}CO$ of up to 900 pmC is high compared to the activity of ~100 pmC usually encountered for radiocarbon dating (for which the AMS facilities are optimized). For stratospheric samples even $^{14}CO$ values of more than 3000 pmC can be reached. Thus the dilution of the CO derived $CO_2$ sample by a factor of 5 to 30 with $^{14}C$-free $CO_2$ is done previous to AMS analysis.

The CO derived $CO_2$ samples of 10-100 µl are often stored after the IRMS measurement at low temperature. The dilution procedure is done on a separate dilution line. We start the dilution process by drying each sample with $P_2O_5$ to remove $H_2O$. Subsequently the sample is transferred into a calibration volume (0.75 ml), sealed and the exact pressure is recorded. The pressure is measured with a piezoresistive

pressure transducer and range between 30 and 200 hPa. Afterwards, the sample is transferred back into its sample bottle. We then flush the dilution line several times with the $CO_2$-free dilution gas MG-$CO_2$. The next step consists of sealing the MG-$CO_2$ gas in the calibration volume at a pressure close to 900 hPa. Finally we add this quantity of MG-$CO_2$ gas to the sample. The mixture is subsequently transferred into a break seal sample bottle in which the diluted sample is send to the AMS facility.

The pressure ratios between the sample and the dilution gas in the calibration volume is called the dilution factor $\alpha$ (see equation 2.5). Its accuracy will directly determine the precision of the final $^{14}$CO concentration. Therefore the calibration of the pressure transducer and its linearity over the whole pressure range of 10-1000 hPa is important. We assume an error of 0.3-1% in the dilution process.

### 2.8.2 AMS measurements

Prior to the AMS analysis the $CO_2$ samples are reduced to graphite. The reduction takes place in an excess of purified hydrogen, using Fe powder at typically 580 °C as a catalyst:

$$CO_2 + 2H_2 \quad \overset{(Fe,\,580\,^\circ C)}{\leftrightarrow} \quad C + 2H_2O$$

The water from the reduction process is cryogenically trapped. The resulting carbon-catalyst mixture is pressed into copper or aluminum target holders for the AMS analysis, in which the $^{14}$C/C ratios of the graphite samples are measured [Wallace et al., 1987], [Rom, 2000a].

The Accelerator Mass Spectrometry is basically a sequence of two large mass spectrometers with an accelerator for the destruction of molecular isobars in between. Thus the carbon isotopes $^{12}$C,$^{13}$C and $^{14}$C are separated by their different masses and counted directly. There are several variations amongst the different AMS systems for $^{14}$C, but the main are [Rom et al., 1998] and [Wijma et al., 1998]:

- Negative-ion source: This produces isobars from $^{14}$N (as nitrogen does not produce negative ions)
- (Van de Graaff or Pelletron) Tandem accelerator with an Ar gas stripper operated at ∼+3 MV for $^{14}C^{3+}$ (sometimes a foil stripper is used)
- High energy mass spectrometer
- Detector for the rare isotope

- Computer-control system with data acquisition

The pmC$_S$ value of the diluted $CO_2$ sample we get from the AMS facilities is measured relative to a solid IAEA standard material (C-6 sucrose, C-3 cellulose) and is corrected for the accelerator blank. These corrections are specific to each AMS facility and its graphitization procedure and vary among the different accelerators.

### 2.8.3 Derivation of the final $^{14}$CO data

In order to obtain the $^{14}$CO concentrations, we need the $^{14}C/^{12}C$ ratio reported from the AMS laboratories, the CO mixing ratio of the sampled air and the dilution factor for the CO derived $CO_2$ sample [Rom et al., 2000b]. This ratio is measured relative to a standard with known $^{14}C/^{12}C$ ratio and is reported in percent Modern Carbon (pmC). Because of its origin from archeological dating, a normalization to $\delta^{13}C = -25\,‰$ is applied to correct for fractionation effects in the carbon isotope composition. Because we are only interested in the $^{14}C/^{12}C$ ratio, this normalization is, however, not meaningful in the case of atmospheric CO sample.

The first step is to converted the measured pmC$_S$ values to $^{14}C/^{12}C$ ratios. Depending on the definition of pmC used by the different accelerators, the activity of the sample is either given relative to the present activity of the standard, or relative to the "absolute" activity of the standard in 1950. This results in constant or time-dependent pmC values respectively, because of the activity of the sample decreasing in pace with the standard or relative to the absolute standard from 1950. In equation 2.5 we use the first pmC definition and therefore correct for the time elapsed since 1950.

For absolute atmospheric $^{14}$CO concentration at standard conditions (STP) first the pmC value of the diluted sample has to be transformed into a non-$\delta^{13}C$-corrected $^{14}C/^{12}C$ ratio:

$$^{14}R_S(x,t) = \frac{pmC_S}{100} \cdot \frac{(1+\delta^{13}C_S/1000)^2}{(1-25/1000)^2} \cdot {}^{14}R_{std} \cdot e^{-\lambda(t-1950)} \cdot e^{\lambda(t-x)} \qquad (2.5)$$

with $^{14}R_S(x,t)$ : $^{14}C/^{12}C$ ratio of the diluted sample (sampled in year $x$ and analyzed in year $t$)

pmC$_S$ : specific activity of the diluted sample (from the AMS)

$\delta^{13}C_S$ : $\delta^{13}C$ value of the diluted sample

$^{14}R_{std} = 1.189 \times 10^{-12}$ : $^{14}C/^{12}C$ ratio of an absolute international standard

$\lambda = ln2/5730\,yr^{-1}$ : decay constant of $^{14}C$

The next step is to deduce the activity of the original, undiluted air sample from the activity of the target. The dilution gas (pure $CO_2$, Messer-Griesheim,

Mainz) was supposed to be free of radiocarbon. Blank tests of this gas have been carried out at three of the AMS facilities and a pmC value of ~0.5% was measured. With equation 2.5 the resulting activity for the dilution gas ($\delta^{13}$C =−42.465 ‰) is $^{14}R_{dil} = 5.686 \times 10^{-15}$. Thus the original conversion from the activity of the diluted gas to the one of the original undiluted gas has changed from

$$\begin{aligned} {}^{14}R_{COs} &= {}^{14}R_S \cdot (\alpha + 1) \qquad \text{to} \\ {}^{14}R_{COs} &= ({}^{14}R_S - {}^{14}R_{dil}) \cdot (\alpha + 1) + {}^{14}R_{dil} \end{aligned} \tag{2.6}$$

with $^{14}R_{COs}$ : $^{14}C/^{12}C$ ratio of the original (undiluted) air sample,

$^{14}R_{dil}$ : $^{14}C/^{12}C$ ratio of the diluting gas (MG-$CO_2$) and

$\alpha = p_{Dil}/p_{Sam}$ : dilution ratio (pressure ratio of the undiluted sample and the dilution gas)

The final step is to obtain the $^{14}$CO concentration from the activity of the original sample.

$$[^{14}CO]_s = {}^{14}R_{COs} \cdot [CO]_s \cdot \frac{[^{12}CO]}{[^{14}CO] + [^{13}CO]} \cdot L^* \tag{2.7}$$

with $[^{14}\mathrm{CO}]_s$ : final $^{14}$CO concentration [molecules cm$^{-3}$ (STP)],

$[\mathrm{CO}]_s$ : CO mixing ratio of the original air sample [ nmol/mol ],

$[^{12}\mathrm{CO}]\cdot([^{14}\mathrm{CO}]+[^{13}\mathrm{CO}])^{-1} \cong 0.989$ : constant within 0.5 ‰ and

$\mathrm{L}^* = 2.6868 \times 10^{10}$ cm$^{-3}$: modified Loschmidt constant.

We assume an overall uncertainty for the $^{14}$CO measurement of maximal 3%. This includes errors arising from the dilution, the graphitization process and the precision of the final AMS measurement of ~ 1% each.

## 2.9 Summary of the different analytical precisions

The different analytical procedures for measuring CO and $CH_4$ mixing and isotope ratios have been documented in this chapter. Table 2.5 gives an overview of the numbers of samples processed during this thesis and the analytical precision we attribute to each measurement.

| | | |
|---|---|---|
| CO | mixing ratio | ±3 nmol/mol |
| | $\delta^{13}C$ | ±0.3 ‰ |
| | $\delta^{18}O$ | ±0.4 ‰ |
| | n | 370 |
| $CH_4$ | mixing ratio | ±2 nmol/mol |
| | $\delta^{13}C$ | ±0.08 ‰ before Aug 1998 |
| | | ±0.04 ‰ after Aug 1998 |
| | $\delta D$ | ±1 ‰ |
| | n | 520 |

**Table 2.5:** Summary of the different analytical precision of CO and $CH_4$ mixing and isotope ratios and the number of samples processed during this thesis (n).

# Chapter 3

# Seasonal cycles of atmospheric $CH_4$

In the following two chapters we report measurements of atmospheric $CH_4$ and CO mixing ratios and their isotopic composition at the baseline air Global Atmospheric Watch (GAW) station Izaña. The measurements have been carried out as part of the European $^{14}$CO-OH-Europe Project, for which mainly CO and its stable isotopes together with $^{14}$CO have been investigated at several stations (listed in Table 3.1). Sampling at Izaña started in late 1996 and nearly three annual cycles can now be interpreted in terms of seasonal cycles, synoptic scale variability and consequences for the methane and carbon monoxide budgets.

Here we report the first measured $\delta$D seasonality for atmospheric background $CH_4$, which was measured with the MISOS system. We also report measurements of $CH_4$ mixing ratios and $\delta^{13}$C at Izaña. To support the analysis also $SF_6$ mixing ratios are provided. Finally we summarize the results from an inverse model study by Bergamaschi et al. [2000a] which uses our Izaña records together with $\delta^{13}$C records from five other globally distributed stations.

## 3.1 GAW station Izaña, Tenerife

The Global Atmospheric Watch (GAW) station Izaña is located on Tenerife (28° N, 16° W), one of the Canary Islands, about 400 km west of the African coast. The station complex is located on a mountain plateau at 2370 m above sea level (Figure 3.1). A characteristic meteorological feature is the existence of a trade wind inversion, which usually shields the observatory from emissions on the island. Between January 1996 and October 1997, the station was above at least one inversion layer on 86 % of all nights [Schaefer, 1998]. During the summer months (June to August) this

| | country | location | altitude [m a.s.l.] | sampling period | |
|---|---|---|---|---|---|
| Izaña | Tenerife Spain | 28° N 16° W | 2370 | Mai 96- | Spanish Meteorological Service |
| Mt. Sonnblick | Austria | 47° N 13° E | 3106 | Sep 96- | Institute for Meteorology, Salzburg |
| Schauinsland | Germany | 48° N 8° E | 1205 | 95 | Umwelt Bundesamt Schauinsland |
| Kollumerwaard | Netherlands | 53° N 6° E | 0 | 97- | University of Groningen |
| Spitsbergen | Norway | 79° N 12° W | 474 | Mar 96- | Norwegian Institute for Air Research |
| Alert | Canada | 82° N 62° W | 210 | Jul 96 -Dec 98 | Atmospheric Environment Service |
| Happo | Japan | 36° N 137° E | 1840 | Feb 97- | University of Tokyo |
| Kaashido | Male | 5° N 73.5° E | 0 | Sep 98 | Kaashido Observatory |

**Table 3.1:** Sampling stations

percentage increased to 100 %, while it is lowest during winter (73-96 %). During daytime the station may be subject to contamination from boundary layer air due to local upslope winds and hence local trace gas sources. During nighttime, these local wind systems are absent at the station and sampled air usually represents the free troposphere. Air sampling was therefore restricted to nighttime (see section 3.1.1). The dominant air flow at the station is from western to north eastern directions, with air masses mainly coming from the North Atlantic. Frequently, air masses arriving at Izaña have crossed the North American continent. To a lesser extent also air masses which passed Europe or the African continent are encountered [Schmitt et al., 1988] [Schmitt & Volz-Thomas, 1997] (see section 3.2.2 for a detailed discussion).

### 3.1.1 Air sampling

The air inlet is installed on top of a tower next to the main station building, at a height of 13 m above ground, and connected via 25 m 1/2 inch teflon (PFA) tubing to the sampling equipment inside the building. In order to prevent condensation, the

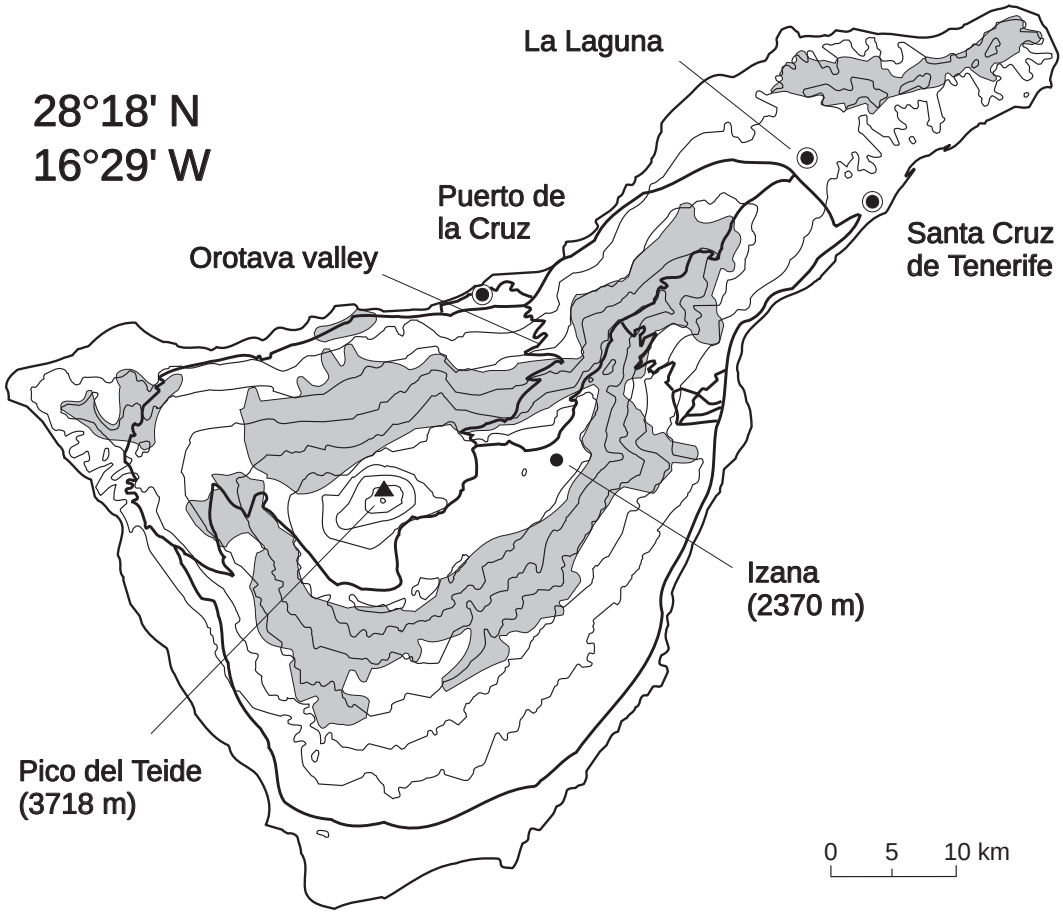


**Figure 3.1:** Map of Tenerife with the location of the GAW Izaña observatory.

whole sampling line is heated 5-10 K above ambient temperature. For the filling of the air bags used for the 2-week continuous samples a clock-controlled valve restricts the sampling to nighttime hours between 21:00 and 7:00 LT. As described in section 2.1.4 duplicate continuous samples are taken. This allows a quality control over the whole analytical procedure, including air sampling, GC analysis and isotope measurements. In addition to the continuous samples also spot samples are collected at intervals of two weeks. Again sampling is restricted to nighttime hours. For a detailed description of the sampling procedure see section 2.1.4. During the three-year sampling period 128 continuous and 86 spot samples have been taken and analyzed.

### 3.1.2 Back trajectories

Back trajectories for air masses arriving at Izaña were obtained from the Atmospheric/Ocean Chemistry Experiment (AEROCE) Trajectory Archive for the period 1991-1997. They are calculated on hypothetical isentropic surfaces, as described by

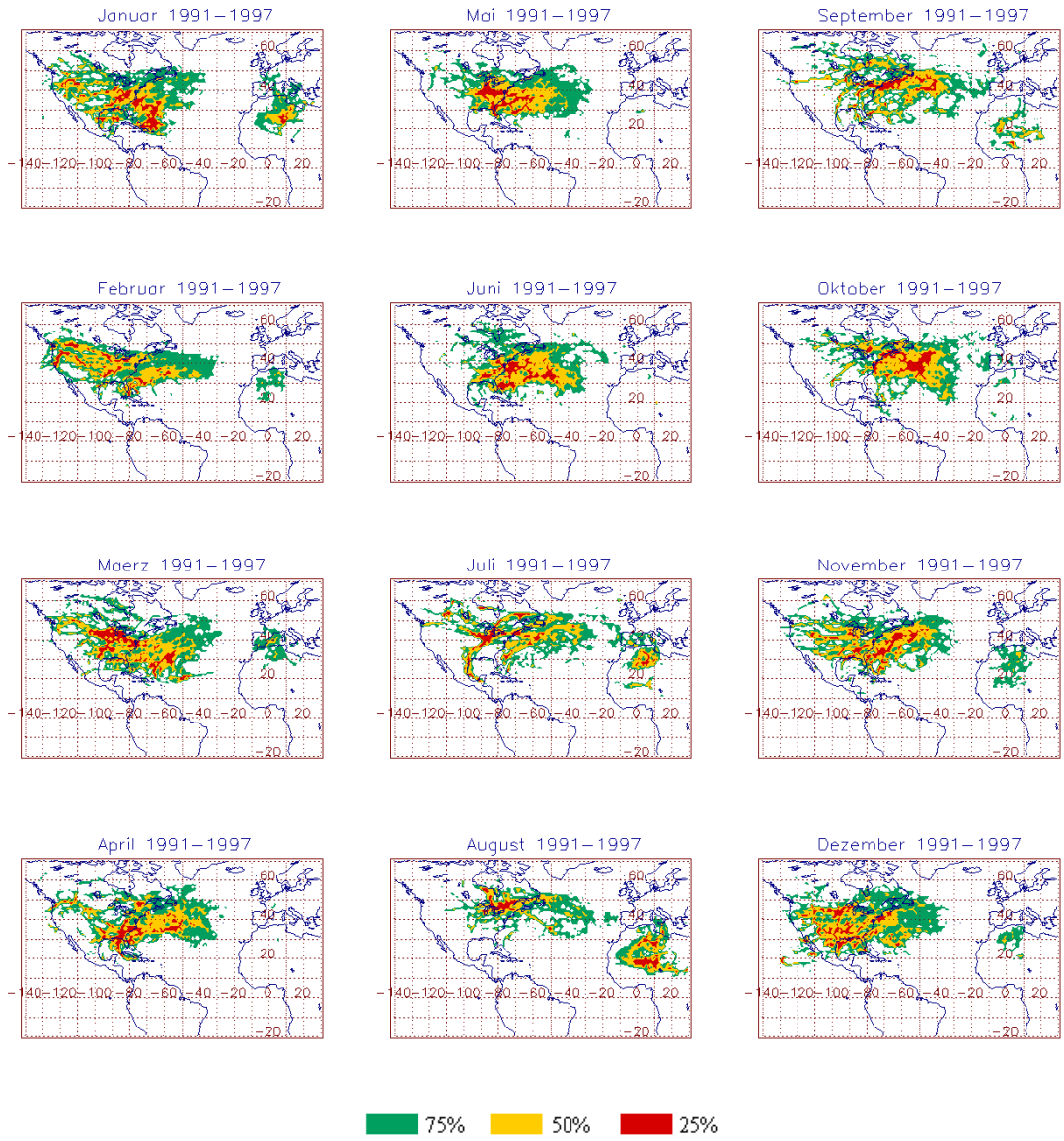


**Figure 3.2:** Isentropic flow probability fields for Izaña for 1991-1997 (January-December). Residence time from all available trajectories were combined to calculate isoplethe maps. Red areas represent 25%, yellow areas 50% and green areas 75% of the total time of all trajectories. The applied geometrical correction factor compensates for the decrease of the probabilities with increasing distance (which fall off with the square of the distance) [Schaefer, 1998].

Merrill [1994]. Individual trajectories are calculated for the four corners of a 1° x 1° square around Izaña (the position of Izaña constitutes the center of the square), for the 10 days prior to their arrival at Izaña. The divergence of the four single trajectories can be regarded as a measure of the reliability of the individual calculations. From 1998 onwards back trajectories were provided by the Spanish Meteorological Service Tenerife. Further, we used the HYSPLIT 4.0 (HYbrid Single-Particle Lagrangian Integrated Trajectory) program from NOAA to calculate 10-day back trajectories. We compared the calculated trajectories of the three different methods and found a good agreement.

The origin of the different air masses reaching Izaña during the year is summarized in Figure 3.2. Based on the AEROCE database, Schäfer [1998] has evaluated the origin of air masses reaching Izaña in terms of isentropic flow probability fields. In figure 3.2 the residence time from all available trajectories are used in order to calculate isoplethe maps for Izaña for 1991-1997 (January-December). The monthly isentropic flow probability fields are normalized by a geometrical factor which compensates for the decrease of the raw probabilities with increasing distance [Merill, 1994]. It is obvious that air masses from very different origins reach the remote station Izaña. Thus important source regions like Europe and North America, as well as very clean maritime or African air can be characterized by our isotopic studies of $CH_4$ and CO in chapter 3 and 3 respectively.

## 3.2 Atmospheric $CH_4$ and $SF_6$ records at Izaña

### 3.2.1 Seasonal cycles and interannual variations

The atmospheric record of $CH_4$ mixing ratio is shown in Figure 3.3. We plot our 2-week-continuous and spot samples together with $CH_4$ mixing ratios from the NOAA/CMDL monitoring network. The fit curves applied to all three data sets were calculated with a low pass convolution filter of the form

$$f(t) = N \cdot exp(-(\frac{t}{\Delta T})^2) \tag{3.1}$$

in the frequency domain by Fast Fourier Transformation (FFT). Before the filter is applied, the data are linear interpolated on daily basis for spot samples and on weekly basis for continuous samples [Jöckel et al., 2000b]. $N$ is a normalization constant, $t$ is time and $\Delta T$ the time window of the low pass filter. Three time window widths $\Delta T$ of 1 week, 2 weeks and 4 weeks were calculated for the spot samples. However, the 2-week-interval of the continuous samples made it necessary to use a 4-week filter for those samples. For the direct comparison of the different data sets we use the

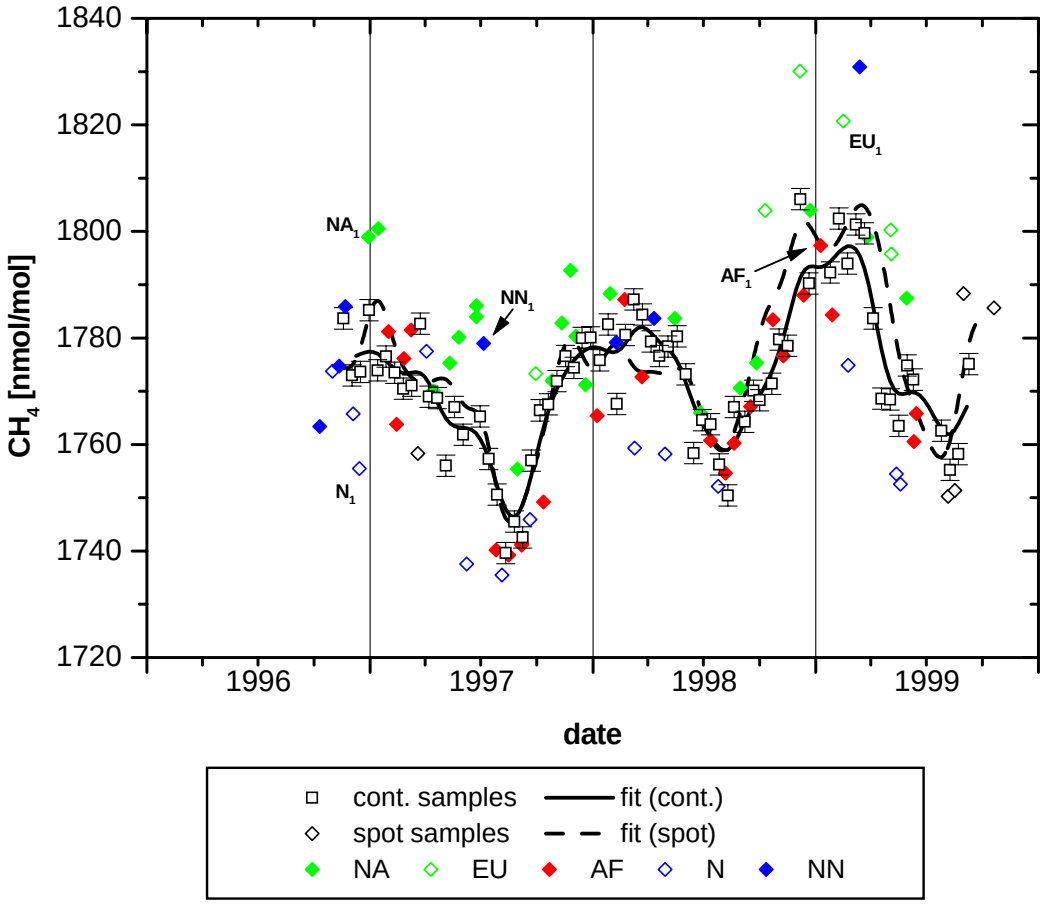


**Figure 3.3:** Record of $CH_4$ mixing ratio at Izaña. 2-week-continuous samples and spot samples are shown together with fit curves (FFT with a 4-week filter). With the help of back trajectories the spot samples are attributed to five sectors (see section 3.2.2), i.e. North America (NA), Europe (EU), Africa (AF) and North Atlantic (low (N) and high (NN) latitudes).

four-week filter for all reported FFT fit curves. The 4-week filter underestimated the amplitudes of the seasonal cycles when the minima and maxima were defined by few data points. We estimated the error in the calculated amplitudes of the seasonal cycles by calculating the difference observed for the maximum and minimum points for the different time window calculations (1 week, 2 weeks and 4 weeks).

While spot samples show considerable synoptic scale variability (which will be further discussed in section 3.2.2), the continuous samples clearly define a seasonal cycle with a peak-to-peak amplitude of about 30 nmol/mol. A sharp increase is apparent in autumn, a flat decrease in spring, and a relatively short dip during the summer months, with a half-minimum-half-width of about four months. The annual trend was calculated from the running mean of the FFT fit as $6.5 \pm 1.6$ nmol/mol $yr^{-1}$,

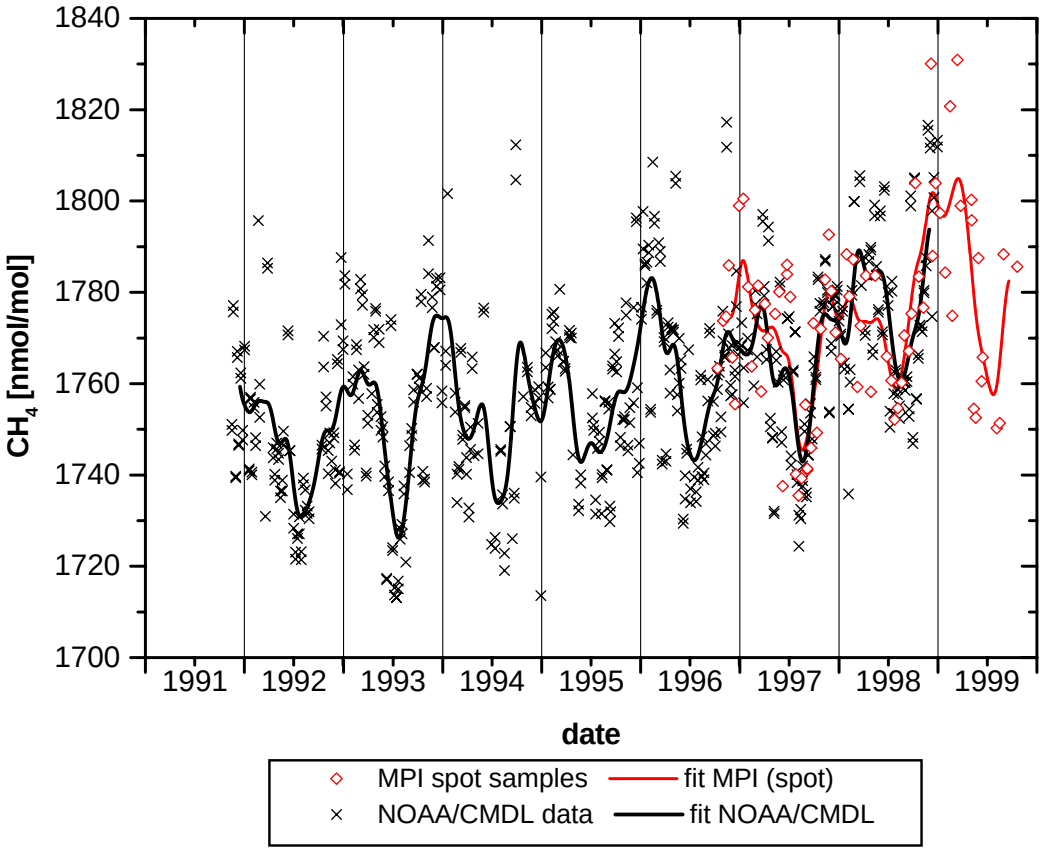


**Figure 3.4:** Records of $CH_4$ mixing ratios at Izaña. MPI spot and 2-week-continuous samples and measurements from the NOAA/CMDL monitoring network are plotted together with fit curves (FFT with a 4-week filter).

thus establishing a significant $CH_4$ increase over the observed period.

We compare our three year record of $CH_4$ mixing ratios to measurements from the NOAA/CMDL monitoring network starting at Izaña in 1991 [Dlugokencky et al., 1994b]. Both data sets are shown in Figure 3.4 together with their respective FFT fit curves (four-week filter). Based on the FFT fit curves we note the general good agreement between both data sets. Some discrepancies are nevertheless apparent which reflect the variability of $CH_4$ mixing ratios due to the large synoptic scale variations at Izaña occurring on time scales of less than 24 h.

Atmospheric $SF_6$ mixing ratios at Izaña which are reported in Figure 3.5 show a pronounced linear increase of $0.197 \pm 0.004$ pmol/mol $yr^{-1}$. $SF_6$ is known to be a virtually inert tracer of anthropogenic origin with a lifetime of about 2300 years. Its mixing ratio exhibit a significant North-South gradient and important enhancements over industrialized sources regions such as North America or Europe [Maiss

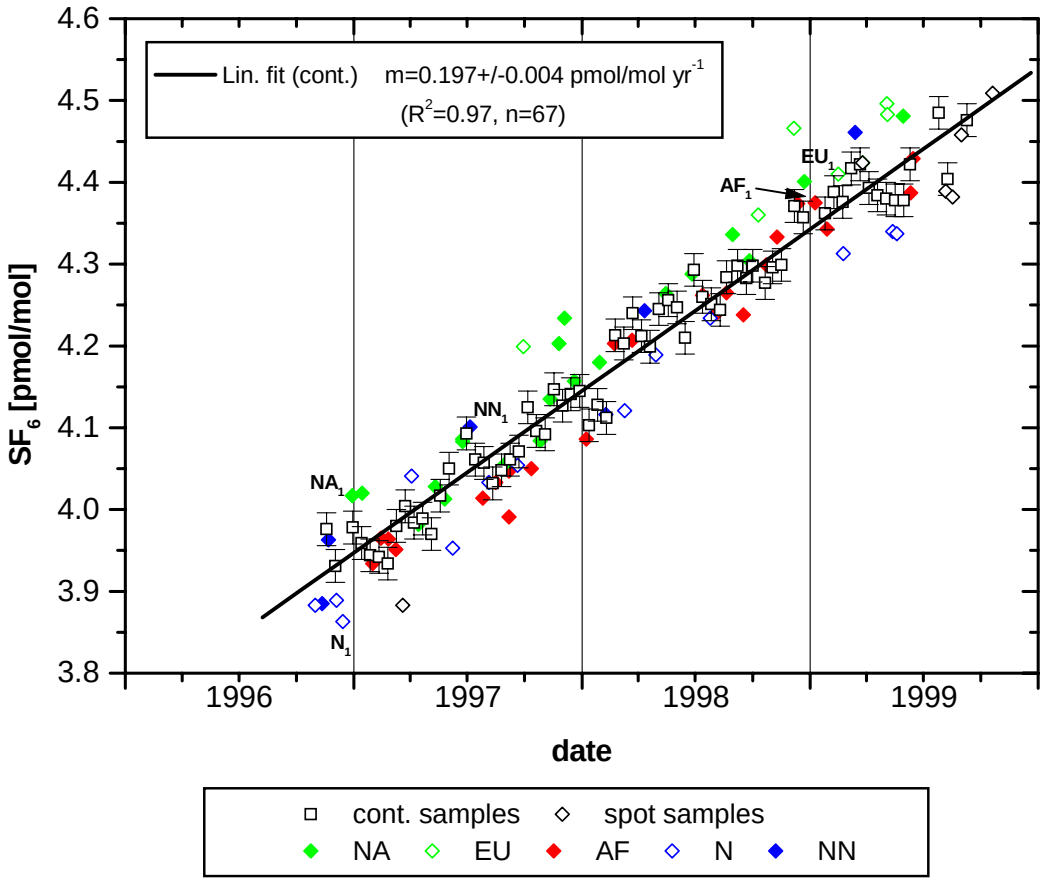


**Figure 3.5:** Record of the $SF_6$ mixing ratio at Izaña. 2-week-continuous samples and spot samples are shown together with a linear fit through the continuous samples. The error bars are the $\pm 0.02$ pmol/mol precision of the GC measurements. With the help of back trajectories the spot samples are attributed to five sectors (see section 3.2.2), i.e. North America (NA), Europe (EU), Africa (AF) and North Atlantic (low (N) and high (NN) latitudes).

& Brenninkmeijer, 1998] [Maiss & Levin, 1994]. The back trajectories indicate that deviations from the linear fit towards higher values can in most cases directly be attributed to air masses coming from North America or Europe. Similarly deviations towards lower values are found for air masses from Africa or North Atlantic (see Table 3.2).

### 3.2.2 Synoptic scales variations

Figure 3.3 shows that many of the spot samples deviate considerably from the mean seasonal cycle of $CH_4$ mixing ratios. There are several events, where the $CH_4$ difference of subsequent samples (time interval usually $\sim$ 2 weeks) is larger than the

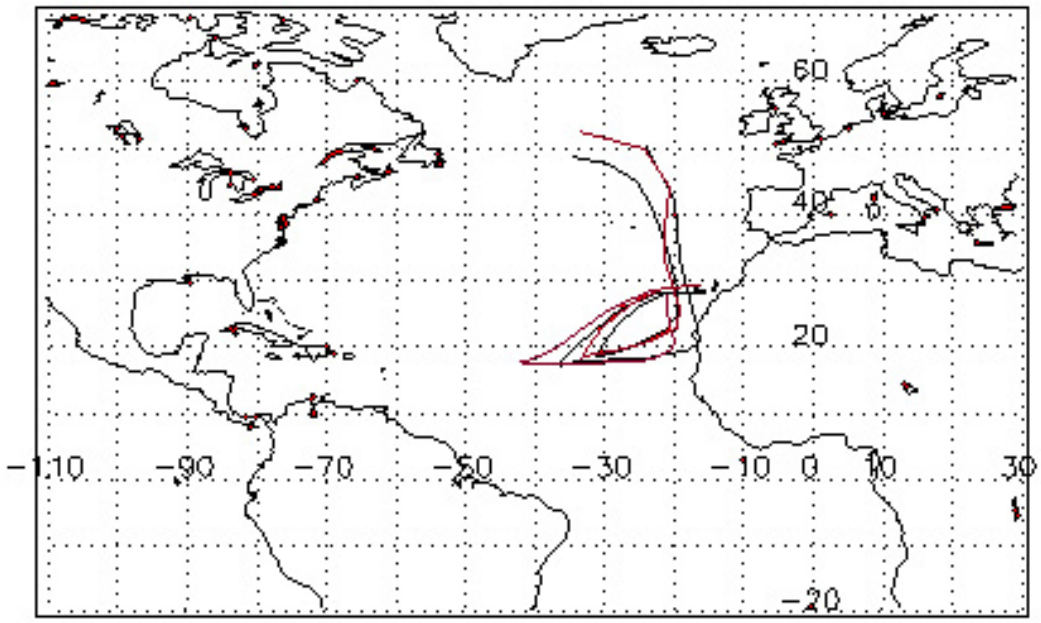


**Figure 3.6:** Sample $N_1$: 14 Dec 1996 (10day back-trajectory).

peak-to-peak amplitude of the mean seasonal cycle ($\sim$ 30 nmol/mol). Using back-trajectories, these variations can be attributed to significant changes in the meteorological situation, leading to the advection of very different air masses.

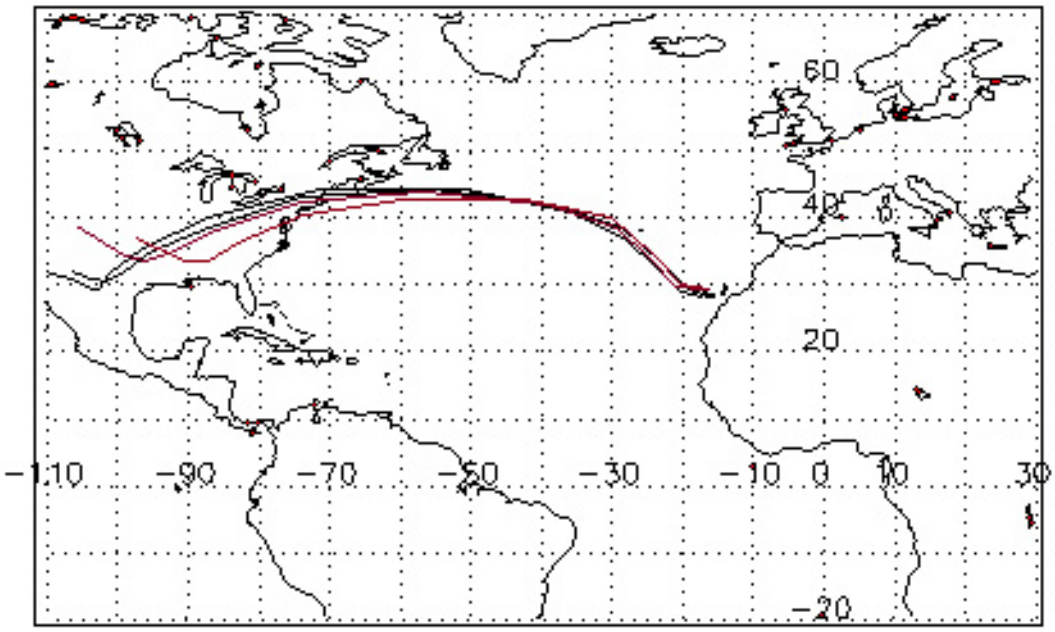


**Figure 3.7:** Sample $NA_1$: 29 Dec 1996 (10day back-trajectory).

An instructive example are the samples taken on the 14 and 29 December 1996, labeled as sample $N_1$ and sample $NA_1$ in Figure 3.3. The air collected by sample $N_1$ circulated over the North Atlantic for 10 days without any contact with continental source areas, thus representing clean marine air (see back-trajectory in figure 3.6). In contrast sample $NA_1$ collects air originating from the North American continent which was rapidly transported to Izaña. The back-trajectory shown in figure 3.7 indicates that the transport time from the American East coast to Izaña was about 3 days. This influence from North America results in a $CH_4$ mixing ratio in sample $NA_1$ which is 43 nmol/mol higher than in sample $N_1$.

Back trajectories are used in the same way to determine the origin of air captured in all spot samples taken between June 1996 and October 1999, with the exception of six samples for which no back trajectories were available. Furthermore back trajectories have been classified into the five following areas of origin:

- North American continent (NA)
- Europe including Mediterranean area (EU)
- African continent (AF)
- North Atlantic (0°-50° N) (N)
- High latitude North Atlantic (50°-70° N)(NN).

In Figures 3.3 to 3.17 spot samples are plotted with different symbols indicating to which of the five groups they belong.

Similar to samples $N_1$ and $NA_1$ as examples for group N and NA typical samples for the remaining three groups can be chosen. Two typical samples with air coming mainly from Africa and Europe respectively were taken on the 10 January and the 15 February 1999. They are labeled $AF_1$ and $EU_1$ in Figure 3.3. In Figure 3.8 the corresponding back trajectory is shown for sample $AF_1$. During the 10 day period prior to their arrival at Izaña, these air masses have circulated over North Africa. $CH_4$ mixing ratios for this sample are $\sim 25$ nmol/mol lower than for sample $EU_1$. Here air masses have crossed vast regions of the European continent (see back trajectories in figure 3.9).

Trajectories coming from the North Atlantic are separated in two groups, N and NN, in order to distinguish the very clean maritime air over the North Atlantic from the considerably more polluted air masses at higher latitudes. Even if air masses from the high latitude North Atlantic had no direct contact with source regions before reaching Izaña, the remote high Northern Hemisphere is relatively well mixed and thus highly affected by the continental source regions of North America, Europe and Siberia. Sample $NN_1$ taken on 7 July 1997 has been chosen as an typical example

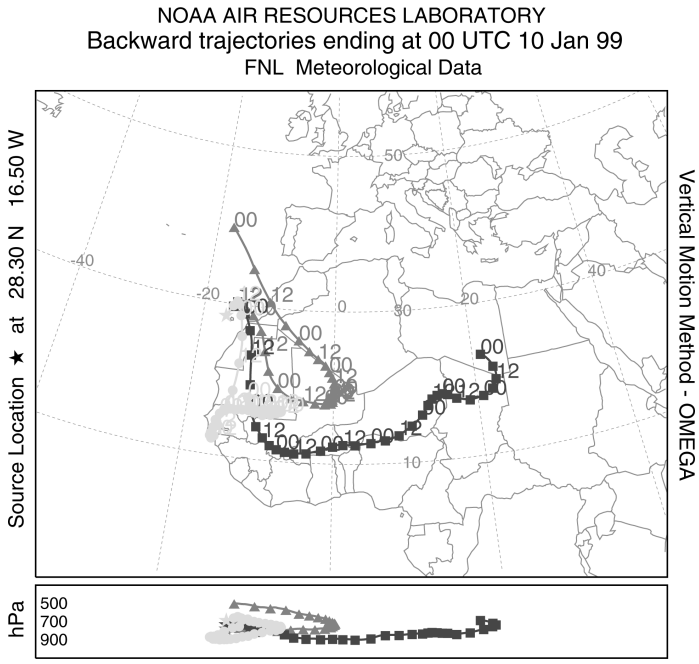


**Figure 3.8:** Sample $AF_1$: 10 Jan 1999 (10day back-trajectory).

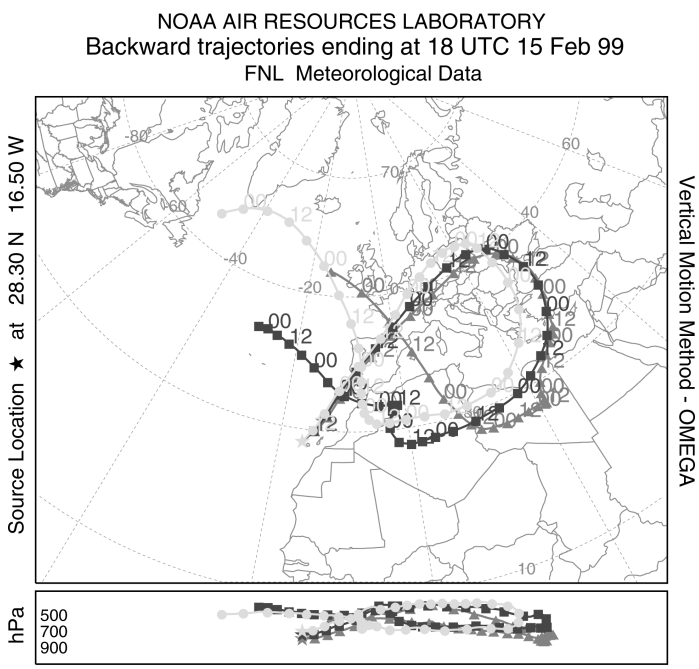


**Figure 3.9:** Sample $EU_1$: 15 Feb 1999 (10day back-trajectory).

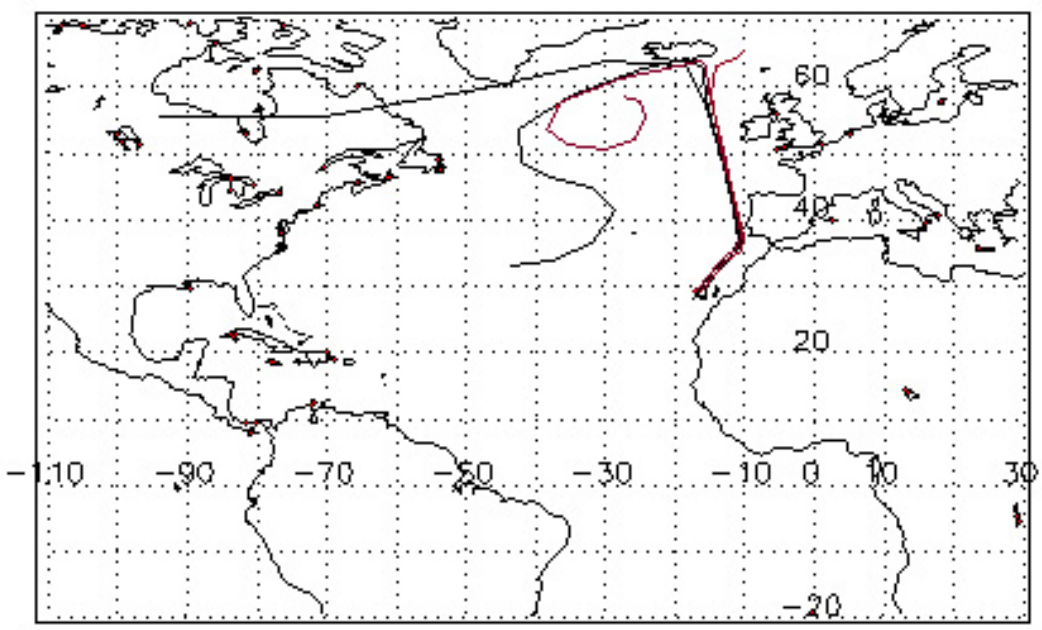


**Figure 3.10:** Sample $NN_1$: 7 July 1997 (10day back-trajectory).

for the high latitude North Atlantic. In figure 3.10 the corresponding back trajectory is shown. Air masses came directly from the high North ($> 60°$ N) with less certain origins before.

Clearly the assignment of spot samples to the five sectors with the help of back trajectories is not always unambiguous. For example, all air masses classified as coming from North America must have crossed the Atlantic. We assigned trajectories to the low North Atlantic (N) if they had nearly no contact with continental regions within the 10 days prior to their arrival at Izaña. A complicating factor in the classification of these air masses is that they often reach Izaña after turning clockwise around the station, thus touching the African coast. We still consider these samples to be representative for group N, i.e. maritime air masses. A similar effect is seen for samples attributed to the high latitude North Atlantic (group NN). These air masses have partly traveled over Ireland or Spain, but are still considered to be representative for the high latitude North Atlantic. Finally, air masses from the African continent have partly also traveled over the European continent, mostly Spain. Again we consider these samples to be representative for group AF.

If we look at the deviation of the $CH_4$ mixing ratio of each of the spot samples from the seasonal cycle derived from the continuous samples, a common pattern becomes apparent. Figure 3.3 shows, that spot samples of North American or European origin and from the remote high Northern Hemisphere all have higher mixing ratios

| | $\Delta SF_6$ [pmol/mol] | $\Delta CH_4$ [nmol/mol] | $\Delta\delta^{13}C$ [‰] | $\Delta\delta D$ [‰] | n |
|---|---|---|---|---|---|
| North America (NA) | $+0.04 \pm 0.03$ | $+10.7 \pm 6.2$ | $-0.02 \pm 0.10$ | $-1.6 \pm 2.8$ | 22 |
| Europa (EU) | $+0.08 \pm 0.03$ | $+27.8 \pm 8.3$ | $-0.10 \pm 0.04$ | $-3.6 \pm 2.0$ | 6 |
| Africa (AF) | $-0.02 \pm 0.03$ | $-3.3 \pm 7.2$ | $+0.01 \pm 0.06$ | $-0.3 \pm 2.1$ | 25 |
| North Atlantic (N)(0°- 50° N) | $-0.04 \pm 0.04$ | $-14.8 \pm 8.7$ | $+0.04 \pm 0.13$ | $+0.8 \pm 1.2$ | 16 |
| North Atlantic (NN)(50°- 70° N) | $+0.02 \pm 0.05$ | $+14.7 \pm 15.6$ | $+0.01 \pm 0.11$ | $-2.5 \pm 2.9$ | 8 |

**Table 3.2:** Residuals in mixing ratios of $SF_6$ and $CH_4$ together with the residuals of $\delta^{13}C$ and $\delta D$. The number $n$ of samples attributed to each of the five groups is given.

than the mean seasonal trend. In contrast all samples from the low North Atlantic, area N, have significantly lower mixing ratios. In order to quantify the synoptic scale variations we define residuals ($\Delta CH_4$) as the difference between the measured mixing ratio and the value of the fitted seasonal cycle.

Table 3.2 shows the clear relationship between the origin of air masses from one of the five sectors and the corresponding residuals. The air masses from the American continent, Europe and high latitude North Atlantic show significant $CH_4$ enhancements of $11.7 \pm 9.5$ nmol/mol, $25.5 \pm 10.9$ nmol/mol and $17.4 \pm 12.3$ nmol/mol, respectively. In contrast, air masses from Africa and from the North Atlantic show $CH_4$ depletions of $-7.3 \pm 4.7$ nmol/mol and $-8.6 \pm 8.6$ nmol/mol.

These enhancements and depletions are directly linked to the source/sink strengths above the respective regions. Assuming an average residence time of 1 to 3 days over the source region and a mixing height of 1 to 12 km a $CH_4$ residual of 10 nmol/mol corresponds to a source strength of 0.1 to 3.3 mg $CH_4$ $m^{-2}\,h^{-1}$. This is in the range of reported $CH_4$ emission rates. For example, for the region of Fraserdale, Ontario, Kuhlmann et al. [1998] estimated the $CH_4$ fluxes to be 0.2 to 0.5 mg $CH_4$ $m^{-2}\,h^{-1}$. While our calculation is only an illustrative estimate it shows the potential to derive trace gas fluxes from the observed variability of mixing ratios. With the availability of high resolution transport models it should be possible to substantially improve these estimates. The observed variability of atmospheric mixing ratios at remote stations could thus be used to infer integrated source fluxes [Engardt & Holmen, 1999].

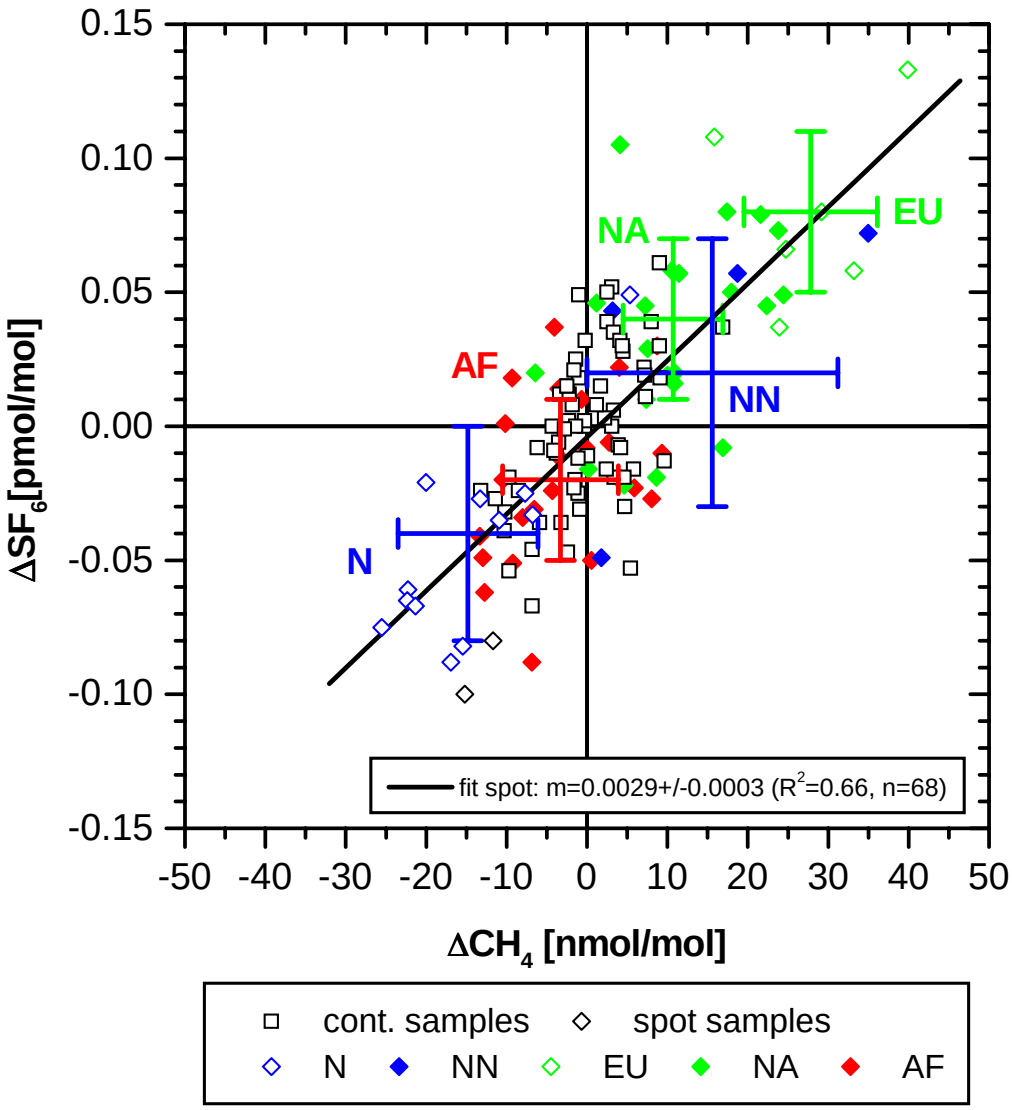


**Figure 3.11:** $CH_4$ residuals vs. $SF_6$ residuals. 2-week-continuous samples and spot samples are shown together with the regression through the spot samples. The average values ($\pm 1\sigma$ range) for spot samples from North America (NA), Europe (EU), Africa (AF) and North Atlantic (high (NN) and low (N) latitudes) are also indicated (according to Table 3.2).

Residuals for the $SF_6$ mixing ratios can also directly be linked to the origin of air masses (Table 3.2), similar to the $CH_4$ residuals. Again, North America and Europe act as sources of $SF_6$, while air masses from the North Atlantic and Africa are generally depleted, largely due to dilution. Figure 3.11 illustrates the generally very high correlation between $CH_4$ and $SF_6$ residuals. Also shown in this figure are the ranges of the residuals for air masses from the above five regions, clearly illustrating

that the varying influence from these regions largely determine the overall $\Delta CH_4$-$\Delta SF_6$ correlation.

In addition, however, it is important to note, that both $CH_4$ and $SF_6$ exhibit strong latitudinal gradients at the latitude of Izaña. The varying latitudinal origin of different air masses is therefore directly reflected in highly correlated variations of both trace gases. With an average inter-hemispheric difference of $\Delta SF_6 \approx 0.3$ pmol/mol [Levin & Hesshaimer, 1996] and $\Delta CH_4 \approx 90$ nmol/mol ($\sim 50$ to $\sim 120$ nmol/mol depending on season) [Dlugokencky et al., 1994c], the expected slope is $\Delta SF_6/\Delta CH_4 \approx 0.0033$ (0.0025 to 0.0060) pmol/mol $SF_6$/ nmol/mol $CH_4$. This is virtually identical to the slope obtained from the regression through the spot samples (Figure 3.11), $0.0028 \pm 0.0003$ pmol/mol $SF_6$/ nmol/mol $CH_4$ ($R^2 = 0.58$, n = 59).

Even though most of the samples from air masses coming from the African continent (sector AF) also have lower mixing ratios, there are 6 samples which have higher mixing ratios than the mean annual cycle. These observations occur in late winter between January and March for the years 1997 to 1999. Two different scenarios could explain these outliers. First, for three of those samples the corresponding back trajectories show that air masses have also traveled over the European continent before crossing Africa on their way to Izaña. Second, the dry season with maximum biomass burning in North Africa is exactly during this time period of February/March [Hao & Liu, 1994]. This would explain enhanced $CH_4$ levels, if biomass burning events have been encountered by the air masses on their way to Izaña. The question of biomass burning events will be addressed in section 4.2 when we discuss the CO isotope measurements done on the same samples.

## 3.3 Atmospheric $\delta^{13}C$ record at Izaña

### 3.3.1 Seasonal cycles and interannual variations

The $\delta^{13}C$ data are shown in Figure 3.12. As for $CH_4$ mixing ratios, the continuous samples define the seasonality much clearer than the spot samples. The peak-to-peak amplitude is $\sim 0.2$ ‰ and a small but significant $\delta^{13}C$ trend of $0.029 \pm 0.035$ ‰ $yr^{-1}$ was determined. A striking feature of the $\delta^{13}C$ seasonality is that it is out of phase with the $CH_4$ mixing ratios, with the $\delta^{13}C$ maximum occurring 1-2 months earlier than the $CH_4$ minimum. If the $\delta^{13}C$ seasonality was driven predominantly by the KIE of the sinks (i.e. mainly $CH_4$ + OH), then a clear anti-correlation between $\delta^{13}C$ and $CH_4$ would result. The different phases of $\delta^{13}C$ and $CH_4$, however, clearly indicate that in addition to the KIE of the sinks also the mixture of sources visible

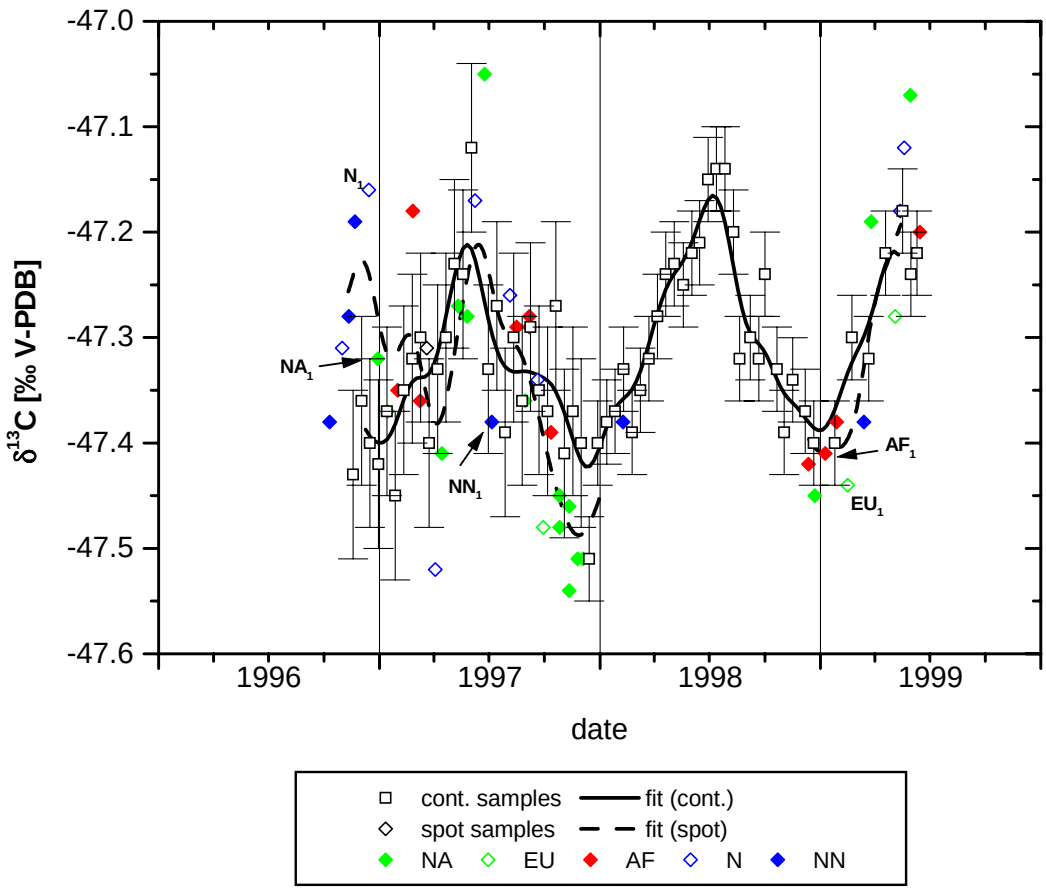


**Figure 3.12:** Record of $\delta^{13}C$ at Izaña. 2-week-continuous samples and spot samples are shown together with fit curves (FFT with a 4-week filter). With the help of back trajectories the spot samples are attributed to five sectors: North America (NA), Europe (EU), Africa (AF) and North Atlantic (low (N) and high (NN) latitudes).

at Izaña varies during the season. We return to this point in section 3.5.

### 3.3.2 Synoptic scale variations

We first investigate how the deviations in $CH_4$ mixing ratios are linked to deviations in the isotopic signature. Figure 3.13 shows the $\delta^{13}C$ residuals versus $CH_4$ residuals. Most samples with negative $CH_4$ residuals show a $\delta^{13}C$ enrichment which is compatible with the KIE=1.0039 of the $CH_4$ + OH sink (or $1.005 \pm 0.001$ of the combined OH and soil sink)[Saueressig, 1999]. One single sample (sample $N_1$), however, shows a significantly larger enrichment, which could be due to an additional influence from the $CH_4$ + Cl sink. Figure 3.6 shows that the air collected in December 1996 in this sample circulated over the Atlantic for 10 days, where the Cl sink could have played a significant role. However, a very high contribution of the Cl sink of $\sim 1/3$ would

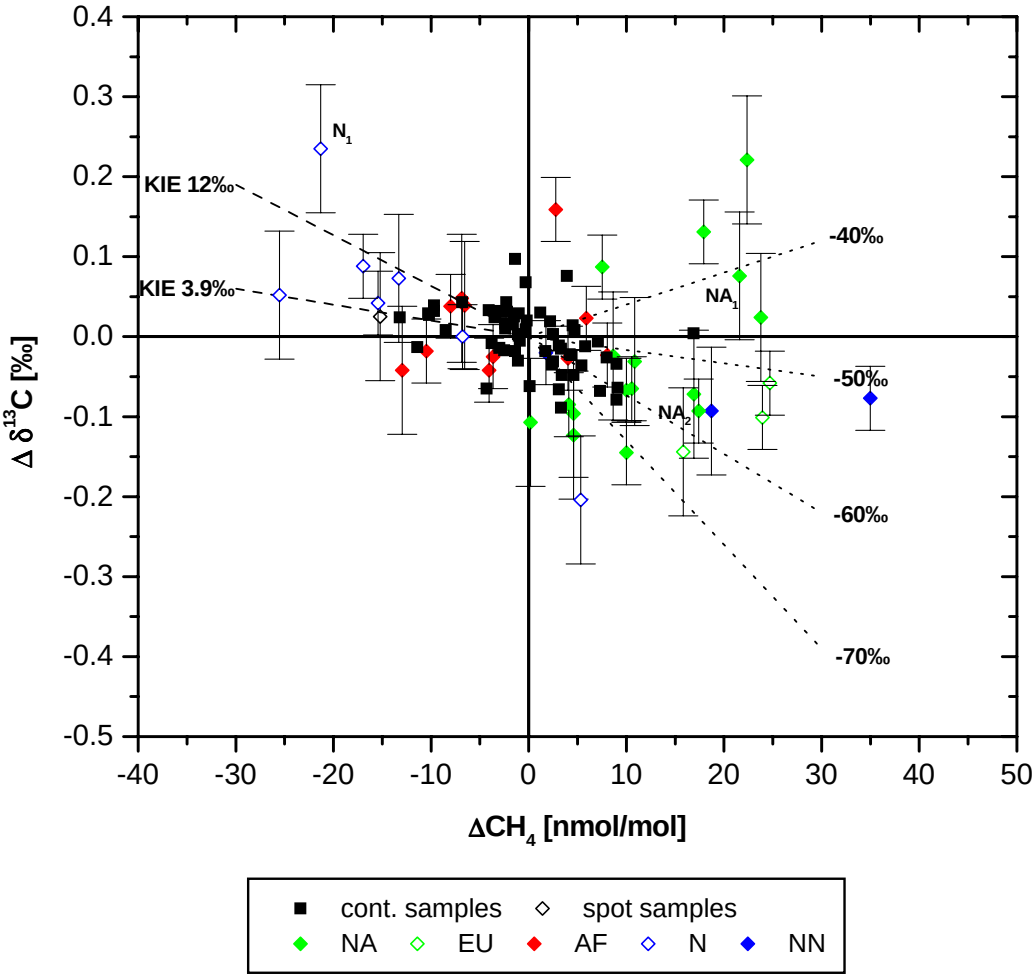


**Figure 3.13:** $\delta^{13}C$ residuals versus $CH_4$ residuals. Mixing lines (dash-dotted) are shown for admixture of $CH_4$ with different $\delta^{13}C$ signatures and the kinetic isotope effects of the sinks (Rayleigh process according equation 3.2).

be required to fully explain the $\delta^{13}C$-$CH_4$ residual of this particular sample.

On the side of $CH_4$ sources (i.e. positive $CH_4$ residuals), a generally much larger $\delta^{13}C$ variability is apparent, directly indicating significant differences in the $\delta^{13}C$ signatures of different source areas. We depict the two samples which have large positive $CH_4$ residuals (and for which also $\delta D$ data are available), termed samples $NA_1$ and $NA_2$. Sample $NA_1$ shows a relatively enriched $\delta^{13}C$ signature of the admixing source of around $-40$ ‰ V-PDB, while sample $NA_2$ has a typical biogenic signature, $\delta^{13}C \approx -60$ ‰ V-PDB. Both samples originate from the North American continent, however from different latitudes. Sample $NA_1$ passed over the industrialized regions of the United States and south eastern Canada and is likely to be mainly influenced by anthropogenic sources, the mix of which may contain some non-biogenic sources,

such as e.g. natural gas or $CH_4$ from coal mining. In contrast, sample $NA_2$ (taken in July 1997) passed over the Canadian wetlands, which during summertime represent a large biogenic $CH_4$ source, which is consistent with the derived $\delta^{13}C \approx -60$ ‰ V-PDB. This interpretation is also consistent with the δD residuals, shown in Figure 3.16.

### 3.3.3 Calculation of the KIE

Correlations between isotopic signatures and mixing ratios are widely used to extract information about the isotopic signatures of the sources or the kinetic isotope effects (KIE) of the sinks. We consider a single well-mixed closed domain ("one-box model"), with one source with a constant isotopic signature and one sink with a well-defined, constant KIE. Isotopic signatures plotted versus inverse mixing ratio form a straight line (approximated for small deviations around the annual mean value). From the point of view of the sources this line represents the mixing line between the atmospheric reservoir and the admixing source. From the point of view of the sinks the line describes a Rayleigh distillation process. The intersection between the regression line and the $\delta$-axis represents the $\delta$-signature of the source, and the slope of the line is directly linked to the KIE. For small variations of the isotopic signature, the Rayleigh equation can be approximated as:

$$\delta_f - \delta_i = [\delta_i + 1000] * [1 - \frac{1}{KIE}] * ln\frac{c_i}{c_f} \approx [\delta_i + 1000] * [1 - \frac{1}{KIE}] * [\frac{c_i}{c_f} - 1] \quad (3.2)$$

where $\delta$ represents the isotopic signature, $c$ the mixing ratio, and the indices $i$ and $f$ indicate the initial and final values.

We already noted in section 3.3 that a clear phase shift between the $\delta^{13}C$ cycle and the $CH_4$ mixing ratios is apparent. This phase shift is directly reflected in a strong deviation of the actual $\delta^{13}C$-$1/CH_4$ correlation from a straight line, which is most clearly seen when we look at the correlation between the corresponding fit curves. This is illustrated in Figure 3.14 after subtraction of the (small) linear trends in $CH_4$ and $\delta^{13}C$.

The correlation between the $\delta^{13}C$ and $1/CH_4$ forms a distorted ellipse. The relatively large opening of the 'ellipse' is reflected in the very poor correlation between the individual data points, with correlation coefficients of $R^2 = 0.28$ (n=61) and $R^2 = 0.10$ (n=45) for the continuous and spot samples respectively. The opening of the ellipse mainly reflects the impact of the seasonality of $CH_4$ sources, which causes the observed phase shift between $CH_4$ and $\delta^{13}C$. Furthermore, the spot samples are more strongly influenced by synoptic scale variations linked to the advection of

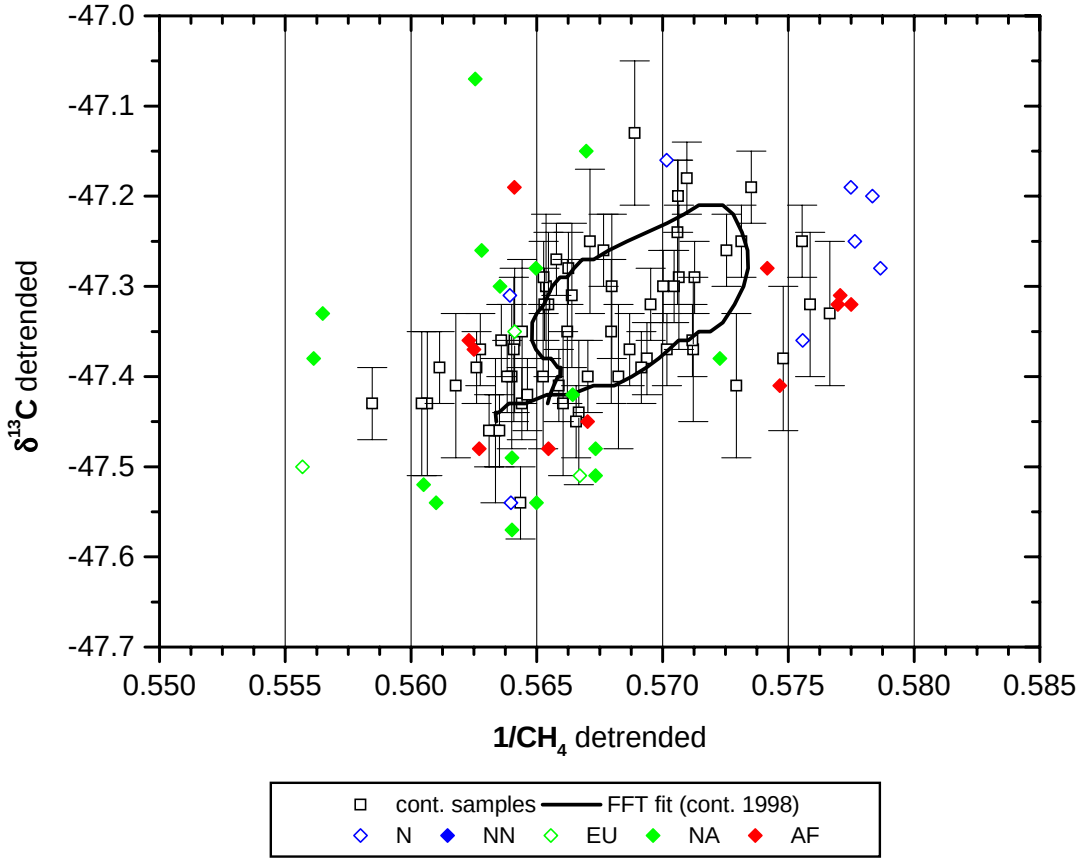


**Figure 3.14:** $\delta^{13}C$ -1/$CH_4$ correlation for spot and 2-week-continuous samples. From the $CH_4$ and $\delta^{13}C$ values a small linear trend has been subtracted. The plotted ellipse is based on the FFT fit through continuous samples from 1998 which have also been detrended.

air masses which bear very different $\delta^{13}C$ signatures depending on the prevailing sources/sinks. The source and sink effects have been discussed in section 3.2.2. For sample $N_1$ we considered a substantial influence of the Cl sink. Consequently the correlation coefficient of the spot samples is even poorer than that for the continuous samples. However, when using the subset of continuous samples from 1998, a distinctly higher correlation coefficient of $R^2 = 0.41$ (n=27) is calculated. This might be due to the higher accuracy for these samples (±0.08 ‰ and ±0.04 ‰ before and after August 1998, see section 2.6.2), but may also reflect some interannual variability. We plot through the continuous samples of 1998 the corresponding FFT fit, which has previously also been detrended. Due to the interannual differences occurring between 1996 and 1999 the subtraction of a linear fit for the data from 1998 leads to an ellipse which is not closed. The slope of the regression line through this subset of samples corresponds to an apparent KIE of 1.009 ± 0.003. This is

larger than the expected average isotope fractionation $KIE_{avg}$:

$$KIE_{avg} = f_{OH}KIE_{OH} + f_{soil}KIE_{soil} \tag{3.3}$$

with $f_{OH}$ and $f_{soil}$ representing the fractional contribution of the OH sink and soil sink respectively ($f_{OH}+f_{soil} = 1$). Inserting $KIE_{OH}^{13C} = 1.0039 \pm 0.0002$ [Saueressig, 1999], $KIE_{soil}^{13C} = 1.022 \pm 0.04$ [Tyler, 1994] and $f_{soil} = 0.06 \pm 0.03$ [Born et al., 1990] yields $KIE_{avg}^{13C} = 1.005 \pm 0.001$($1\sigma$ uncertainties). The discrepancy to the measured apparent KIE may indicate some influence of the $CH_4$ + Cl sink, which is associated with an extraordinarily large KIE of about 1.066 (at 298 K, slightly increasing with decreasing temperature) [Crowley et al., 1999] [Saueressig et al., 1995] [Tyler et al., 1998]. Similar deviations between the apparent KIE and the KIE calculated from the combined OH and soil sink were also observed in the extratropical SH, at the stations Baring Head and Scott Base [Allen et al., 1999]. The $CH_4$ and $\delta^{13}C$ data from these stations also showed a very pronounced elliptical phase behavior with the tilt of the major axis being a good measure for the kinetic isotope effect [Allen et al., 1999]. At Izaña, however, the calculation of the average isotope fractionation $KIE_{avg}$ from the $\delta^{13}C$-1/$CH_4$ correlation has to be interpreted with some caution, in particular in view of (1) the not fully consistent correlation patterns in 1997 and 1998, (2) the very large distortion and opening of the 'ellipse' derived from the fit curves, and (3) the influence of seasonally varying sources on the apparent KIE (see also section 3.5 and [Bergamaschi et al., 2000c]).

## 3.4 Atmospheric $\delta$D record at Izaña

### 3.4.1 Seasonal cycles and interannual variations

A significant seasonal cycle is also evident for δD, which is shown in Figure 3.15. The extremely high precision in our δD measurements has enabled us, to our knowledge for the first time, to clearly establish a seasonal δD cycle at an atmospheric background station. Marik [1998] has previously measured δD at the three stations Neumayer, Izaña, and Alert, using conventional sample preparation followed by IRMS analysis (precision ±5 ‰). His records for the 1991-1997 period show no obvious seasonal cycle at any of these stations due to the relatively low precision of the single measurements. However, after calculating monthly mean values over the whole 1991-1997 period, seasonal cycles of 4 ‰ became apparent for Alert and Neumayer, but not for Izaña. In contrast, the measurements presented here, clearly establish a seasonal cycle at Izaña with a peak-to-peak amplitude of about 3.5 ‰. The δD maximum in mid-August coincides with the minimum of $CH_4$ mixing ratios.

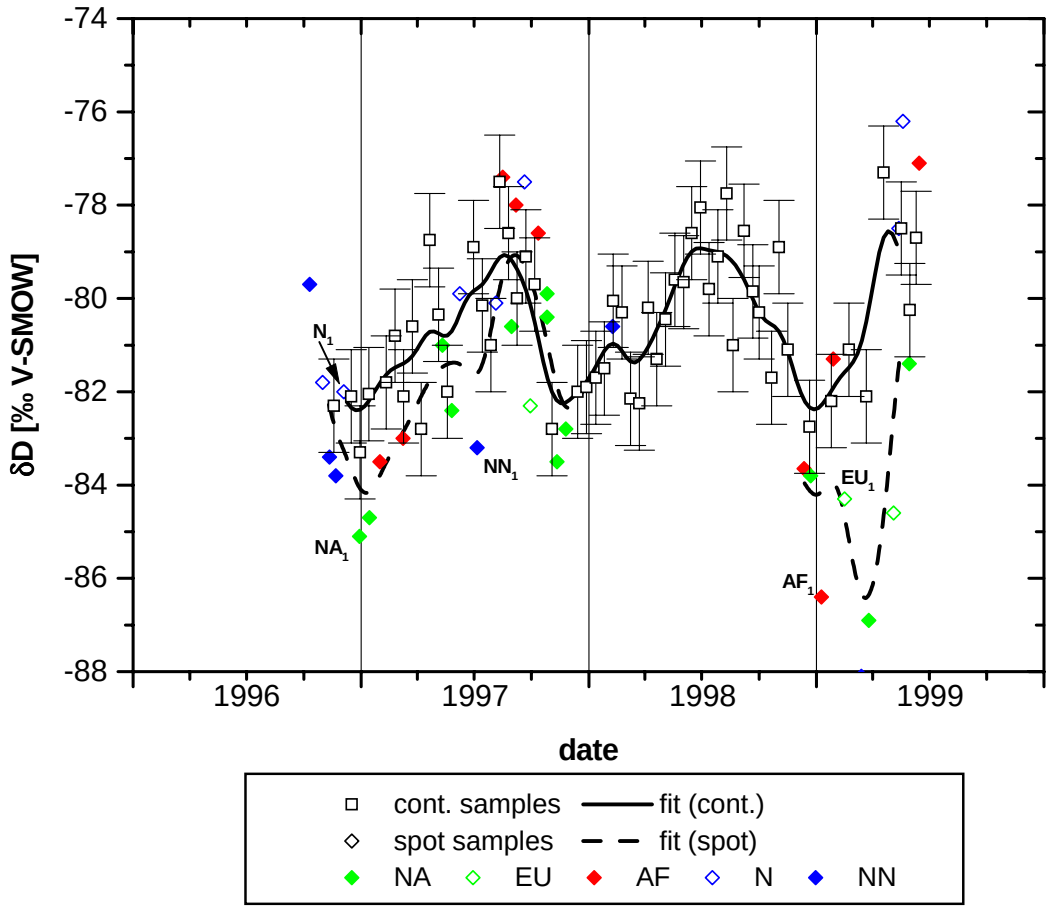


**Figure 3.15:** Record of δD at Izaña. 2-week-continuous samples and spot samples are shown together with fit curves (FFT with a 4-week filter). With the help of back trajectories the spot samples are attributed to five sectors: North America (NA), Europe (EU), Africa (AF) and North Atlantic (low (N) and high (NN) latitudes).

This suggests a, in contrast to $\delta^{13}$C , much closer link of the δD seasonality to the KIE of the sinks, and a smaller influence of seasonal variations of the sources. This will be discussed in the next section and compared to model results in section 3.5. A small but significant positive δD trend $0.21 \pm 0.49$ ‰ $\mathrm{yr}^{-1}$ is discernible from the FFT fit through the continuous samples.

In 1997 δD measurements were made regularly on spot and continuous samples. The comparison of the two data sets with the help of the calculated FFT fits shows that the spot samples are slightly depleted compared to the continuous samples. Only few samples (mostly from the North Atlantic and Africa) are enriched compared to the background defined by the continuous samples. δD sources are very light ($\sim -260$ ‰) compared to the atmospheric value of $\sim -79$ ‰. Thus we expect spot

samples which have recently been influenced by source regions prior to their arrival at Izaña to have depleted δD values. Nevertheless, the extremely low δD values for some samples in 1999 are not consistent with their corresponding $CH_4$ mixing ratios. In section 3.4.3 we show that even δD sources of less than $-400$ ‰ cannot account for the measured δD values of less than $-68$ ‰. As δD measurements are very sensitive to the exchange with $H_2O$ we cannot exclude that these spot samples in 1999 have been contaminated. If the drying unit during the sampling process has started to be less effective, this would mainly affect the corresponding δD measurements.

### 3.4.2 Synoptic scale variations

In Figure 3.16 δD residuals are plotted versus $CH_4$ residuals in order to quantify the synoptic scale variations occurring in the δD signals of the spot samples. Compared to $\delta^{13}C$ , δD residuals generally correlate much better with the $CH_4$ residuals since the typical δD signatures of atmospheric sources lead to a much smaller spread of mixing lines. Sample 3 exhibits a derived δD signature of below $-300$ ‰ V-SMOW, which is typical for biogenic sources. Sample 2 lies slightly above the $-300$ ‰ mixing line, but considering the given error bars the difference is not significant.

### 3.4.3 Calculation of the KIE

Figure 3.17 shows that a compact correlation exists between δD and $1/CH_4$. Considering the set of continuous samples, a $R^2 = 0.54$ (n=54) is calculated. Thus 54% of the variations in δD are explained by variations in $1/CH_4$. The plot of the detrended FFT fit curves (δD fit vs. inverse of $CH_4$ fit) forms a very flat ellipse not very different from the regression line through the data. The δD data closely follow the idealized relationship outlined above for the one-box model with one source and one sink. The main underlying reason for this behavior is the large KIE of $1.294 \pm 0.04$ [Saueressig, 1999] associated with the $CH_4$ + OH reaction, and the fact that the majority of sources have δD values far away from atmospheric $CH_4$. Typical δD values of (terrestrial) biogenic sources are around $-350$ to $-280$ ‰ V-SMOW [Bergamaschi, 1997] [Bergamaschi et al. 1998b], [Levin et al., 1993], [Wahlen, 1993], [Whiticar et al., 1986] and also $CH_4$ from natural gas (even if thermogenic) has δD values significantly depleted relative to atmospheric $CH_4$ of around $-150$ to $-280$ ‰ V-SMOW [Schoell, 1980]. The only source for which δD are reported which are enriched relative to atmospheric $CH_4$ is biomass burning with δD values $\sim -30$ ‰ V-SMOW [Wahlen, 1993]. Recent measurements, however, yielded much more depleted values of $-233 \pm 2$ ‰ for large scale laboratory combustion and $-210 \pm 16$ ‰ for forest and pasture burning in the Brazilian Amazon [Snover et al., 1999].

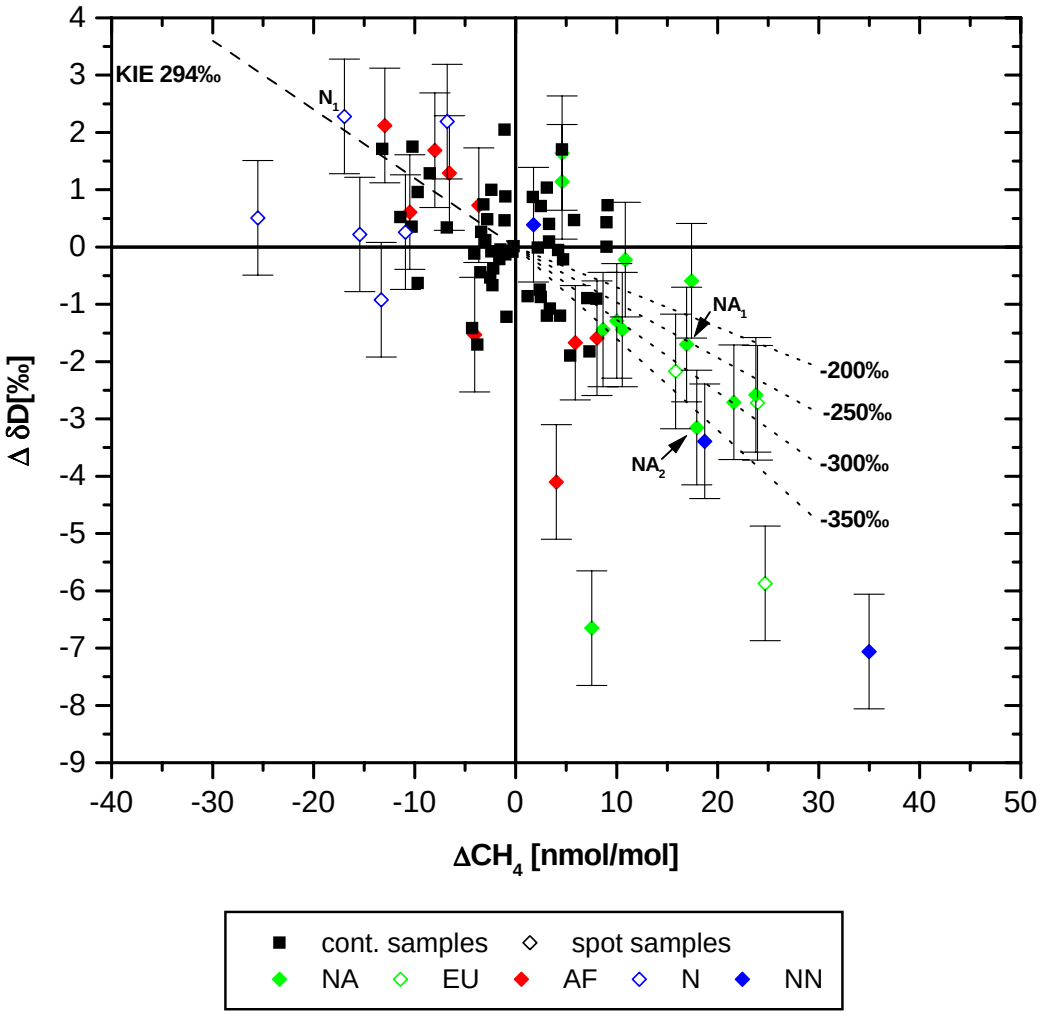


**Figure 3.16:** δD residuals versus $CH_4$ residuals. Mixing lines (dash-dotted) are shown for admixture of $CH_4$ with different δD signatures and the kinetic isotope effects of the sinks (Rayleigh process according equation 3.2).

In contrast to δD, the KIE$^{13}C$ in the reaction $CH_4$ + OH is relatively small, 1.0039 [Saueressig, 1999]. Sources exhibit a wide range of $\delta^{13}$C values, typically $-80$ ‰ to $-50$ ‰ V-PDB for biogenic sources, $-50$ to $-30$ ‰ V-PDB for thermogenic $CH_4$, and $-28$ to $-12$ ‰ V-PDB for $CH_4$ from biomass burning (depending on the mix of C3 and C4 plants) [Levin et al., 1993] [Stevens & Engelkemeir, 1988] [Wahlen, 1993]. Consequently, air masses originating from different source regions may bear very different $\delta^{13}$C signatures (see also section 3.2.2), but are expected to always have a δD signature close to $-300$ ‰ V-SMOW, unless largely influenced by biomass burning (in case of enriched δD values for this source). This fact is most clearly reflected in the very high correlation between δD and $1/CH_4$ of the

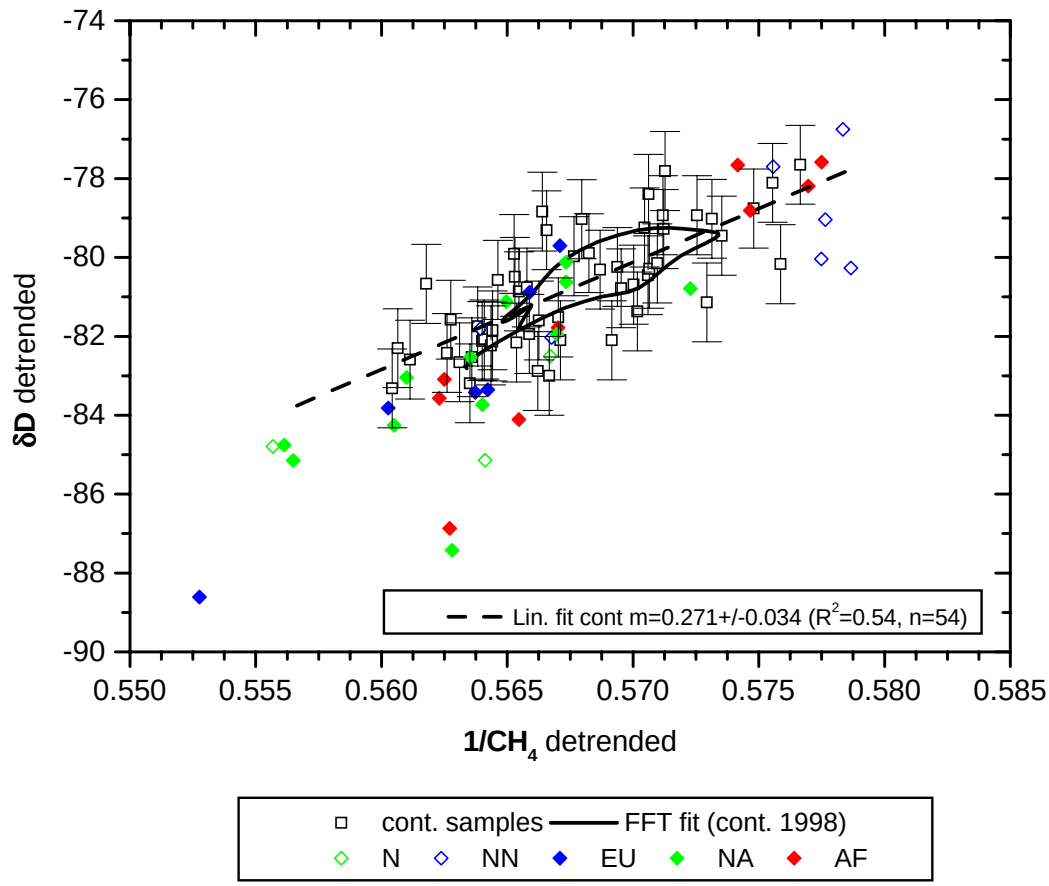


**Figure 3.17:** δD-1/$CH_4$ correlation for spot and 2-week-continuous samples. From the $CH_4$ and δD values a small linear trend has been subtracted. The plotted ellipse is based on the FFT fit through continuous samples from 1998 which have also been detrended.

spot samples ($R^2 = 0.74$), compared to a correlation coefficient of $R^2 = 0.10$ for the corresponding $\delta^{13}C$ -1/$CH_4$ correlation.

The compact δD-1/$CH_4$ correlation defines the slope of the linear regression relatively precisely. Using the regression through the continuous samples, we derive an average KIE of $1.23 \pm 0.04$. Since this value reflects the seasonal (rather than synoptic scale) δD variation, and mixing within the hemispheres occurs relatively fast (time scale a few weeks to months), this estimate can be considered to be representative at least for the Northern Hemisphere. In contrast, the value derived from the regression through the spot samples may to a larger extent be influenced by the source and sink areas relevant for Izaña, such as North America and Europe ($CH_4$ sources) or the North Atlantic and Africa ($CH_4$ sinks). The result of the regression through the spot samples, $KIE^D_{avg} = 1.24 \pm 0.03$ is, however, virtually identical to

the result derived from the continuous samples.

## 3.5 Comparison to model results

In order to simulate the global distribution of $CH_4$ mixing ratios, $\delta^{13}C$ and $\delta D$, our measurements from Izaña were used in a three-dimension inverse model by Bergamaschi et al. [2000a]. This study used the first two years of our $CH_4$ records (1996 to 1998) together with data from a number of other sources. Observational data for $CH_4$ mixing ratios were taken from the NOAA/CMDL network (38 stations) [D. Dlugokencky, data retrieved from ftp:// ftp.cmdl.noaa.gov/ccg/$CH_4$/]. For $\delta^{13}C$ records from Scott Base (Antarctica), Baring Head (New Zealand)(data of the National Institute of Water and Atmospheric Research (NIWA), New Zealand [Lowe et al., 1999]), Pt. Barrow (Alaska), Olympic Peninsula (Washington) and Mauna Loa (Hawai) [P. Quay, University of Washington, Seattle, data retrieved from Carbon Dioxide Information Analysis Center, Oak Ridge, Tennessee, USA, http://cdiac.esd.ornl.gov/ndps/quay.html] were used. For $\delta D$ only the data from Izaña was included.

The model setup is similar to the one used by Hein et al. [1997]. Atmospheric transport is simulated with the TM2 model [Heimann, 1996], with a horizontal resolution of $\sim 8°$ latitude by $10°$ longitude, and 9 layers in the vertical dimension. Meteorological fields (advection, and subgridscale vertical transport) are based on 12-hourly ECMWF (European Community Medium Range Weather Forecast) analyzes for the year 1987. For the treatment of the isotopic composition the TM2 was configured for three tracers, representing the principal isotopomers of methane, $^{12}CH_4$, $^{13}CH_4$, $^{12}CH_3D$ (with a mean abundance as listed in table 1.4.1 of 98.8 %, 1.1 %, and 0.06 %, respectively).

The principal $CH_4$ sources considered are swamps, bogs, rice paddies, domestic animals (incl. animal waste), biomass burning (separated into forest and savanna burning), landfill sites, and fossil fuel related emissions (separated into coal, oil/gas, and Siberian gas). The spatio-temporal emission patterns used for these sources were as described by Hein et al. [1997], except for bogs and biomass burning, for which the distributions of Fung et al. [1991] and [Hao & Liu, 1994] were used respectively.

Possible small $\delta^{13}C$ calibration offsets among the three $\delta^{13}C$ laboratories were treated as additional parameters to be optimized by the inversion. A posteriori results for these calibration offsets were, however, not significantly different from zero. Together with Marik [1998] this was the first time $\delta D$ measurements were included for a better understanding of the methane budget.

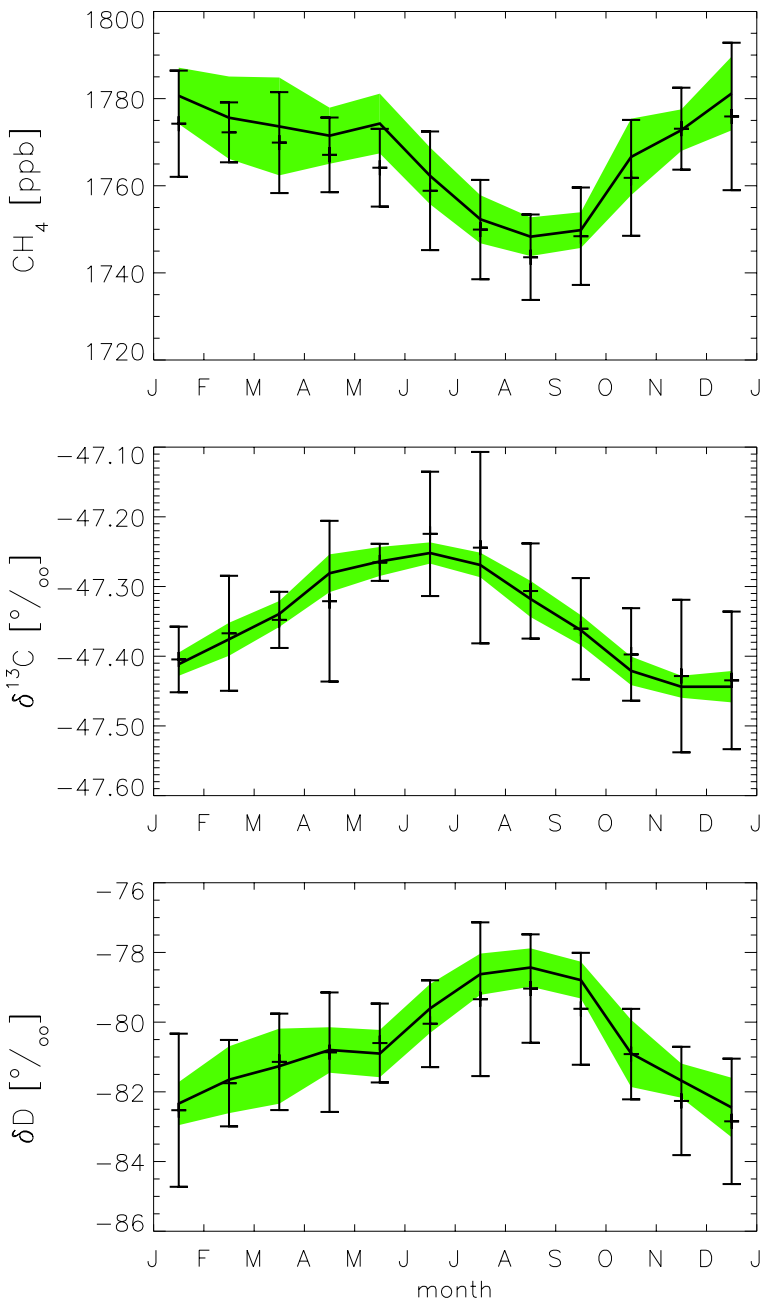


**Figure 3.18:** Comparison of observational data with results from an inverse model [Bergamaschi et al., 2000a]: (a) $CH_4$ mixing ratios, (b) $\delta^{13}C$ , and (c) $\delta D$. Model results are given as monthly mean values (solid line) and standard deviation ($1\sigma$) of daily model data (shaded area). Observational data are detrended and their monthly mean values are shown as black bars, with the error bars representing the $1\sigma$ standard deviation from the fitted curve.

inv_903.set

Figure 3.18 shows the results from the inverse model along with the observational data from Izaña. Model data are given as monthly mean values (solid line) $\pm 1\sigma$ standard deviation of the daily data (shaded area). Observational data are detrended and their monthly mean values are shown as black bars, with the error bars representing the $1\sigma$ standard deviation from the fitted curve (over the 2-year record 1996 - 1998). Both spot and continuous samples were used in this case, with a stronger weight on the continuous samples in the fit procedure (by a factor of 2; thus in this representation the mean seasonal cycle is mainly determined by the continuous samples, but the given standard deviation by the spot samples). The figure shows the excellent agreement between inverse model and observational data for $CH_4$ mixing ratios, $\delta^{13}C$ , and $\delta D$. Note that also the phase behavior of $CH_4$, $\delta^{13}C$ , and $\delta D$ is exactly reproduced by the model, i.e. a time lag of two months between $\delta^{13}C$ maximum and $CH_4$ minimum, and a coincidence of $\delta D$ maximum and $CH_4$ minimum.

Another output of the model was the calculation of the contribution of the individual sources on the seasonal cycles. In Figure 3.19 this is shown for $CH_4$ mixing ratios, $\delta^{13}C$ and $\delta D$. The seasonal $CH_4$ cycles of the sources with assumed constant emissions throughout the year (animals, waste, and fossil sources) are mainly influenced by the seasonality of the OH sink, while in particular $CH_4$ from bogs, rice paddies and biomass burning show a significantly different phase behavior, largely determined by their emission seasonality. The sum of all individual sources is shown in black (and equals the seasonal $CH_4$ cycle shown in Figure 3.18). For $\delta^{13}C$ and $\delta D$ the contribution of the individual sources is given in Figure 3.19 b and 3.19 c as:

$$[\delta_j(t) - \delta_{avg}] * f_j(t) - const \tag{3.4}$$

with $\delta_j(t)$ representing the modeled isotopic signature of source $j$ at the observational site at time $t$ (as determined by the original isotopic signature of the emission and the KIEs of the sinks during the transport to Izaña), $\delta_{avg}$ the annual mean value of the total $\delta$ at the station, $f_j(t)$ the relative contribution of source $j$ (as determined from modeled $CH_4$ mixing ratios) and *const* an offset chosen so that the integral over (3.4) becomes zero. Again, the sum of the individual sources is shown in black. For $\delta^{13}C$ , the most prominent seasonal cycle is seen for bogs, with an overall amplitude of about 50 % of the total seasonal $\delta^{13}C$ cycle. This large influence is mainly due to the significantly increasing $CH_4$ mixing ratios from this source in autumn (Figure 3.18 a), combined with its relatively low $\delta^{13}C$ (a posteriori $\delta^{13}C = -64.2 \pm 2.8$ ‰). As for $CH_4$ mixing ratios, a significant contribution to $\delta^{13}C$ also arises from rice paddies. In contrast to $CH_4$, however, biomass burning exhibits a much more pronounced influence, due to its very enriched $\delta^{13}C$ values. This component has indeed

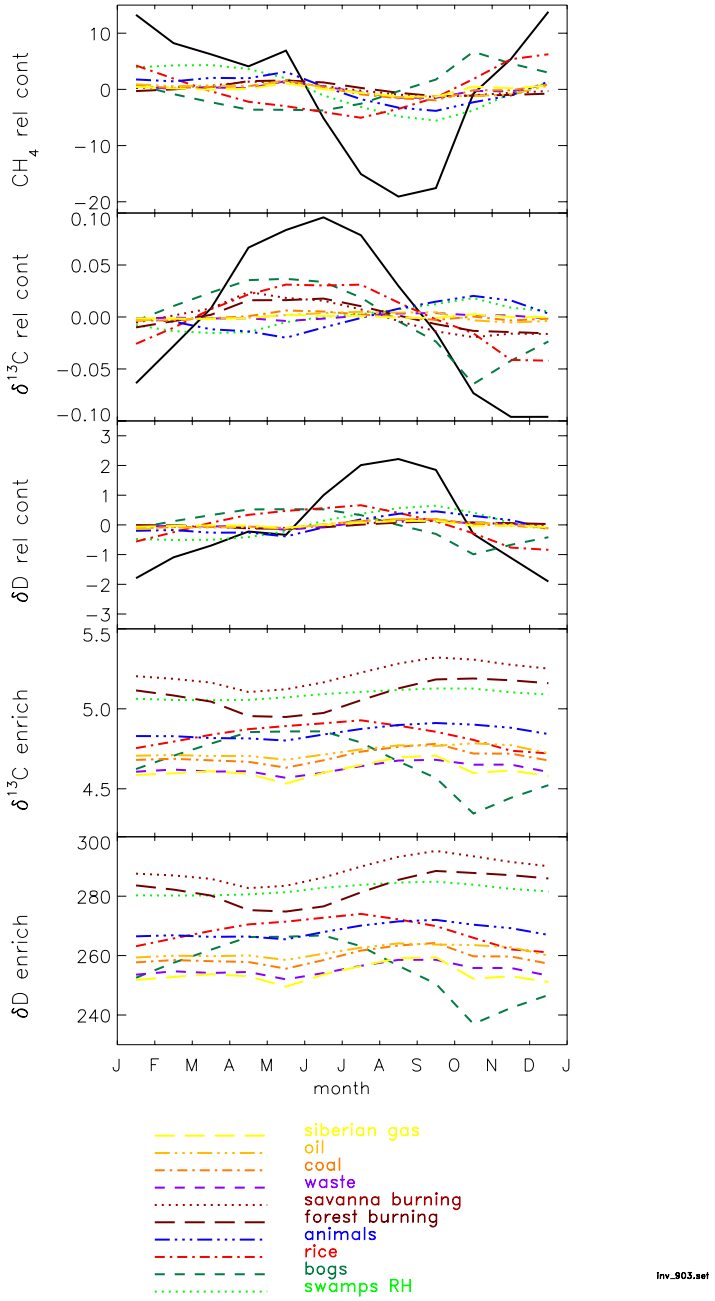


**Figure 3.19:** Contribution of the different sources to the modeled seasonal cycles [Bergamaschi et al., 2000a] of (a) $CH_4$ mixing ratios, (b) $\delta^{13}C$, and (c) $\delta D$. The black curves represent the sums of the individual sources and equal the seasonal cycles shown in Figure 3.18. (d) $\delta^{13}C$ enrichment of $CH_4$ from the individual sources. (e) $\delta D$ enrichment of $CH_4$ from the individual sources.

a significant impact on the overall $\delta^{13}C$ seasonality. Test runs performed with the biomass burning source strength set to zero showed a $\delta^{13}C$ maximum only one month prior to the $CH_4$ minimum. In contrast to $\delta^{13}C$ , the relative influence of biomass burning is much weaker on $\delta D$, while again bogs and rice paddies constitute the two sources with the largest impact. The results shown in Figure 3.19 refer to an inversion with an a posteriori $\delta D$ value from biomass burning of $-203 \pm 20$ ‰. In general, the behavior of the individual sources and the overall $\delta D$ seasonal cycles largely mirrors the behavior seen for $CH_4$ mixing ratios.

Finally, in Figure 3.19 the isotopic enrichment in the $CH_4$ of the individual sources (corresponding to equation 4.1 in 4.5) can be seen, reflecting the integrated influence of the sinks (i.e. mainly OH) during the transport from the source areas to the station (Figure 3.19). $CH_4$ from savanna burning undergoes the strongest isotopic enrichment on its way from the tropical emission regions (with high OH concentrations) to Izaña. In contrast, $CH_4$ from fossil sources and landfills exhibit a relatively week isotopic enrichment, since it encounters less OH during its transport from mid latitudes of the northern hemisphere to Izaña. The largest seasonal cycle is evident for bogs, with the emission peak in late summer constituting a source of fresh (i.e. little enriched) $CH_4$, which later undergoes significant isotopic enrichment.

## 3.6 Conclusion

Izaña is located at 28° N, where trace gases, such as $CH_4$ and $SF_6$ exhibit large latitudinal gradients. Furthermore, Izaña is directly influenced by sources from the North American continent, and to a lesser extent by European sources. Consequently, atmospheric $CH_4$ mixing ratios show considerable variability, with short term synoptic scale variations often exceeding the mean seasonal cycle. In order to define the mean seasonal cycle, continuous air sampling proved to be very helpful, while exclusive spot sampling at a 2-week frequency would provide an only fragmentary picture at this station. Significant seasonal cycles of $\delta^{13}C$ and $\delta D$ were detected, with peak-to-peak amplitudes of 0.2 ‰ and 3.5 ‰, respectively. $\delta^{13}C$ shows a significant phase shift with respect to $CH_4$ mixing ratios, resulting in an 'elliptical' behavior in the phase diagrams, attributed to a seasonally varying source mixture. In contrast, $\delta D$ showed a compact correlation with inverse $CH_4$ mixing ratios, allowing an estimate of the average KIE of atmospheric sinks of $1.23 \pm 0.04$. This apparent KIE is consistent with recent measurement of the KIE in the $CH_4$ + OH reaction [Saueressig, 1999], resulting in an average KIE of $1.28 \pm 0.01$, when corrected for a small influence of the soil sink. Application of an 3-D inverse model allowed an excellent reproduction of

observed mean seasonal cycles of $CH_4$, $\delta^{13}C$ , and $\delta D$, including their phase behavior. Thus the isotopic information (atmospheric records, source signatures, and kinetic isotope effects of the sinks) can be regarded as consistent with our present knowledge of the atmospheric $CH_4$ cycle and its description in the model. Visualization of the contribution of the individual sources showed the significant influence of bogs and rice paddies on $CH_4$, $\delta^{13}C$ , and $\delta D$ at Izaña, and in addition a significant influence of biomass burning on $\delta^{13}C$ . Observed short term variations of $CH_4$ mixing ratios could be clearly linked to changing synoptic situations, leading to the advection of very different air masses. Further evidence for the influence of transport on $CH_4$ mixing ratios arose from the significant correlation between $CH_4$ and $SF_6$ residuals. The American continent and Europe act as significant $CH_4$ and $SF_6$ sources, while air masses from Africa and the North Atlantic usually showed depleted mixing ratios of these trace gases. Isotope analysis helped to identify different $CH_4$ sources such as the Canadian wetlands or the industrialized regions of the United States and Southeastern Canada. At stations as Izaña, which are subject to direct influence from sources and sinks, measurements of short term variations may be utilized to infer integrated sources or sink strengths, when combined with high resolution atmospheric transport models with an exact model meteorology for the time period of observations.

# Chapter 4

# Seasonal cycles of atmospheric CO

In this chapter we present the Izaña records of CO and its isotopes, $\delta^{13}C$, $\delta^{18}O$ and $^{14}CO$, from July 1996 to August 1999. These are the first long term records of the isotopic composition of CO at subtropical latitudes. We infer seasonal cycles as well as interannual variations of CO mixing and isotopic ratios for the three-year period analyzed during this research period. Air masses sampled at Izaña have a wide range of latitudinal and longitudinal origins (chapter 3). We therefore use back-trajectories to discuss the large synoptic scale variations encountered for CO and its isotopes. Most of the time clean tropospheric conditions are encountered at the Izaña observatory.

The Izaña records of the stable CO isotopes, $\delta^{13}C$ and $\delta^{18}O$, have been used together with CO isotope records from four other globally distributed stations in an inverse model study by Bergamaschi et al. [2000b]. Through optimization of the agreement between modeled and measured mean annual CO mixing and isotopic ratios, estimations of the CO budget as well as the isotopic signature of different CO sources have been improved. The main results of this study concerning the Izaña records are summarized in section 4.5.

Finally we compare the Izaña records to CO isotope measurements done at a number of other stations. At Spitsbergen, a remote station at high northern latitude, CO isotope measurements have already started in 1995. We also use CO isotopes records from UBA Schauinsland, Germany, and Sonnblick, Austria, which are representative for continental stations at mid latitudes. In contrast more polluted air masses have been encountered at Kollumerwaard, The Netherlands, and during the BERLIOZ campaign in summer 1998, for which CO, $\delta^{13}C$, $\delta^{18}O$ and $^{14}CO$ have been investigated.

## 4.1 Atmospheric CO mixing ratios at Izaña

The meteorological situation of the Izaña station has been discussed in detail in the previous chapter. Its location on the Island of Tenerife at 2370 m altitude allows the sampling of air from the free troposphere, especially during night time when inversion layers shield the observatory from the marine boundary layer and locally polluted air masses from the island. We consider the seasonal cycles and annual trends derived from our three-year record of atmospheric CO and its isotopes (section 4.1 to 4.4) to be representative for the subtropical North Atlantic. The large synoptic scale variations occurring in the spot sample measurements are classified with the help of their corresponding back-trajectories. We smooth the data sets for CO mixing ratios, $\delta^{13}C$ , $\delta^{18}O$ and $^{14}CO$ (based on the spot and 2-week-continuous samples) by applying a low pass convolution filter in the frequency domain (by Fast Fourier Transformation (FFT)). Both the classification of spot samples and the FFT fits are done in the same way as for $CH_4$ in the previous chapter. The 3-year record of CO mixing ratios measured on spot and continuous samples are shown in Figure 4.1. The spot samples are attributed to five different sectors as discussed in section 3.2.2, e.g. the American continent, Europe, Africa and the North Atlantic (low and high latitudes). A FFT fit with a filter of four weeks (see equation 3.1) is applied to both data sets of CO mixing ratios, e.g. our spot and continuous samples. With the help of these fit curves we discuss the seasonal cycles and inter-annual trends observed over the three years of our analysis. While both fits display a similar picture for the evolution of CO mixing ratios, some differences are also apparent.

Comparing the fits through our spot and continuous samples it is remarkable that, despite of the large degree of variability of the spot samples, the two fits agree very well from November 1996 to February 1998. Only during spring 1998 fit curves differ by 15 nmol/mol because of spot samples with very low CO mixing ratios while no spot samples with higher mixing ratios than the continuous samples have been encountered. Flasks sampled in June/July 1998 by the NOAA/CMDL network (discussed below) captured events of significantly higher ($\Delta$ CO >30 nmol/mol) CO mixing ratios. This explains the consistently higher CO mixing ratios of the continuous samples compared to our spot samples during this period.

From July to October 1998 a significant contamination of the continuous samples of up to 15 nmol/mol was observed. For these samples problems have occurred during the transfer of the air sample from the bags into the cylinders (see section 2.1.4). In Figures 4.1 to 4.10 these contaminated continuous samples are labeled. They are omitted in the calculation of FFT fit curves. In November 1998 the filling

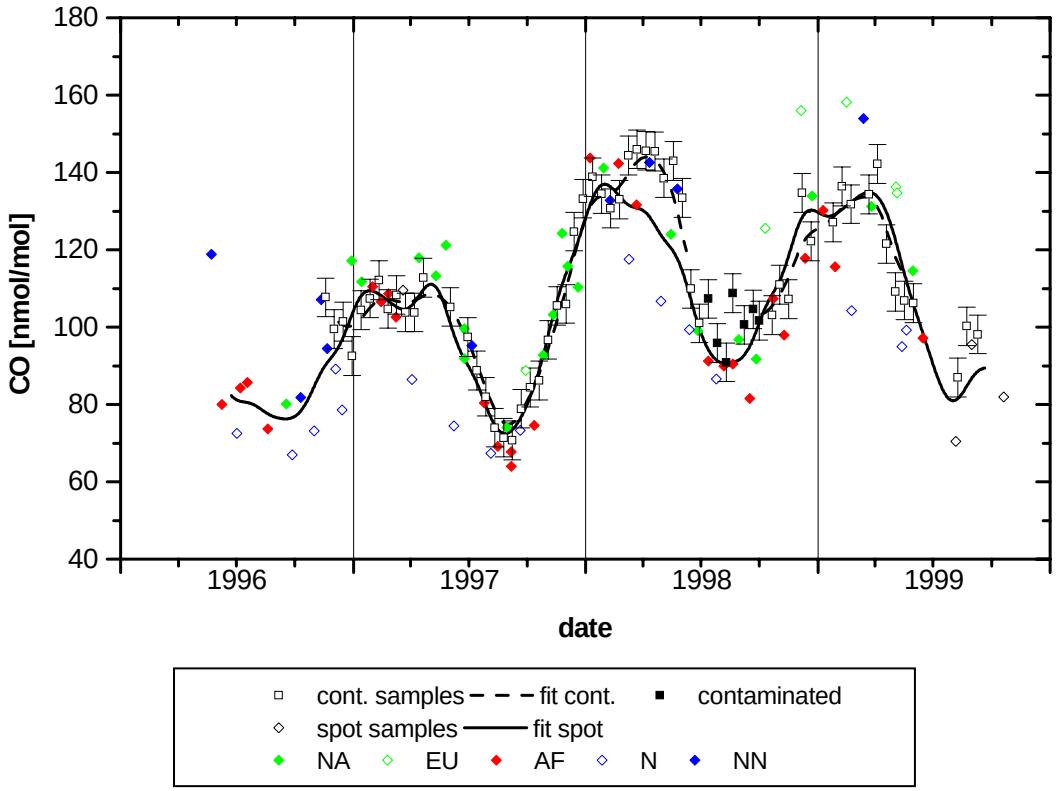


**Figure 4.1:** Record of CO mixing ratio at Izaña. 2-week-continuous samples and spot samples are shown together with fit curves (FFT with a 4-week filter). With the help of back trajectories the spot samples are attributed to five sectors: North America (NA), Europe (EU), Africa (AF) and North Atlantic (low (N) and high (NN) latitudes).

procedure of the continuous samples has been checked and the agreement between the fit curves calculated for spot and continuous samples is again very good. We note that the motivation for taking continuous samples at Izaña was to enable us to extract background values at this station which is known for its large synoptic scale variations. The good agreement between background CO values derived from continuous and spot samples with the help of the FFT fits was unexpected. Thus background CO mixing ratios representative for the subtropics can be inferred from spot samples (taken biweekly) after an appropriated smoothing of the data. For the following discussion of the seasonal cycles, synoptic scale variations and annual trends we will refer to the FFT fit through our spot samples.

### 4.1.1 Seasonal cycles and interannual variations

The seasonal cycle of CO mixing ratios with its minimum in late summer and its maximum during winter/spring is mainly due to the seasonality of its main sink, i.e. oxidation by OH. The high OH concentrations during summer reduce the lifetime of CO to a few weeks compared to an average lifetime of two to three months during winter.

For the three-year period of our study significant interannual variations were encountered. During the maximum in winter/spring 1997/1998 and the minimum in late summer 1998 CO mixing ratios were above the corresponding values one year earlier by 30 nmol/mol and 20 nmol/mol respectively. This strong increase in CO mixing ratios is not maintained during the third seasonal cycle. The maximum in late 1998 and early 1999 with around 130 nmol/mol and the minimum in late summer 1999 with 70-80 nmol/mol are closer to the values before 1998. The calculated trend of the CO mixing ratio for the period from June 1996 to June 1999 is +9.1±4.8 %/yr(derived from the running mean through the FFT fit). This very high trend of the CO mixing ratio is mainly due to the huge increase between 1997 and 1998.

The strong interannual variations in the seasonal cycles are also reflected in the corresponding peak-to-peak amplitudes. The amplitudes of the seasonal cycles in 1996/1997 and 1997/1998 nearly increased by a factor of two, from $\sim$ 35 nmol/mol to $\sim$ 70 nmol/mol respectively. In the following section 4.2 we discuss possible scenarios explaining the exceptionally high CO growth rates in 1998.

### 4.1.2 Comparison to NOAA/CMDL CO measurements

We compare our three year record of CO mixing ratios to measurements from the NOAA/CMDL monitoring network starting at Izaña in 1991 [Novelli et al., 1998a]. Both data sets are shown in Figure 4.2 together with their respective FFT fit curves (four-week filter). Based on the FFT fit curves we note the general good agreement between both data sets. Some discrepancies are nevertheless apparent which could reflect a difference in the reference scales as well as the natural variability of CO mixing ratios due to the large synoptic scale variations at Izaña occurring on time scales of less than 24 h. The MPI samples and the NOAA/CMDL samples have not been collected at the same time. A direct inter-comparison between our spot samples and the NOAA/CMDL flasks is therefore questionable even for the few occasions on which they were both taken on the same day. During the winter/spring plateaus differences between the two fits are mainly due to the variability of mixing ratios of

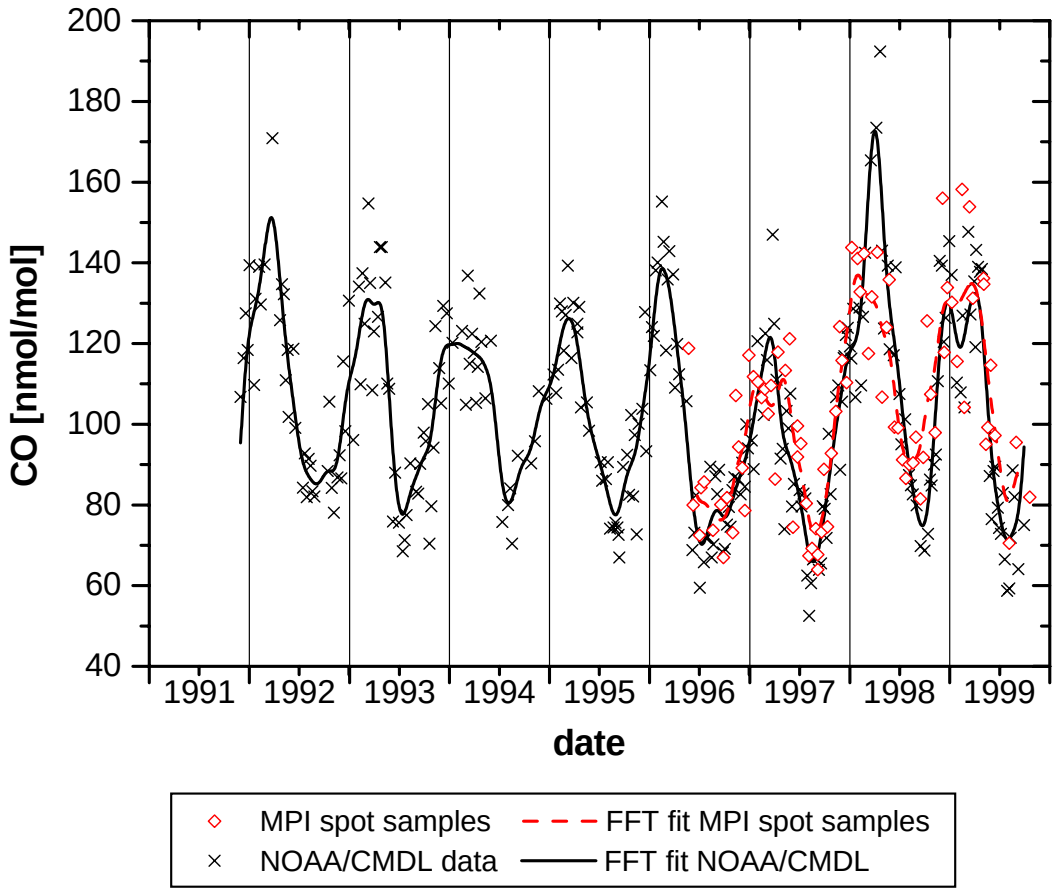


**Figure 4.2:** Records of CO mixing ratios at Izaña. MPI spot samples and measurements from the NOAA/CMDL monitoring network are plotted together with fit curves (FFT with a 4-week filter).

up to 40 nmol/mol seen in both data sets.

It is, however, apparent that for all four summer minima the NOAA/CMDL flasks are on average lower. We compared the FFT fits from both data sets for the four summer periods between June and October (1996-1999). On average the FFT fit through the NOAA/CMDL measurements lies 7.7%±3.8% below the fit through the MPI data. Thus from this three year inter-comparison of CO mixing ratios no systematic difference appears in the 100-170 nmol/mol range whereas there is a clear difference in the 50-100 nmol/mol range. This confirms results from two laboratory inter-comparison organized by NOAA/CMDL in 1994 and 1999 [Novelli et al., 1994] [Brenninkmeijer et al., 2000]. In this inter-comparison CO mixing ratios based on relative measurements using NOAA/CMDL standards have been consistently lower by 8.2% in the 50 nmol/mol range than absolute measurements of CO mixing ratios at NIWA [Novelli et al., 1998a] and MPI [Brenninkmeijer et al., 2000]. The drift in

the NOAA CO scale is discussed in Masari et al. [2000].

Novelli et al. [1998a] reported for the globally-averaged CO mixing ratio a decrease of approximately 2 nmol/mol $yr^{-1}$ in the long term trend for the period from 1990 through 1995. The reasons for this decrease in mixing ratios in the background atmosphere are not yet fully understood (see section 1.6). The period of decreasing CO mixing ratios is also seen in the Izaña record shown in Figure 4.2. Thus the large increase of CO mixing ratios in 1998 observed in our study has been exceptional for the 1990s and marked a change in the previously decreasing growth rates.

### 4.1.3 Synoptic scale variations

The synoptic scale variations of the spot samples which have already been discussed for the $CH_4$ mixing ratios (section 3.2.2) are also significant for CO. During all three winters subsequently taken spot samples can differ by more than 40 nmol/mol. These large variations in CO mixing ratios often reflect the impact of source regions, as can be seen from the corresponding back-trajectories. We note, however, that the latitudinal gradient in CO mixing ratios reaches its maximum during winter. This effect is seen for two samples taken on the 12th and 24th of April in 1998 which differ by 40 nmol/mol. While the air of the first sample came from the high North Atlantic (>60° N), air masses for the second traveled for several days between 20° and 40° N. Their mixing ratios of 140 nmol/mol and 100 nmol/mol are close to background values for their respective latitudinal origin (see Figure 1.6 in section 1.7.1).

As the latitudinal gradient in CO mixing ratios is smaller during summer, synoptic scale variations are less pronounced. Still mixing ratios of subsequent samples can differ by more than 10 nmol/mol. We note that samples of African or low North Atlantic origin are far more frequent during the summer months (70% from sectors AF and N during June-October for the years 1996-1998), than samples attributed to the Northern sectors, e.g. NA, NN and EU. This pattern is confirmed by the statistical analysis of AEROCE back-trajectories for the years 1991 to 1997 done by Schäfer [1997]. The main results of this study have been summarized in section 3.1.2. Figure 3.2 shows that the influence from the North American continent on air masses reaching Izaña is less important from June to October than for the winter and spring months. Under most conditions the Izaña station is meteorologically separated from Europe [Armerding et al., 1997]. Only during few episodes do we see the impact of European emissions (mainly in winter/spring 1998/1999).

In order to quantify the synoptic scale variations we calculate the residuals ($\Delta$ CO) of the spot samples. As defined in section 3.2.2 we calculate the difference between measured mixing ratios and the value of the FFT fit curve (representing

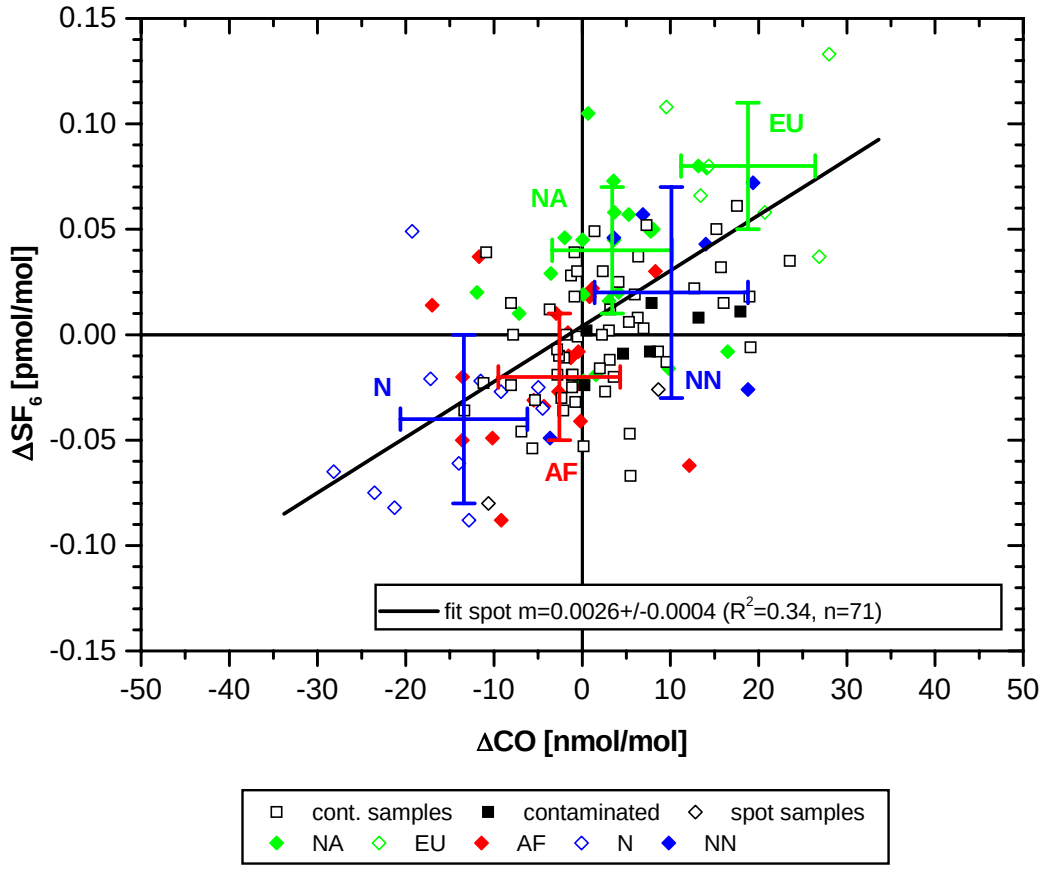


**Figure 4.3:** CO residuals versus $SF_6$ residuals for spot and 2-week-continuous samples. A linear fit through the spot samples is applied. The average values ($\pm 1\sigma$ range) for samples from North America (NA), Europe (EU), Africa (AF) and North Atlantic (low (N) and high (NN) latitudes) are also indicated (according to Table 4.1).

the mean annual cycle) at the time of sampling. In table 4.1 the $\Delta$ values for CO and $SF_6$ mixing ratios are listed for spot samples from the different sectors. The residuals calculated for $\delta^{13}C$ , $\delta^{18}O$ and $^{14}CO$ are also given and will be discussed in the following sections. We plot the $\Delta SF_6$ against the $\Delta CO$ residuals in Figure 4.3 and a clear relationship between the origin of air masses from one of the five sectors and the residuals is apparent.

The enhancements/depletions are directly linked to the source/sink strengths in the respective sectors. As in the case of $CH_4$ and $SF_6$, North America and Europe act as a CO source, while air masses from the North Atlantic (0° to 50° N) and Africa are generally depleted, largely due to dilution and also to some extent due to chemical destruction. The simplified calculation of trace gas fluxes done in section

| | $\Delta$ CO [ nmol/mol ] | $\Delta\ \delta^{13}$C [ ‰ ] | $\Delta\ \delta^{18}$O [ ‰ ] | $\Delta\ ^{14}$CO [ molec./cm$^3$ ] | $\Delta$ SF$_6$ [ pmol/mol ] | n |
|---|---|---|---|---|---|---|
| NA | $+3.4 \pm 6.8$ | $+0.3 \pm 0.5$ | $+0.6 \pm 0.8$ | $+0.6 \pm 1.0$ | $+0.04 \pm 0.03$ | 22 |
| EU | $+18.8 \pm 7.6$ | $+0.4 \pm 0.3$ | $+2.2 \pm 0.7$ | $+2.4 \pm 1.6$ | $+0.08 \pm 0.03$ | 6 |
| AF | $-2.6 \pm 6.9$ | $-0.2 \pm 0.4$ | $-0.4 \pm 1.0$ | $-0.3 \pm 0.8$ | $-0.02 \pm 0.03$ | 25 |
| N | $-13.4 \pm 7.2$ | $-0.5 \pm 0.5$ | $-1.8 \pm 1.0$ | $-2.6 \pm 1.5$ | $-0.04 \pm 0.04$ | 16 |
| NN | $+10.1 \pm 8.7$ | $+0.2 \pm 0.5$ | $+1.5 \pm 1.2$ | $+2.7 \pm 1.3$ | $+0.02 \pm 0.05$ | 8 |

**Table 4.1:** Residuals of CO mixing and isotopic ratios together with SF$_6$ residuals for spot samples. The average $\Delta$ values are given together with $\pm 1\sigma$ standard deviations and the number of samples n from North America (NA), Europe (EU), Africa (AF) and North Atlantic (low (N) and high (NN) latitudes).

3.2.2 (average residence time of 1 to 3 days over the source region and a mixing height of 1 to 12 km) gives for CO residuals of 10 nmol/mol a corresponding source strength of 1.2 to 5.8 mg CO m$^{-2}$ h$^{-1}$.

Both effects, the influence of source regions of the North American and European continent and the latitudinal gradients for CO mixing ratios lead to the observed correlation of CO and SF$_6$ residuals. For the regression through the spot samples (Figure 4.3) we obtain a slope of $+0.0026 \pm 0.004$ pmol/mol SF$_6$ ( nmol/mol CO)$^{-1}$ (R$^2$=0.34, n=34). With the extremely different lifetimes of SF$_6$ and CO it is not surprising that the ratio between both interhemispheric gradients can vary between 0.002 and 0.01 pmol/mol SF$_6$ ( nmol/mol CO)$^{-1}$ during winter and summer respectively.

## 4.2 Atmospheric $\delta^{18}$O record from Izaña

Three annual cycles of the isotopic composition of atmospheric CO have been measured at Izaña during this thesis. In Figure 4.4 the $\delta^{18}$O record is shown. Again FFT fits (with a 4-week filter) are applied through the 2-week-continuous samples and spot samples.

### 4.2.1 Seasonal cycles and interannual variations

For $\delta^{18}$O we observe a similar seasonal cycle as for the CO mixing ratios. The minima and maxima during winter/spring and summer respectively are in phase with the CO mixing ratios. The $\delta^{18}$O cycle is mainly driven by the OH seasonality and the heavy technological source ($\delta^{18}$O value of +23.5 ‰ [Stevens & Krout, 1972] and

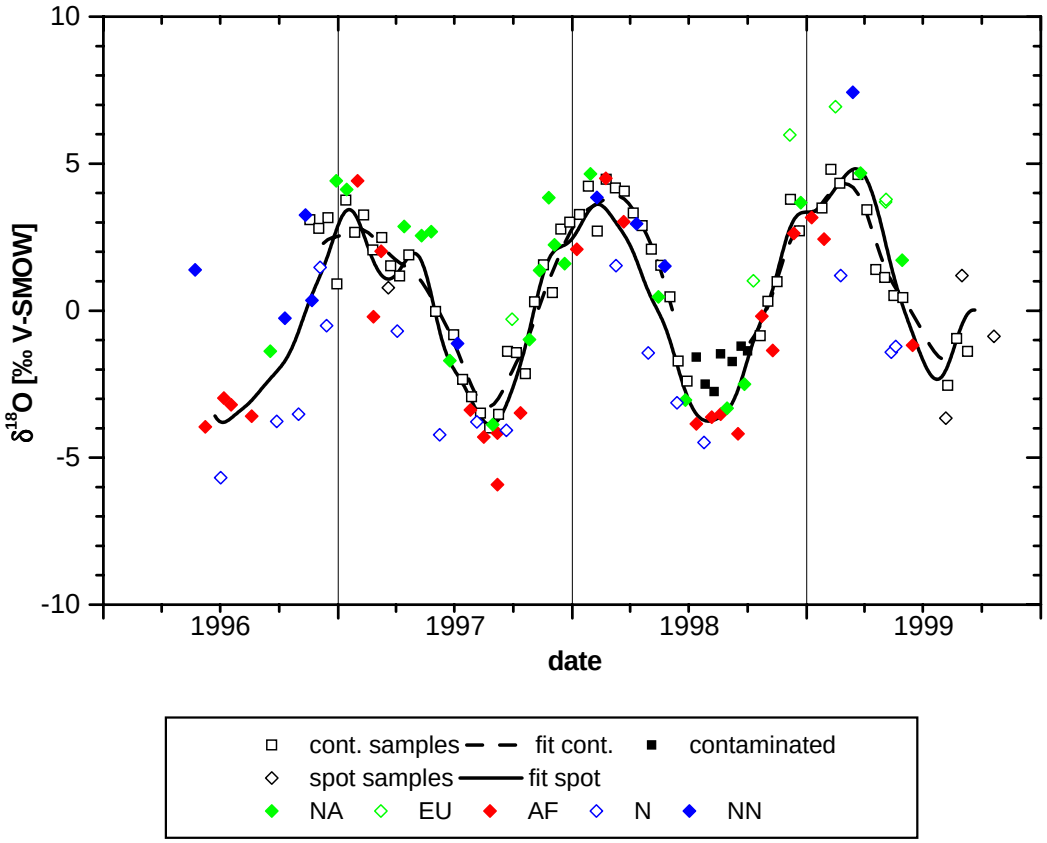


**Figure 4.4:** Record of $\delta^{18}$O (CO) at Izaña. 2-week-continuous samples are shown together with spot samples and fit curves (FFT with a 4-week filter). With the help of back trajectories the spot samples are attributed to five sectors: North America (NA), Europe (EU), Africa (AF) and North Atlantic (low (N) and high (NN) latitudes).

[Brenninkmeijer, 1993]). The fit through the spot samples indicates a large seasonal cycle with a peak-to-peak amplitude close to 8 ‰. In the summer months $\delta^{18}$O values reach $-4$ ‰, while single samples can be as light as $-6$ ‰. During high OH levels the large inverse kinetic isotope effect (KIE) of $\sim -10$ ‰ [Röckmann et al., 1998c] leads to a preferential removal of the $C^{18}O$ isotopomer. Thus a $\delta^{18}$O minimum is induced near the maximum in OH levels. In January/February the seasonal $\delta^{18}$O cycle peaks around values of 3-5 ‰ for the fits and 4-7 ‰ for single spot samples. During this period of low OH levels the heavy technological source builds up in the Northern Hemisphere leading to enhanced $\delta^{18}$O values.

While no trend appears in the minima from 1996 to 1998 (not enough samples have yet been analyzed for summer 1999) the maxima are getting progressively enriched throughout the three-year period. The annual $\delta^{18}$O trend inferred from

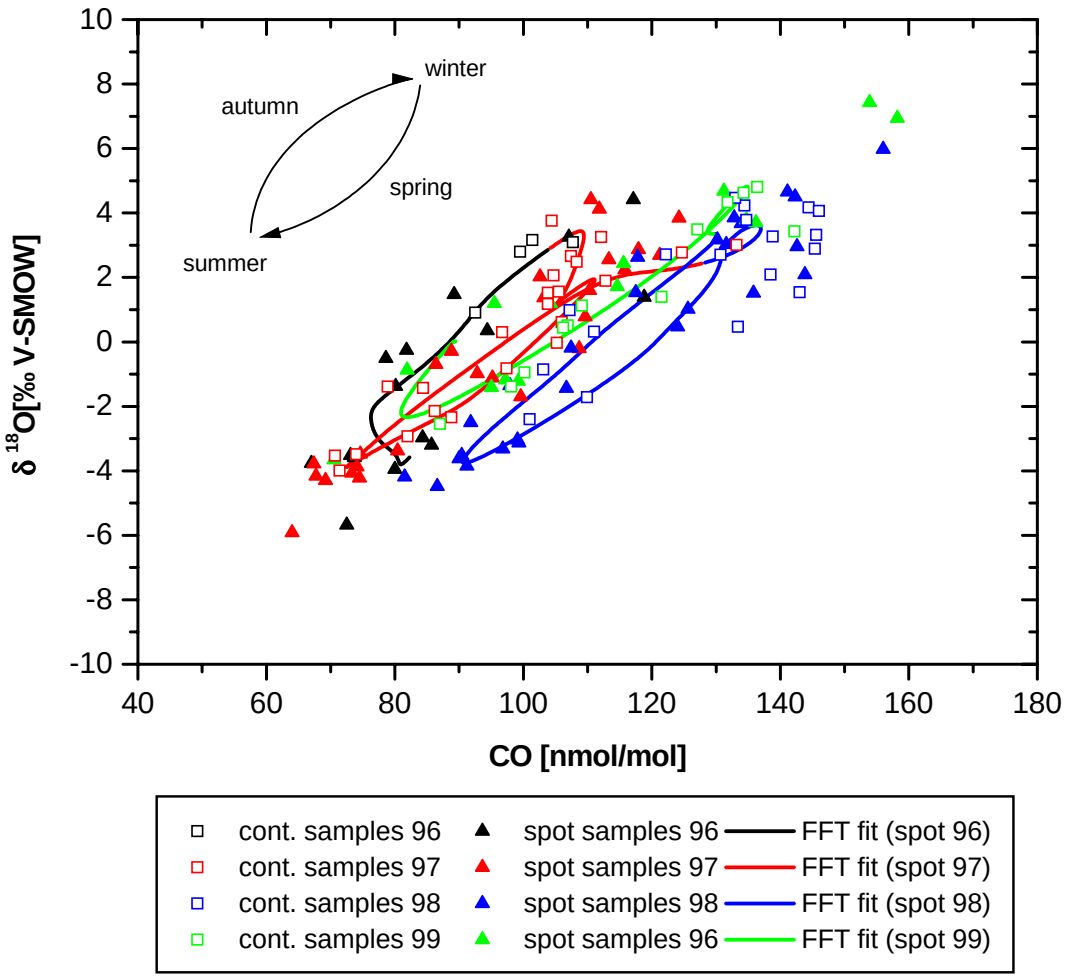


**Figure 4.5:** $\delta^{18}$O values for continuous and spot samples are plotted against CO mixing ratios. The samples and calculated FFT fit curves (spot samples) are labeled for the four different years 1996 to 1999.

the FFT fit through the spot samples for the period of June 1996 to June 1999 is $+0.43 \pm 0.40$ ‰ yr$^{-1}$. No significant difference between the fit curves through the smooth record of continuous samples and the by far more scattered spot samples can be observed in Figure 4.4. The contaminated continuous samples in summer 1998 (see previous section) are not included in the fit calculation.

In Figures 4.5 the $\delta^{18}$O values of the continuous and spot samples are plotted against CO mixing ratios. We differentiate between samples of the four years 1996 to 1999 of our study. The FFT fit curve calculated for the spot samples is also shown for the four different years.

The apparent correlation between CO mixing ratios and $\delta^{18}$O underlines the

similarity of the two seasonal cycles. Nevertheless, we observe an ellipsoid-shaped curve for a given year. The transitions from winter to summer and summer to winter are slightly different. For a given CO mixing ratio, the corresponding $\delta^{18}O$ values are 1 to 2 ‰ lower in spring than in autumn. This implies a small phase shift between the two seasonal cycles, caused either by a seasonality of CO and $\delta^{18}O$ sources or sinks. In section 4.5 the underlying reason for this small phase shift between CO and $\delta^{18}O$ will be discussed together with results obtained by the inverse CO model study [Bergamaschi et al., 2000b].

The other interesting feature in Figure 4.5 are the observed interannual differences. It has already been apparent in the seasonal cycles shown in Figures 4.1 and 4.4 that CO mixing ratios and $\delta^{18}O$ variations were very different in 1998 compared to 1997 and 1999. In Figure 4.5 the positive trend towards higher CO mixing ratios from 1996 to 1998 can be seen, while values for 1999 are closer to those from 1997. For $\delta^{18}O$ this results in approximately 2 ‰ lower $\delta^{18}O$ values for a given CO mixing ratio in 1998 compared to 1997 or 1999. With the simple 1-box model presented in section 1.6 we calculated the change in OH concentrations necessary for a 1 ‰ decrease in $\delta^{18}O$ . Assuming OH concentration of $10^6$ molec./cm$^3$, OH levels would need to increase by 15% in order to explain the observed shift. With present interannual OH variations supposedly of the order of $\sim 0.5\%$ [Krol et al., 1998] the more than 2 ‰ lower $\delta^{18}O$ values of 1998 relative to 1997 and 1999 can not be explained by a change in the sink process. Thus an important change in CO sources is a more likely explanation for our observations.

The most plausible explanation are the intense biomass burning events occurring in late 1997 and early 1998 in the tropics [Levine, 1999]. The atmospheric disequilibrium caused by this sudden increase in source activity could explain why unusually high CO mixing ratios have been measured up until the minimum of the seasonal cycle in 1998. Even if the source signature of biomass burning is around +10 ‰, high OH levels in the tropics would reduce the original high $\delta^{18}O$ values due to the inverse KIE of −10 ‰. Nevertheless, the same feature of lower $\delta^{18}O$ values for a given CO mixing ratio in 1998 have also been observed at higher latitudes (at the Sonnblick observatory in Austria (47° N, 13° E) [Gros et al., 2000] and at Spitsbergen (79° N, 12° E) [Röckmann et al., manuscript in preparation]). Even intense biomass burning events in the tropics cannot account for the observed increase of nearly 30 nmol/mol in the CO mixing ratios at Spitsbergen during the summer minimum from 1997 to 1998 (see section 4.6). Thus also emissions from the biomass burning source at higher latitudes (>30° N) which can significantly fluctuate from one year to the other [Dywer & Gregoire, 1998] should be considered.

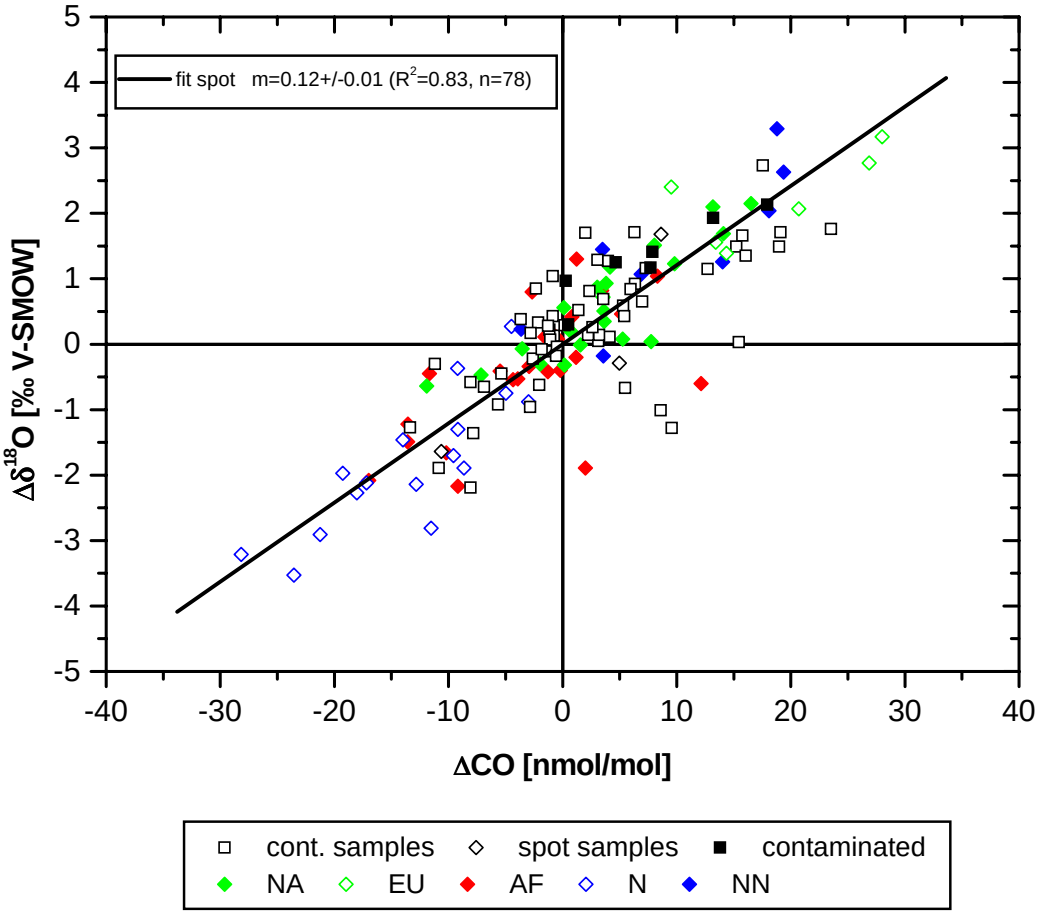


**Figure 4.6:** Residuals calculated for CO mixing ratios and $\delta^{18}O$ for continuous and spot samples are plotted together with respective linear fits. With the help of back trajectories the spot samples are attributed to five sectors: North America (NA), Europe (EU), Africa (AF) and North Atlantic (low (N) and high (NN) latitudes).

### 4.2.2 Synoptic scale variations

Next, we address the significant synoptic scale variations in $\delta^{18}O$ that can exceed 2 ‰ during summer and 5 ‰ during winter/spring. The reason for the large variations during maximum $\delta^{18}O$ values in January to March are similar to those already discussed for CO mixing ratios in the previous section. The latitudinal gradient for $\delta^{18}O$ is largest during this period (see Figure 4.16), with typical values of 2 ‰ at low latitudes and $\sim$ 8 ‰ at high latitudes of the Northern Hemisphere [Bergamaschi et al., 2000b]. In Table 4.1 the $\Delta\delta^{18}O$ residuals for air samples from the different sectors are given and are plotted against $\Delta$CO mixing ratio residuals in Figure 4.6.

Again a clear relationship exists between the origin of air masses from one of the five sectors and the residuals. Air masses from low latitudes, e.g. low North Atlantic (N) and Africa (AF), are considerably depleted by $-1.8 \pm 1.0$ ‰ and $-0.4 \pm 1.0$ ‰ respectively. In contrast, air masses from the North (North American continent (NA), Europe (EU) and the high North Atlantic (NN)) are significantly enriched by $+0.6 \pm 0.8$ ‰, $+2.23 \pm 0.7$ ‰ and $+1.5 \pm 1.2$ ‰ respectively. These enhancements/depletions are directly linked to the source/sink strength in the respective regions. The positive $\Delta\ \delta^{18}$O residuals from Northern source regions are due to the (dominating) heavy technological source. In contrast, in the tropical and subtropical regions, apart from biomass burning, light sources dominate and are further depleted in the OH sink process. For the regression through the spot samples we obtain a slope of $+0.121 \pm 0.006$ ‰/ nmol/mol ($R^2$=0.83, n=78). This is close to values calculated from North hemispheric CO and $\delta^{18}$O gradients for summer (~20 nmol/mol, ~3 ‰) and winter (~60 nmol/mol, ~6 ‰) of $0.15 \pm 0.02$ ‰ (nmol/mol)$^{-1}$ and $0.1 \pm 0.2$ ‰ (nmol/mol)$^{-1}$ respectively. Thus for air masses of varying latitudinal origin the strong latitudinal CO and $\delta^{18}$O gradients at the latitude of Izaña lead to highly correlated variations of these tracers.

## 4.3 Atmospheric $\delta^{13}$C record from Izaña

The main characteristics of the $\delta^{13}$C record shown in Figure 4.7 are the relatively smooth records for continuous and spot samples compared to those from CO mixing ratios and $\delta^{18}$O . On the other hand, large differences are observed for the position of the summer minima over the 3-year period. We note that, despite of the good agreement between the FFT fits through the spot and continuous samples, the four week filter does not catch the sharp summer minima as well as desirable. For the calculation of the seasonal $\delta^{13}$C amplitudes and trends we therefore use a FFT fit with a 2-week filter through the spot samples .

### 4.3.1 Seasonal cycles and interannual variations

As for CO and $\delta^{18}$O , the $\delta^{13}$C cycle is controlled by source and sink processes. However, in contrast to the $\delta^{18}$O cycle where the dominant (technological) source and the KIE of the OH sink are in phase, the two major contributions to the $\delta^{13}$C cycle partly attenuate each other. On the source side the extremely depleted methane oxidation source ($\sim -52$ ‰) leads to the sharp summer minima when its relative contribution to CO levels is highest [Bergamaschi et al., 2000b]. On the sink side the positive KIE (+2 ‰ at 500 hPa and +5 ‰ 1000 hPa [Stevens et al., 1980]) forces

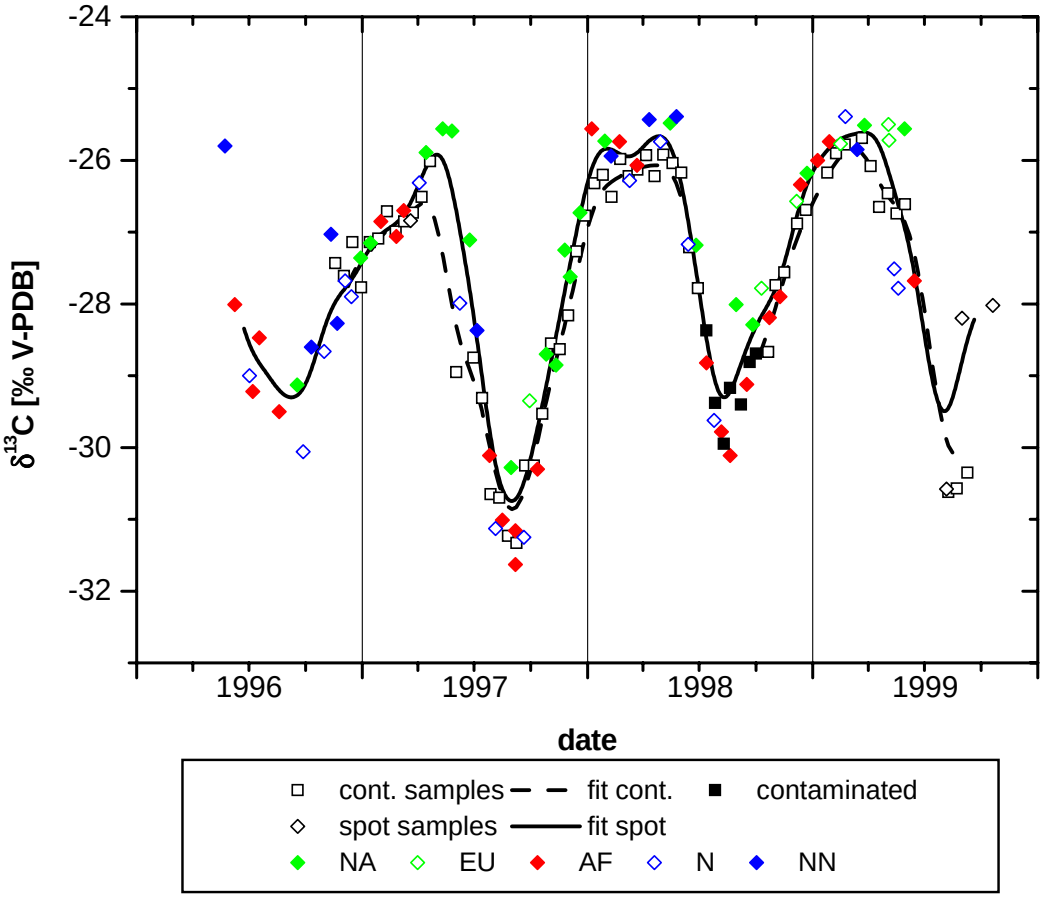


**Figure 4.7:** Record of $\delta^{13}$C (CO) at Izaña. 2-week-continuous samples are shown together with spot samples and fits (FFT with a 4-week filter). With the help of back trajectories the spot samples are attributed to five sectors: North America (NA), Europe (EU), Africa (AF) and North Atlantic (low (N) and high (NN) latitudes).

$\delta^{13}$C towards higher values in spring/summer. These effects were best seen in 1997. First, $\delta^{13}$C values seemed to stabilize in February/March around $-27$ ‰. Second, in April/May a short positive dip of nearly 1 ‰ is apparent for both spot and continuous samples. This is attributed to the positive KIE when OH levels start to rise in spring. Third, the sharp decrease of more than 5 ‰ over the summer months led to minimum values in September 1997 of less than $-31$ ‰. While the absolute contribution from the very light methane oxidation source stays more or less constant over the year, its relative contribution to CO mixing ratios increases significantly during summer and causes the sharp decrease in $\delta^{13}$C. Finally, during autumn and winter $\delta^{13}$C values increase again by nearly 6 ‰ until they reach the winter/spring plateau of $\sim -26$ ‰. During this time the enhanced atmospheric lifetime of CO (when OH levels decrease)

leads to a piling up of CO from the important sources of the Northern Hemisphere which have $\delta^{13}$C signatures of close to $-27$‰.

For 1998, the situation is somewhat different. During the first five months $\delta^{13}$C values stabilized around $-26$‰ before they reached the summer minimum slightly earlier and at 1.5‰ higher values than 1997. For 1999, not all samples are yet analyzed but a huge seasonal cycle (comparable to the one in 1997) of more than 5‰ can already be seen. Thus large interannual variations with amplitudes of the seasonal cycles varying from 5-6‰ in 1997 and 1999 to 3.5‰ in 1996 and 1998 have been observed.

### 4.3.2 Synoptic scale variations

In contrast to CO mixing ratios and $\delta^{18}$O values, the synoptic variations for $\delta^{13}$C are less pronounced. Table 4.1 shows that, nevertheless, a small but significant relationship between the origin of air masses from different sectors and the calculated $\Delta\ \delta^{13}$C residuals exists. Air masses from the American continent, Europe and high Northern latitudes are generally enriched (by $+0.3\pm0.5$‰, $+0.4\pm0.3$‰ and $+0.2\pm0.5$‰ respectively) compared to the mean annual cycle. While air masses from the African continent and the low North Atlantic are depleted by $-0.2\pm0.4$‰ and $-0.5\pm0.5$‰ respectively.

Another interesting feature of the synoptic scale variations of $\delta^{13}$C is that they are not smaller during the $\delta^{13}$C minimum in late summer than during the large plateau in winter and spring. This stands in contrast to the results for CO and $\delta^{18}$O . $\delta^{13}$C from combustion processes is close to $-27$‰. For spot samples influenced by technological sources (e.g. from the North American or European sector) this leads to stronger deviations from the summer background value of $-32$‰ to $-30$‰ than for winter/spring values that are already close to $-27$‰. In Figure 4.16 the seasonal cycle of $\delta^{13}$C is plotted as a function of latitude (extracted from model results [Bergamaschi et al., 2000b]). The figure shows a small gradient of less than 2‰ for latitudes $> 10°$ N from January to May compared to $\sim 4$‰ between July and September.

## 4.4 Atmospheric $^{14}$CO record from Izaña

In this section we present the three year record of $^{14}$CO measurements for Izaña. In Figure 4.8 spot samples (selected by sectors) and 2-week-continuous samples are plotted together with their respective fit curves (FFT with a 4-week filter).

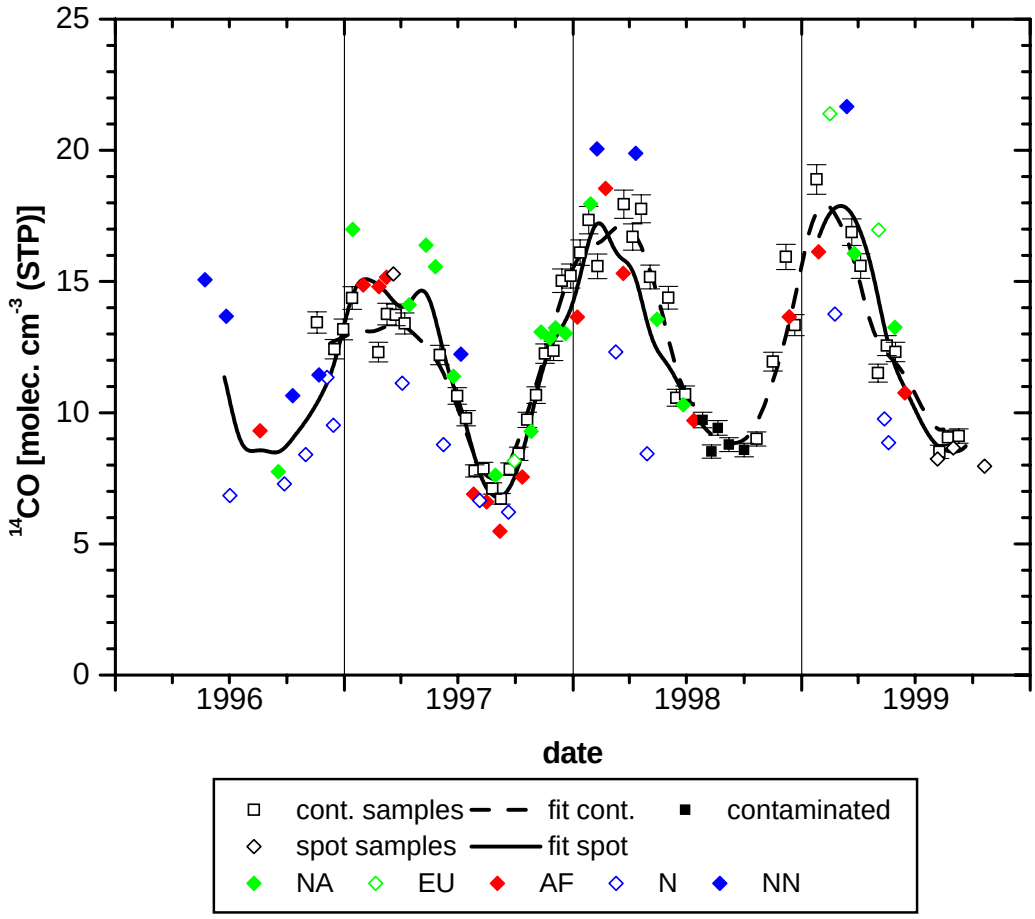


**Figure 4.8:** Record of $^{14}$CO at Izaña. 2-week-continuous samples are shown together with spot samples and fits (FFT with 4-week filter). With the help of back trajectories the spot samples are attributed to five sectors: North America (NA), Europe (EU), Africa (AF) and North Atlantic (low (N) and high (NN) latitudes).

### 4.4.1 Seasonal $^{14}$CO cycles and interannual variations

$^{14}$CO displays a seasonal cycle similar to CO mixing ratios. The winter maxima in Februar/March increased from $\sim$ 15 molec./cm$^3$ in 1997 to 17 molec./cm$^3$ and 18 molec./cm$^3$ in 1998 and 1999 respectively. The summer minima in August/September varied between 7.5 and 9 molec./cm$^3$. While the continuous samples show a smooth record with well defined seasonal cycles, the spot samples are significantly more scattered. However, both data sets define seasonal cycles with a peak-to-peak amplitude of 8.9$\pm$0.8 molec./cm$^3$.

From the fit through the continuous samples (no $^{14}$CO spot samples were measured during summer 1998) a small but significant positive trend of +0.5$\pm$0.25 molec.

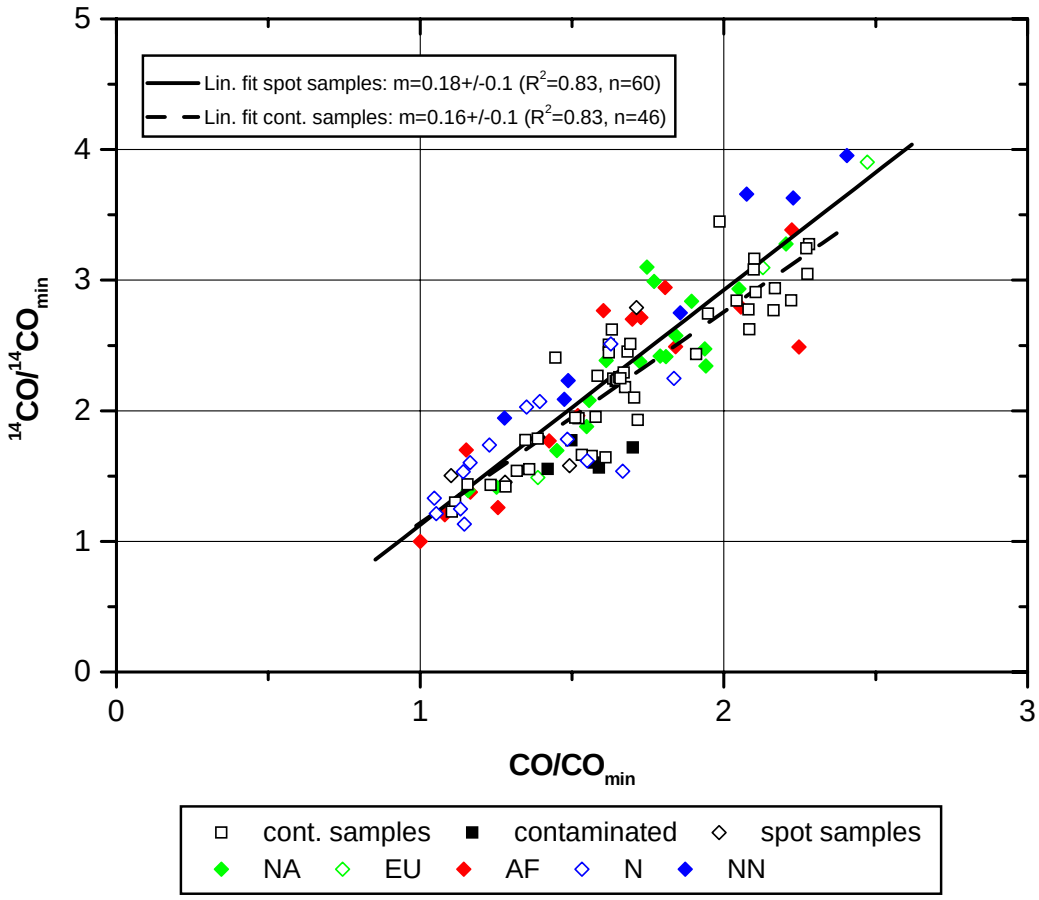


**Figure 4.9:** Normalized $^{14}$CO concentrations are plotted against normalized CO mixing ratios. Shown are 2-week continuous samples and spot samples (selected by sectors) together with a linear fit through the spot samples.

cm$^{-3}$ yr$^{-1}$ is obtained for the period 1997 to mid 1999. We expect slightly increased $^{14}$CO concentrations in 1998 due to a higher production rate of $^{14}$CO, which depends on the solar cycle activity (Jöckel, personnal communication).

As already mentioned for the CO and $\delta^{18}$O records, continuous samples were contaminated between July and October 1998. No correction for the $^{14}$CO concentration is necessary, if the contamination was $^{14}$CO free. If the total added CO (15-20 nmol/mol) was of biogenic origin (an increase of 10 nmol/mol from recycled CO of biogenic origin leads only to a 0.38 molec./cm$^3$ increase in $^{14}$CO), then corresponding $^{14}$CO concentration would be at most 0.57 to 0.76 molec./cm$^3$ too high. However, this only changes the calculation of the annual $^{14}$CO trend within the range given above. The seasonal $^{14}$CO cycle is mainly controlled by the OH sink, because the main source of $^{14}$CO is cosmogenic and hardly exhibits a seasonal cycle

[Volz et al., 1981]. The common OH sink for CO and $^{14}$CO explains why these trace gases are in phase over the whole period of our analysis. We therefore observe in Figure 4.9 a compact correlation between CO mixing ratios and $^{14}$CO concentrations for the continuous samples as well as for the spot samples. In order to compare the amplitudes of the CO and $^{14}$CO cycles, we use normalized CO mixing ratios and $^{14}$CO concentrations in Figure 4.9. The normalization is obtained by dividing the CO mixing ratio and $^{14}$CO concentration of each sample by the respective values of the lowest sample, which are $CO_{min}$=64 nmol/mol and $^{14}CO_{min}$=5.48 molec./cm$^3$ for the spot sample taken on the 6.9.1997. We obtain slopes of +1.8±0.1 molec./cm$^3$ (nmol/mol)$^{-1}$ and +1.6±0.1 molec./cm$^3$ (nmol/mol)$^{-1}$ for the regression through the spot and continuous samples respectively.

One may have expected in first instance a slope of 1 molec./cm$^3$ (nmol/mol)$^{-1}$, if $^{14}$CO and CO exhibit a similar seasonal gradient due to their common OH sink. However, the gradient is steeper for $^{14}$CO than for CO. A 10% change in CO corresponds to a 16% to 18% change in $^{14}$CO. The explanation for the smaller decline in CO relative to $^{14}$CO is that CO sources increase at the same time, while they stay constant for $^{14}$CO. The $^{14}$CO to CO ratio depends only on the $^{14}$CO source (and the Stratosphere-Troposphere Exchange (STE)) and the CO sources. Thus variations of the $^{14}$CO source and the STE would only be seen in interannual variations of the $^{14}$CO to CO ratio, whereas the CO sources induce a latitudinal gradient of the $^{14}$CO to CO ratio. For $^{14}$CO measurements at high latitudes (Spitsbergen, 79° N, 12° E) a $^{14}$CO to CO ratio close to one has been found [Röckmann, 1998a]. At the latitude of Izaña the relative contribution of the $CH_4$ oxidation source to CO mixing ratios is significantly higher than at higher latitudes. This is especially true during the summer minimum. Thus when the common sink, the oxidation by OH, starts to decrease CO and $^{14}$CO levels during summer we still see a significant contribution to CO mixing ratios from $CH_4$ oxidation (which is also higher in this period of enhanced OH levels). This explains why the amplitude of the seasonal cycle at Izaña is higher for $^{14}$CO than for CO. Concerning the interannual variations of the $^{14}$CO to CO ratio, we found no significant differences between the four years of our analysis. The annual variations of the $^{14}$CO cosmogenic source can be quantified [Jöckel et al., 1999], [Jöckel et al., 2000a], however, they are too small to be directly seen in Figure 4.9. Interannual variations of the recycled $^{14}$CO source would also only lead to small changes in $^{14}$CO (a 10 nmol/mol change in CO only yields the already mentioned 0.38 molec./cm$^3$ change in $^{14}$CO). Altogether, our $^{14}$CO data does not suggest any important changes in total CO sources and STE during the years of our study. This stands in contrast with the significant interannual changes which we

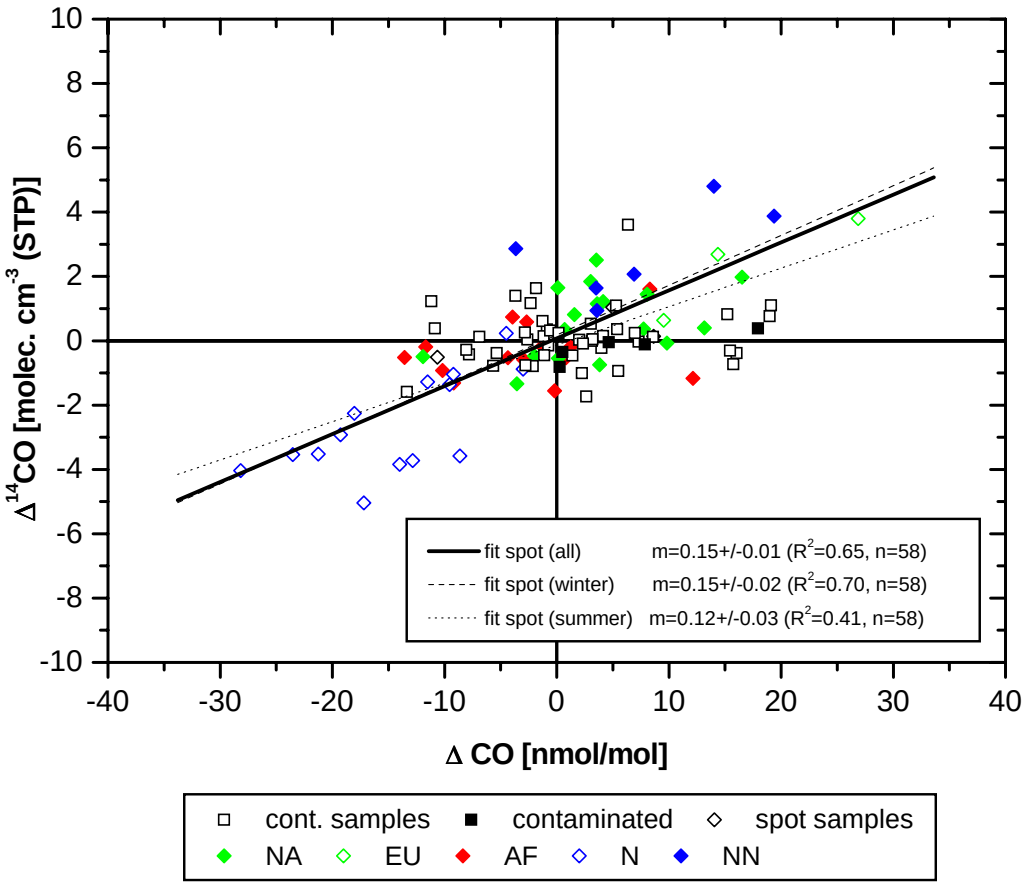


**Figure 4.10:** Residuals of $^{14}$CO concentrations versus residuals of CO mixing ratios. Plotted are 2-week continuous samples and spot samples (selected by sectors). Linear fits through all spot samples and for the subsets of summer and winter values are shown.

observed for $\delta^{18}$O at Izaña (see section 4.2).

### Synoptic scale variations

For the spot samples, large synoptic scale variations occur in the $^{14}$CO concentration. The reason for this has already been mentioned for CO mixing ratios and $\delta^{18}$O . Depending on the latitudinal origin of air masses reaching Izaña, corresponding $^{14}$CO concentrations, as well as CO mixing ratios and $\delta^{18}$O , can vary significantly. During winter $^{14}$CO concentrations are, for example, 5-10 molec./cm$^3$ lower for spot samples attributed to the low North Atlantic than for those from high latitudes. During summer this latitudinal gradient is still apparent, but with variations of 2-5 molec./cm$^3$ less pronounced.

In Figure 4.10 we plot residuals of $^{14}$CO concentrations against residuals of mixing

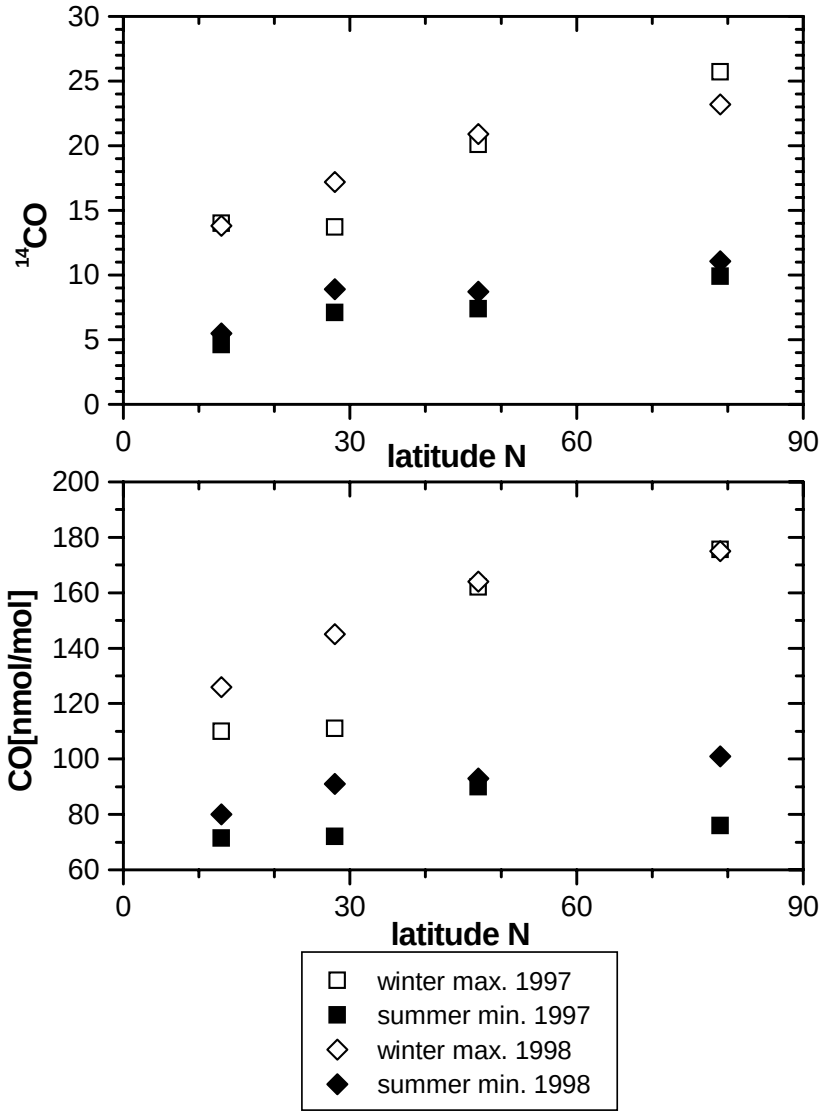


**Figure 4.11:** $^{14}$CO and CO measurements at stations of different latitudinal location.

ratios for continuous and spot samples (see Table 4.1). If the deviations of $^{14}$CO concentrations from the mean seasonal cycle are related to the varying latitudinal origin of different air masses, we should observe a correlation to $\Delta$CO residuals. We find a slope of $+0.15 \pm 0.01$ molec./cm$^3$ $^{14}$CO (nmol/mol CO)$^{-1}$ for the linear fit through the spot samples ($R^2$=0.65, n=58). As expected, spot samples from the low North Atlantic and Africa (sectors N and AF) have low or negative $\Delta^{14}$CO and $\Delta$CO values, while positive $\Delta^{14}$CO and $\Delta$CO values dominate for spot samples from higher latitudes (sectors NN, NA and EU). With an average annual mean of $\sim$70 nmol/mol for the latitudinal gradient of the North hemisphere [Novelli et al., 1998a], this would

result in a corresponding latitudinal $^{14}$CO gradient of 10.5±0.7 molec./cm$^3$.

We compare this estimated $^{14}$CO gradient to $^{14}$CO measurements at stations of different latitudinal locations. In Figure 4.4.1 the $^{14}$CO and CO summer minima and winter maxima in 1997 and 1998 are given for four different stations, i.e. Spitsbergen, Sonnblick, Izana (see Table 3.1) and Barbados (13° N, 53° W) [Mak & Southon, 1998].

Clearly the latitudinal gradient for $^{14}$CO concentrations as well as CO mixing ratios is less pronounced during summer than during winter. For CO mixing ratios this has already been reported by [Novelli et al., 1998a] and for $^{14}$CO by [Mak et al., 1994]. The correlation in Figure 4.4.1 is therefore higher for winter samples ($R^2$=0.70) than for summer samples ($R^2$=0.41) and our derived North hemispheric latitudinal $^{14}$CO gradient of $\Delta^{14}$CO =$\sim$ 10.5 molec./cm$^3$ is in agreement with the observed difference in $^{14}$CO concentrations of 11±1.5 molec./cm$^3$ between Barbados and Spitsbergen during winter. We address the large interannual differences in CO and $^{14}$CO between 1997 and 1998 at Izaña in section 4.6 where the records of Spitsbergen and Izaña are compared over the three year period 1996 to 1999.

## 4.5 Comparison to model results

Records of CO mixing ratios and its stable isotopes can be used to infer the source distribution of CO and its source strengths. CO mixing ratios have been simulated with global chemistry transport models, [Brasseur et al., 1998] [Crutzen & Zimmermann, 1991] and [Bergamaschi et al., 2000c], mostly based on CO data from the globally distributed network of 49 NOAA/CMDL sites [Novelli et al., 1998a]. From this CO budgets have been calculated which are partly summarized in Table 1.4 in section 1.6.

The first two years of our three year record of CO mixing ratios and its stable isotopes at Izaña have been used together with records from four other stations for an inverse CO modeling study by Bergamaschi et al. [2000b]. The model setup of this study is similar to the one described in section 3.5 for the inverse $CH_4$ model study [Bergamaschi et al., 2000a]. We report the main results from this study with regard to the Izaña records presented in the previous section of this thesis. We note that inverse modeling of CO and its isotopic composition is inherently difficult because of the short lifetime of CO and its strong coupling with OH.

With the inverse modeling technique source emissions are inferred from observed mixing ratios. Thus information on source strengths are retrieved and the agreement

between the model and observational data is optimized. The isotopic information is included by treating the CO isotopomers, $^{13}$C and $^{18}$O, as independent tracers. This allows the simultaneous optimization of modeled atmospheric mixing and isotope ratios with respect to the measurements.

The three North Hemisphere stations on which the inverse model study was based were part of the MPI sampling network listed in Table 3.1, i.e. $\delta^{13}$C and $\delta^{18}$O data from Alert (82.5° N, 62.5° W; 210 m asl) and Spitsbergen (78.9° N, 11.9° W; 473 m asl) were included together with the Izaña data. The Spitsbergen data set is shown in Figure 4.17 in section 4.6 where we compare the two long term records of Spitsbergen and Izaña. The data from the two Southern Hemisphere stations, Baring Head (41.4° S, 174.9° E; 80 m asl) and Scott Base (77.8° S, 167.5° E; 200 m asl), came from the National Institute of Water and Atmospheric Research (NIWA). Thus the observational data of $\delta^{13}$C and $\delta^{18}$O which were used in the inverse CO study came from globally distributed sites. As has been shown for Izaña, they all exhibit pronounced seasonal cycles and together they define large latitudinal gradients [Bergamaschi et al., 2000b].

### 4.5.1 Mean seasonal cycle of CO mixing ratios

In Figure 4.12 the contribution of individual sources to atmospheric CO mixing ratios is shown for Izaña. Plotted are also monthly mean values calculated for the period 1993-1995 from NOAA/CMDL CO mixing ratios at Izaña. The error bars indicate ±2 standard deviations. The time period 1993-1995 was chosen because of a previous inverse model study based on CO mixing ratios from the NOAA/CMDL network [Bergamaschi et al., 2000c]. The shown seasonal amplitude of 45±15 nmol/mol together with CO mixing ratios varying between 50 and 160 nmol/mol cover the wide range of seasonal cycles we measured for the period 1996-1999 shown in Figure 4.1.

The large seasonal CO cycle is driven by the OH cycle with maximum OH levels during summer and minimum OH levels during winter. This directly influences the lifetime of CO, which is 2-3 months in winter and only a few weeks in summer. The effect of changing CO lifetimes due to changing OH levels is best seen in the contribution of the technological source to atmospheric CO mixing ratios at Izaña. The inverse model considers the technological source to be constant throughout the year, with total emissions of 478 Tg yr$^{-1}$ (90% from the North hemisphere) (see Figure 4.13 for the latitudinal and seasonal distribution of CO sources and corresponding references). However, while CO from technological sources accounts for more than 50 nmol/mol during winter, its contribution to atmospheric CO mixing ratios drops to 10-20 nmol/mol during summer. The relative contribution of $\sim$ 1/3 of the tech-

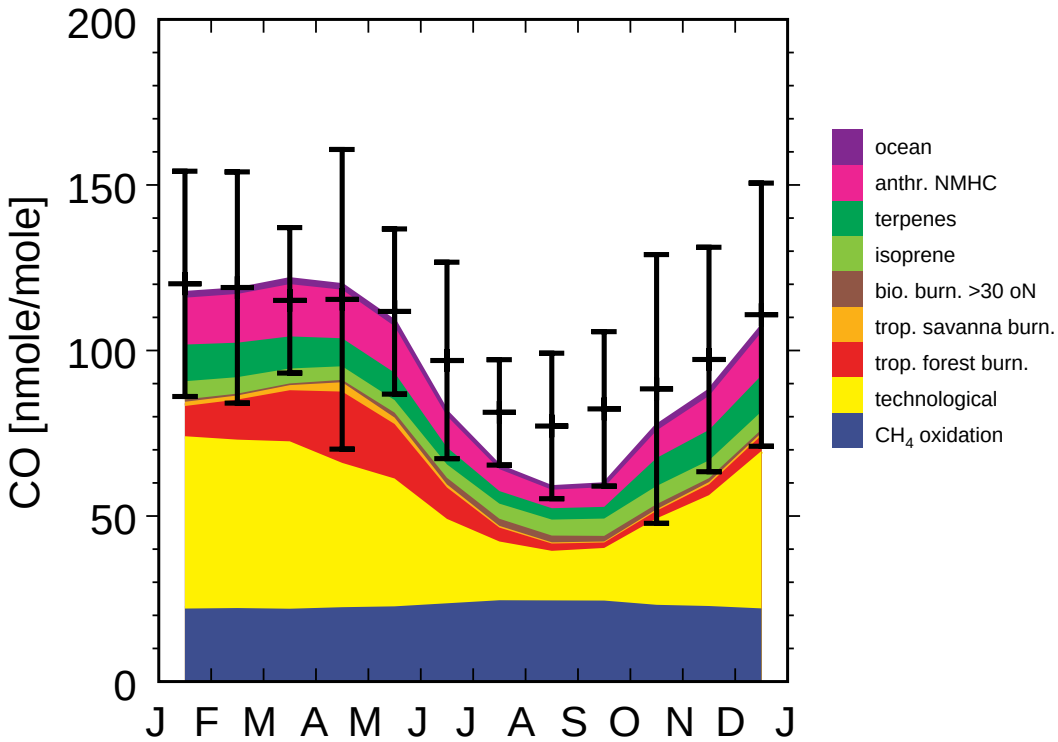


**Figure 4.12:** Contribution of individual sources to atmospheric CO mixing ratios at Izaña. Observational data (symbols) are given as monthly mean values ±2 standard deviations [Bergamaschi et al., 2000b].

nological source to CO mixing ratios remains nearly constant throughout the year.

The influence of the $CH_4$ oxidation on CO mixing ratios is very different. With assumed total emissions of 830 Tg yr$^{-1}$ (see section 1.6) the emissions in the North Hemisphere are comparable to those from the technological source, but exhibit a small seasonal cycle. The contribution to atmospheric CO mixing ratios remains with 20±2 nmol/mol nearly constant throughout the year. This results in a relative contribution to CO mixing ratios which is much larger during summer (40%) than winter (15%). The reason for the different seasonal influence of the two important CO sources, technological and $CH_4$ oxidation, on CO mixing ratios is their different latitudinal source distribution. While the technological source has its maximum between 20° N and 60° N, $CH_4$ oxidation is most important in the tropics between 30° S and 30° N. Thus the discussed influence of seasonally changing OH levels and CO lifetimes is by far more important for the technological source than for $CH_4$ oxidation. The contribution of the remaining CO sources to CO mixing ratios at Izaña will be discussed in more detail together with the isotopic composition of CO.

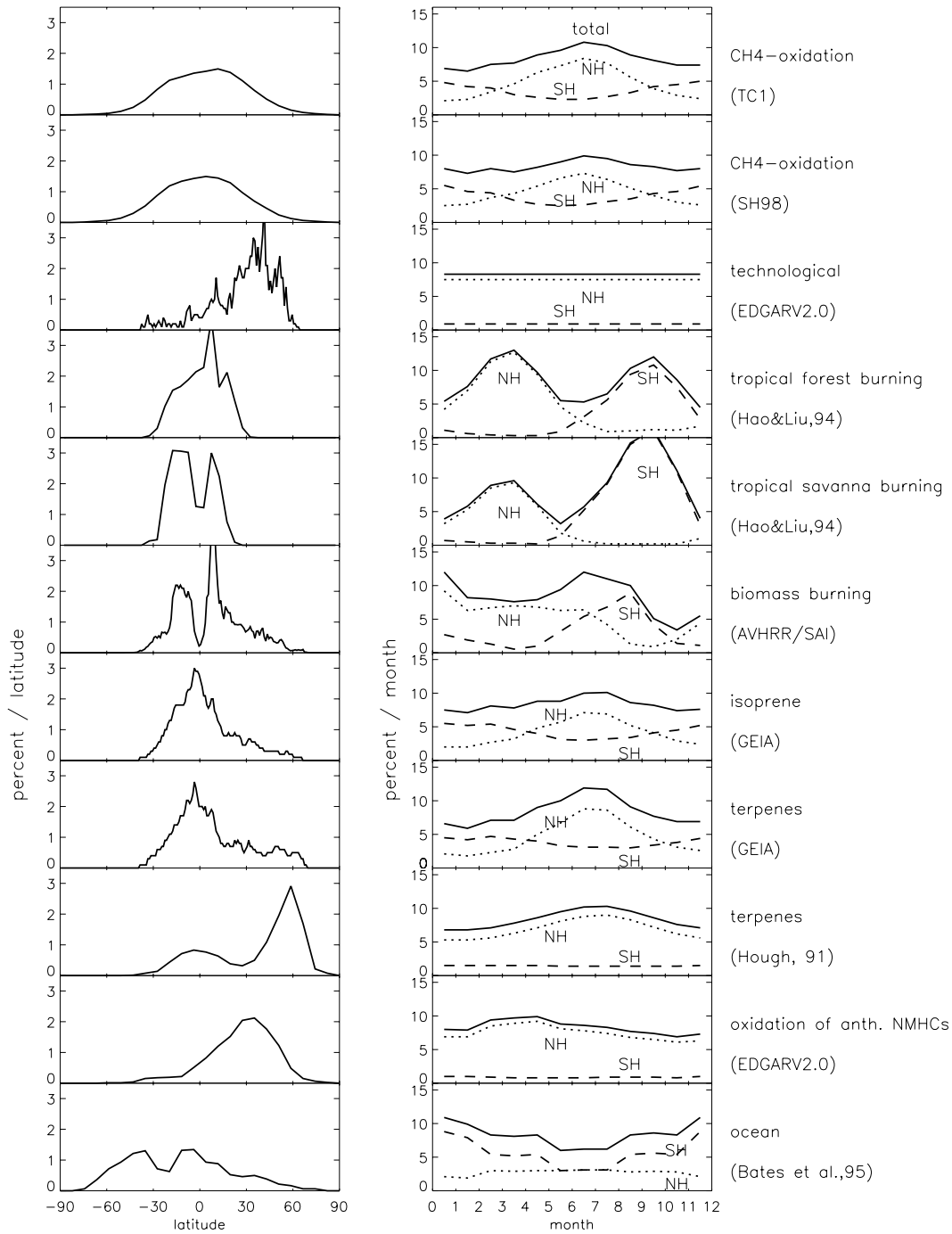


**Figure 4.13:** Latitudinal and seasonal distribution of CO sources. (left) Percentage of average annual emissions per 1° latitude band. (right) Percentage of total emissions per month. Emissions in the SH (dashed line) and NH (dotted line) are indicated separately [Bergamaschi et al., 2000c].

Fig. 1

### 4.5.2 Mean seasonal cycles of $\delta^{13}$C and $\delta^{18}$O

The phase behavior of the mean seasonal cycles of CO mixing and isotope ratios is summarized in Figure 4.5.2. The observed and simulated mixing ratios, $\delta^{18}$O and $\delta^{13}$C of atmospheric CO at Izaña are shown. Observational data are given as monthly mean values ±2 standard deviations. Also given are the a priori and a posteriori model simulations (shown as monthly mean values ±2 standard deviations of the daily model data).

The seasonal cycles of CO mixing ratios and $\delta^{18}$O are in phase. Both values are highest from January to April and lowest from July to October. For $\delta^{13}$C the plateau from January to May is even more pronounced while the minimum values are reached slightly later in August and for a shorter time span. We note the difference in the a priori and a posteriori results for $\delta^{13}$C. In order to reproduce the $\delta^{13}$C values measured at Izaña and the other stations, the model increased the CO yield from $CH_4$ oxidation to 84%. Present estimates for the CO yield from $CH_4$ oxidation range from 0.7 to 0.94 [Kanakidou et al., 1999].

With the help of Figure 4.15 we discuss the driving forces of the mean annual cycles observed at Izaña for $\delta^{13}$C and $\delta^{18}$O of atmospheric CO. The $\delta^{13}$C and $\delta^{18}$O data given in Figure 4.15 are monthly mean values of the time period from mid-1996 to mid-1998, again with error bars corresponding to ±2 standard deviations. This inconsistency in time periods chosen for the monthly mean values of CO mixing ratios (1993-1995) and its isotopic composition (1996-1998) could introduce a systematic error. But the monthly mean values derived from the NOAA/CMDL Izaña record for 1993-1995 do not differ from those in 1996-1998. The latter have been shown in Figure 4.1 where also the agreement between the NOAA/CMDL and our CO mixing ratios was discussed (the systematically lower NOAA/CMDL values at levels between 50 and 90 nmol/mol are taken into account by allowing the large range of ±2 standard deviations).

Before we discuss how the inverse model results help to understand the mean seasonal cycles observed at Izaña, we define the notation used in the inverse model and plotted in Figure 4.15. $\delta^{13}$C$_i$(x,t) and $\delta^{18}$O$_i$(x,t) illustrate the isotopic enrichment due to the sinks during transport. They are defined by the equation 4.1

$$\delta_i(x,t) = \delta_i(source) + \epsilon_i(x,t) \tag{4.1}$$

where $\delta_i(source)$ is the source signature and $\epsilon_i(x,t)$ a model parameter which calculates the isotopic effect due to removal of CO during transport (for each source $i$). The total $\delta^{13}$C and $\delta^{18}$O signature in atmospheric sources is the average of the $\delta^{13}$C$_i$(x,t) and $\delta^{18}$O$_i$(x,t) from the individual sources $i$ (shown for Izaña in Figure

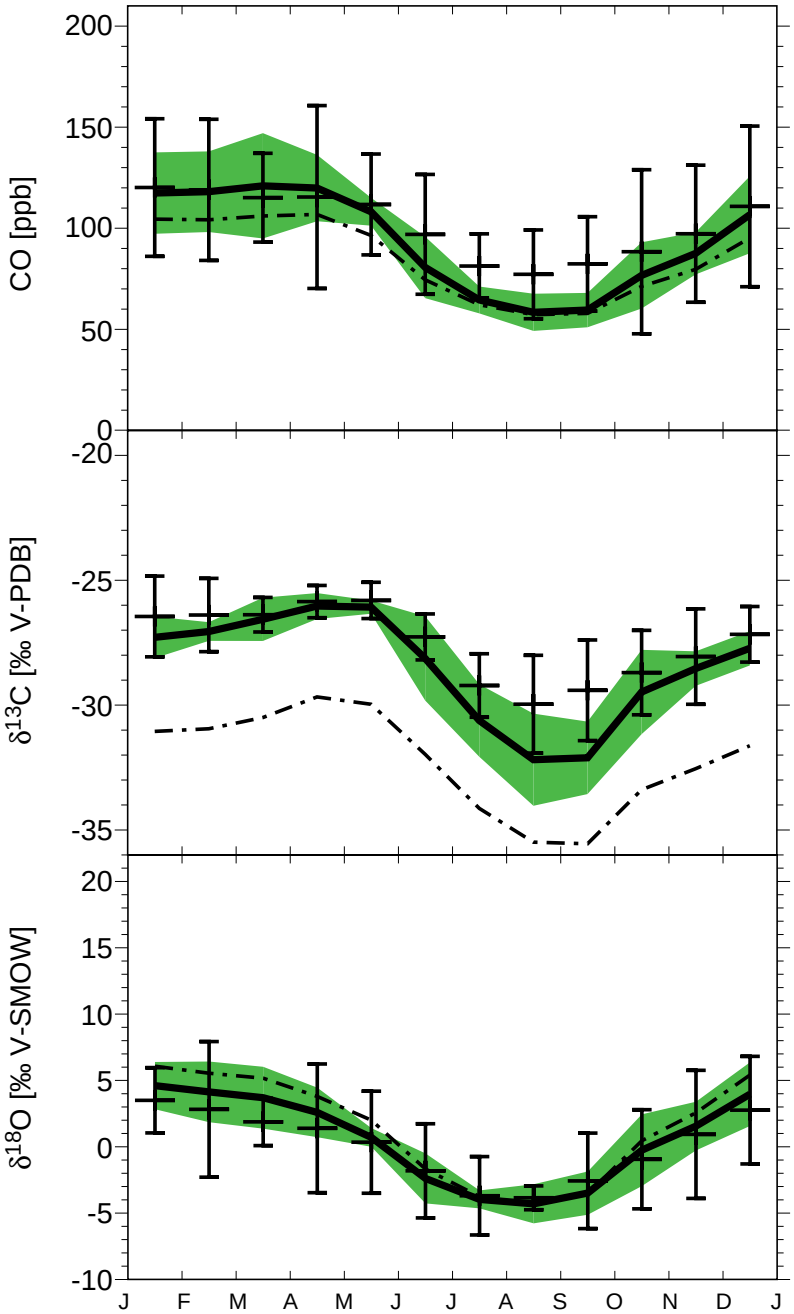


**Figure 4.14:** Observed and simulated mixing ratios, $\delta^{18}$O and $\delta^{13}$C of atmospheric CO at Izaña. Observational data (symbols) are given as monthly mean values ±2 standard deviations. A posteriori model simulations are shown as monthly mean values (solid line) ±2 standard deviations of the daily model data (shaded area). A priori results are shown as thin dash-dotted lines [Bergamaschi et al., 2000b].

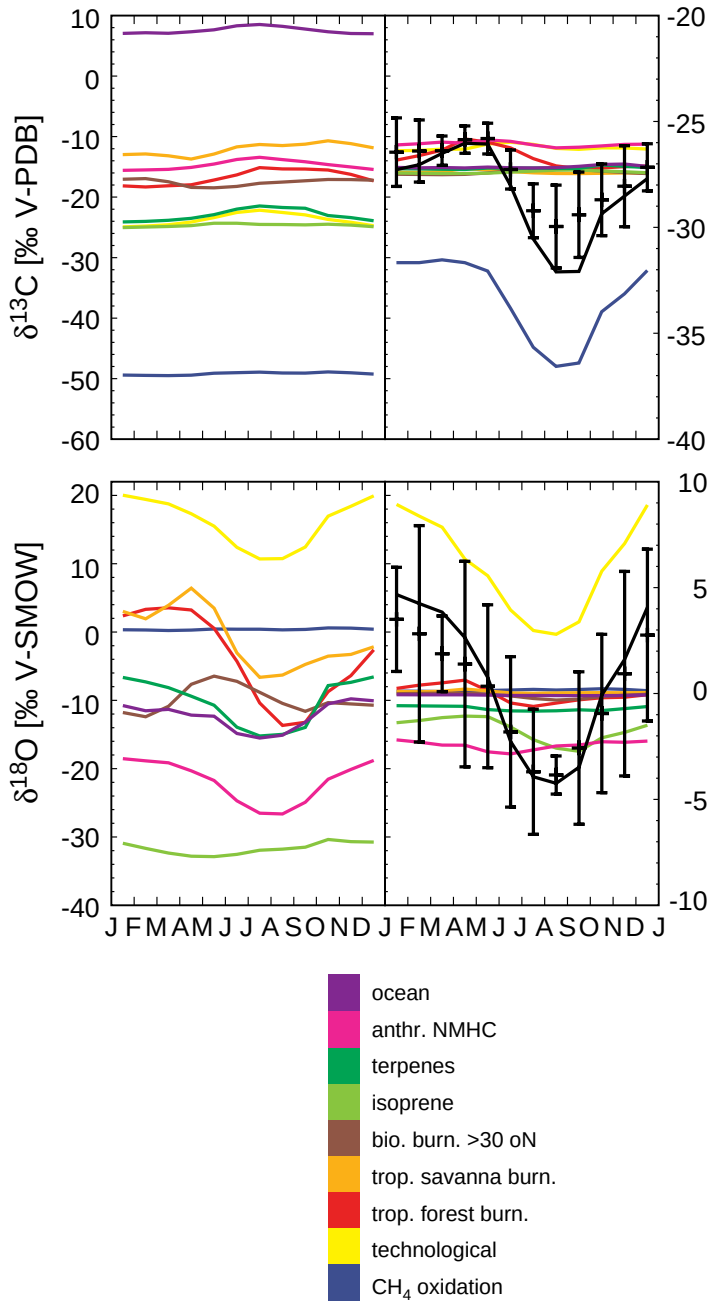


**Figure 4.15:** Influence of individual sources at Izaña: (top, left) $\delta^{13}C_i(x,t)$ illustrates the isotopic enrichment due to the sinks during transport; (top, right) visualization of the influence of the individual sources on atmospheric $\delta^{13}C$. The optimized model results for the monthly mean values are plotted (black solid line); (bottom, left and right) the same for $\delta^{18}O$. Observational data (symbols) are given as monthly mean values $\pm 2$ standard deviations [Bergamaschi et al., 2000b].

4.15), weighted with their relative contribution $f_i$. In order to illustrate the influence of the individual sources on the modeled $\delta^{13}$C and $\delta^{18}$O the inverse model also allows to plot (solid line through the observational data)

$$[\delta_i(x,t) - \delta_{mean}]f_i + \delta_{mean}] \tag{4.2}$$

with

$$f_i = \alpha_i c_i(x,t) / \sum \alpha_i c_i(x,t) \tag{4.3}$$

where $\delta_{mean}$ represents the average $\delta^{13}$C or $\delta^{18}$O of the measurements at Izaña and $\alpha_i$ and $c_i(x,t)$ represent source strength and CO mixing ratios respectively.

We now discuss the mean seasonal cycles for $\delta^{13}$C and $\delta^{18}$O at Izaña, which were calculated from the first 2-years of measurements shown in Figure 4.7 and Figure 4.4 respectively. This is done with the help of the inverse model results plotted in Figure 4.15. For $\delta^{13}$C this presentation illustrates the large influence of the seasonally varying relative contribution of CO from $CH_4$ oxidation on the seasonal $\delta^{13}$C cycle at Izaña. The 5 ‰ decrease in $\delta^{13}$C values from May to August is nearly exclusively due to the increasing relative contribution of $CH_4$ oxidation when CO mixing ratios decrease during the same period. We already noted that the absolute contribution of $CH_4$ oxidation is nearly constant throughout the year. The CO+OH sink reaction does not induce important seasonal variation for $\delta^{13}$C through its kinetic isotope effect (KIE). While the KIE is responsible for the absolute value of $\delta^{13}C_i$(x,t) for each source (see equation 4.1 and Figure 4.15(top-left)), only sources with strong seasonal varying source strengths, e.g. biomass burning, exhibit a isotopic enrichment with a seasonal pattern. For CO from $CH_4$ oxidation not only the absolute contribution but also $\delta^{13}C_i$(x,t) and $\delta^{18}O_i$(x,t) remain almost constant throughout the year.

For the mean seasonal cycle of $\delta^{18}$O of atmospheric CO at Izaña we note the dominant influence of the technological source. As discussed for the CO mixing ratios, the emissions from technological sources are assumed constant throughout the year. However, the isotope effect of the main CO sink, oxidation by OH, is opposite in sign for $\delta^{18}$O (inverse isotope effect) and much more pronounced compared to $\delta^{13}$C . Thus nearly 7 ‰ of the annual cycle of 9 ‰ is explained by the influence of the technological source on the $\delta^{18}$O signal. This explains why the $\delta^{18}$O cycle is highly correlated to the OH cycle and to the CO mixing ratios.

It is clear that the global distribution of the five sites used in the inverse study defined large latitudinal gradients. These seasonal varying latitudinal gradients are shown in Figure 4.16 for CO mixing ratios as well as for $\delta^{13}$C and $\delta^{18}$O .

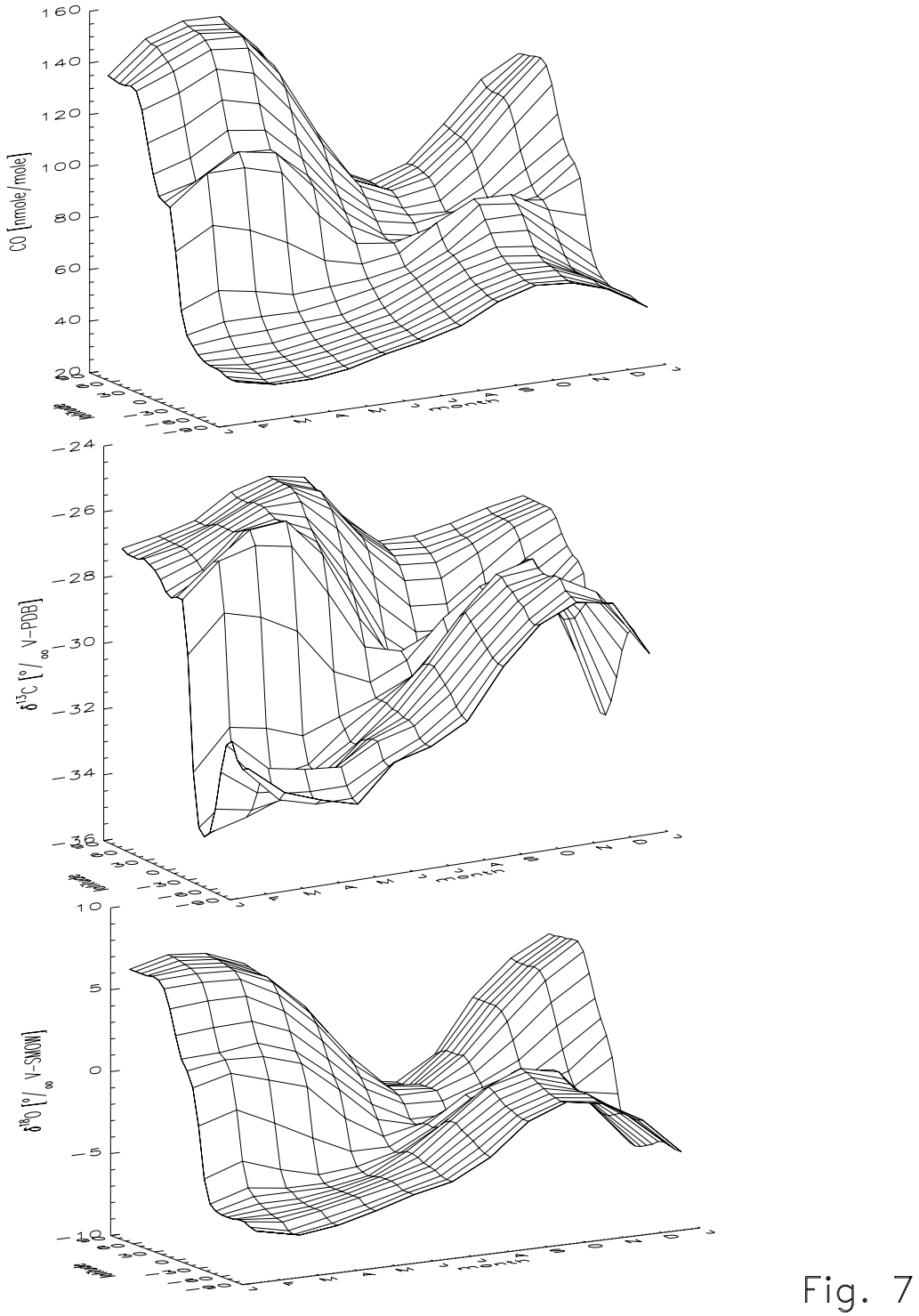


**Figure 4.16:** Seasonal cycles in the free troposphere (vertical and zonal average) as function of latitude: surface plots for (top) CO mixing ratios, (middle) $\delta^{13}$C , and (bottom) $\delta^{18}$O [Bergamaschi et al., 2000b].

## 4.6 Comparison to the Spitsbergen record

CO isotope measurements at Spitsbergen (79° N, 12° W) started in spring 1995 (see Table 3.1). Since spring 1996 spot samples have been taken regularly by the Norwegian Institute for Air Research (NILU) and sent for analysis to the MPI. In Figure 4.17 the CO mixing ratio and isotope record for Spitsbergen is shown and compared to the Izaña record. We also plot a fit through data from the Sonnblick observatory (47° N, 13° E), which represents the background values of this continental station situated in the Austrian Alps [Gros et al., 2000]. Thus long term records are shown for three stations which are representative for high latitudes, mid-latitudes (free troposphere) and subtropical latitudes of the Northern Hemisphere respectively.

All three CO records exhibit the well known, strongly OH driven, seasonal cycle. During the winter maxima strong differences between the Spitsbergen and the Izaña record are apparent. In 1998 CO mixing ratios are nearly 70 nmol/mol higher in Spitsbergen compared to Izaña, whereas the difference is less during winter 1998 (~30 nmol/mol). CO values for Sonnblick are lower but still comparable to those from Spitsbergen during winter. Thus the strong increase in CO mixing ratios at Izaña discussed in section 4.1 is not seen for the two stations at higher latitudes. The summer minima at Izaña and Spitsbergen are very close for 1997 and 1998. This reflects the much smaller latitudinal CO gradient during the summer months (see Figures 1.6 and 4.16). For Sonnblick CO levels were higher in summer 1997. Regional sources can influence the low summer values at this continental station, nevertheless in 1998 values were close to background values found at Izaña and Spitsbergen.

A similar pattern is seen for the $^{14}$CO concentrations at the three stations. The latitudinal $^{14}$CO gradient of these three stations has already been discussed in section 4.4. As for CO mixing ratios, large interannual differences between $^{14}$CO concentrations at Izaña and Spitsbergen are apparent for the winter months in 1997 and 1998. Again the strong increase observed in the Izaña record for this period (see section 4.4) is not seen in the records from Spitsbergen and Sonnblick. Altogether Izaña seemed to be more representative for lower latitudes from mid-1996 to mid-1997. This would explain why CO and $^{14}$CO values at Izaña were comparable to measurements at Barbados (see Figure 4.4.1) during this period. This is also confirmed by the stable isotopes records from both stations [Mak et al., 2000].

The $\delta^{13}$C records shown in Figure 4.17 for Izaña, Sonnblick and Spitsbergen highlight the influence of the OH seasonality and the contribution of the $CH_4$ oxidation on the seasonal $\delta^{13}$C cycle. Due to the pronounced seasonal CO cycle at Spitsbergen the kinetic isotope effect in the CO + OH reaction leads to a signif-

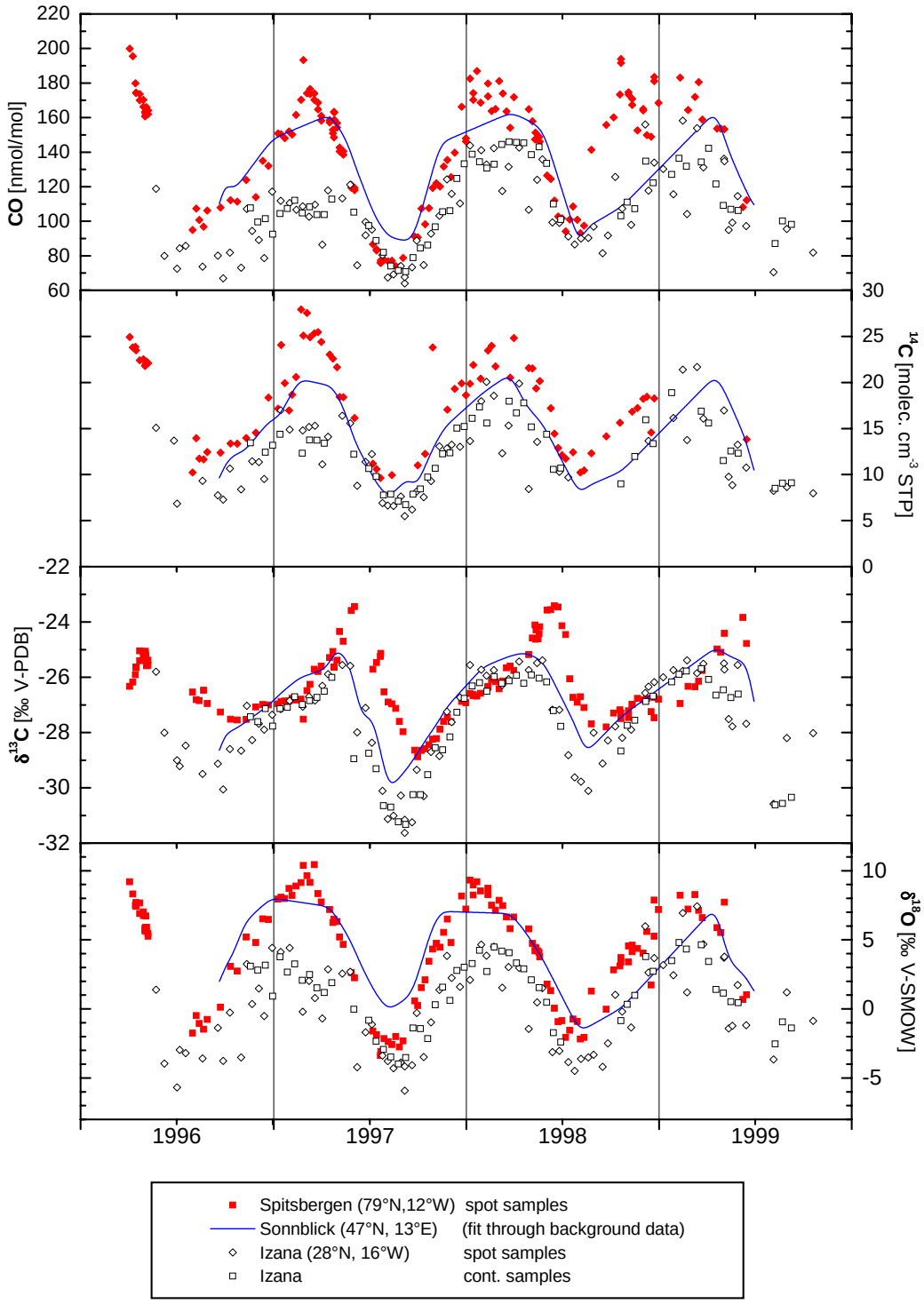


**Figure 4.17:** CO mixing and isotope ratios records from three stations, Spitsbergen, Sonnblick and Izaña (see Table 3.1).

icant phase shift between CO and $\delta^{13}C$ of $\sim$ 3months. During rising OH levels, and therefore decreasing CO levels, the remaining CO gets progressively enriched (KIE($\delta^{13}C$ ) of 1.004 to 1.005 in the lower troposphere [Stevens et al., 1980]). With decreasing CO levels the contribution of the very light $CH_4$ oxidation source gets relatively more important and a sharp decrease in $\delta^{13}C$ is observed from June to October. This effect has already been discussed for the Izaña $\delta^{13}C$ variations. The considerably lower $\delta^{13}C$ values during summer/autumn at Izaña compared to Spitsbergen reflect that $CH_4$ oxidation is a relatively more important source at lower latitudes. Bergamaschi et al. [2000b] calculated the contribution from $CH_4$ oxidation to total CO levels. During the summer months $CH_4$ oxidation accounts only for approximately 1/5 of CO mixing ratios at Spitsbergen, whereas it is 1/2 at Izaña (see Figure 4.12). The $\delta^{13}C$ signal at Sonnblick is between those from Spitsbergen and Izaña, in accordance with the latitudinal gradient shown in Figure 4.16. Only during the winter maximum is $\delta^{13}C$ higher than at the other stations. This reflects again that regional sources from combustion processes with heavy $\delta^{13}C$ source signatures are more important at this continental station. Concerning the interannual variability between 1997 and 1998 we note that in all three records the summer minimum in 1997 was lower than in the previous and subsequent years. This effect is yet not fully understood [Gros et al., 2000], [Röckmann, 1998a].

The $\delta^{18}O$ cycles shown in Figure 4.17 reflect the seasonality of the OH sink which is enhanced by the CO source shift from isotopically light sources in summer towards isotopically heavy combustion sources in winter. This leads to the strong latitudinal gradient between the three $\delta^{18}O$ records which is largest in winter. Again the higher contribution of combustion sources during low CO concentrations in summer can be seen for the continental station Sonnblick.

## 4.7 The BERLIOZ campaign

In July and August 1997 we have taken samples during the Berlin-Ozone Experiment (BERLIOZ) in the surroundings of Berlin. The BERLIOZ campaign was part of the BMBF-Project for tropospheric studies (TFS) in which Ozone and its precursors were studied [Becker et al., 1998]. We compare these measurements taken in the continental boundary layer to long term measurements at two European stations, e.g. Kollumerwaard (Netherlands) and Umweltbundesamt (UBA) Schauinsland (Germany). While the Kollumerwaard station is located in the boundary layer a few km from the North See, the UBA station is located at the top of the Schauinsland at 1205 m a.s.l.. With an elevation about 1000 m above the regional level

(e.g., the broad Rhine valley), it is usually above the ground level inversion layer during night, but within the ground level boundary layer during day-time. Samples are usually taken in the early morning when the night-time inversion still shields the station from local emissions.

The BERLIOZ samples were collected at the Papsthum station (53° N, 13° E) approximately 60 km northwest from Berlin. Between the 20th July and 6th August 1998 twenty high pressure aluminum cylinders (Scott Marin Inc., 5 l) were taken with the compressor system described in section 2.1.1. The CO mixing and isotopic ratios from the BERLIOZ samples are shown in Figure 4.18 together with the 1998 data sets from the Kollumerwaard station (53° N, 6° E, 0 m a.s.l.) and the Schauinsland station (48° N, 8° E, 1205 m a.s.l.)(see also Table 3.1). The FFT fits through the Izaña and Spitsbergen records are also shown which indicate the background signals from high northern and subtropical latitudes.

The previously discussed seasonal cycles of CO and its isotopes are indicated by the FFT fit curves. The CO mixing ratios at both monitoring stations are very scattered, ranging from $\sim$ 110 nmol/mol in summer to values as high as 220 nmol/mol and 300 nmol/mol for Schauinsland and Kollumerwaard respectively. These large variations make it difficult to extract a distinct seasonal cycle. The BERLIOZ samples had CO mixing ratios ranging between 136 and 192 nmol/mol on the 20th/21th July, while they reached background concentrations between the 3rd and 6th of August (109 to 152 nmol/mol).

$^{14}$CO measurements were much less affected by local and regional sources and therefore distinct annual cycles are apparent for 1998 at both monitoring stations. Most $^{14}$CO values lie within the fit curves for Izaña and Spitsbergen, indicating that the seasonal cycles are mainly defined by the OH sink, i.e. the latitudinal location of Kollumerwaard and Schauinsland. The BERLIOZ data vary between 8 and 11 molec./cm$^3$ and exhibit the same scatter as observed for the monitoring stations during the summer minimum.

The $\delta^{13}$C signals of Kollumerwaard and Schauinsland exhibit a similar seasonal cycle as discussed for Sonnblick in section 4.6. The scatter of the BERLIOZ data is relatively high especially on the 20th/21th July. But apart from one outlier with an extremely low $\delta^{13}$C signal of less than 30 ‰, the variability is within the range of $\delta^{13}$C values observed at the monitoring stations during the same period. The reasons for the up to 2 ‰ depleted value for the outlier sampled on the 21th July at 2 p.m. are not yet clear. For samples from the boundary layer with high levels of carbon containing compounds, such as formaldehyde, cross interference may occur during the analysis.

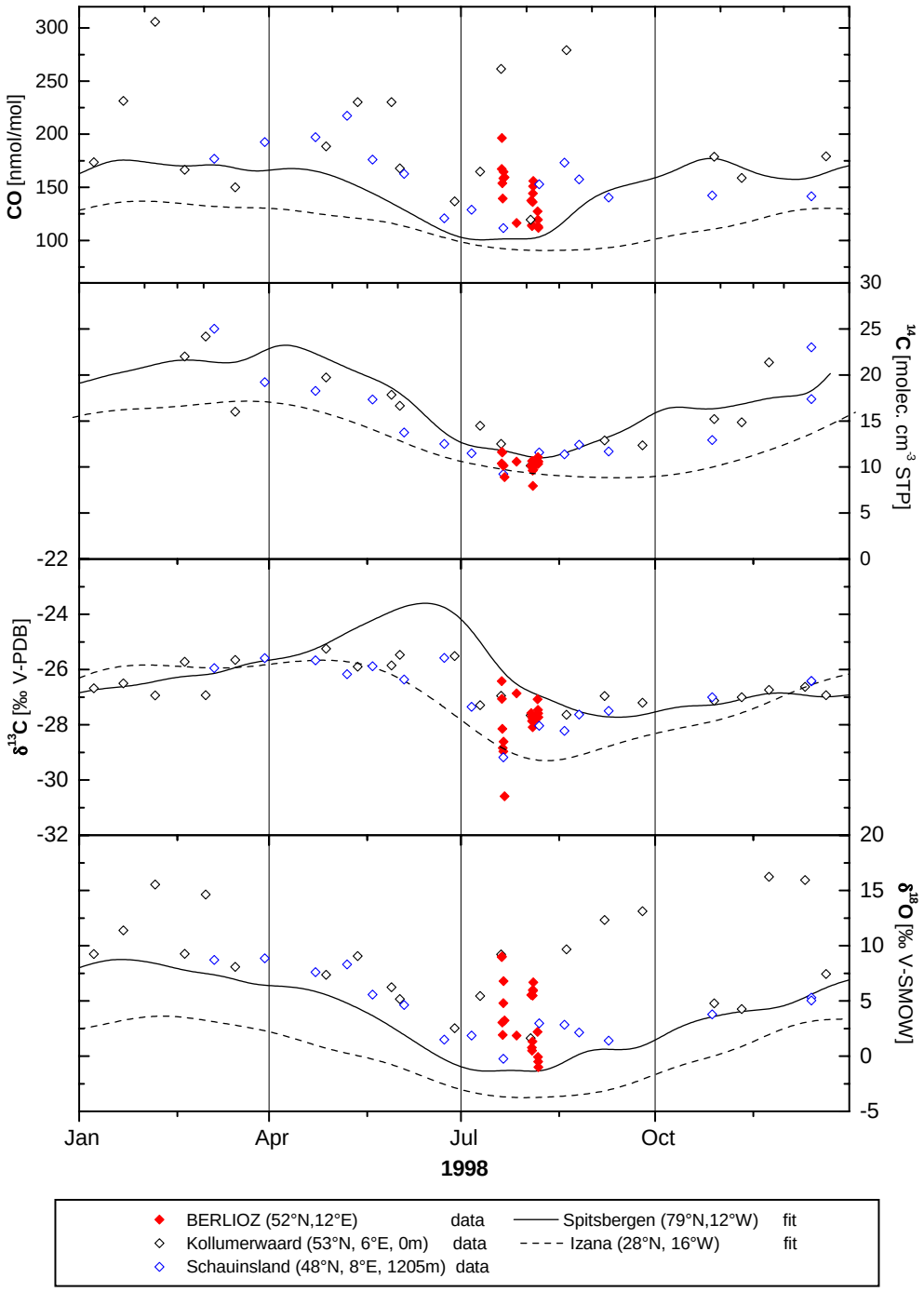


**Figure 4.18:** CO mixing and isotope ratios records from the BERLIOZ campaign together with the 1998 records from two monitoring stations, e.g. Kollumerwaard and Schauinsland (see Table 3.1). FFT fit curves from Spitsbergen (2-week filter) and Izaña (4-week filter) are shown.

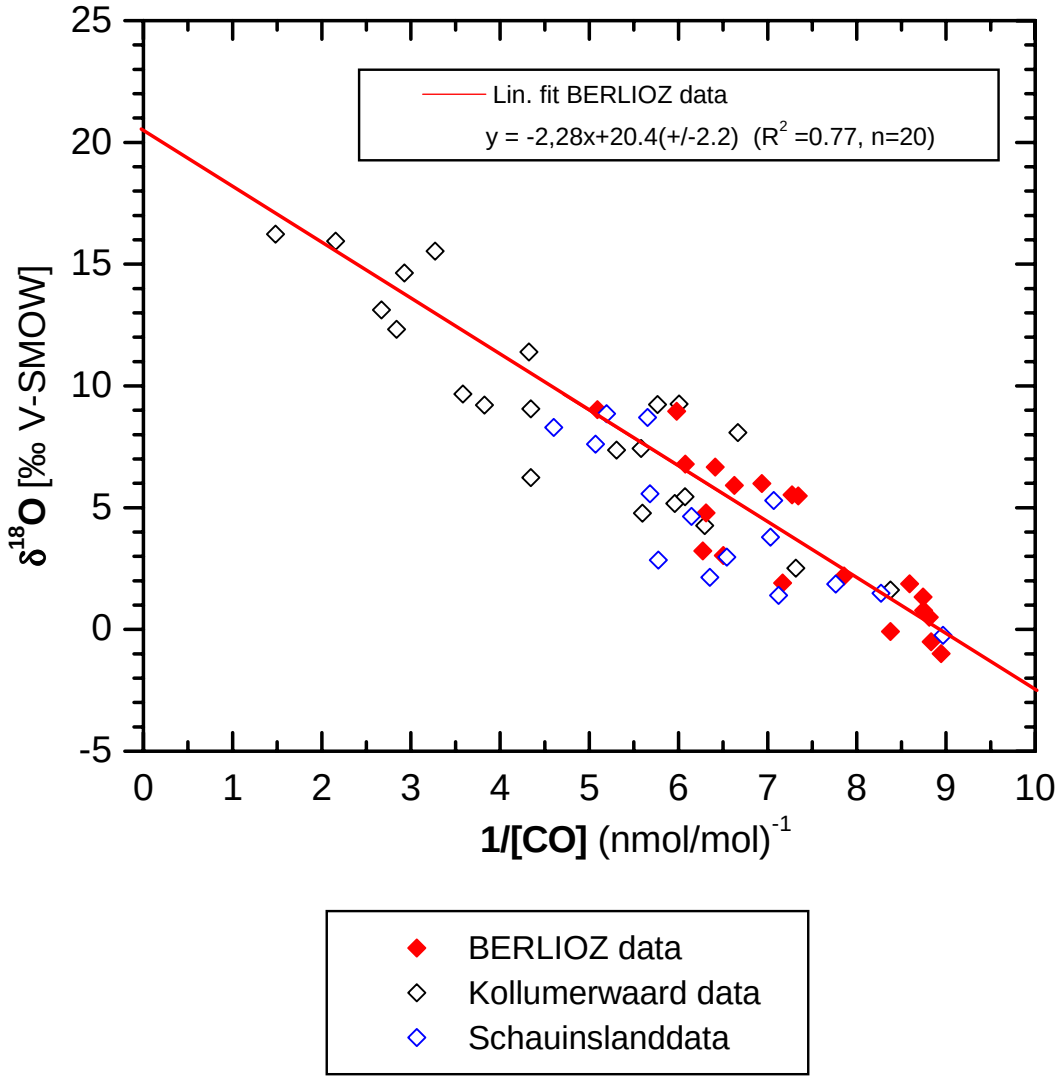


**Figure 4.19:** $\delta^{18}$O values are plotted against the inverse concentration for the BERLIOZ data and for Kollumerwaard and Schauinsland data from 1998. A linear fit through the BERLIOZ data is applied.

In Figure 4.19 we show how the variability of the $\delta^{18}$O signals at the monitoring stations as well as for the BERLIOZ samples can be explained by the contribution of combustion sources. CO from combustion sources is enriched in $^{18}$O and nearly matches the isotopic composition of atmospheric oxygen which has a $\delta$ value of 23.5 ‰. Because combustion is the only large source of enriched CO, CO and $\delta^{18}$O values are correlated for samples affected by local combustion sources [Brenninkmeijer & Röckmann, 1997]. By plotting $\delta^{18}$O values against the inverse concentration, the intercept with the linear fit gives the $\delta^{18}$O value of unmodified CO from combustion processes (mainly traffic). For the BERLIOZ data the ap-

plied linear fit had an high correlation coefficient of $R^2$=0.77 and an intercept of 20.4±2.2 ‰. The Kollumerwaard and Schauinsland data all lie close to the dilution line defined by the fit. This underlines that $\delta^{18}O$ variations at continental stations, which are influenced by local and regional sources, are mainly due to the admixing of CO from combustion processes, which dominates the fractionation process of the OH sink.

## 4.8 Conclusion

The seasonal cycles observed for CO mixing and isotopic ratios at Izaña are mainly explained by the OH seasonality. While continuous samples were representative of the background signal at the subtropical station Izaña, large variations occurred in the measured CO, $^{14}CO$ and $\delta^{18}O$ values of spot samples. These short term synoptic scale variations often exceeded the mean seasonal cycles. We showed with the help of back trajectories that air masses from very different origins reach the remote station Izaña. Thus important source regions like Europe and North America, as well as very clean maritime or African air were characterized by our isotopic study. For some samples from the African continent biomass burning events were detected in the CO and $\delta^{18}O$ signals between January and March 1997 to 1999. The large range of latitudinal origins of the air masses allowed to confirm and estimate the large latitudinal gradients occurring in the CO, $^{14}CO$, $\delta^{13}C$ and $\delta^{18}O$ signals at Izaña.

The first two years of our three year record of CO mixing ratios and its stable isotopes at Izaña have been used together with records from four other stations for an inverse CO modeling study by Bergamaschi et al. [2000b]. This made it possible to quantify the seasonal variation in the contribution of CO sources which were responsible for the small phase shift observed in the $\delta^{13}C$ record relative to CO. This is mainly due to the changing relative contribution of the $CH_4$ oxidation source to CO levels.

Through the comparison of our Izaña measurements to the Spitsbergen record we could address the question of the large interannual differences seen at Izaña between 1997 and 1999. While the measurements of CO and its isotopic composition at Izaña resulted in values that were close to measurements at the tropical station Barbados from mid-1996 to mid-1997, values in 1998 are more representative of higher latitudes and thus the difference to the Spitsbergen record was less pronounced. This explanation for the observed interannual variations mainly between 1997 and 1998 is further supported by our $SF_6$ measurements at Izaña. Figure 3.5 shows that $SF_6$ concentrations in 1997 where slightly lower compared to the interannual trend, while

they were on average slightly higher in 1998. This is especially true for the continuous samples which are considered to be representative of the background signal at Izaña. This is a further indication that in addition to large CO sources at the end of 1997, which we attribute to a larger biomass burning source in this year, the large scale meteorological situation also changed. Further analysis of back-trajectories, as has been done by Schäfer [1997] for the period 1992 to 1997, should allow to distinguish these two factors which influenced the Izaña record.

Finally long term records of CO and its isotopic composition from two continental stations, Schauinsland and Kollumerwaard, were compared to measurements during the BERLIOZ campaign in July/August 1998. While the observed $^{14}$CO and $\delta^{13}$C variations were comparable to those from high northern and subtropical latitudes and defined a latitudinal gradient, the observed variations in CO and $\delta^{18}$O were much larger at these continental sites and were explained by the influence of combustion processes.

# Chapter 5

# Antarctic firn air records

Temporal trends of atmospheric trace gases represent a crucial information for the understanding of their global budget. Using Antarctic firn air the atmospheric trend of methane isotopic ratios over much of the present century has been reconstructed. High volume air samples were extracted at several depth levels at two sites in East Antarctica. Methane concentrations and its $^{13}C/^{12}C$ and D/H ratio were determined by gas chromatography, mass spectrometry and infrared spectroscopy. A firn air transport model was applied to reconstruct past atmospheric trends in methane and its isotopic composition. Also results from an atmospheric model are presented, which explores changes in methane sources and OH sink compatible with our reconstructed atmospheric trends.

Historical information about the isotopic ratios of $CH_4$ in the atmosphere is still limited. [Stevens & Engelkemeir, 1988] pioneered the investigation of atmospheric $\delta^{13}C$ trends in the northern and southern hemispheres. Since then other attempts have been made for long-term monitoring of this signal at various sites ([Quay et al., 1996] [Lowe et al., 1999], and references therein), including $\delta D$ Marik [1998], thus providing some information over the last decade. The recent analysis of the Cape Grim air archive and firn air samples, collected at Law Dome in Antarctica, have extended the history of $\delta^{13}C$ to the last 20 years [Francey et al., 1999]. This study showed an increase of $\sim$0.6 ‰ in $\delta^{13}C$ since 1978, while the $CH_4$ mixing ratio increased by $\sim$200 nmol/mol. The authors concluded that global $CH_4$ sources and sinks probably remained constant since 1982, and that the trend observed in $\delta^{13}C$ reflects the slower equilibration of isotopic signals in the atmosphere compared to mixing ratios. Other historical information on $CH_4$ isotopic trends is provided by ice core measurements. The only such record to date, suggests an increase in $\delta^{13}C$ of $\sim$2 ‰ since pre-industrial times [Craig et al., 1988]. The authors interpreted this in terms of a biomass burning source strength in the present-day $CH_4$ budget, which

would amount to about 50 $\mathrm{Tg\,yr^{-1}}$.

The present study is part of the European Project FIRETRACC (Firn Record of Trace Gases Relevant to Atmospheric Chemical Change Over 100 Years) which included several laboratories:

- CNRS Laboratoire de Glaciologie et Géophysique de l´Environnement(LGGE), France
- British Antarctic Survey (BAS), UK.
- School of Environmental Sciences, University of East Anglia, UK.
- Physics Institute , University of Bern, Switzerland.
- MPI, Mainz, Germany

We use air captured in Antarctic firn (unconsolidated snow), spanning several decades due to the time required for gas diffusion in this porous medium. The advantage of firn lies in the possibility of extracting much larger amounts of air compared to ice-cores, which makes it possible to study with greater accuracy and smaller risk of contamination the decadal to secular history of trace gases of low abundance, including their isotopic composition. An additional rational for collecting very high sample volumes was to allow measurements of $^{14}CO$ with an abundance of about 20 molecules per $cm^3$ (STP) and other ultra rare atmospheric trace gases.

In this chapter we focus on measurement and modeling of $CH_4$ mixing ratios including its stable isotopes, $^{13}C$ and D, from two drilling sites in Antarctica in order to reconstruct their evolution in the atmosphere over the last 50 years. In a second step these reconstructed trends are interpreted with the help of an atmospheric model in terms of changing ratios of natural to anthropogenic methane sources over time. Because of the high sensitivity of $\delta D$ levels to changes in OH mixing ratios, this will be done with regard to potential changes in the OH sink.

## 5.1 Antarctic sampling sites

The first drilling conducted by the British Antarctic Survey (BAS) took place in Dronning Maud Land (DML) (77° S, 10° W; 2300 m asl) in January 1998. The site has a mean annual temperature of $-38\,^{\circ}\mathrm{C}$ and a relatively high snow accumulation rate (60 $\mathrm{kg\,m^{-2}\,yr^{-1}}$) compared with the Antarctic plateau. Eighteen firn air samples were taken starting from the surface to the firn-ice transition zone at 73.5 m. Similarly, in January 1999 drilling and firn air sampling was conducted by BAS and

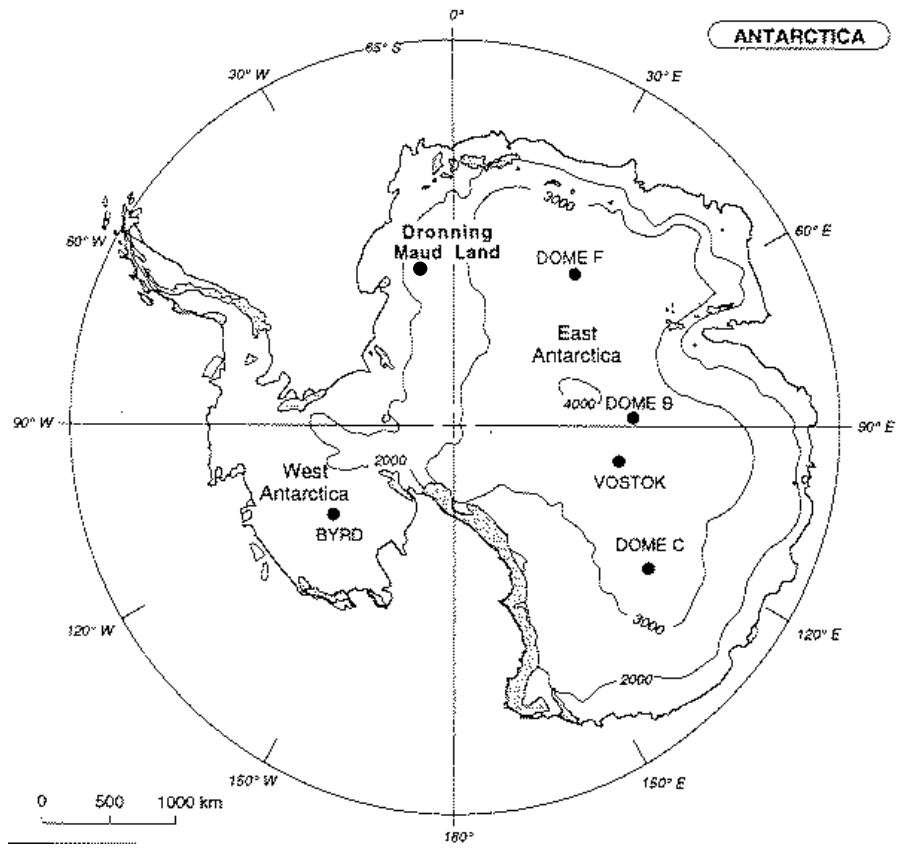


**Figure 5.1:** FIRETRACC drilling sites

| site | location | T | Acc | Alt | P | depth |
|---|---|---|---|---|---|---|
| Dronning Maud Land | 77° S, 10° W | −38 | 60 | 2300 | 730 | 73.5 |
| Dome C | 75° S, 123° W | −53 | 30 | 3240 | 655 | 99.5 |

**Table 5.1:** Location, annual mean surface temperature $T$ (°C), accumulation rate $Acc$ ($\mathrm{kg\,cm^{-2}\,yr^{-1}}$), altitude $Alt$ (m), atmospheric pressure $P$ (hPa) and $depth$ (m) of the firn-ice transition at both Antarctic drilling sites.

the Laboratory of Glaciology and Geophysics of the Environment (LGGE) at Dome Concordia (DC) (75° 06′ S, 123° 23′ E, 3233 m asl). This is an extremely cold site (−53 °C) with a low accumulation rate (30 $\mathrm{kg\,m^{-2}\,yr^{-1}}$), resulting in a deeper firn-ice transition (99 m) than DML. This time 20 air samples were taken down to 99.5 m. In Figure 5.1 the location of the two drilling sites in East Antarctica is shown and in Table 5.1 their climatic parameters are listed.

The sampling of firn air was first documented by Schwander [1993]. Here we describe a modified set-up for the extraction of large firn air samples of up to 1000 l. Drilling progressed stepwise in intervals of 1 to 5 m. At each level the drill was withdrawn and the hole sealed close to the bottom with a 5 m (DML) or 3 m (DC) long inflatable rubber bladder. Two continuous, 105 meter long, 3/8 inch PFA tubes passed through the bladder, connected the pumping system at the surface to the bottom of the hole. Through one of those tubes, ending just below the aluminum end cup of the bladder, air was drawn continuously at a high flow rate (25 $\mathrm{l\,min^{-1}}$) to waste. The sample air itself was drawn at a lower flow rate (15 $\mathrm{l\,min^{-1}}$) via the other tube, which ended about 10 cm lower. Both inlets were separated by a set of metal baffles. The function of these baffles (originally devised by M. Bender, Princeton University) is to prevent any possible contamination from the bladder material or leakage past the seal from reaching the sample inlet at the very bottom of the hole.

The quality of the sampling was continuously monitored with an infrared $CO_2$ analyzer (Li-Cor) attached to the sample air stream and calibrated with a standard gas. Stable $CO_2$ levels (at $\pm$ 0.1 µmol) were usually encountered after about 10 min flushing following inflation of the bladder. Purging and filling the different types of sample flasks at each depth level usually required about 2 hours and 1200 liters of firn air. The maximum difference in $CO_2$ mixing ratio observed between the start and the end of sampling was 1 µmol at DC.

A high purity air extraction system was deployed consisting of a 2-stage metal bellows pump (Parker) for filling small cylinders, i.e. for LGGE 0.5 l CSIRO glass flasks pressurized at 25 psi. Subsequently the air emerging from the metal bellow pump was fed into a three-stage, oil-free, modified RIX SA3 piston compressor [Mak & Brenninkmeijer, 1994a], which allowed the high volume air samples for the MPI to be compressed to $\sim$ 120 bars in 5 or 10 l aluminum cylinders (Scott Marrin). See section 2.1 for a detailed description of the cylinders and compressor system respectively.

## 5.2 Firn air measurements

The D measurements of $CH_4$ presented here are the first from firn air. For $^{13}C$ we report in addition to our analysis those from a second laboratory, LGGE.

The high volume samples allowed a wide range of trace gases to be analyzed. At the MPI GC analysis for CO, $CH_4$, $CO_2$, $N_2O$ and $SF_6$ was performed. Further, mass spectrometry was applied after the extraction of $CO_2$ and CO for $^{13}C$ and $^{18}O$ isotope analysis. Analysis of the $^{14}C$ content of CO, $CH_4$ and $CO_2$ were done by

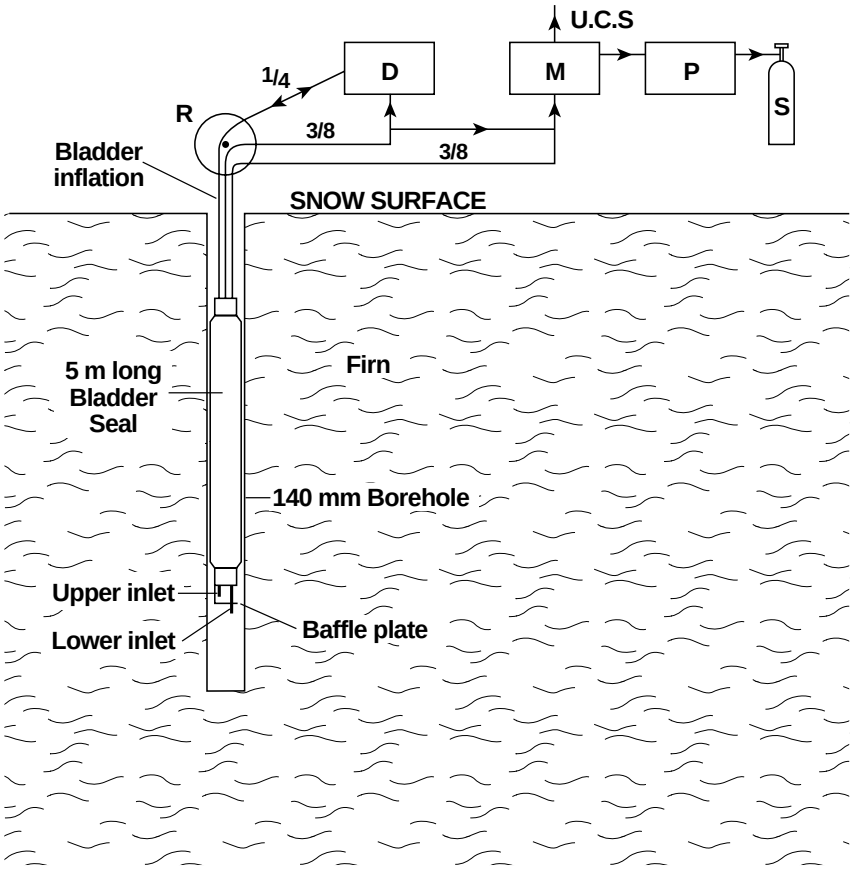


**Figure 5.2:** Firn air sampling at Dronning Maud land and Dome C. D: 2-stage, 4-leads diaphragm compressor for inflation of the bladder; M: 2-stage, 2-leads metal bellows compressor for the medican pressure ultra clean samples (U.C.S); P: modified 3-stage RIX compressor for the filling of high volume sample cylinders (S); R: 3-section reel with 2×110 m 3/8 Inch PFA and 1×110 m 1/4 Inch for the bladder.

accelerator mass spectroscopy (AMS). In this chapter we mainly concentrate on $CH_4$ and its isotopes, $^{13}C$ and D.

At LGGE aliquots of firn air were first used for the determination of $CH_4$ and $CO_2$ by gas chromatography (Varian 3300). Working reference gases are calibrated against the NOAA/CMDL scale at LGGE and the overall precision for the firn air samples is estimated to be $\pm 4\,\mathrm{nmol/mol}$ and $\pm 0.4\,\mu\mathrm{mol/mol}$ respectively. Then, $^{13}C/^{12}C$ of $CH_4$ was measured with a Finigan GC-Combustion interface coupled to a Finnigan MAT 252 isotope-ratio mass spectrometer.

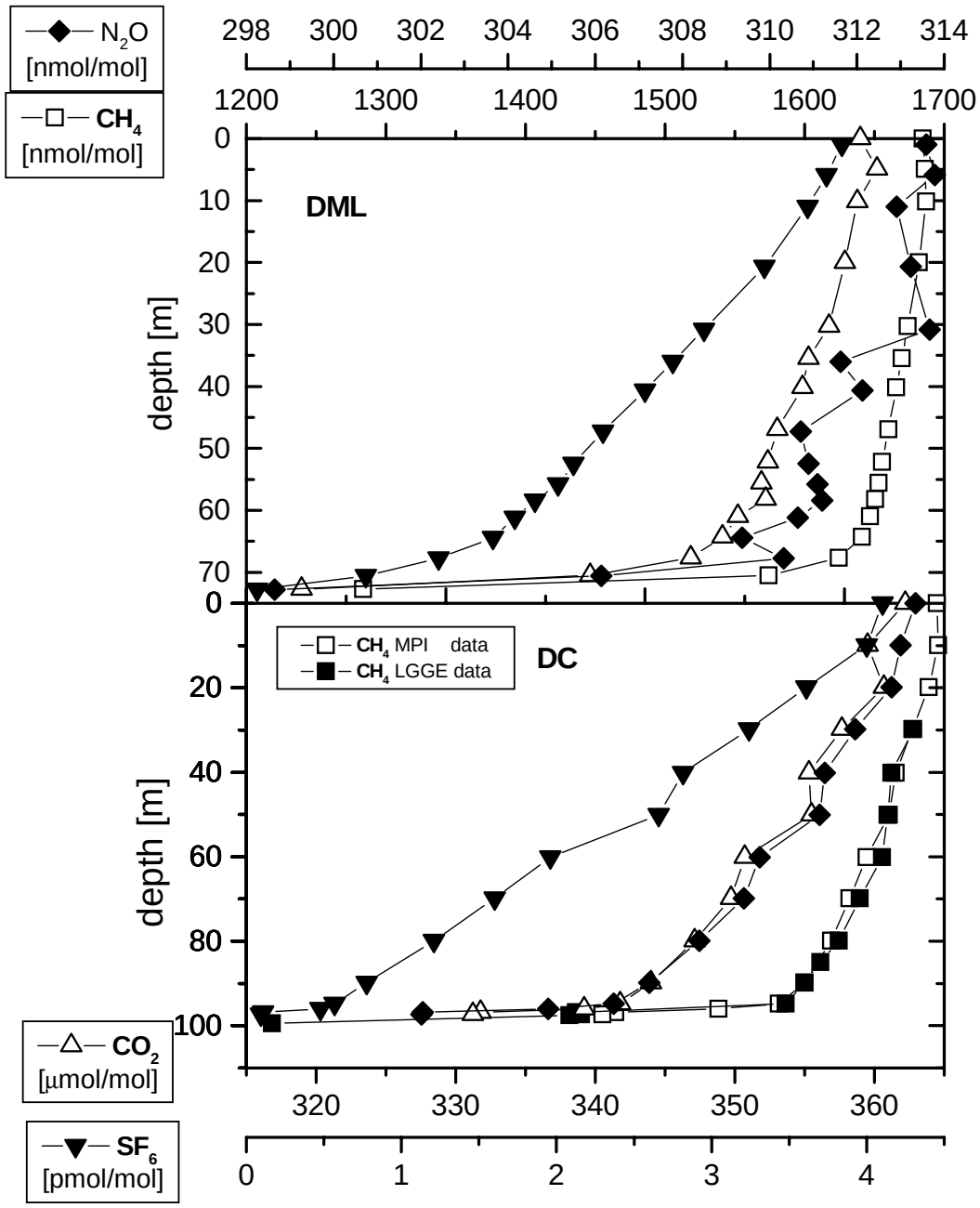


**Figure 5.3:** $CH_4$, $CO_2$, $N_2O$ and $SF_6$ mixing ratios of firn air at DML and DC plotted against depth.

### 5.2.1 Mixing ratios

The data for DML and DC in Figure 5.3 show the expected decrease in the mixing ratios of $CH_4$, $CO_2$, $N_2O$, CO and $SF_6$ with depth. For $CH_4$ the mixing ratios at DML (January 1998) ranged from contemporary atmospheric levels of 1684±2 nmol/mol at the surface to 1284±2 nmol/mol at the firn-ice transition at 73.5 m. $CH_4$ mix-

ing ratios at DC (January 1999) were 1694±2 nmol/mol at the surface and went down to 1218 ±10 nmol/mol near the close-off zone at 99.5 m. Thus a change in concentrations of more than 400 nmol/mol has been observed, reflecting the underlying increase of methane concentration over time. The two ambient air measurements from January 1998 and 1999 indicate an atmospheric increase of +0.6 %/yr for 1998, in agreement with measurements from the NOAA/CMDL network.

At DC methane mixing ratios have been measured by both MPI and LGGE. The two methane series agreed well within the uncertainty of the measurements (see Figure 5.3). One notable exception are the samples taken at a depth of approximately 97 m, where the MPI results were significantly higher than those of LGGE. The difference was also observed for $\delta^{13}C$ ($CH_4$) and for $CO_2$. The most plausible explanation lies in the sequence of sampling, and in the difficulty of recovering firn air in the low open porosity close-off region. The LGGE flasks were the first to be filled after inflating the bladder and the MPI flasks followed. At this specific depth level, the prolonged pumping may have created a route towards lower depths thus filling MPI flasks with shallower and therefore younger air. For this reason only the LGGE results are considered at the DC depth of 97 m in the following discussion and interpretation.

### 5.2.2 $\delta^{13}C$ of $CH_4$ in firn air

For the further analysis of the firn profiles we also consider $\delta^{13}C$ measurements which have been carried out at LGGE. For Dronning Maud Land $\delta^{13}C$ was measured on the same high volume samples, while for Dome C the $\delta^{13}C$ measurements from LGGE were done on separate glass flasks.

The $^{13}C$ analyses at LGGE were performed on a Finnigan MAT-252 mass spectrometer, coupled to a Finnigan GC / combustion interface in continuous flow mode (CF-IRMS). A custom pre-concentration unit was used to isolate $CH_4$ from the major air constituents. This unit included a sample loop of 150 ml, a Haysep D column (20 cm length, 1/8 inch ID) held at −130 °C with a pentane-ice slush, and a 3 m capillary focussing trap also held at −130 °C and identical to the main separation column (GS-Q, 30 m length, 0.32 mm ID). After pre-concentration, methane was separated from the residual trace gases on the capillary column, combusted to $CO_2$ and injected with helium into the mass spectrometer for measurement of masses 44, 45 and 46. Isotopic calibration was performed against a pure $CO_2$ working standard with a $^{13}C/^{12}C$ ratio of −45.98±0.02 ‰ versus PDB, which is close to the carbon isotopic ratio of methane in the atmosphere. This value was determined by intercalibration with the MPI standard and with other laboratories measuring methane

isotopes. Simultaneously with the firn air measurements the external accuracy of the CF-IRMS was determined by regularly analyzing a tank of atmospheric air sampled at Baring Head, New Zealand, on 27 May 1997 by D. Lowe (National Institute of Water and Atmospheric Research, NIWA), with a $\delta^{13}C$ of $-47.16 \pm 0.05$ ‰ versus PDB. The firn air samples were each measured at least four times, using a sample size of only 80 ml STP. The mean reproducibility on replicate firn air samples and the NIWA standard was $\pm 0.05$ ‰.

For the international isotope standard NZCH [Brenninkmeijer, 1990] our measurements gave a value of $-47.13$ ‰, close to the $\delta^{13}C$ value of $-47.12$ ‰ based on a laboratory intercomparison [Röckmann, 1998a]. The low abundance of $CH_4$ in the older firn air samples necessitated the recovery of $CH_4$ after the MISOS D/H measurements for subsequent combustion, instead of splitting samples as is usually done [Bergamaschi et al., 2000a]. The resulting measurement error in $\delta^{13}C$ was estimated to be $\pm 0.08$ ‰ for the DML data. The recovery was improved in 1999 and the measurement error thus reduced to $\pm 0.04$ ‰ for the DC data. Regarding the LGGE measurements of the DML samples (Figure 5.4), made on residual air in the MPI flasks, a $+0.25$ ‰ correction was applied, which takes into account a mass spectrometer non-linearity effect caused by peak intensity differences between standard and sample on this set of measurements.

The $\delta^{13}C$ values for DML and DC are shown in Figures 5.4 a and b respectively. At the surface the $\delta^{13}C$ values were $-47$ ‰ in January 1998 (DML) and January 1999 (DC). With increasing depth the firn air methane was progressively depleted in $^{13}C$ and reached $-50$ ‰ at the firn-ice transition. The $\delta^{13}C$ measurements of both isotope laboratories are plotted together and a good agreement of approximately 0.02 ‰ can be observed between the LGGE and MPI profiles. Only near the firn-ice transition of DC (Figure 5.4b) did the LGGE measurements become slightly lighter relative to those of MPI, most probably due to the sampling artifact discussed in section 5.2.1.

For DML (Figure 5.4a) the LGGE data are significantly less scattered. The contamination effects due to the recovery of the methane from the MISOS system, as discussed above, might have been more important than expected. Both laboratories did measure a significant variation of nearly 0.3 ‰ in the top 10 m in the DC record (Figure 5.4b), most probably reflecting seasonal thermal fractionation of gas isotopes in cold firn compared to the relatively warm surface of the austral summer [Severinghaus & Brook, 1999]. This phenomenon impacts the firn composition only over the upper 10-15 m and has no effect deeper down, provided that there was no abrupt climate change at the surface over the time period covered by the firn air

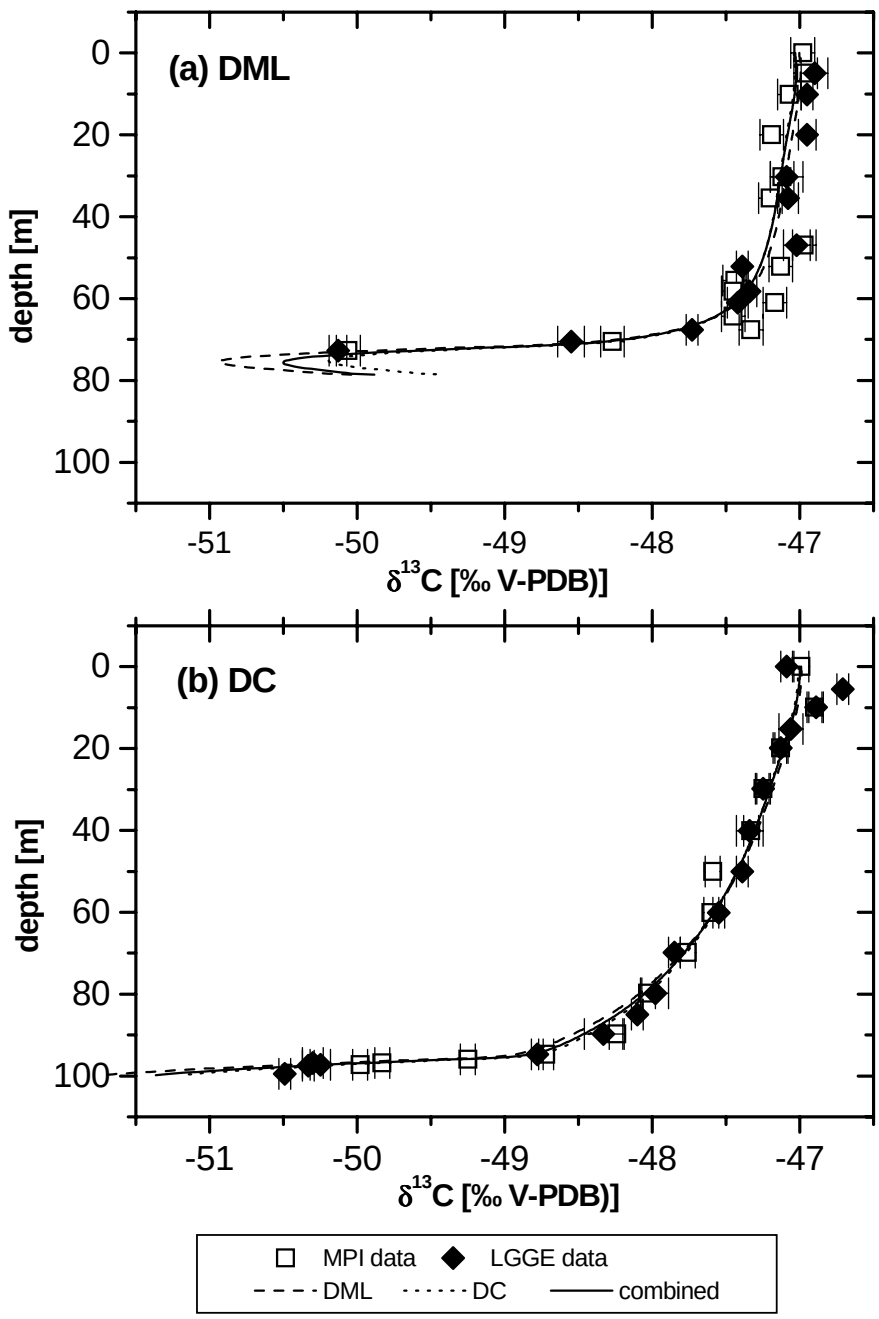


**Figure 5.4:** $\delta^{13}C$ of $CH_4$ in firn air at (a) DML and (b) DC, measured by MPI and LGGE. Error bars are $1\sigma$ analytical precision and $1\sigma$ scattering on replicate measurements for MPI and LGGE respectively. Lines running through the data are firn model results for the best atmospheric $\delta^{13}C$ scenarios (as a function of time in figure 5.11) for DML, DC and the combination of both sites (see section 5.5.1).

samples.

The measured total $\delta^{13}C$ range of nearly 3 ‰ from top to bottom of the two profiles is very large compared to direct atmospheric measurements. For example, the seasonal amplitude observed at a remote southern hemisphere station, Baring Head (41° S, 175° E), is around 0.4 ‰ and the observed trend is smaller than 0.05 ‰ $yr^{-1}$ [Lowe et al., 1994].

### 5.2.3 δD of $CH_4$ in firn air

The δD measurements are shown for DML and DC in Figures 5.5 a and b respectively. The values obtained for ambient air samples were −70 ‰ at DML in January 1998 and as light as −80 ‰ at the firn-ice transition at 73.5 m. For DC they were −72 ‰ in January 1999 and reached −82 ‰ at 97.5 m. The δD measurement error including sample preparation is estimated to be ±1 ‰. The ambient air at DML and DC was 2 to 3 ‰ enriched compared to the shallowest firn air. Opposite to the $\delta^{13}C$ signal, thermal fractionation seems to be overwhelmed by the seasonality of the atmospheric signal for δD propagating in the shallow firn. As we will show later, the firn integrates seasonal variations after the first few meters. This means that the recent annual average should be −74.3 ‰. The strong kinetic isotope fractionation of nearly 300 ‰ in the $CH_4$ + OH reaction drives a strong seasonal δD cycle which reaches its maximum in May, when OH levels are beyond the summer maximum. For January ambient air measurements for δD are expected to be close to the annual mean value and not 2 to 3 ‰ enriched as observed. The measured difference between the ambient air samples and the first firn air samples is not expected and has no explanation at the moment. The fact that coherent atmospheric scenarios from DML and DC can be drawn from the firn profiles (section 5.5) suggests that there was no significant artifact in the firn (supposedly temperature, chemical composition, or density related) disturbing the δD signal, and that at least the relative trend in δD is robust.

As for the $\delta^{13}C$ variation, the observed δD range of ∼10 ‰ from top to bottom is high compared to present atmospheric variations. For instance, a seasonal cycle of 4 ‰ in East Antarctica has been deduced for Neumayer Station (70° S, 8° W), after calculating monthly mean values over a 6 year period [Marik, 1998] (see also section 3.2 for seasonal cycles and the atmospheric trend at Izaña)

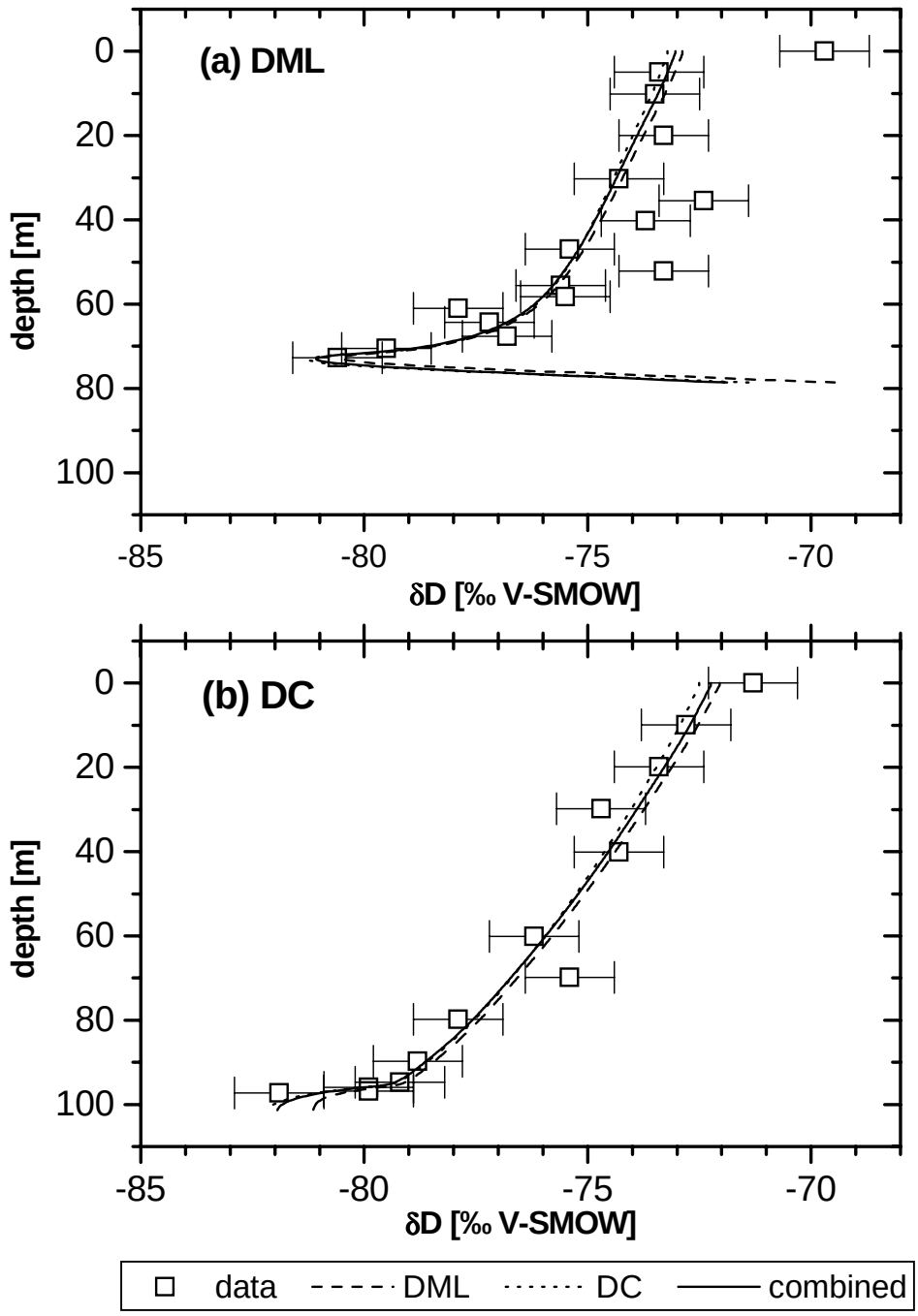


**Figure 5.5:** δD of $CH_4$ in firn air at (a) DML and (b) DC. Error bars are $1\sigma$ analytical precision. Lines running through the data are firn model results for the best atmospheric δD scenarios (which are shown as a function of time in figure 5.12) for DML, DC and the combination of both sites (see section 5.5.1).

## 5.3 Properties of firn

Firn is a porous medium which results from the densification of dry snow at the surface of polar ice sheets and glaciers. Its structure is discussed in section 5.3.1. Firn is permeable to gases and the diffusivity of these gases decreases with the increasing density of the firn with depth. Variations in atmospheric trace gas mixing ratios occurring at the surface continuously propagate downwards by molecular diffusion and are influenced by the effect of gravitation, which will be discussed in sections 5.3.3 and 5.3.2 respectively. During these processes the atmospheric variations are attenuated by diffusive mixing. In general, light gases such as methane diffuse faster downwards whereas gravitational settling favors the accumulation of the heavier gases in the deepest part of the firn. These two main processes modify mixing ratios as well as isotopic ratios.

### 5.3.1 The firn structure

Figure 5.6 indicates the typical depth, density and age ranges for polar ice sheets [Schwander, 1989]. The firn layer at polar sites can be separated into four different zones that are relevant for the transport of gases through this permeable medium.

- The mixing zone:
  In this snow-layer close to the surface (0 to 10-25 m depth) the air can be mixed by winds, atmospheric pressure variations or thermal gradients. If strong annual temperature gradients occur thermal diffusion effects can be important [Leuenberger et al., 2000]. At the surface the density is typically around 300 $\mathrm{kg\,m^{-3}}$.

- The diffusion zone:
  This zone covers most of the firn layer (10-25 m to 60-110 m depth). It is defined as the zone where transport through the open pores takes place until the diffusion gets zero (the open porosity can still be non-zero). The transport of gases in this zone is due to mass differences of the molecules (gravitation effect), to the concentration gradient (diffusion effect) and the downward movement of air created by the trapping of gas in the firn close-off zone.

- The non-diffusion zone:
  Here the air begins to be trapped into bubbles and open pores and bubbles coexist. The diffusion is already zero, while the open porosity is still non-zero. The average gas age increases rapidly in this zone (up to 100 years), because no dilution with younger air masses from above takes place any longer.

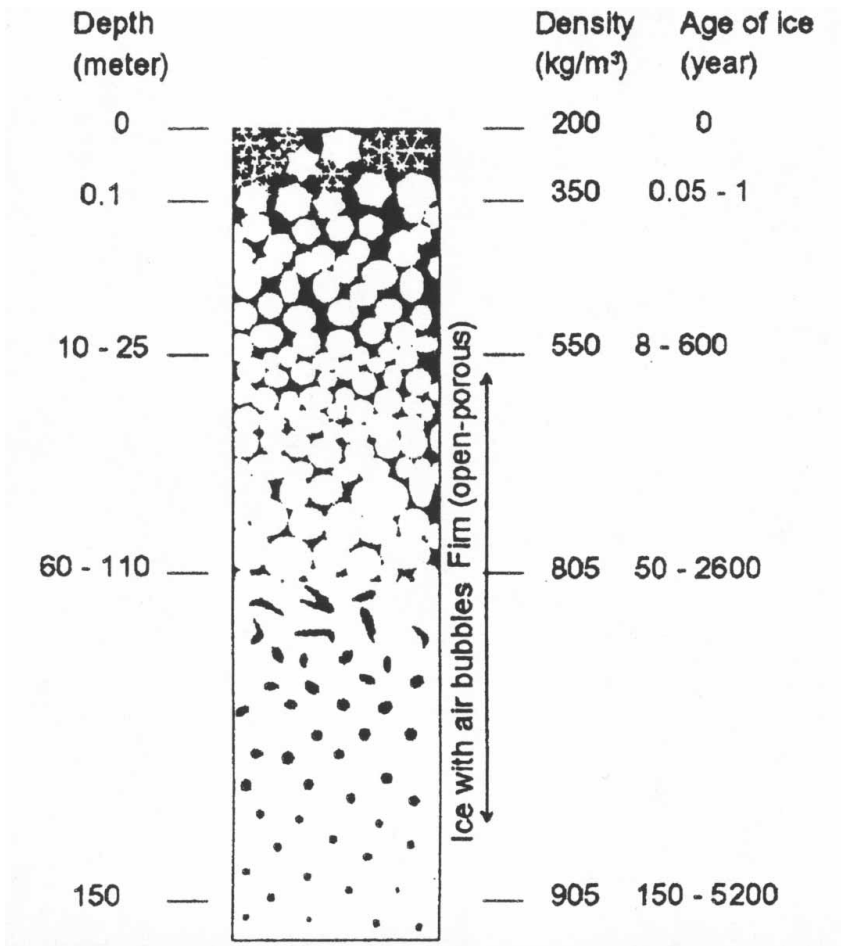


**Figure 5.6:** Diagram of the snow-ice transformation, indicating the typical depth, density and age ranges for polar ice sheets [Schwander, 1989].

Nevertheless, the firn air is even at this depth considerably younger than the surrounding ice, which can be up to 2600 years old. The air in the remaining open pores and the bubbles is transported downwards with the advection of the ice layers.

- The close-off zone (firn-ice transition):
  From this zone onwards all porosity is closed and the gas trapped in bubbles is descending with the ice layers. This downward movement only depends on the snow accumulation rate at the surface. The density of the ice at the close-off zone is close to 850 $\mathrm{kg\,m^{-3}}$ [Arnaud, 1997] (this value has changed since [Schwander, 1989] in Figure 5.6).

The factors determining gas transport and mixing in the firn are molecular weight, the molecular diffusion coefficients of the considered trace gas, pressure, temperature, and the porosity and tortuosity profiles of the firn matrix. The firn is characterized by three profiles that can be measured as a function of depth (z) and two climatic parameters:

- the density profile $\rho(z)$
- the closed porosity profile $\epsilon(z)$
- the tortuosity profile $\gamma(z)$
- the mean annual surface temperature $T$
- the accumulation rate at the surface $Acc$

The porosity profile $\epsilon(z)$ is closely linked to the density profile of the firn:

$$\epsilon(z) = 1 - \frac{\rho(z)}{\rho_{ice}} \tag{5.1}$$

The effective diffusivity of a specific gas in the firn will depend on the porosity profile and on the molecular diffusivity of the pure gas in air. The tortuosity profile of the firn reflects the influence of the firn structure on the effective diffusion coefficient $D(z)$ (in $m^2/s$):

$$\gamma(z) = \frac{D(z)}{D_m} \tag{5.2}$$

For this study the density profiles of both drilling sites have been measured by the BAS and a smoothed fit through these measurements has been used in the firn diffusion model discussed in section 5.4. In Figure 5.7 the density profiles of both sites are shown.

The open porosity profile can be directly measured [Arnaud, 1997]. In our study we use the open porosity calculated by J.M. Barnola (personal communication). Figure 5.7 also shows the open and total porosity profiles of both sites.

### 5.3.2 Gravitation processes in firn

The air in the open firn pores is considered to be hydrostatic . Therefore the classic results for an isotherm atmosphere can be applied to the air below the mixing zone [Craig et al., 1988b]. The concentration of air in firn is then given by the barometric equation:

$$c_{air}(z) = c_{air}(0) \cdot exp(-\frac{M_{air} g z}{RT}) \tag{5.3}$$

$z$ : depth (m)

$M_{air}$ : molecular air mass ($29 \times 10^{-3}$ kg mole$^{-1}$)

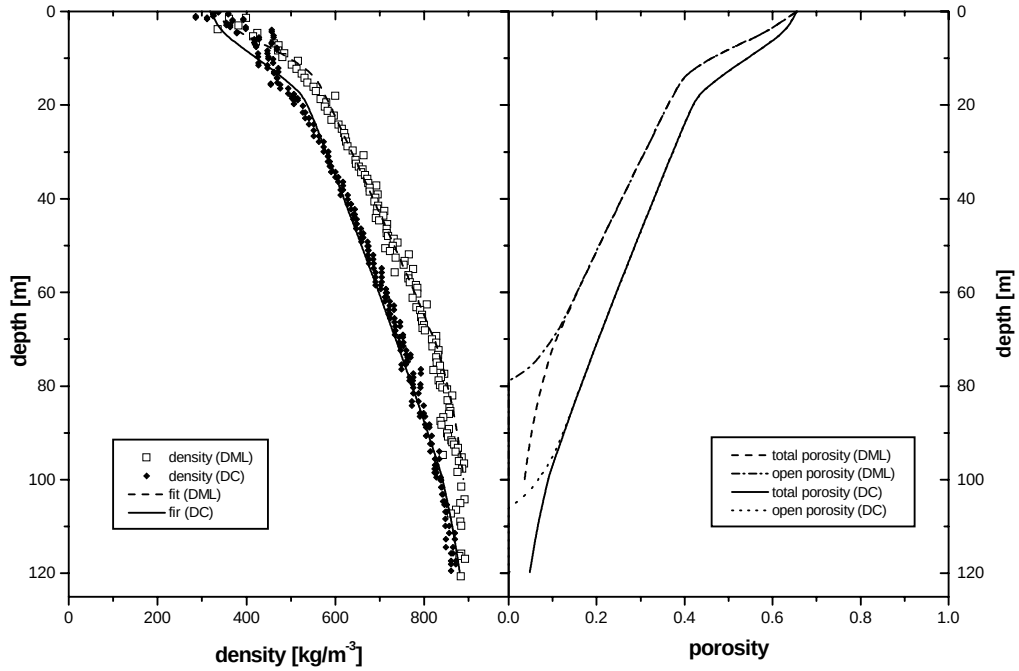


**Figure 5.7:** density profiles for DML (dashed line) and DC (dotted line)

$g$ : gravitation constant (9.81 $\mathrm{m\,s^{-2}}$)
$R$ : perfect gas constant (8.314 $\mathrm{J\,mole^{-1}\,K^{-1}}$)
$T$ : temperature (K)

Equation 5.3 allows to calculate the gravitational effect in firn at depth $z$ for two gases with mass difference $\Delta M$:

$$\Delta(z) = \Delta M \frac{gz}{RT} \cdot 1000 \tag{5.4}$$

$$\text{with} \qquad \Delta = 1000 \cdot (\frac{R}{R_0} - 1)$$

where $R$ is the concentration ratio at a given depth and $R_0$ is the atmospheric concentration ratio of both gases. For isotopes $\Delta$ is the $\delta$ value defined in section 1.4.1.

This theoretical value of the gravitation effect in firn can be compared to measurements shown in figure 5.8. The depth profiles for $\delta O_2/N_2$, $\delta^{29}N_2$, $\delta Ar/N_2$ and $\delta^{34}O_2$ are plotted for DML (Rolf Neubert, personal communication). The fact that $N_2$, $O_2$ and Ar exhibit no significant temporal trend in the atmosphere is used to separate the gravitation effect from diffusion effects due to concentration gradients. The

measured $\delta^{29}N_2$ value of 0.33±0.008 ‰ at 71 m is close to the theoretical value of 0.35 ‰ (equation 5.4). The $\delta^{34}O_2$ value of 0.69±0.04 ‰ (measured at 71 m) directly reflects the factor of ΔM=2 between $^{32}O_2$ and $^{34}O_2$.

We note that the observed changing concentration ratios between gases due to gravitation effects in the firn reflect that the effective distance covered by a gas is much longer than the depth at which the sample was taken. For the scale height ($z_0 = RT/Mg$) defined by equation 5.3 the calculated values for $O_2$ and $N_2$ are 6224 m and 5446 m respectively (T=235 K at DML). The mixing ratios of both gases are, however, already attenuated at depths of less than 100 m. This phenomena of increasing effective distances covered by gases with increasing depth of the firn is addressed in the next section.

Note that in Figure 5.8 all isotope ratios deviate significantly from the theoretical value between 0 m and 20 m. This is due to thermal diffusion effects in the mixing zone of DML, which is discussed in section 5.3.4.

### 5.3.3 Diffusion processes in firn

In the troposphere and stratosphere turbulent processes dominate mixing and transport processes and molecular diffusion can be neglected. In contrast, the separation of molecules by molecular diffusion can be observed in the higher atmospheric layers above 80 km, i.e. the mesosphere. In this region temperature and pressure are low enough and result in mean free paths of several cm. Here molecules of different mass separate and the very light molecules such as hydrogen are even lost to free space. A similar effect of gas separation due to molecular diffusion can be observed in firn.

For the discussion of diffusion effects in firn we assume that we are in a Knudsen regime (mean free path ≫ radius of the molecules), where the diffusion is characterized by a single diffusion coefficient. The mean free paths of molecules in firn are in the range of $10^{-8}$ m, whereas the dimension of the pores is in the order of $10^{-4}$ m. This implies that molecules collide less frequently with the firn structure than between themselves.

In a first step the temperature and pressure dependence of diffusion coefficients are discussed. Bzowzki et al. [1990] calculated the diffusion coefficient $D_{ij}$ for a binary mixture of gases $i$ and $j$:

$$D_{ij} = \frac{3}{8}\sqrt{(\frac{m_i + m_j}{m_i m_j})\frac{kT}{\pi}} \cdot \frac{1}{\sigma_{ij}^2 \Omega_{ij}^*(T_{ij}^*)} \tag{5.5}$$

$m_i$: mass of molecule $i$

$\sigma_{ij}$ : characteristic parameter of the inter-molecular potential (distance). For a

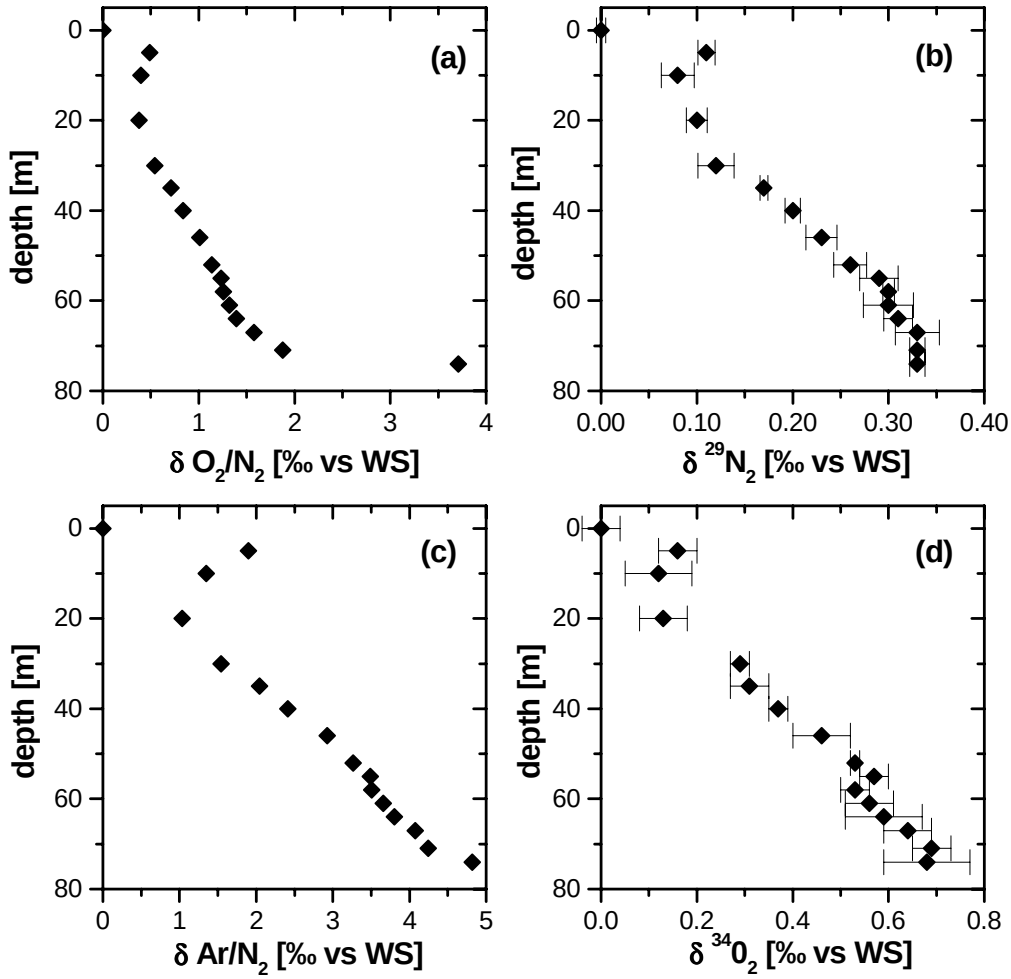


**Figure 5.8:** Depth profiles for $\delta O_2/N_2$, $\delta^{29}N_2$, $\delta Ar/N_2$ and $\delta^{34}O_2$ for DML. $\delta$ values are given relative to a working standard (WS) of the atmospheric isotope (Rolf Neubert, personal communication).

potential energy equal to zero this corresponds to the distance between molecules

$\Omega_{ij}$ : collision integral of the diffusion

$\Omega^*_{ij} = \Omega_{ij}/(\pi\sigma^2_{ij})$: reduced collision integral

$T^*_{ij} = kT/\epsilon_{ij}$: reduced temperature

$\epsilon_{ij}$ : characteristic parameter of the inter-molecular potential (energy), represents the maximum of attraction between the molecules

The collision integral of the diffusion $\Omega_{ij}$ is a function of temperature and of the force between the molecules. To obtain the temperature and pressure dependence of

the diffusion coefficient equation 5.5 can be transformed to:

$$D(T,P) = D_{T_0,P_0} \cdot \frac{P_0}{P} \cdot (\frac{T}{T_0})^{3/2} \frac{\Omega^*(T_0^*)}{\Omega^*(T^*)} \tag{5.6}$$

For the last term, $\Omega^*(T_0^*)/\Omega^*(T^*)$, the temperature dependence varies with the considered gas. For the overall temperature dependence Schwander et al. [1993] proposed an exponent of 1.85 for all gases. For the temperature range relevant for firn air Trudinger et al. [1997] found that the exponent can vary between 1.8 and 1.95, resulting in diffusion coefficients which vary less than 1%. We therefore consider the pressure and temperature dependence to be:

$$D(T,P) = D_{T_0,P_0} \cdot \frac{P_0}{P} \cdot (\frac{T}{T_0})^{1.85} \tag{5.7}$$

The equation 5.5 can also be used to calculate the diffusion coefficients for gases for which measurements are not yet available. In this case the diffusion in air is calculated for a mixture of 21.2% of oxygen and 78.8% of nitrogen after Blancs law [1908]:

$$\frac{1}{D_{gas/air}} = \frac{0.788}{D_{gas/N_2}} + \frac{0.212}{D_{gas/O_2}} \tag{5.8}$$

Finally equation 5.5 can be used to infer the diffusion coefficients of isotopes:

$$\frac{D(M_1)}{D(M_2)} = \sqrt{\frac{M_2(M_1 + M_{air})}{M_1(M_2 + M_{air})}} \tag{5.9}$$

The ratio of diffusion coefficients is in this case only mass dependent.

Table 5.2 lists the diffusion coefficients calculated with equations 5.5 and 5.9 for the gases which are used in this study. They are also given relative to the diffusion coefficient of $CO_2$, which is the value used in the firn air diffusion model in section 5.4.

For the flux through firn we neglect the thermal diffusion and only consider the molecular diffusion and the discussed gravitational effect:

$$\vec{j} = \vec{j}_{diff} + \vec{j}_{grav} = -D(\frac{\delta c}{\delta z} + \frac{Mgc}{RT}) \tag{5.10}$$

$\vec{j}$ : total flux, sum of the flux due to diffusion $\vec{j}_{diff}$ and gravitation $\vec{j}_{grav}$
$D$ : Diffusion coefficient ($m^2$ $s^{-1}$)
In the firn diffusion model from Rommelaere et al. [1997] (see section 5.4) equation 5.10 is solved with respect to conservation of the air and the considered trace gas in the firn.

| gas | mass [$10^{-3}$kg mol$^{-1}$] | diffusion coefficient [cm$^2$ s$^{-1}$] | $D_{gas}/D_{CO_2}$ |
|---|---|---|---|
| $CO_2$ | 44.01 | 0.1203 | 1 |
| $CH_4$ | 16.043 | 0.1702 | 1.415 |
| $SF_6$ | 146.056 | 0.0747 | 0.621 |
| $O_2$ | 31.9988 | 0.1596 | 1.326 |
| $N_2$ | 28.0135 | 0.1583 | 1.316 |
| $^{12}CH_4$ | 16 | 0.1702 | 1.415 |
| $^{13}CH_4$ | 17 | 0.1671 | 1.3889 |
| $CH_3D$ | 17 | 0.1671 | 1.3889 |
| $^{14}N^{15}N$ | 29 | 0.1569 | 1.304 |
| $^{16}N^{18}N$ | 34 | 0.1573 | 1.308 |

**Table 5.2:** Summary of diffusion coefficients (calculated after equations 5.5 and 5.9 at 253 K and 1013 hPa). Also diffusion coefficients relative to $CO_2$ are given (values used in the firn air diffusion model in section 5.4).

### 5.3.4 Thermal Diffusion in firn

Figures 5.8 shows a considerable thermal diffusion effect for firn samples taken in DML at depths of 1 m to 20 m. Between winter and summer temperature gradients occur in the mixing zone. As mentioned in section 5.3.2 no molecular diffusion is expected for the considered gases because of lacking temporal concentration gradients. However, the diffusion coefficients are temperature dependent and therefore the different isotopes diffuse with different velocities. Usually this results in an enrichment of heavy molecules in colder zones.

The impact of the thermal diffusion effect has also been detected for the DC samples [M. Leuenberger, personal communication, 1999]. Because of the lower temperature of DC compared to DML we even detected the thermal fractionation in our $\delta^{13}C$ profile in Figure 5.4. At depths of 1 m to 15 m at DC a deviation of nearly 0.3 ‰ occurs. For $\delta D$ we would expect an effect of the same range, because mass difference and diffusion coefficient are the same as for $\delta^{13}C$ . However, a 0.3 ‰ shift is too small to be detected on our $\delta D$ measurements for which reproducibility is $\pm 1$ ‰.

## 5.4 Firn air diffusion model

Schwander et al. [1993] developed the first model that accounted for the diffusion of gases and an additional modification due to gravitational effects for the interpretation of firn air measurements. Since, two other firn diffusion models from Trudinger et al. [1997] and Rommelaere et al. [1997] have been used in several firn air studies, e.g. [Etheridge et al., 1998] and [Arnaud, 1997].

We apply the firn air transport model developed by Rommelaere et al. [1997] in order to reconstruct the atmospheric history of the methane isotopic ratios from the convoluted firn air signals. The main assumptions in this model are that the climatic parameters (temperature and accumulation rate) and firn structural variables have remain constant in time, and thus also the firn diffusivity profile and depth of the firn-ice transition.

The main assumptions of the firn diffusion model are in detail:

- Isotherm firn
  The model applies only to stable climatic conditions where temperature gradients are limited to the top firn layer, i.e. the well-mixed zone. Otherwise the firn is considered to be constantly at the mean annual temperature of the site.

- Constant accumulation rate and firn structure over the modeled period
  The model is not valid during important climatic changes, which would modify the firn structure and the accumulation rate. In our study we limit the reconstructed atmospheric records to the last 50 years, where this assumption is justified.

- No direct air entraining with the downward movement of the firn layer
  The transport of gases takes place in a porous medium which moves downwards and increases in density $\rho(z)$. Nevertheless, the firn layers do not entrain the air in the open porosity unless they reach the close-off zone. From here the air is trapped in bubbles and moves downwards with the surrounding ice layers.

- Effective diffusion coefficient and tortuosity
  The effective diffusion coefficient is considered to be the product of the molecular diffusion coefficient and a tortuosity function, which is only determined by the firn structure. Once this tortuosity function is established for one molecule, it can be used to calculate the effective diffusion coefficient of any trace gas.

The profile of effective diffusivity is the main unknown in the model [Fabre, 1999]. We infer it, as proposed by Fabre et al. [1999], by calibration with a trace gas of well-

known atmospheric evolution. Here we use the $CO_2$ history, based on atmospheric $CO_2$ monitoring since 1958 [Keeling and Whorf, 1994] and ice core measurements [Etheridge et al., 1996]. Once the effective diffusivity profile has been calibrated for $CO_2$ the mixing ratio of any trace gas in the atmosphere can be computed by inversion techniques from its firn profile, its molecular diffusivity and its mass as described by Rommelaere et al. [1997]. This is true for all gases which do not react with the surrounding snow or ice.

In order to validate the diffusivity profiles for DML and DC, calibrated with $CO_2$ measurements, we apply the firn model to known atmospheric $CH_4$ records. A fit through atmospheric measurements from Palmer Station [NOAA/CMDL], starting in 1978, and ice core measurements [Etheridge et al., 1992] is taken as input of the firn model (see Figure 5.9a). The model-generated DML and DC methane profiles are shown in Figure 5.9b together with our measurements. The agreement between the data and the model reconstruction based on the $CO_2$-calibration is excellent for DML. For DC a difference of $\sim$10 nmol/mol is observed around 90 m, representing less than the equivalence of one year of atmospheric evolution during industrial times. The mixing ratio of 1240 nmol/mol from the deepest firn air sample in DC could not be reproduced by the firn diffusion model, because density data suggest that this level is below the close-off zone, whereas the model requires open pores for the reconstruction of firn air mixing ratios. The large MPI air samples could not be filled at this depth, because of the limited amount of air which could be pumped from this depth. Therefore, no $\delta D$ and $\delta^{13}C$ measurements from the MPI were available at 99 m and the corresponding $\delta^{13}C$ measurement from LGGE has not been included in the reconstruction of past atmospheric $\delta^{13}C$ trends.

### 5.4.1 Firn air age distribution

The firn air model allows the calculation of the age distribution of any trace gas as a function of depth. This is shown in Figure 5.10 for $CH_4$ and $SF_6$ at DML and DC. At both sites contemporary air was still contributing significant to the firn air of the top 40 m, while the average gas age rapidly increased towards the close-off zone. The deeper close-off (non-diffusive zone) at DC compared with DML resulted in broader age distributions.

The age distribution can be very different from site to site. In general, there is a trade off between high, "cold" sites with low accumulation rates and lower, "warmer" sites, which tend to have higher accumulation rates. Cold sites will have a deep firn-ice transition zone and thus cover a broader time scale than warmer sites with a more swallow close-off zone. On the other hand higher accumulation rates will result

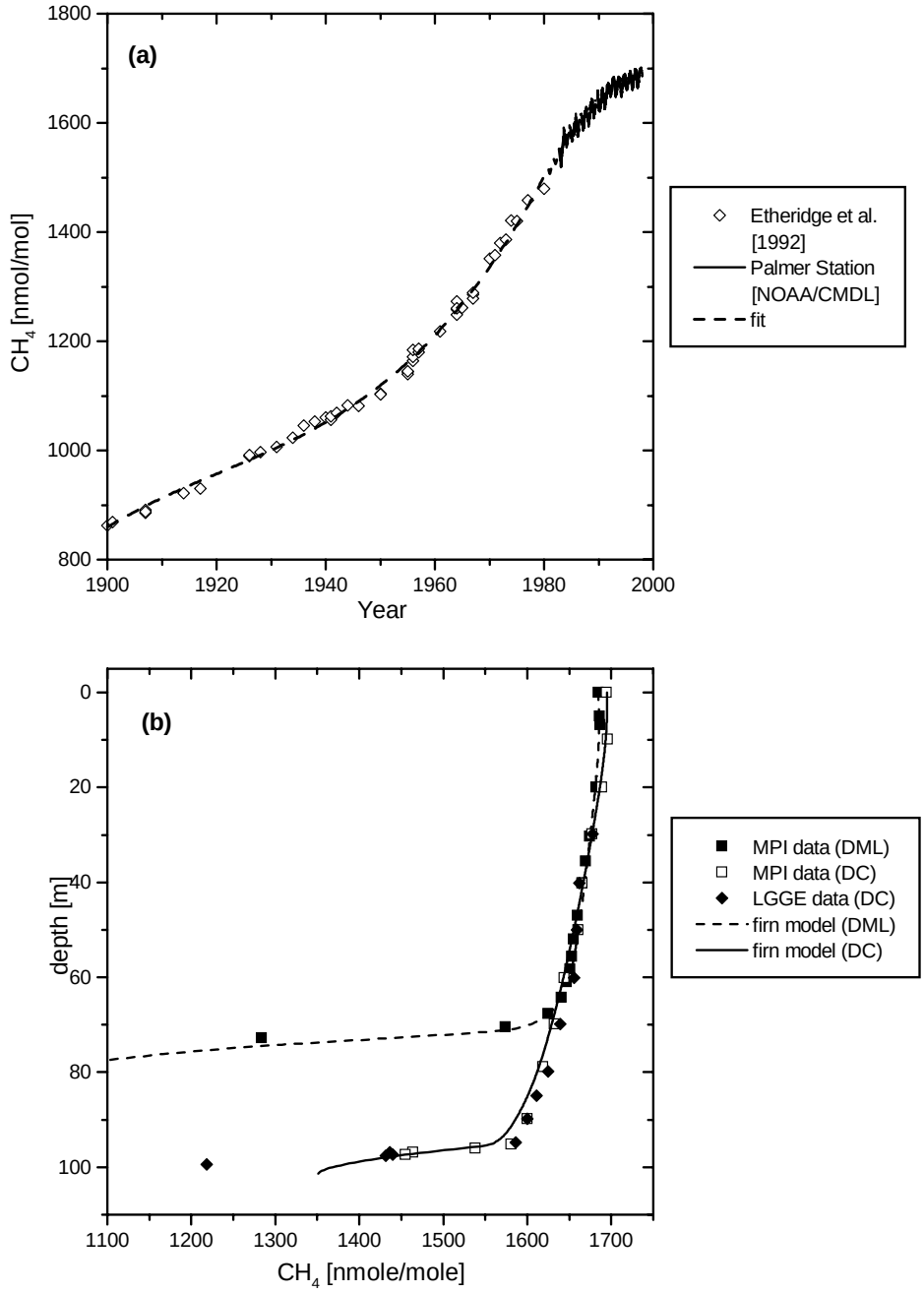


**Figure 5.9:** (a) Atmospheric methane mixing ratios since 1900 based on ice-core measurements [Etheridge et al., 1992] and direct atmospheric measurements from Palmer Station (64° S, 64° W) [NOAA/CMDL] starting in 1978. A fit through both data sets is applied. (b) Measured $CH_4$ mixing ratios are plotted against depth for DML and DC and compared to firn model results.

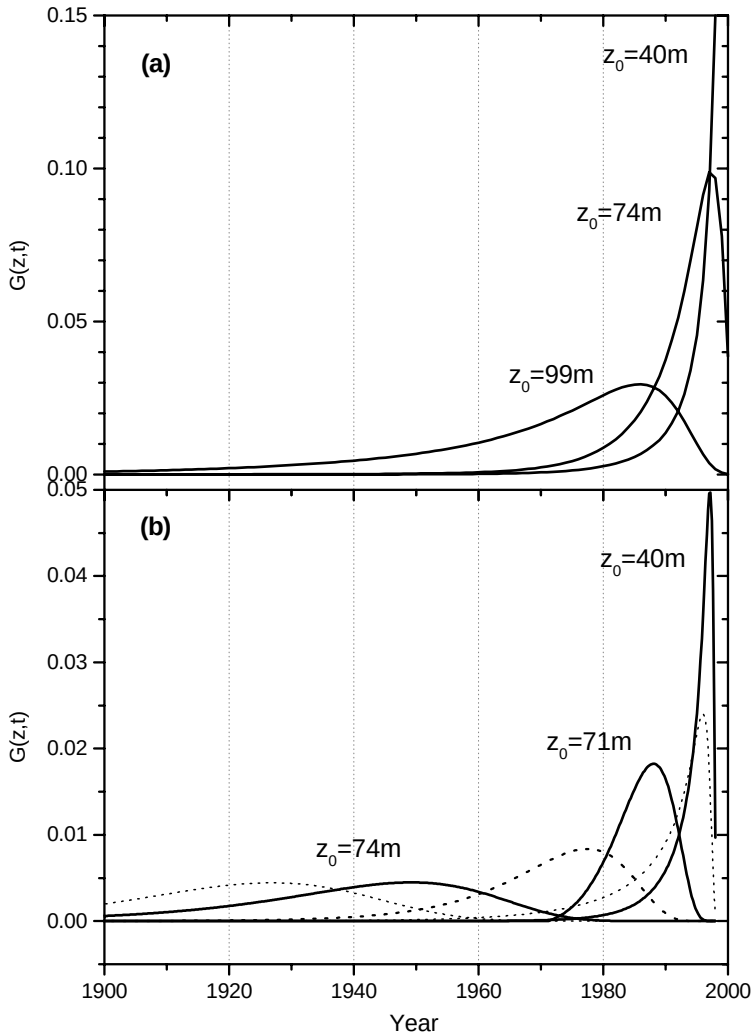


**Figure 5.10:** (a) firn air age distribution for $CH_4$ at depth $z_0$ for DC, plotted as the transfer function G(z,t) (model output) for different values of $z_0$. (b) firn air age distribution for $CH_4$ (continuous line) and $SF_6$ (dotted line) at DML.

in a higher time resolution. For DC with an annual mean temperature of $-53\,^{\circ}$C the firn ice transition is 20 m deeper than at DML, which is 15° warmer. At the same time the lower accumulation rate of DC results in age distributions which are larger than in DML. Another characteristic of the firn air age distribution concerns gases of different masses which are analyzed on the same sample, i.e. the same depth. At a given depth, the age of a light molecule is less and its age distribution broader compared to heavier gases. For DML the light $CH_4$ molecule is nearly 20 years

younger than the heavier $SF_6$, for which the downward diffusion of recent $SF_6$ takes considerably longer to dilute the old air at the bottom.

## 5.5 Past trends of atmospheric $\delta^{13}$C and $\delta$D

In the case of isotopic ratios, the inversion technique with the firn air model cannot be readily applied because the comparatively high measurement errors in the isotopic composition are magnified by the model inversion and result in a reconstructed isotopic history of considerably uncertainty. We have instead used a Monte Carlo approach where scenarios of temporal trends in the isotopic composition of atmospheric methane were tested against the firn air profiles with the diffusion model run in forward mode.

Since the firn model is linear with regard to mixing ratios, each isotopomer ($^{12}CH_4$, $^{13}CH_4$ and $CH_3D$), which was previously derived from a $\delta$ value and the $CH_4$ concentration (equation 1.3), was calculated separately by the firn model. Subsequently the model results were recombined to give $^{13}CH_4/^{12}CH_4$ and $CH_3D/^{12}CH_4$ ratios and the $\delta$ values calculated, using again equation 1.3, and compared with the measured $\delta$ values. The diffusion coefficient for methane and its isotopomers in air was calculated after Bzowski et al. [1990].

### 5.5.1 Monte Carlo modeling

The atmospheric evolution (the firn model input) was parameterized as a third-order polynomial defined on the time interval 1950 to 1998 (DML) and 1999 (DC). Sensitivity studies showed that atmospheric $CH_4$ changes prior to 1950 hardly influenced the reconstructed firn air records at DML and DC.

The polynomial scenarios were set up with four free parameters: the $\delta$ value and yearly rate of change in 1950 and in 1999. 10.000 depth profiles (the firn model output) for $\delta^{13}$C and $\delta$D were calculated with the firn model for DML and for DC, varying the polynomial coefficients, i.e the four free parameters, at random within the limits given in Table 5.3.

The resulting firn model depth profile, which best reproduced the measurements, defines the most likely reconstructed atmospheric $CH_4$ isotopic evolution of the past 50 years. In order to obtain this best scenario we define the error function

$$E = \sum_{i=1}^{n} \sqrt{(m(d_i) - \sigma(d_i))^2} \times \frac{\Delta\sigma(d_i)}{\sum \Delta\sigma(d_i)} \tag{5.11}$$

where $\sigma(d_i)$ are the observations and $m(d_i)$ the model results at depth $d$. The measurement error $\Delta\sigma(d_i)$ is introduced in order to give different weights to mea-

| Monte Carlo parameters | parameter space | best scenario | envelope |
|---|---|---|---|
| $\delta^{13}$C (1950) [‰ ] | −52.0 to −46.0 | −48.75 | ±0.5 |
| $\delta^{13}$C (1950) [‰ $yr^{-1}$ ] | ±1 | 0.0 | ±0.1 |
| $\delta^{13}$C (1999) [‰ ] | −47.1 to −46.9 | −47.0 | ±0.05 |
| $\delta^{13}$C (1999) [‰ $yr^{-1}$ ] | ±0.5 | 0.03 | ±0.02 |
| δD (1950) [‰ ] | −85.0 to −50 | −73.8 | ±3.9 |
| δD (1950) [‰ $yr^{-1}$ ] | ±2 | −0.58 | ±0.6 |
| δD (1999) [‰ ] | −74.0 to −70.0 | −72.2 | ±0.3 |
| δD (1999) [‰ $yr^{-1}$ ] | ±2 | +0.82 | ±0.16 |

**Table 5.3:** Range of free parameters and best scenarios used in Monte Carlo runs of the firn air diffusion model to get the best agreement between modeled and measured firn profiles.

surements done at LGGE and MPI, and for DML and DC. For $\delta^{13}$C the measurement errors varied depending on the isotope laboratories and the year of analysis (MPI(1998, DML)=±0.08 ‰, MPI(1999, DC)=±0.04 ‰, LGGE(DML, DC)=± 0.05 ‰). δD measurements had a reproducibility of ±1 ‰ for both sites and were only measured at MPI. The ambient air δD values at the surface were not used in the Monte Carlo runs because they are clearly different from the annual mean (section 5.2.3).

As there are no known methane sources in the remote high latitude southern hemisphere and the tropospheric air is well mixed, the profiles from DML and DC should represent an identical history. We therefore combined the two sites and performed a third Monte Carlo (MC) run (again with 10.000 parameter sets) using identical free parameters for both locations, and tested against both profiles.

### 5.5.2 The positive $\delta^{13}$C trend

The reconstructed atmospheric evolution of $\delta^{13}$C is shown in Figure 5 for the three Monte Carlo runs. The main common feature of the different scenarios is the positive trend in the $\delta^{13}$C signal over the last 50 years. Among the large range of parameters considered (Table 5.3) the best defined scenario for each of the three MC runs all lie within a much narrower range. For the scenario with the best fit to the combined DML and DC measurements we calculate an error envelope defined by scenarios for which the corresponding modeled depth profiles were within a 0.3 ‰ range of each measurement and for which the MC error (equation 5.11) was within 5% of the best scenario. In Table 5.3 this best scenario is given together with its error envelope and

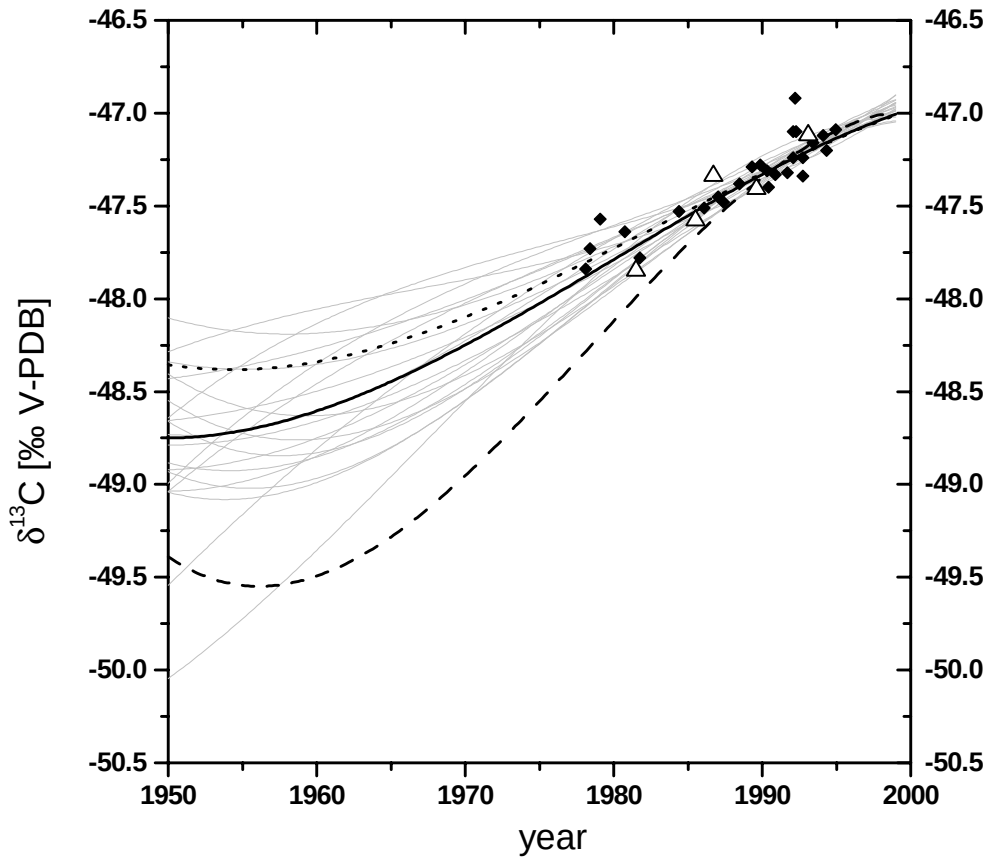


**Figure 5.11:** Atmospheric scenarios of $\delta^{13}$C evolution for the last 50 years, reproducing the firn air profiles of DML and DC, based on Monte Carlo runs of a firn air diffusion model. The best scenario reproduces both firn air profiles. The thin solid lines represent error envelopes around the best scenario (see text). In addition $\delta^{13}$C values from the Cape Grim Air Archive (solid symbols) and other firn measurements (open symbols) [Francey et al., 1999] are shown.

it is also plotted in Figure 5.11. Here we plot sufficient envelope scenarios to define the outer limits of the error envelope. The calculated firn profiles corresponding to the best scenarios for DC and DML are plotted with the measurements in Figure 5.4. For the annual trends and for the absolute $\delta^{13}$C values the Monte Carlo approach has constrained the initial range in the parameter space by at least a factor of 2.

The best scenarios generated separately for DML and DC have a very consistent trend for $\delta^{13}$C of $+0.04\pm0.01$ ‰ yr$^{-1}$ over the last 15 years, but differ by nearly 1 ‰ in 1950. The best scenario for DC starts around $-48.3\pm0.5$ ‰ in 1950 and ends after a positive trend over the last 50 years around $-47.0\pm0.05$ ‰ in 1999. Whereas the best scenario for DML starts around $-49.4\pm0.7$ ‰ in 1950, but is in very good

agreement with the DC scenario from 1985 onwards. For the combined DC and DML Monte Carlo run Figure 5.11 shows that the resulting atmospheric scenario is very close to the already extracted best DC scenario. With more samples taken in the deep DC firn compared to DML, together with the improved measurement error at the MPI in 1999, the scenarios are altogether better defined by the DC measurements. The best DML scenario lies clearly outside the error envelope for the combination of DML and DC, because it reproduces the DC data less precisely at depths around 90 m (see Figure 5.4 b). An interesting feature is the turning point observed in the modeled $\delta^{13}$C profile near the firn-ice transition zone in DML (75 m). Below 70 m effective diffusion is zero at DML and the firn air age increases dramatically over short distances. In this non-diffusion zone the atmospheric trend towards lighter $\delta^{13}$C values is directly reflected in the firn profile.

In Etheridge et al. [1998] a detailed $\delta^{13}$C record, based on atmospheric methane measurements from the Cape Grim Air Archive and data from Antarctic firn air, was published for the time period 1978 to 1993. While their overall trend is comparable to our reconstructed trend over this period, there is a significant offset of nearly 0.4 ‰ between the two data sets. Their $\delta^{13}$C values have subsequently been linked with the NZCH standard [Francey et al., 1999], which now allows a direct comparison with our data. The two data sets now agree within their error specification. From 1978 onwards, their observed mean trend over the last 17 years is $+0.04$ ‰ yr$^{-1}$, which is identical to our mean DC/DML positive $\delta^{13}$C trend of $+0.04\pm0.01$ ‰ yr$^{-1}$ over the same period. Thus the significantly higher trend reported earlier by Stevens et al. [1988], $\sim+0.14$ ‰ yr$^{-1}$ from 1978 to 1988, is further questioned.

### 5.5.3 The observed minimum in the $\delta$D record

The past atmospheric evolution of $\delta$D is unknown. Even if D/H measurements are difficult, and have a measurement uncertainty of $\pm1$ ‰, $\delta$D can be reconstructed with as much confidence as $\delta^{13}$C from firn air samples. Corrections for diffusion and gravitation are basically mass dependent and therefore identical for both stable isotopes. However, the $\delta$D variation from top to bottom in the firn air were more than 10 ‰. This makes the reconstruction of the past atmospheric $\delta$D evolution very sensitive to its trend over the last few decades, as will be shown below.

Figure 5.12 shows the results for $\delta$D. The reconstructed scenarios start in 1950 at values between $-81$ ‰ and $-67$ ‰. They show a clear minimum of between $-83$ ‰ and $-79$ ‰ in the 1970s and have strikingly similar slopes of $0.55\pm0.05$ ‰/year over the last two decades. Scenarios with lower starting values tend to have their minima in the early 1980s at higher values. Even with a wide parameter range (Table

5.3), the best fits through the DML and DC data, separately and combined, gave a very coherent picture. Thus the Monte Carlo technique is able to constrain not only the starting point significantly, but also the present mean atmospheric value of $-72.2\pm0.3$ ‰ and the $\delta$D trend over the recent decades. The envelope for the combined scenarios was chosen in a way similar to that for the $\delta^{13}$C record. Again the set of scenarios shown corresponds to modeled depth profiles (see Figure 5.5) which fitted each measurement within a 3 ‰ range and for which the associated error was again within 5 % of the best scenario. As for $\delta^{13}$C, the modeled profiles for DML showed a change in trend towards enriched isotopic values in the non-diffusive zone near the firn-ice transition. This reflects the atmospheric trend prior to 1975.

Our $\delta$D reconstruction is so far unique and cannot be compared with any other time series covering several years or decades. In terms of absolute values, and for discussion of the methane budget (section below), the intercalibration in $\delta$D between MPI and other laboratories measuring $\delta$D of $CH_4$ must be addressed. The $\delta$D source signatures considered by Marik [1998] and used here for the discussion, had to be shifted by an offset of $+5.7$ ‰. This factor has been established by comparing parallel methane $\delta$D data sets at a remote station [Bergamaschi et al., 2000a].

## 5.6 The effects of changing sources and sinks

After reconstructing atmospheric scenarios the next step is to infer changes in the methane sources and sinks that can explain these scenarios. In the following section the two main features of the atmospheric records, the positive $\delta^{13}$C trend and the observed minimum in the $\delta$D record, will first be qualitatively explained. The changes in the isotopic composition of methane in a period of increasing mixing ratios combined with the delay due to the atmospheric response time [Tans, 1997] lead to complex connections, which are analyzed in detail using an atmospheric model.

The uninterrupted positive trend in $\delta^{13}$C (Figure 5.11) seems to suggest a shift from light to heavier sources during recent decades. The present-day $\delta^{13}$C value of about $-47$ ‰ [Quay et al., 1999] is not the weighted mean isotopic composition of all sources because of the fractionation accompanying the sink processes (oxidation with OH and Cl in the atmosphere and bacterial oxidation in soils). Estimation of the isotopic composition of $CH_4$, averaged over all sources, is based either on the sum of methane sources weighted by their isotopic signatures (bottom-up) or on the present atmospheric isotopic values taking into account relative contribution of the sinks and their kinetic isotopic effect (KIE)(top-down).

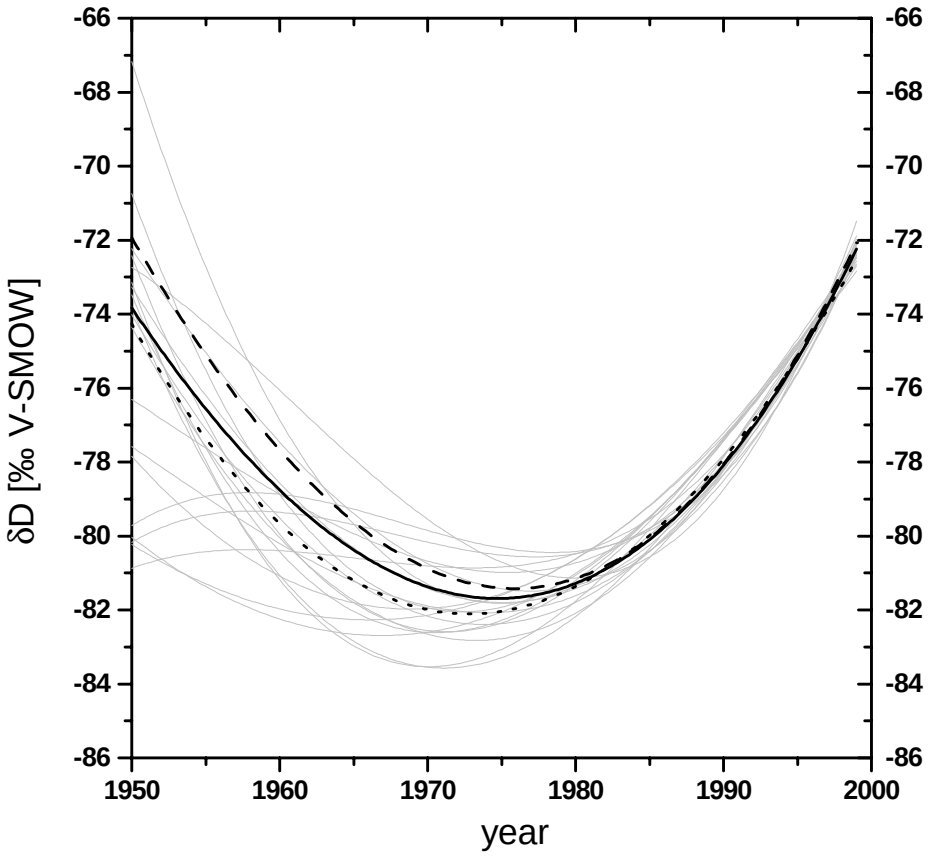


**Figure 5.12:** Atmospheric scenarios of δD evolution for the last 50 years, reproducing the firn air profiles of DML and DC, based on Monte Carlo runs of a firn air diffusion model. The best scenario reproduces both firn air profiles. The thin solid lines represent error envelopes around the best scenario (see text).

Using source distributions from Lelieveld et al. [1998] and isotopic source signatures listed in Table 1.2 (chapter 1), the first approach gives $\delta_S(^{13}\mathrm{C})$=−53.5±2.6 ‰ for the mean isotopic composition of the $CH_4$ sources. The high error reflects the current uncertainties in the methane budget and in the measured isotopic composition of sources. The second approach gives a $\delta^{13}\mathrm{C}$ value for the mean source of $\delta_S(^{13}\mathrm{C}) = -52.0\pm0.8$ ‰. This calculation is based on a sink distribution from Lelieveld et al. [1998], and KIEs for the OH sink (88 %, with mean OH mixing ratios of $5\times10^{-6}$ molecules/cm$^3$), oxidation in soils (5 %) and for the stratosphere (7 %) of 1.0039±0.0004 [Saueressig, 1999], 1.021±0.005 [King et al., 1989] and 1.012 [Brenninkmeijer et al., 1995] respectively (see Table 1.2). This second approach can

only be applied to an equilibrium state, as has been shown by Tans [1997]. In reality the rising $CH_4$ levels in the past have influenced the present atmospheric $\delta^{13}C$ values [Lassey et al., 2000]. During non-equilibrium states excess source methane leads to a smaller difference between the atmospheric and the mean source value.

The non-equilibrium effect can be well identified in the reconstructed δD signal. The observed minimum in δD (Figure 5.12) is partly explained by the large difference between the atmospheric value and the mean isotopic source composition. For an identical sink and source distribution as above and isotopic source signatures from Table 1.2 (chapter 1) bottom-up calculations lead to $\delta_S$(D)=$-283\pm13$ ‰. With an atmospheric global average of $-79$ ‰ (chapter 3 and our firn measurements) and the corresponding KIE factors for the sink processes ($KIE^D_{OH}$=1.294±0.018 [Saueressig, 1999], $KIE^D_{stratos}$=1.19±0.02 [Irion et al., 1996], and $KIE^D_{soil}$=1.066 [Wahlen, 1993]), top-down calculations give a mean source signature of $\delta_S$(D)=$-274\pm10$ ‰. Again the high error in the bottom-up calculation is due to current uncertainties, not only in the methane budget but also in the measured isotopic composition of sources. We note that the bottom-up calculation considers a steady-state situation, whereas the top-down calculation is affected by the far-from-equilibrium state of the current atmosphere. Calculations by Marik [1998] show that, if $CH_4$ sources remained constant from now on, then atmospheric δD values would reach their equilibrium state only after more than 20 years.

The non-equilibrium state between sources and sinks leads to the observed decreasing trend for δD between 1950 and the minimum around 1975. High $CH_4$ growth rates have led to excess source methane which is extremely depleted in δD relative to the atmospheric value. After the stabilization and subsequent slowing down of the $CH_4$ growth rates at the beginning of the 1980s [Dlugokencky et al., 1994c], a strong δD increase of $+0.55\pm0.05$ ‰ $yr^{-1}$ is observed, clearly reflecting the shift towards the heavier atmospheric equilibrium values. The atmospheric model introduced in the next section will take into account the non-equilibrium state of methane mixing ratios and isotopes in the atmosphere.

### 5.6.1 Atmospheric model results

To quantify the constrains imposed on the methane budget by long-term atmospheric records of methane mixing ratios and isotope ratios, including their seasonal variations and annual trends, Marik designed an atmospheric eight-box model (BOSCAGE-8) [Marik, 1998]. He uses our data set of $\delta^{13}C$ and δD trends over the past 50 years for new model runs with BOSCAGE-8 [Bräunlich et al., 2000b].

The modeled tracers are $CH_4$ (including $^{13}C$ and D) and $SF_6$. The model has

a time resolution of two weeks and $SF_6$ measurements are used to calibrate the inter-box exchange time. The $CH_4$ source distribution and seasonality is taken from [Hein et al., 1997], while the source signatures for $\delta^{13}C$ and $\delta D$ are taken within the range given by present publications (see Table 1.2). The free parameters of the model are the total emission of each source type. Changing sinks will be considered by discussing two different model runs: case A with OH levels kept constant at the present value, and case B with decreasing OH levels in periods of growing $CH_4$ and CO mixing ratios. The sink KIE factors are taken with the values mentioned above.

The model outputs have to reproduce:
(1) the present atmospheric values for $\delta^{13}C$ and $\delta D$ from Neumayer station (70° S, 8° W) [Marik, 1998]
(2) methane mixing ratios since 1800 based on Antarctic ice-core records [Etheridge et al. 1998]
(3) present-day atmospheric $CH_4$ distribution based on the NOAA/CMDL monitoring network.
In order to limit the range of scenarios tested in our simulation of long-term $CH_4$ and isotopic trends in the high latitude Southern hemisphere, we consider two main assumptions about the evolution of methane sources. First, they are divided into two categories, natural and anthropogenic, with the natural source (wetlands and 30 % of the total biomass burning) kept constant over the last 200 years. Second, the increasing anthropogenic source (rice paddies, ruminants, landfills, fossil fuel, and 70 % of the total biomass burning) is related to human population growth, as suggested by Khalil & Rasmussen [1985]. This assumption will be discussed in more detail together with the model results. In Table 5.4 the temporal scenarios since pre-industrial times of methane source strengths (natural and anthropogenic) and the mean $\delta^{13}C$ and $\delta D$ source signatures for the two cases A (OH constant) and B (OH decreasing) are listed. The corresponding Antarctic $\delta^{13}C$ and $\delta D$ trends calculated with the BOSCAGE-8 model are shown in Figure 5.13 together with the best estimate from the firn air measurements.

Until 1980 the assumption of an anthropogenic methane source strength proportional to human population is in agreement with changing methane mixing ratios over the past 200 years. After 1980, however, decreasing $CH_4$-growth rates [Dlugokencky et al., 1994c] make it necessary to decouple the two variables. Therefore we lowered the annual increase of methane sources in 1983 from $\sim$+6.3 $Tg\,yr^{-1}$ (+1.3 %/yr) to $\sim$+1 $Tg\,yr^{-1}$ (+0.2 %) until 1991 and we kept it constant afterwards for case A (constant OH). The decreasing OH levels until 1978 in case B result in a slightly lower annual methane source increase before 1983 (+5 $Tg\,yr^{-1}$).

| | Case A OH constant | | | Case B OH decreasing | | |
|---|---|---|---|---|---|---|
| | 1800 | 1950 | 1999 | 1800 | 1950 | 1999 |
| total source [ $Tg\,yr^{-1}$ ]: | 211 | 354 | 519 | 262 | 375 | 517 |
| nat. sources | 135 | 135 | 135 | 200 | 200 | 200 |
| anth. sources | 76 | 219 | 384 | 62 | 175 | 317 |
| $\delta^{13}C$ source [ ‰ ] | −55.9 | −53.1 | −52.0 | −55.6 | −53.4 | −52.0 |
| $\delta D$ source [ ‰ ] | −274 | −266 | −262 | −274 | −267 | −262 |
| source signatures: | $\delta^{13}C$ | $\delta D$ | | $\delta^{13}C$ | $\delta D$ | |
| nat. sources | −59.6 | −286 | | −57.9 | −281 | |
| anth. sources | −49.3 | −254 | | −48.3 | −250 | |

**Table 5.4:** Emission rates, mean $\delta^{13}C$ and $\delta D$ of natural and anthropogenic sources of $CH_4$ used as input to the BOSCAGE-8 atmospheric model. Results are given for two cases: A (OH constant), and B (OH decreasing).

For $\delta^{13}C$ the comparison of the modeled and firn-based reconstructed evolution of the atmospheric trend over the past 50 years is encouraging (see Figure 5.13a). Both cases A and B fall within the envelope of scenarios given by the firn model. The positive $\delta^{13}C$ trend corresponds to a calculated increase of the anthropogenic methane source, which implies a positive trend in the mean $\delta^{13}C$ source as listed in Table 5.4). In contrast, the results for $\delta D$ scenarios differ significantly from the reconstructed atmospheric $\delta D$. For both cases A and B the calculated $\delta D$ values show a pronounced minimum around 1980, which happens later and is 1 to 3 ‰ lighter than the firn air-derived $\delta D$ scenario. As a consequence, the trend over the last 20 years is stronger than reconstructed from the firn profiles (+0.7 instead of 0.55 ‰ $yr^{-1}$). If real, the enhanced gradient over the last two decades would lead to firn profiles depleted by more than 1 ‰ compared to our $\delta D$ measurements at DML and DC.

The main parameter which influences the position of the $\delta D$ minimum, is the time at which the growth of methane sources started to slow down. The response time of atmospheric $\delta D$ is nearly instantaneous when the source growth rate decreases, because the sink processes gain over the sources and drive the atmosphere towards its equilibrium value. This implies a shift in the $\delta D$ trend from negative to positive values, whereas the positive growth rate of mixing ratios only change in strength from 1 %/yr to 0.2 %/yr. This makes mixing ratios less sensitive than the isotopic

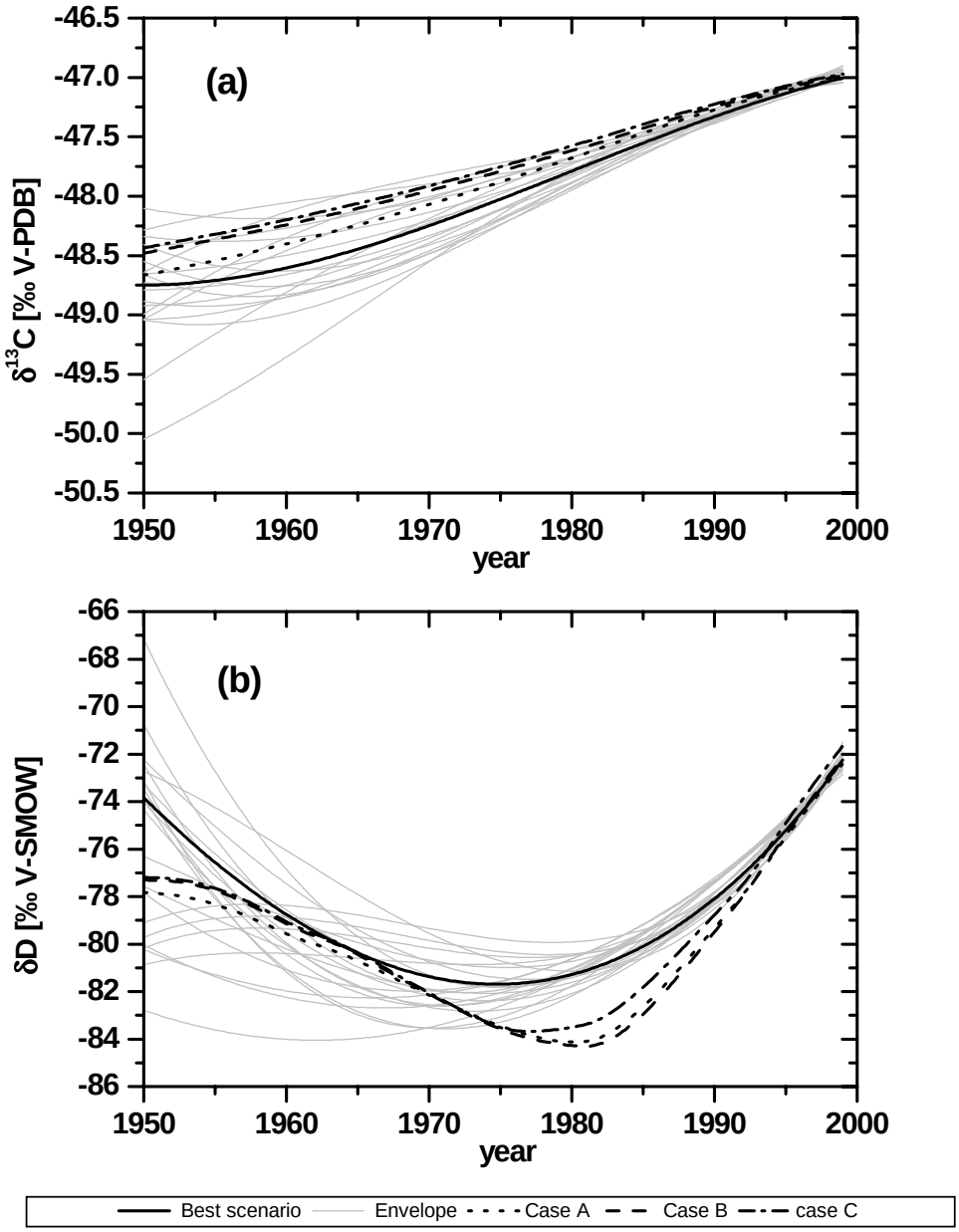


**Figure 5.13:** (a) Comparison of three outputs (Case A-C) of the atmospheric methane isotope model BOSCAGE-8 with the reconstructed best atmospheric $\delta^{13}C$ scenario over the last 50 years from DML and DC. In case A OH levels are kept constant over the last 200 years; in case B OH levels are linearly decreasing by 23 % from 1885 to 1978. In case C the growth rate of methane sources is optimized to better fit the recent trend in mixing ratios and isotopes. (b) Same for δD.

ratios to any change in the total methane source strength.

For the BOSCAGE-8 runs shown in Figures 5.13 (a) and (b) for $\delta^{13}C$ and $\delta D$, respectively, the growth in the methane source was adapted in order to shift the minimum towards 1975, while trends in mixing ratios and $\delta^{13}C$ still had to be reproduced. For this case C the other model parameters were kept unchanged compared to case A. This approach implied for constant OH levels (case A), methane source strengths that changed earlier and less abruptly. The growth rates are stepwise reduced from 1974 onwards (before 1974: 6.6 $Tg\,yr^{-1}$ (1.4 %); 1974-1981: 5 $Tg\,yr^{-1}$ (1 %); 1981-1991: 1.6 $Tg\,yr^{-1}$; short period of decline from 1991 to 1994: from 526 to 519Tg) and the methane source strength stays constant at 519 $Tg\,yr^{-1}$ after 1994. This scenario of total methane emissions (figure 5.13, case C) best reproduces the observed atmospheric mixing ratios and our reconstructed trends in $\delta^{13}C$ and $\delta D$. Although the $\delta^{13}C$ trend for case C agrees with the firn-based reconstruction, for $\delta D$ the scenario C (Figure 5.13b) still lies outside the uncertainty envelope of the firn-based scenario. The calculated $\delta D$ minimum happens either ~5 years too early or is 1-2 ‰ too light.

Another parameter influencing the $\delta D$ minimum is, however, the fractionation factor in the sink process. Sensitivity tests made with the BOSCAGE-8 model in order to shift the minimum by about 1 ‰ towards heavier values, resulted in a reduction of the mean tropospheric KIE factor from 1.27 to 1.22, a reduction of the total sink contribution of OH from 88 % to 81 % towards the soil sink and a reduction of the $KIE_{OH}$ from 1.294 to 1.250. For the mean $\delta D$ source this would result in a shift from −262 ‰ to −255 ‰, with $\delta D$ source signatures being at the lower end of their error specification. The tests described above, although limited, give some indications on the sensitivity of the model output to key parameters. Thus additional work is needed before the best constraints on the methane budget from our data set can be extracted.

### 5.6.2 Discussion

When assuming that OH levels remained unchanged over the last 200 years, only the increasing anthropogenic source is responsible for growing methane mixing ratios and the positive $\delta^{13}C$ and $\delta D$ trend towards a heavier equilibrium state in both isotopes. Assuming a constant natural source of 135 $Tg\,yr^{-1}$, the ratio between natural and anthropogenic sources has decreased since pre-industrial times from ~1.8 to ~0.4. With the mean anthropogenic source being more than 10 ‰ enriched in $\delta^{13}C$ relative to the mean natural source, the global $CH_4$ source would have become ~4 ‰ heavier in $\delta^{13}C$ compared to 1800 and 2 ‰ heavier since 1950 (Table 5.4). This potential 2 ‰ shift is close to our reconstructed trend of 1.7±0.7 ‰. Thus even if for all these

values the far-from-equilibrium state of the atmosphere is taken into account by the model, the atmospheric $\delta^{13}C$ trend still closely reflects the underlying trend of the mean methane source. The situation is different for $\delta D$. Here the difference between mean anthropogenic and natural source is more than 30 ‰, making the present global source up to 12 ‰ heavier in $\delta D$ than compared to pre-industrial values. This time the atmospheric shift in $\delta D$ values is not comparable to the differences in the mean sources, because of the already mentioned far-from-equilibrium state of the present atmosphere. For the last 50 years the expected shift of 7 ‰ is less directly seen in the reconstructed scenarios than for $\delta^{13}C$.

When assuming that the OH sink increased by 23% between 1885 and 1978 [Thompson & Cicerone, 1986; Marik, 1998] the $CH_4$ increase since pre-industrial times is due to a combination of increasing anthropogenic sources and a decreasing sink. In addition, the ratio between natural and anthropogenic sources since pre-industrial times becomes more important (from ~3.2 to ~0.6), in order to compensate for the more important sink in pre-industrial times. As we still assume that the natural and anthropogenic sources remained constant and proportional to human population respectively, we need to compensate for the higher isotopic fractionation in the past during elevated OH levels by shifting natural and anthropogenic sources towards heavier values. $\delta D$ is far more sensitive to changing OH levels than $\delta^{13}C$, because of the huge fractionation of ~300 ‰ in this sink process. The mean anthropogenic and natural $\delta D$ source have thus both to be changed in the range of +5 ‰ in order to compensate for the increased sink.

Overall, our interpretation of the temporal trends deduced from the firn air profiles suffers from several caveats:
(1) the lack of intercalibration between laboratories measuring methane isotopes on sources and in the atmosphere (we note that this concerns the absolute $\delta D$ and $\delta^{13}C$ values, but not the trends derived in this study),
(2) the large range of $\delta$ values for the sources,
(3) the large uncertainties in the fractionation factors for the different sinks,
(4) the limited number of free parameters (e.g. not including the strength of individual sources, changing natural sources, etc.) tested in the BOSCAGE-8 model so far.
Altogether, this makes it difficult to quantify the evolution of individual methane sources since pre-industrial times from the firn air data alone. Concerning the OH sink, the expected $\delta D$ trends calculated by BOSCAGE-8 also suffer from the problems listed above. Even if $\delta D$ is very sensitive to OH changes, we can not confidently differentiate between the two considered cases A and B with our firn profiles. Still,

any future attempt to produce a methane budget over the corresponding time period should be tested against the temporal evolution of the three tracers now available: the mixing ratio and the two stable isotopes.

## 5.7 Conclusion

Detailed firn air measurements of the stable isotopes $^{13}C$ and D in methane, together with methane mixing ratios from two Antarctic sites, Dronning Maud Land and Dome Concordia, allowed us to estimate the temporal evolution of these three signals over the last approximately 50 years. They extend and complete existing records of $\delta^{13}C$ of $CH_4$ and appear to be the first ever reported for past $\delta D$ of $CH_4$. A Monte Carlo approach using a firn diffusion model enables us to extract from the firn profiles the most plausible scenarios of atmospheric trends. We found very similar reconstructed trends for $\delta^{13}C$ and $\delta D$ for the two Antarctic sites, thus allowing us to combine both firn air profiles and to increase the precision of the reconstruction. We revealed a positive $\delta^{13}C$ shift of 1.7±0.7‰ over the last 50 years, with a trend of +0.04±0.01 ‰ $yr^{-1}$ over the last 15 years. The latter trend compares very well with previously published $\delta^{13}C$ measurements based on the Cape Grim air archive and Law Dome firn air [Francey et al., 1999]. The reconstructed trends of $\delta D$ revealed a decrease until ∼1975 followed by a gradual increase of 0.55±0.05 ‰ $yr^{-1}$ over the last two decades. The $\delta D$ minimum reflects the non-equilibrium state between atmospheric methane and its sources and sinks in a period of a changing budget.

We tested different scenarios of a changing methane budget against our temporal reconstruction with the help of an atmospheric eight-box model from Marik [1998]. Assuming constant sinks and natural sources over the last 200 years, and an increase in the anthropogenic sources proportional to human population, the model reproduced reasonably well the temporal trend of methane and its stable isotopes until 1975. The minimum in our $\delta D$ record at that time required a decrease in the growth rate of methane emissions from 6.3 Tg $yr^{-1}$ to 5 Tg $yr^{-1}$ until 1981, with a further drop afterwards to 1.6 Tg $yr^{-1}$ until 1991, before methane source strength stabilized from 1994 onwards (after a short period of decline from 1991 to 1994). We also assumed a change in the sink strength over the considered time period, mainly to change the ratio between the isotopically lighter natural sources and the isotopically heavier anthropogenic sources, which drives the equilibrium of $\delta^{13}C$ and $\delta D$ towards heavier values.

Our present knowledge of the atmospheric $CH_4$ cycle, including the isotopic information based on atmospheric records, source signatures and kinetic isotope effects

of the sinks, permitted us to reproduce our observed positive $\delta^{13}C$ trend and the main features of our firn-based $\delta D$ trend. Nevertheless, the difference in the calculated and observed $\delta D$ record over the last two decades indicates that there may still be some ambiguity in the actual KIE factors, the sink distribution and the applied models. The importance of the methane isotope data from firn air of the last 50 years presented here will increase with higher precision of the source signatures for $\delta D$ and of the fractionation factors of the sink process. The comparison with firn air measurements going further back in time together with a Northern hemisphere record, defining an inter-hemispheric gradient, would also put important constraints on the global methane budget. All this will considerably improve our knowledge of changes in the atmospheric source and sink processes of methane that have caused the large increase in methane mixing ratios since pre-industrial times.

# Bibliography

[Allen et al., 1999] Allen, W., M. R. Manning, A. J. Gomez, D. C. Lowe and K.R.Lassey, *Modelling the variation of d13C in atmospheric methane: phase ellipses and the kinetic isotope effect*, submitted to Global Biogeochem. Cycles, 1999.

[Anderson, 1996] Anderson, B. L., *Modeling isotopic fraction in systems with multiple sources and sinks with application to atmospheric $CH_4$*, Global Biogeochemical Cycles, 10, No. 1, 191-196, 1996.

[Armerding et al., 1997] Armerding, W., F. J. Comes, H. J. Crawack, O. Forberich, G. Gold, C. Ruger, M. Spiekermann, J. Walter, E. Cuevas, A. Redondas, R. Schmitt and P. Matuska, *Testing the daytime oxidizing capacity of the troposphere: 1994 OH field campaign at the Izana observatory, Tenerife*, J. Geophys. Res., 102, D9, 10,603-10,611, 1997.

[Arnaud, 1997] Arnaud, L., *Modelisation de la transformation de la neige en glace a la surface des calottes polaires; Etudes du transport des gaz dans ces milieux poreux.*, Laboratoire de Glaciologie et Geophysique de l'Environnemen-CNRS, 1997.

[Bates et al., 1995] Bates, T. S., K. C. Kelly, J. E. Johnson and R. H. Gammon, *Regional and seasonal variations in the flux of oceanic carbon monoxide to the atmosphere*, J. Geophys. Res., 100, 23.093-23.101, 1995.

[Becker et al., 1998] Becker, K. H., F. Fiedler, R. Winkler, D. Möller, V. A. Mohnen, U. Platt, E. Reimer and A. Volz-Thomas, *BERLIOZ-Operationsplan*, Version 3.15, Berlin, 1998.

[Bekki et al., 1994] Bekki, S., K.S. Law and J.A. Pyle, *Effect of ozone depletion on atmospheric $CH_4$ and CO concentrations*, Nature, 371, 595-597, 1994.

[Bergamaschi et al., 1994] Bergamaschi, P., M. Schupp and G. W. Harris, *High-precision direct measurements of $^{13}CH_4/^{12}CH_4$ and $^{12}CH_3D/^{12}CH_4$ ratios in at-*

*mospheric methane sources by means of a long-path tunable diode laser absorbtion spectrometer*, Applied Optics, 33,, 7704-7716, 1994.

[Bergamaschi & Harris, 1995] Bergamaschi, P. & G.W. Harris, *Measurements of stable isotope ratios ($^{13}CH_4/^{12}CH_4$; $^{12}CH_3D/^{12}CH_4$) in landfill methane using a tunable diode laser absorption spectrometer*, Global Biogeochem. Cycles, 9, 4, 439-447, 1995.

[Bergamaschi, 1997] Bergamaschi, P., *Seasonal variations of stable hydrogen and carbon isotope ratios in methane from Chinese rice paddy*, J. Geophys. Res., 102, D21, 25 383-25 393, 1997.

[Bergamaschi et al., 1998a] Bergamaschi, P., C. A. M. Brenninkmeijer, M. Hahn, T. Röckmann, D. H. Scharffe and P. J. Crutzen, *Isotope analysis based source identification for atmospheric $CH_4$ and CO across Russia using the Trans-Siberian railroad*, J. Geophys. Res., 103, 8227-8235, 1998.

[Bergamaschi et al. 1998b] Bergamaschi, P., C. Lubina, R. Königstedt, H. Fischer, A. C. Veltcamp and O. Zwaagstra, *Stable isotopic signatures ($\delta^{13}C$, $\delta D$) of methane from European landfill sites*, J. Geophys. Res., 103, D7, 8251-8265, 1998.

[Bergamaschi et al., 2000c] Bergamaschi, P., R. Hein, M. Heimann and P. J. Crutzen, *Inverse modeling of the global CO cycle: 1. Inversion of atmospheric mixing ratios*, J. Geophys. Res.,105, D2, 1909-1927 , 2000.

[Bergamaschi et al., 2000b] Bergamaschi, P., R. Hein, C. A. M. Brenninkmeijer and P. J. Crutzen, *Inverse modeling of the global CO cycle: 2. Inversion of $^{13}C/^{12}C$ and $^{18}O/^{16}O$ ratios*, J. Geophys. Res., 105, D2, 1928-1946, 2000.

[Bergamaschi et al., 2000a] Bergamaschi, P., M. Bräunlich, T. Marik and C. A. M. Brenninkmeijer, *Measurements of $CH_4$ and its carbon and hydogen isotopes at Izaña, Tenerife - seasonal cycles and synoptic scale variations*, J. Geophys. Res., 105, D11, 14,531-14,546, 2000.

[Bigeleisen & Mayer, 1947] Bigeleisen, J. and M. G. Mayer, *Calculation of equilibrium constants for isotopic exchange reactions*, J. Chem. Phys., 15, 261-267, 1947.

[Bönisch, 1997] Bönisch, H., *Aufbau einer teilautomatisierten Aufbereitungsapparatur für Methan aus Heidelberger Luft*, Diploma Thesis, Institut für Umweltphysik, Universität Heidelberg, 1997.

[Born et al., 1990] Born, M., H. Dürr and I. Levin, *methane consumption in aerated soils of the temperate zone*, Tellus, 42, B, 2-8, 1990.

[Bräunlich, 1996] Bräunlich, M., *Gaschromatographische Messungen von atmosphaerischem $N_2O$ in Heidelberger Luft*, Diploma Thesis, Institut für Umweltphysik, Universität Heidelberg, 1996.

[Bräunlich et al., 2000a] Bräunlich, M., P. Bergamaschi and C. A. M. Brenninkmeijer, *Isotopic composition of CO at Izana, tenerife*, manuscript in preparation

[Bräunlich et al., 2000b] Bräunlich, M., O. Aballain, T.Marik, P. Jöckel, C. A. M. Brenninkmeijer, J. Chapellaz, J.-M. Barnola, R. Mulvaney and W. Sturges, *Changes in the atmospheric methane budget over the last decades inferred from $^{13}C$ and D isotopic analysis of Antarctic firn air*, submitted to J. Geophys. Res, 2000.

[Brasseur et al., 1998] Brassuer, G. P., D. A. Hauglustaine, S. Walter, P. J. Rasch, J.-F. Müller, C. Granier and X.X.Tie, *MOZART: A Global chemical transport model for ozone related chemical tracers,1, Model description*, J. Geophys. Res., 103, 28.265-28.289, 1998.

[Brasseur, 1999] Edited by Brasseur, G. P., J. J. Orlando and G.S.Tyndall, *Atmospheric Chemistry and Global Change*, Oxford University Press, 1999.

[Brenninkmeijer & Louwers, 1985] Brenninkmeijer, C. A. M. and M. C. Louwers, *Vacuum actuated high-vacuum glass valve*, Anal. Chem, 57, 960, 1985.

[Brenninkmeijer, 1990] Brenninkmeijer, C. A. M., *A light carbonate standard for $^{13}C$ analysis of atmospheric methane*, INS-R–913,1990.

[Brenninkmeijer, 1991] Brenninkmeijer, C. A. M., *Robust, high efficiency, high-capacity cryogenic trap*, Anal. Chem., 63, 1182-1184, 1991.

[Brenninkmeijer et al., 1992] Brenninkmeijer, C. A. M., M. R. Manning, D. C. Lowe, R. J. Sparks, G. Wallace and A. Volz-Thomas, *Interhemispheric asymmetry in OH abundance inferred from measurements of atmospheric $^{14}CO$*, Nature, 356, 50-54, 1992.

[Brenninkmeijer, 1993] Brenninkmeijer, C. A. M., *Measurement of the abundance of $^{14}CO$ in the atmosphere and the $^{13}C/^{12}C$ and $^{18}O/^{16}O$ ratio of atmospheric CO, with application in New-Zealand and Antarctica*, J. Geophys. Res., 98, 10,595-10,614, 1993.

[Brenninkmeijer et al., 1995] Brenninkmeijer, C.A.M., D.C. Lowe, M.R. Manning, R.J. Sparks and P.F.J. van Velthoven, *The $^{13}C$, $^{14}C$, and $^{18}O$ isotopic composi-*

*tion of CO, $CH_4$, and $CO_2$ in the higher southern latitudes lower stratosphere*, J. Geophys. Res., 100, D12, 26 163-26 172, 1995.

[Brenninkmeijer et al., 1996] Brenninkmeijer, C.A.M., R. Müller, P.J. Crutzen, D.C. Lowe, M.R. Manning, R.J. Sparks and P.F.J. van Velthoven, *A large $^{13}CO$ deficit in the lower Antarctic stratosphere due to "ozone hole" chemistry: Part I, Observations*, Geophys. Res. Lett., 26 163-26 172, 1996.

[Brenninkmeijer & Röckmann, 1996] Brenninkmeijer, C. A. M. and T. Röckmann, *Russian doll type cryogenic traps: Improved design and isotope separation effects*, Anal. Chem., 68, 3050-3053, 1996.

[Brenninkmeijer & Röckmann, 1997] Brenninkmeijer, C. A. M. and T. Röckmann, *Principal factors determining the $^{18}O/^{16}O$ ratio of atmospheric CO as derived from observations in the southern hemispheric troposphere and lowermost stratosphere*, J. Geophys. Res., 102, 25477-25485, 1997.

[Brenninkmeijer & Bergamaschi, 1998] Brenninkmeijer, C. A. M. and P. Bergamaschi, *A Safety Pressure Relief Valve for Glass Systems*, Anal. Chem., 70, 1652-1653, 1998.

[Brenninkmeijer et al., 2000] Brenninkmeijer, C. A. M., C. Koeppel, T. Röckmann, D. S. Scharffe, M. Bräunlich and V. Gros, *Absolute measurements of the abundance of atmospheric carbon monoxide*, J. Geophys. Res., in press, 2000.

[Brown, 1995] Brown, M., *The singular value decompostion method applied to the deduction of the emissions and the isotopic composition of atmospheric methane*, J. Geophys. Res., 100, 11,425-11,446, 1995.

[Brunke et al., 1990] Brunke, E. G., H. E. Scheel and W. Seiler, *Trends of troposheric CO, $N_2O$ and $CH_4$ as observed at Cape Point, South Africa*, Atmos. Environm., 24A, No. 3, 585-595, 1990.

[Burke et al., 1988] Burke Jr., R.A., T.R. Barber and W.M. Sackett, *Methane flux and stable hydrogen and carbon isotope composition of sedimentary methane from the Florida Everglades*, Global Biogeochem. Cycles, 2, 4, 329-340, 1988.

[Bzowski et al., 1990] Bzowski, J., J. Kestin, E. A. Mason and F. J. Uribe, *Equilibrium and transport properties of gas mixtures at low density: Eleven polyatomic gases and five noble gases*, J. Phys. Chem. Ref. Data, 19, 5, 1179-1232, 1990.

[Cantrell et al., 1990] Cantrell, A.C., R.E. Shetter, A.H. McDaniel, J.G. Calvert, J.A. Davidson, D.C. Lowe, S.C. Tyler, R.J. Cicerone and J.P.Greenberg, *Carbon*

*Kinetic Isotope Effect in the Oxidation of Methane by the Hydroxyl Radical*, J. Geophys. Res., 95D, 22, 455-462, 1990.

[Chanton et al., 1997] Chanton, J.P., G.J. Whiting, N.E. Balir, C.W. Lindau and P.K. Bollich, *Methane emission from rice: Stable isotopes, diurnal variations, and $CO_2$ exchange*, Global Biogeochem. Cycles, 11, 1, 15-27, 1997.

[Chappellaz et al., 1990] Chappellaz, J.A., J.M. Barnola, D. Raynaud, Y.S. Korotkevich and C. Lorius, *Ice-core record of atmospheric methane over the past 160,000 years*, Nature, 345, 127-131, 1990.

[Cliff & Thiemens, 1997] Cliff, S. S. and M. H. Thiemens, *The $^{18}O/^{16}O$ and $^{17}O/^{16}O$ ratios in atmospheric nitrous oxide: a mass-independent anomaly*, Science, 278, 1774-1776, 1997.

[Conny et al., 1997] Conny, J. M., R. M. Verkouteren and L. A. Currie, *Carbon 13 composition of tropospheric CO in Brazil: A model scenario during the biomass burn season*, J. Geophys. Res., 102, 10,683-10,693, 1997.

[Conny, 1998] Conny, J. M., *The isotopic characterization of carbon monoxide in the troposphere*, Atmos. Environm., Atmos. Environm., 32, (14-15), 2669-2683, 1998.

[Coplen, 1994] Coplen, T. B., *Reporting of stable hydrogen, carbon, and oxygen isotopic abundances*, Pure & Appl. Chem., 66 No. 2, 273-276, 1994.

[Craig, 1954] Craig, H., *Carbon 13 in plants and the relationships between 13 and carbon 14 variations in nature*, J. Geol., 62, 115-149, 1954.

[Craig, 1957] Craig, H., *Isotopic standards for carbon and oxygen and correction factors for mass-spectrometric analysis of carbon dioxide*, Geochim. Cosmochim. Acta, 12, 133-149, 1957.

[Craig et al., 1988] Craig, H., C. C. Chou, J. A. Welhan, C. M. Stevens and A. Engelkemeir, *The Isotopic Composition of Methane in Polar Ice Cores*, Science, 242, 1535-1538, 1988.

[Craig et al., 1988b] Craig, H., Y. Horibe and T. Sowers, *Gravitational separation of gases and isotopes in polar ice caps.*, Sciences, 242, 1675-1678, 1988.

[Crowley et al., 1999] Crowley, J., G. Saueressig, P. Bergamaschi, H. Fischer and G. W. Harris, *Carbon kinetic isotope effect in the reaction $CH_4$ +Cl: A relative rate study using FTIR spectroscopy*, J. Phys. Chem., 303, 268-274, 1999.

[Crutzen & Zimmermann, 1991] Crutzen, P. J. and P. H. Zimmermann, *The changing photochemistry in the troposphere*, Tellus, 43(AB), 136-151, 1991.

[Crutzen, 1995] Crutzen, P. J., *On the role of $CH_4$ in atmospheric chemistry: Sources, sinks and possible reductions in anthropogenic sources*, Ambio, 24, 52-55, 1995.

[Deines, 1980] Deines, P., The isotopic composition of reduced organic carbon, in *The Terrestrial Environment* (ed. by A. P. Fritz and J. Fontes), Elsevier Scientific Publishing Company, Amsterdam, 1980.

[DeMore, 1993] DeMore, W.B., *Rate constant ratio for the reactions of OH with $CH_3D$ and $CH_4$*, J. Phys. Chem., 97, 33, 8564-8566, 1993.

[Dlugokencky et al., 1994a] Dlugokencky, E.J., K.A. Masarie, P.M. Lang, P.P. Tans, L.P. Steele and E.G. Nisbet, *A dramatic decrease in the growth rate of atmospheric methane in the northern hemisphere during 1992*, Geophys. Res. Lett., 21, 1, 45-48, 1994.

[Dlugokencky et al., 1994b] Dlugokencky, E.J., P.M. Lang, K.A. Masarie and L.P. Steele, *Atmospheric methane mixing ratios – The NOAA/CMDL global cooperative air sampling network, 1983-1993*, http://cdiac.esd.ornl.gov/ftp/db1008, 1994.

[Dlugokencky et al., 1994c] Dlugokencky, E. J., P. P. Steele, P. M. Lang and K. A. Masaire, *The growth rate and distribution of atmospheric methane*, J. Geophys. Res., 99, 17,021-17,043, 1994.

[Dlugokencky et al., 1996] Dlugokencky, E.J., E.G. Dutton, P.C. Novelli, P.P. Tans, K.A. Masarie, K.O. Lantz and S. Madronich, *Changes in $CH_4$ and CO growth rates after the eruption of Mt. Pinatubo and their link with changes in tropical tropospheric UV flux*, Geophys. Res. Lett., 23, 20, 2761-2764, 1996.

[Dumke et al., 1989] Dumke, I., E. Faber and J. Poggenburg, *Determination of stable carbon and hydrogen isotopes of light hydrocarbons*, Anal. Chem, 61, 2149-2154, 1989.

[Dywer & Gregoire, 1998] Dywer, E. and J. M. Gregoire, *A global analysis of vegetation fires using satellite images-spatial and temporal dynamics*, Ambio, 27, 175-181, 1998.

[Ehhalt & Volz, 1974] Ehhalt, D. H. and A. Volz, *Coupling of the $CH_4$ with the $H_2$ and CO cycle: Isotopic Evidence*, 1974.

[Engardt & Holmen, 1999] Engardt, M. and K. Holmen, *Model simulations of anthropogenic $CO_2$ transport to an Arctic monitoring station during winter*, Tellus, Ser. B, 44, 282-294, 1999.

[Etheridge et al., 1992] Etheridge, D.M., G.I. Pearman and P.J. Fraser, *Changes in tropospheric methane between 1841 and 1978 from a high accumulation-rate Antarctic ice core*, Tellus, 44B, 282-294, 1992.

[Etheridge et al., 1996] Etheridge, D. M., L. P. Steele, R. L. Langenfelds, R. J. Francey, J.-M. Barnola and V. I. Morgan, *Natural and anthropogenic changes in atmospheric $CO_2$ over the last 1000 years from air in Antarctic ice and firn*, J. Geophys. Res.,, 101, NO. D2, 4115-4128, 1996.

[Etheridge et al., 1998] Etheridge, D. M., L. P. Steele, R. J. Francey and R. L. Langenfelds, *Atmospheric methane between 1000 AD and present: Evidence of antropogenic emissions and climatic variability*, J. Geophys. Res., 103, 15979-15993, 1998.

[Fabre, 1999] Fabre, A., J.-M. Barnola, L. Arnaud and J. Chappellaz, *Determination of gas diffusivities in polar firns: comparison between experimental measurements and inverse modelling*, GRL, 27, NO. 4. 557-560, 2000.

[Francey et al., 1999] Francey, R. J., M. R. Manning, C. E. Allison, S. A. Coram, D. M. Etheridge, R. L. Langenfelds, D. C. Lowe and L. P. Steele, *A history of $\delta^{13}C$ in atmospheric $CH_4$ from Cape Grim Air Archive and Antarctic firn air*, J. Geophys. Res.,, 104, D19, 23,631-23,643, 1999.

[Fung et al., 1991] Fung, I., J. John, J. Lerner, E. Matthews, M. Prather, L.P. Stelle, and P.J. Fraser, *Three-dimensional model synthesis of the global methane cycle*, J. Geophys. Res.,, 94D, 11, 11,089-11,104, 1991.

[Games & Hayes, 1976] Games, L.M. & J.M. Hayes, *On the mechanisms of $CO_2$ and $CH_4$ production in natural anaerobic environments*, Environ. Biogeochem., 1, 51-73, 1976.

[Gellene, 1993] Gellene, G. I., *Symmetry-dependent isotopic fractionation in the formation of $He^{2+}$*, J. Phys. Chem., 97, 34-39, 1993.

[Gierczak et al., 1997] Gierczak, T., R.K. Talukdar, S.C. Herndon, G.L. Vaghjiani and A.R. Ravishankara, *Rate coefficients for the reaction of hydroxyl radicals with methane and deuterated methane*, J. Phys. Chem., A, 101, 3125-3134, 1997.

[Gonfiantini, 1978] Gonfiantini, R., *Standards for stable isotope measurements in natural compounds*, Nature, 271, 534-536, 1978.

[Gros et al., 2000] Gros, V., M. Bräunlich, T. Röckmann, P. Jöckel, P. Bergamaschi, C. A. M. Brenninkmeijer, W. Rom, W. Kutschera, A. Kaiser, H. E. Scheel, M. Mandel, J. v. d. Plicht and G. Possnert, *Detailed analysis of the isotopic composition of CO and characterization of the air masses arriving at Mt. Sonnblick (Austrian Alps)*, submitted, 2000.

[Guenther et al., 1995] Guenther, A., C. N. Hewitt, D. Erickson, R. Fall, C. Geron, T. Graedel, P. Harley, L. Klinger, M. Lerdau, W. A. McKay, T. Pierce, B. Scholes, R. Steinbrecher, R. Tallamraju, J. Taylor and P. Zimmerman, *A global model of natural volatile organic compound emissions*, JGR, 100, No. D5, 8873-8892, 1995.

[Haan et al., 1996] Haan, D., P. Martinerie and D. Raynaud, *Ice core data of atmospheric carbon monoxide over Antarctica and Greenland during the last 200 years*, Geophys. Res. Lett., 23, No. 17, 2235-2238, 1996.

[Haan & Raynaud, 1998] Haan, D. and D. Raynaud, *Ice core record of CO variations during the last two millenia: Atmospheric implications and chemical interactions with the Greenland ice*, Tellus, 50, Ser.B, 253-262, 1998.

[Hao & Liu, 1994] Hao, W. M. and M. H. Liu, *Spatial and temporal distribution of tropical biomass burning*, Global Biogeochem. Cycles, 8, 4, 495-503, 1994.

[Hein et al., 1997] Hein, R., P.J. Crutzen and M. Heimann, *An inverse modeling approach to investigate the global atmospheric methane cycle*, Global Biogeochem. Cycles, 11, 1, 43-76, 1997.

[Heimann, 1996] Heimann, M., *The global atmospheric tracer model TM2*, Technical Report No. 10,1996.

[Hodder et al., 1994] Hodder, P. S., C. A. M. Brenninkmeijer and M. H. Thiemens, *Mass independent fractionation in tropospheric carbon monoxide*, ICOG proceedings, US Geological Circulair 1107, 1994.

[Hogan & Harriss, 1994] Hogan, K.B. & R.C. Harriss, *Comment on 'A dramatic decrease in the growth rate of atmospheric methane in the Northern Hemisphere during 1992' by E.J. Dlugokencky et al.*, Geophys. Res. Lett., 21, 22, 2445-2446, 1994.

[Hough, 1991] Hough, A. M., *Developement of a Two-Dimensional Global Tropospheric Model: Model Chemestry*, J. Geophsys. Res., 96, No. D4, 7325-7362, 1991.

[Houweling et al., 1998] Houweling, S., F. Dentener and J. Lelieveld, *The impact of nonmethane hyydrocarbon compounds on troposheric photochemistry*, J. Geophys. Res., 103, D9, 10673-10696, 1998.

[Huff & Thiemens, 1998] Huff, A. K. and M. H. Thiemens, *$^{17}O/^{16}O$ and $^{18}O/^{16}O$ isotope measurements of atmospheric carbon monoxide and its sources*, Geophys. Res. Lett., 25, 3509-3512, 1998.

[IPCC, 1995] IPCC (Intergovernmental Panel on Climate Change), *Climate Change 1994: Radiative forcing of climate change and An evaluation of the IPCC IS93 emission scenarios.*, Cambridge University Press, 1995.

[Irion et al., 1996] Irion, F. W., E. J. MOyer, M. R. Gunson, C. P. Rinsland, Y. L. Yung, H. A. Michelsen, R. J. Salawitch, A. Y. Chang, M. J. Newchurch, M. M. Abbas, M. C. Abrams and R. Zander, *Stratospheric observations of CH3D and HDO from ATMOS infrared solar spectra: Enrichments of deuterium in methane and implications for HD*, Geophys. Res. Lett., 23, 2381-2384, 1996.

[Jöckel et al., 1999] Jöckel, P., M. G. Lawrence and C. A. M. Brenninkmeijer, *Simulations of cosmogenic $^{14}CO$ using the three-dimensional atmospheric model MATCH: Effects of $^{14}C$ production distribution and the solar cycle*, J. Geophys. Res., 104, 11,733-11,743, 1999.

[Jöckel et al., 2000a] Jöckel, P., C. A. M. Brenninkmeijer and M. G. Lawrence, *The atmospheric response time of cosmogenic $^{14}CO$ to changes in solar activity*, J. Geophys. Res.,105, 6737-6744, 2000.

[Jöckel et al., 2000b] Jöckel, P., C. A. M. Brenninkmeijer, M. G. Lawrence and P. Siegmund, *Cross tropopause transport of solar proton event induced atmospheric $^{14}CO$: Modeling and observations of the 1989 events*, submitted, 2000.

[Kanakidou et al., 1999] Kanakidou, M., F. J. Dentener, G. P. Brasseur, T. K. Berntsen, W. J. Collins, d. A. Hauglustaine, S. Houweling, I. S. A. Isaksen, M. Krol, M. G. Lawrence, J.-F. Muller, N. Poisson, G. J. Roelofs, Y. Wang and W. M. F. Wauben, *3-D global simulations of tropospheric CO distributions - results of the GIM/IGAC intercomparison 1997 exercise*, Global Change Science, 1, 1-3, 263-282, 1999.

[Kandilar & McRae, 1995] Kandilar, M. and G. J. McRae, *Inversion of the global methane cycle using chance constrained programming: methodology and results*, Chemosphere, 30, 1151-1170, 1995.

[Kato et al., 1999a] Kato, S., H. Akimoto, M. Bräunlich, T. Röckmann and C. A. M. Brenninkmeijer, *Measurements of stable carbon and oxygen isotopic composition of CO in automobile exhausts and ambient air from semi-urban Mainz, Germany*, Geochem. J., 33, 73-77, 1999.

[Kato et al., 1999b] Kato, S., H. Akimoto, T. Röckmann, M. Bräunlich and C. A. M. Brenninkmeijer, *Stable isotopic compositions of carbon monoxide from biomass burning experiments*, Atmosph. Environm., 33, 4357-4362, 1999.

[Kato et al., 2000] Kato, S., J. Kajii, H. Akimoto, M. Bräunlich, T. Röckmann and C. A. M. Brenninkmeijer, *Observed and modeled seasonal variation of* $^{13}C$, $^{18}O$ *and* $^{14}C$ *of atmospheric CO at Happo, a remote site in Japan, and a comparison with other records*, J. Geophys. Res., 105, D7, 8891-8900, 2000.

[Kaye, 1987] Kaye, J. A., *Mechanisms and Observations for Isotope Fractionation of Molecular Species in Planetary Atmospheres*, Reviews of Geophysics, 25 No.8, 1609-1658, 1987.

[Keeling and Whorf, 1994] Keeling, C. D. and T. P. Whorf, *Atmospheric* $CO_2$ *records drom sites in the SIO air sampling network, South Pole,*, 1994.

[Khalil & Rasmussen, 1985] Khalil, M.A.K. & R.A. Rasmussen, *Causes of increasing atmospheric methane: depletion of hydroxyl radicals and the rise of emissions*, Atmos. Environ., 19, 3, 397-407, 1985.

[Khalil & Rasmussen, 1988] Khalil, M. A. K. and R. A. Rasmussen, *Carbon monoxide in the earth's atmosphere: indications of a global increase*, Nature, 332, 242-245, 1988.

[Khalil & Rasmussen, 1994] Khalil, M. A. K. and R. A. Rasmussen, *Global decrease in atmospheric monoxide concentration*, Nature, 370, 639-641, 1994.

[Khalil, 2000] Khalil, M. A. K., *Atmospheric Methane: An Introduction*, In: Atmospheric Methane Its Role in the Global Environment, Springer, Heidelberg, 1-8, 2000.

[King et al., 1989] King, S.L., P.D. Quay and J.M. Lansdown, *The* $^{13}C/^{12}C$ *kinetic isotope effect for soil oxidation of methane at ambient atmospheric concentrations*, J. Geophys. Res., 94, D15, 18 273-18 277, 1989.

[Krol et al., 1998] Krol, M., P. J. v. Leeuwen and J. Lelieveld, *Global OH trends inferred from methylchloroform measurements*, JGR, 103, 10,697-10,711, 1998.

[Kuhlmann et al., 1998] Kuhlmann, A. J., D. E. J. Worthy, N. B. A. Trivett and I. Levin, *Methane emissions from a wetland region within the Hudson Bay Lowland: An atmospheric approach*, J. Geophys. Res, 103, D13, 16.009-16.016, 1998.

[Lassey et al., 1993] Lassey, K.R., D.C. Lowe, C.A.M. Brenninkmeijer and A.J. Gomez, *Atmospheric methane and its carbon isotpoes in the southern hemisphere: Their time series and an instructive model*, Chemosphere, 26, (1-4), 95-110, 1993.

[Lassey et al., 2000] Lassey, K. R., D. C. Lowe and M. R. Manning, *The trend in atmospheric methane* $\delta^{13}C$ *and implications for isotopic constraints on the global methane budget*, Global Biogeochem. Cycles, 14, 1, 41, 2000.

[Lelieveld et al., 1998] J. Lelieveld, P. J. Crutzen and F. J. Dentener, *Changing concentration, lifetimes and climate forcing of atmospheric methane*, Tellus, 50B, 128-150, 1998.

[Leuenberger et al., 2000] M. Leuenberger *Thermal diffusion*, submitted, 2000.

[Levin et al., 1993] Levin, I., P. Bergamaschi, H. Dörr and D. Trapp, *Stable isotopic signature of methane from major sources in Germany*, Chemosphere, 26, 161-177, 1993.

[Levin & Hesshaimer, 1996] Levin, I. & V. Hesshaimer, *Refining of atmospheric transport model entries by the globally observed passive tracer distributions of* $^{85}$*krypton and sulfur hexafluoride (*$SF_6$*)*, J. Geophys. Res., 101, D11, 16 745-16 755, 1996.

[Levin et al., 1999] Levin, I., H. Glatzel-Mattheier, T. Marik, M. Cuntz, M. Schmidt and D. E. Worthy, *Verification of German methane emission inventories and their recent changes based on atmospheric observations*, J. Geophys. Res., 104, 26,125-26,135, 1999.

[Levine, 1999] Levine, J. S., *The 1997 fires in Klaimantan and Sumatra, Indonesia: Gaseous and particulate emissions*, Geophys. Res. Lett., 26, 815-818, 1999.

[Libby, 1946] Libby, W. F., *Atmospheric Helium three and radiocarbon from cosmic radiation*, Phys. Rev., 69, 2, 671-672, 1946.

[Liptay et al., 1998] Liptay, K., J. Chanton, P. Cizepiel and B. Mosher, *Use of stable isotopes to determine methane oxidation in landfill cover soils*, J. Geophys. Res., 103, 8243-8250, 1998.

[Lingenfelter & Flamm, 1963] Lingenfelter, R. E. and E. J. Flamm, *Production of carbon 14 by solar flares*, J. Atmos. Scienc., 21, 134-140, 1963.

[Logan et al. 1981] Logan, J. A., M. J. Prather, S. C. Wofsy and M. B. McElroy, *Tropospheric chemistry: A global perspective*, J. Geophys. Res., 86, 7210-7254, 1981.

[Lowe et al., 1988] Lowe, D. C., C. A. M. Brenninkmeijer, M. R. Manning, R. Sparks and G. Wallace, *Radiocarbon determination of atmospheric methane at Baring Head, New Zealand*, Nature, 332, 522-525, 1988.

[Lowe et al., 1994] Lowe, D.C., C.A.M. Brenninkmeijer, G.W. Brailsford, K.R. Lassey and A.J. Gomez, *Concentration and $^{13}C$ records of atmospheric methane in New Zealand and Antarctica: Evidence for changes in methane sources*, J. Geophys. Res., 99, D8, 16,913-16,925, 1994.

[Lowe et al., 1997] Lowe, D.C., M.R. Manning, G.W. Brailsford and A.M. Bromley, *The 1991–1992 atmospheric methane anomaly: southern hemisphere $^{13}C$ decrease and growth rate fluctuations*, Geophys. Res. Lett., 24, 8, 857-860, 1997.

[Lowe et al., 1999] Lowe, D. C., W. Allan, M. R. Manning, T. Bromley, G. Brailsford, D. Ferretti, A. Gomez, R. Knobben, R. Martin, Z. Mei and R. Moss, *Shipboard determinations of the distribution of $^{13}C$ in atmospheric methane in the Pacific*, J. Geophys. Res., 104, 26,125-26,135, 1999.

[Manning et al., 1997] Manning, M. R., C. A. M. Brenninkmeijer and W. Allan, *Atmospheric carbon monoxide budget of the southern hemisphere: Implications of $^{13}C/^{12}C$ measurements*, J. Geophys. Res., 102, D9, 10,673-10,682, 1997.

[Maiss & Levin, 1994] Maiss, M. and I. Levin, *Global increase of SF6 observed in the atmosphere*, Geophys. Res. Lett., 21, 7, 569-572, 1994.

[Maiss et al., 1996] Maiss, M., L.P. Steele, R.J. Francey, P.J. Fraser, R.L. Langenfelds, N.B.A. Trivett and I. Levin, *Sulfur hexafluoride — a powerful new atmospheric tracer*, Atmos. Environ., 30, 10/11, 1621-1629, 1996.

[Maiss & Brenninkmeijer, 1998] Maiss, M. and C. A. M. Brenninkmeijer, *Atmospheric $SF_6$: trends, sources, and prospects*, Environ. Sci.Technol., 32, 3077-3086, 1998.

[Marik, 1998] Marik, T., *Atmospheric $\delta^{13}C$ and $\delta D$ Measurements to balance the Global Methane Budget*, Umweltphysik, 1998.

[Mak & Brenninkmeijer, 1994a] Mak, J. E. and C. A. M. Brenninkmeijer, *Compressed air sample technology for isotopic analysis of atmospheric carbon monoxide*, J. Atmos. Oceanic Technol., 11, 425-431, 1994.

[Mak et al., 1994] Mak, J. E., C. A. M. Brenninkmeijer and J. Tamaresis, *Atmospheric $^{14}CO$ observations and their use for estimating carbon monoxide removal rates*, J. Geophys. Res., 99, 22915-22922, 1994.

[Mak & Southon, 1998] Mak, J. E. and J. R. Southon, *Assessment of tropical OH seasonality using atmospheric $^{14}CO$ measurements from Barbados*, Geophys. Res. Lett., 25, 2801-2814, 1998.

[Mak & Kra, 1999] Mak, J. E. and G. Kra, *The isotopic composition of carbon monoxide at Montauk Point, Long Island*, Chemosphere Glob. Change Sci., 1, 205-218, 1999.

[Mak et al., 2000] Mak, J. E., G. Kra, T. Sandomenico and M. Bräunlich, *The seasonal varying isotopic composition of the sources of carbon monoxide at Barbados, West Indies*, manuscript in preparation, 2000.

[Masari et al., 2000] in press

[Mauersberger, 1987] Mauersberger, K., *Ozone isotope measurements in the stratosphere*, Geophys. Res. Lett., 14, 80-83, 1987.

[McKay et al., 1963] McKay, C., M. Pandow and R. Wolfgang, *On the chemistry of natural radiocarbon*, J. Geophys. Res., 68, 3929-31, 1963.

[Merill, 1994] Merill, J. T., *Isentropic airflow probability analysis*, J. Geophys. Res., 99, 25,881-25,889, 1994.

[Migeotte, 1948] Migeotte, M.V., *Spectroscopic evidence of methane in the Earth's atmosphere*, Phys. Rev., 73, 519-520, 1948.

[Migeotte, 1949] Migotte, M., *The fundamental band of carbon monoxide at 4.7m in the solar spectrum*, Phys. Rev., 75, 1108-1109, 1949.

[Migeotte & Neven, 1952] Migotte, M. and L. Neven, *Recents progres dans l observation du spectra solaire a la station scientific du Jungfrauhoch*, Soc. R. Sci. Liege, 12, 165-169, 1952.

[Novelli et al., 1994] Novelli, P. C., J. E. Collins, Jr., R. C. Myers, G. W. Sachse and H. E. Scheel, *Reevaluation of the NOAA/CMDL carbon monoxide reference scala*

*and comparisons with CO reference gases at NASA-Langley and the Fraunhofer Institut*, J. Geophys. Res., 99, No. D6, 12,833-12,839, 1994.

[Novelli et al., 1998a] Novelli, P. C., K. A. Masarie and P. M. Lang, *Distribution and recent trends in carbon monoxide in the lower troposphere*, J. Geophys. Res., 103, 19,015-19,033, 1998.

[Novelli et al., 1998b] Novelli, P. C., V. S. Connors, H. G. Reichle, B. E. Anderson, C. A. M. Brenninkmeijer, E. G. Brunke, B. G. Dodderidge, V. W. J. H. Kirchhoff, K. S. Lam, K. A. Masarie, T. Matsuo, D. D. Parish, H. E. Scheel and L. P. Steele, *An internally consistent set of globally distributed atmospheric carbon monoxide mixing ratios devoloped using results from an intercomparison of measurements*, J. Geophys. Res., 103, 19258-19293, 1998.

[Novelli, 1999] Novelli, P. C., *CO in the atmosphere: measurements techniques and related issues*, Global Change Science, 1, 1-3, 115-126, 1999.

[Olivier et al., 1999] Olivier, J. G. J., J. P. J. Bloos, J. J. M. Berdowski, A. J. H. Visschedijk and A. F. Bouwman, *A 1990 global emission inventory of anthropogenic sources of carbon monoxide on 1o x 1o development in the framework of EDGAR/GEIA*, Glob. Change Sci., 1, 1-3, 1-17, 1999.

[Pandow et al., 1960] Pandow, M., C. McKay and R. Wolfgang, *The reaction of atomic carbon with oxygen: Significance for the natural radio-carbon cycle*, J. Inorg. Nucl. Chem., 14, 153-158, 1960.

[Pernaton et al., 1996] Pernaton, E., A. Prinzhofer and F. Schneider, *Reconsideration of methane isotope signature as a criterion for the genesis of natural gas - Influence of migration on isotopic signatures*, REVUE DE L INSTITUT FRANCAIS DU PETROLE, 51, (5), 635-651, 1996.

[Petit et al., 1999] Petit, J. R., J. Jouzel, D. Raynaud, N. I. Barkov, J.-M. Barnola, I. Basile, M. Bender, J. Chappellaz, M. Davis, G. Delaygue, M. Delmotte, V. M. Kotlyakov, M. Legrand, V. Y. Lipenkov, C. Lorius, L. Pépin, C. Ritz, E. Saltzman and M. Stievenard, *Climate and atmospheric history of the past 420,000 years from the Vostok ice core, Antarctica*, Nature, 399, 429-436, 1999.

[Prather, 1996] Prather, M. J., *Time scales in atmospheric chemistry: Theory, GWPs for $CH_4$ and CO, and runaway growth*, Geophys. Res. Lett., 23, 2597-2600, 1996.

[Quay et al., 1988] Quay, P., S.L. King, J.M. Lansdown and D.O. Wilbur, *Isotopic composition of carbon in gases of biogenic origin*, Global Biogeochem. Cycles, 2, 385-397, 1988.

[Quay et al., 1991] Quay, P.D., S.L. King, J. Stutsman, D.O. Wilbur, L.P. Steele, I. Fung, R.H. Gammon, T.A. Brown, G.W. Farwell, P.M. Grootes and F.H. Schmidt, *Carbon isotopic composition of atmospheric $CH_4$: fossile and biomass burning source strengths*, Global Biogeochem. Cycles, 5, 25-47, 1991.

[Quay et al., 1996] Quay, P. D., J. Stutsman and R. J. Francey, $\delta^{13}C$ *of atmospheric $CH_4$ at Cape Grim, 1991-1995*, Baseline Atmospheric Program (Australia) 1991, 110-111, 1996.

[Quay et al., 1999] Quay, P. D., J. L. Stutsman, D. O. Wilbur, A. K. Snover, E. J. Dlugokencky and T. A. Brown, *The isotopic composition of atmsopheric methane*, Global Biogeochem. Cycles, 13, 2, 445-461, 1999.

[Rasmussen & Khalil, 1981] Rasmussen, R.A. & M.A.K. Khalil, *Atmospheric methane ($CH_4$): trends and seasonal cycles*, J. Geophys. Res., 86, C10, 9826-9832, 1981.

[Reichle et al., 1986] Reichle, H. g., V. S. Connors, J. A. Holland, W. D. Hypers, H. A. Wallio, J. C. Casas, B. B. Gormsen, M. S. Saylor and W. D. Hesketh, *Middle and Upper Tropospheric Carbon Monoxide Mixing Ratios as Measured by Satellite-Borne Remote Sensor*, JGR, 91, NO. D10, 10,865-10,887, 1986.

[Reid & Labrie, 1978] Reid, J. and D. Labrie, *Second-harmonic detection with tunable diode lasers-comparison of experiment and theorie*, Appl. Phys., B26, 203-210, 1981.

[Rice & Claypool, 1981] Rice, D.D. & G.E. Claypool, *Generation, accumulation, and resource potential of biogenic gases*, Am. Assoc. Pet. Geol. Bull., 65, 5-25, 1981.

[Robinson & Robins, 1970] Robinson, E. and R. C. Robinson, *Atmospheric background concentrations of carbon monoxide*, Ann. N.Y. Acad. Sci., 174, 89-95, 1970.

[Robbins et al., 1973] Robbins, R. C., L. A. Cavanagh and L. J. Salas, *Analysis of ancient atmospheres*, J. Geophys. Res., 78, 5.341-5.344, 1973.

[Röckmann, 1998a] Röckmann, T., *Measurement and interpretation of $^{13}C$, $^{14}C$, $^{17}O$ and $^{18}O$ variations in atmospheric carbon monoxide*, Thesis, Physics departement, University of Heidelberg, 1998.

[Röckmann & Brenninkmeijer, 1998b] Röckmann, T. and C. A. M. Brenninkmeijer, *The error in conventionally reported 13C/12C ratios of atmospheric CO due to the presence of mass independent oxygen isotope enrichment*, Geophys. Res. Lett., 25, 3163-3166, 1998.

[Röckmann et al., 1998c] Röckmann, T., C. A. M. Brenninkmeijer, G. Saueressig, P. Bergamaschi, J. Crowley, H. Fischer and P. J. Crutzen, *Mass independent fractionation of oxygen isotopes in atmospheric CO due to the reaction CO + OH*, Science, 281, 544-546, 1998.

[Röckmann et al., 1998] Röckmann, T., C. A. M. Brenninkmeijer, P. Neeb and P. J. Crutzen, *Ozonolysis of nonmethane hydrocarbons as a source of the observed mass independent oxygen isotope enrichment in tropospheric CO*, J. Geophys. Res., 103, 1463-1470, 1998.

[Rom et al., 1998] Rom, W., R. Golser, W. Kutschera, A. Priller, P. Steier and E. Wild, *AMS*, Radiocarbon, 40, 1-2, 255, 1998.

[Rom, 2000a] Rom, W., *$^{14}C$ Accelerator Mass Spectronomy Applications in Archaelogy, Biomedicine and in Atmospheric Sciences*, 2000.

[Rom et al., 2000b] Rom, W., C. A. M. Brenninkmeijer, M. Bräunlich, R. Golser, M. Mandl, A. Kaiser, W. Kutschera, A. Priller, S. Puchegger, T. Röckmann and P. Steier, *A. detailed 2-year record of atmospheric $^{14}CO$ in the temperate northern hemisphere*, Nucl.Instr.Meth.Phys.Res.B, in press, 2000.

[Rommelaere et al., 1997] Rommelaere, V., L. Arnaud and J.-M. Barnola, *Reconstructing recent atmospheric trace gas concentrations from polar firn and bubbly ice data by inverse methods*, J. Geophys. Res., 102, 30,069-30,083, 1997.

[Roths, 1992] Roths, J., *Entwicklung einer flugtauglichen, laserspektroskopischen Spurengassensors und dessen Einsatz bei der TROPOZ-II-Flugmesskampagne*, Johannes-Gutenberg-Universität, 1992.

[Rudolph & Ehhalt, 1981] Rudolph, J. and D. H. Ehhalt, *measurements of $C_2$-$C_5$ hydocarbons over the north Atlantic*, J. Geophys. Res., 86, C12, 11959-11964, 1981.

[Rudolph, 1994] Rudolph, J., *Anomalous methane*, Nature, 368, 19-20, 1994.

[Rudolph et al., 1997] Rudolph, J., D. C. Lowe, R. J. Martin and T. S. Clarkson, *A novel method for the compound specific determination of d13C in volatile organic compounds at ppt levels in ambient air*, Geophys. Res. Lett., 24, 659-662, 1997.

[Rust, 1981] Rust, F., *Ruminant methane ($^{13}C/^{12}C$) values: relation to atmospheric methane*, Science, 211, 1044-1046, 1981.

[Saueressig et al., 1995] Saueressig, G., P. Bergamaschi, J.N. Crowley, H. Fischer and G.W. Harris, *Carbon kinetic isotope effect in the reaction of $CH_4$ with Cl atoms*, Geophys. Res. Lett., 22, 1225-1228, 1995.

[Saueressig, 1999] Saueressig, G., *Bestimmung von Isotopentrennfaktoren in den atmosphärischen Methanabbaureaktionen*, MPI Chemie, Abt. Luftchemie, 1999.

[Schütze, 1949] Schütze, M., 1949, *Ein neues Oxidationsmittel für die quantitative Überführung von Kohlenmonoxyd in Kohlendioxyd. Ein Beitrag zur Chemie des Jodpentoxids*, Ber. Dtsch. Chem. Ges, 77b, 484-487, 1949.

[Schaefer, 1998] Schaefer, H., *Meterologische Analyse für Spurengasmessungen am Observatorium Izana (Teneriffa) unter Verwendung von Rückwärtstrajektorien*, Physik, 1998.

[Schmitt et al., 1988] Schmitt, R., B. Schreiber and I. Levin, *Effects on Long-Range Transport on Atmospheric Trace Constituents at the Baseline Station Tenerife (Canary Island)*, Journal of Atmospheric Chemestry, 7, 335-351, 1988.

[Schmitt & Volz-Thomas, 1997] Schmitt, R. and A. Volz-Thomas, *Climatology of Ozone, PAN, CO, and NMHC in the Free Troposhere Over the Southern North Atlantic*, Jour. Atm. Chem., 28, 245-262, 1997.

[Schoell, 1980] Schoell, M., *The hydrogen and carbon isotopic composition of methane from natural gases of various origins*, Geochim. Cosmochim. Acta, 44, 649-661, 1980.

[Schwander, 1989] Schwander, J., *The transformation of snow to ice and the occlusion of gases*, In: The Environmental Record in Glaciers and Ice Sheets, Report of the Dahlem Workshop held in Berlin 1988, March 13-18, John Wiley and Sons, Chichester, 51-67, 1989.

[Schwander et al., 1993] Schwander, J., J. M. Barnola, C. Andrie, M.Leuenberger, A. Ludin, D.Raynaud and B. Stauffer, *The age of the air and the ice at Summit, Greenland*, J. Geophys. Res., 98, 2831-2838, 1993.

[Seiler, 1974] Seiler, W., *The cycle of atmospheric CO*, Tellus, 26, 116/35, 1974.

[Seiler et al., 1984] Seiler, W., H. Giehl, E.-G. Bruncke and E. Halliday, *The seasonality of CO abundance in the Southern Hemisphere*, Tellus, 36b, 219-231, 1984.

[Seinfeld & Pandis, 1998] J. H. Seinfeld, S. N. Pandis *Atmospheric Chemistry and Physics, From Air Pollution to Climate Change*, John Wiley & Sons, N.Y., 1998.

[Severinghaus & Brook, 1999] Severinghaus, J. P. and E. J. Brook, *Abrupt climate change at the end of the Last Glacial Period inferred from trapped air in polar ice, Science*, Science, 286, 930-934, 1999.

[Smiley, 1965] Smiley, W. G., *Note on a reagent for oxidation of carbon monoxide*, Nucl. Sci. Abstr, 3, 391, 1965.

[Smit et al., 1982] Smit, H. G. J., A. Volz, D. H. Ehhalt and H. Knappe, *The isotopic fractionation during the oxidation of carbon monoxide by hydroxyl radicals and its implications for the atmospheric CO-cycle*, Stable Isotopes, 147-152, 1982.

[Snover & Quay, 1999] Snover, A. K. and P. D. Quay, *Hydrogen and carbon kinetic isotope effects during soil uptake of atmospheric methane*, Global Biogeochem. Cycles, 14, 1, 25-39, 2000.

[Snover et al., 1999] Snover, A. K., P. D. Quay and W. M. Hao, *The D/H content of methane emitted from biomass burning*, Global Biogeochem. Cycles, 14, 1, 11-24, 2000.

[Stern & Kaufmann, 1996] Stern, D. I. and R. K. Kaufmann, *Estimates of global anthropogenic methane emissions 1860-1993*, Chemosphere, 33, 159-176, 1996.

[Stevens & Krout, 1972] Stevens, C. M. and L. Krout, *Method for the determination of the concentration and of the carbon and oxygen isotopic composition of atmospheric carbon monoxide*, International Journal of Mass Spectrometry and Ion Physics, 8, 265-275, 1972.

[Stevens et al., 1980] Stevens, C. M., L. Kaplan, R. Gorse, S. Durkee, M. Compton, S. Cohen and K. Bielling, *The kinetic isotope effect for carbon and oxygen in the reaction CO + OH*, Int. J. Chem. Kinet., 12, 935-948, 1980.

[Stevens & Rust, 1982] Stevens, C. M. and F. E. Rust, *The Carbon Isotopic Composition of Atmospheric Methane*, J. Geophys. Res.,, 87, No. C7, 4879-4882, 1982.

[Stevens & Engelkemeir, 1988] Stevens, C.M. & A. Engelkemeir, *Stable carbon isotopic composition of methane from some natural and anthropogenic sources*, J. Geophys. Res., 93, D1, 725-733, 1988.

[Stevens & Wagner, 1989] Stevens, C. M. and A. F. Wagner, *The role of isotope fractionation effects in atmospheric chemistry*, Z. Naturforsch, 44a, 376 - 384, 1989.

[Stevens, 1993] Stevens, C.M., "Isotopic abundances in the atmosphere and sources", in *Atmospheric methane: sources, sinks and role in global change* (ed. by M.A.K. Khalil), Springer-Verlag, Berlin, 1993.

[Tans, 1997] Tans, P.P., *A note on isotopic ratios and the global atmospheric methane budget*, Global Biogeochem. Cycles, 11, 1, 77-81, 1997.

[Thiemens et al., 1995] Thiemens, M. H., T. Jackson, E. C. Zipf, P. W. Erdman and C. v. Egmond, *Carbon dioxide and oxygen isotope anomalies in the mesosphere and stratosphere*, Science, 270, 969-972, 1995.

[Thom et al., 1993] Thom, M., R. Bosinger, M. Schmidt and I. Levin, *The regional budget of atmospheric methane os a highly populated area*, Chemosphere, 26, 143-160, 1993.

[Thompson & Cicerone, 1986] Thompson, A. M. and R. J. Cicerone, *Atmospheric $CH_4$, CO and OH from 1860 to 1985*, Nature, 321, 148-150, 1986.

[Thompson, 1992] Thompson, A. M., *The oxidizing capacity of the Earth´s atmosphere: probable past and future changes*, Science, 256, 1157-1165, 1992.

[Trudinger et al., 1997] Trudinger, C. M., I. G. Enting, D. M. Etheridge, R. J. Francey, V. A. Levchenko, L. P. Steele, D. Raynaud and L. Arnaud, *Modeling air mouvement and bubble trapping in firn*, J. Geophys. Res.,, 102, d6, 6747-6763, 1997.

[Tyler, 1986] Tyler, S.C., *Stable carbon isotope ratios in atmospheric methane and some of its sources*, J. Geophys. Res., 91, D12, 13,232-13,238, 1986.

[Tyler et al., 1988] Tyler, S.C., P.R. Zimmerman, C. Cumberbatch, J.P. Greenberg, C. Westberg and J.P.E.C. Darlington, *Measurements and interpretation of $\delta^{13}C$ of methane from termites, rice paddies, and wetlands in Kenya*, Global Biogeochem. Cycles, 2, 4, 341-355, 1988.

[Tyler et al., 1994] Tyler, S.C., G.W. Brailsford, K. Yagi, K. Minami and R.J. Cicerone, *Seasonal variations in methane flux and $\delta^{13}CH_4$ values for rice paddies in Japan and their implications*, Global Biogeochem. Cycles, 8, 1, 1-12, 1994.

[Tyler, 1994] Tyler, S. C., P. M. Crill and G. W. Brailsford, *$^{13}C/^{12}C$ Fractionation of methane during oxidation in a temperate forested soil*, Geochimica et Cosmochemica Acta, 58, No. 6, 1625-1633, 1994.

[Tyler et al., 1998] Tyler, S. C., H. O. Ajie, A. L. Rice, R. J. Cicerone and E. C. Tuazon, *Experimentally determined kinetic isotope effect in the reaction of CH4 with Cl: Implications for atmospheric CH4*, EOS, Trans., 79, 45, F102, 1998.

[Urey, 1947] Urey, H. C., *The Thermodynamic Properties of Isotopic Substances*, J. Chem. Soc., 562-581, 1947.

[Volz et al., 1981] Volz, A., D. H. Ehhalt and R. G. Derwent, *Seasonal and latitudinal variation of 14CO, and the tropospheric concentration of OH radicals*, J. Geophys. Res., 86, 5163-5171, 1981.

[Wahlen et al., 1989] Wahlen, M., N. Tanaka, R. Henry, B. Deck, J. Zeglen, J.S. Vogel, J. Southon, A. Shemesh, R. Fairbanks and W. Broecker, *Carbon-14 in methane sources and in atmospheric methane: the contribution from fossil carbon*, Science, 245, 286-290, 1989.

[Wahlen, 1993] Wahlen, M., *The global methane cycle*, Annu. Rev. Earth Planet. Sci., 21, 407-426, 1993.

[Wallace et al., 1987] Wallace, G., R. J. Sparks, D. C. Lowe and K. P. Pohl, *The New Zealand accelerator mass spectrometry facility*, Nucl. Instr. Meth, 29(B), 124-128, 1987.

[Wassmann et al., 1992] Wassmann, R., U.G. Thein, M. Whiticar, H. Rennenberg, W. Seiler and W.J. Junk, *Methane emissions from the Amazon floodplain: characterization of production and transport*, Global Biogeochem. Cycles, 6, 1, 3-13, 1992.

[Weinstock, 1969] Weinstock, B., *Carbon monoxide: Residence time in the atmosphere*, Science, 166, 224-225, 1969.

[Whiticar et al., 1986] Whiticar, M.J., E. Faber and M. Schoell, *Biogenic methane formation in marine and freshwater environments: $CO_2$ reduction vs. acetate fermentation — Isotope evidence*, Geochim. Cosmochim. Acta, 50, 693-709, 1986.

[Wijma et al., 1998] Wijma, S., J. v. d. Plicht, A. Zondervan and H. A. Been, *The AMS System*, 1998.

[Zimov et al., 1997] Zimov, S.A., Y.V. Voropaev, I.P. Semiletov, S.P. Davidov, S.F. Prosiannikov, F.S. Chapin III, M.C. Chapin, S. Trumbore and S. Tyler, *North Siberian lakes: A methane source fueled by Pleistocene carbon.*, Science, 277, 800-802, 1997.

# Acknowledgements

During the work on this thesis I benefited tremendously from the support, suggestions and encouragement of many people. I like to especially acknowledge and thank my supervisor Carl Brenninkmeijer for his continuous support, advice and for sharing his great passion for science with us. I thank Prof. Paul Crutzen for making the MPI for chemistry an exciting place to work at. Furthermore, I thank Prof. Ulrich Platt for his guidance throughout this thesis and Prof. Konrad Mauersberger for refereeing.

At the MPI I am especially indebted to the whole 'Brenninkmeijer group' for the support and friendship I received over the last years: Thomas Röckmann, without whom three years in the lab would have been only half as effective and much less fun; Patrick Jöckel for his help with the modeling of the firn data; Valerie Gros for her patience and for our French connection; Manfred Maiss and Andreas Zahn for persuading me to come to Mainz in the first place; Wolfgang Hanewacker, Rolf Hofmann, Claus Koeppel and Dieter Scharffe for keeping pace with the incredible amount of samples and help with trouble of any kind; many thanks also go to Eva Oberländer, Jan Kaiser, Jens Mühle, Shungo Kato, Denis Haan, Jeff Johnson, Michael Hahn and Harald Schäfer.

I have also greatly benefited from the collaboration with Peter Bergamaschi, who guided my first steps measuring methane isotopes and whose modeling of global CO and $CH_4$ isotope data significantly improved the understanding of the Izaña records. I am also indebted to Thomas Marik for his help with the interpretation and modeling of the firn data, for the $\delta D$ measurements (together with Peter) and for being my LATEX guru. Many thanks go also to Gerd Saueressig for providing the $CH_4$ fractionation factors. Doing research at at the MPI would be very different without the excellent support from the Glassbläserei, Werkstätten, Zeichenbüro, Bibliothek, Verwaltung and Sekretariat. Finally I gratefully acknowledge financial support from the Max Planck Gesellschaft through a HSP-II scholarship and from the European Commission DG-XII through the FIRETRACC and CO-OH Europe projects.

My debts extend well beyond the MPI community. In particular I would like to

thank Jerome Chappellaz, Olivier Aballain, Jean-Marc Barnola, Adeline Fabre and Laurent Arnaud from the LGGE in Grenoble for supplying the firn diffusion model and for more than one year of continuous discussion of the firn data. Many thanks go also to Robert Mulvaney from the British Antarctic Survey for his incredible field work in QML and DomeC and William Sturges from the University of East Anglia for his never-ending energy to keep the EU-project FIRETRACC on track.

I am also grateful for the cooperation of our partners in the EU-project CO-OH-Europe: Pilar Ripodas, Emilio Cuevas, Pedro Carretero, Ramon Juega and Ramon Ramon from the Spanish Meteorological Service for collecting the air samples and for supplying the continuous $CH_4$ and CO measurements as well as meteorological data and back-trajectories; Rolf Neubert, Bert Kers, Harro Meijer and Hans van der Plicht from the University of Groningen for providing the Kollumerwaard samples and $^{14}CO$ data; Frank Meinhardt and Rolf Graul from the UBA Schauinsland for their continuous support; Michael Mandl from the Central Institute for Meteorology and Geodynamics in Salzburg for taking the samples at the Sonnblick Observatory; Werner Rom and Walter Kutschera from Vienna University for $^{14}CO$ measurements; the Norwegian Institute for Air Research Spitsbergen and the Norsk Polar Institute for their support and Georg Possnert from the University of Uppsala also for $^{14}CO$ measurements.

Many thanks also to John Mak from the State University of New York at Stony Brook for making the Barbados data available and many discussions. I would also like to thank Andreas Volz-Thomas for organizing the Papsthum station during the BERLIOZ campaign and Dirk Grossmann for his help with the sampling during this time.

I would also like to thank my co-organizers Rolf von Kuhlmann, Steffi Meilinger, Fritz Hanisch, Hermann Bange and Marc von Hobe of the airchemistry and biogeochemistry seminar. Life at the MPI would not have been the same without our DonnerstagDiscussionGroup meetings and I thank all DDG presidents for keeping it alive. Finally I also want to thank the women from the Frauenkommission in Heidelberg and from the Lovelace Project in Mainz for providing the network which made life in science much easier.

After ten years at university and more than twenty years of education altogether, I would like to use this opportunity to thank all the teachers and friends who had to deal with me on this long way. In particular I have to thank: Frau Höher for her early support; Herr Wessling for saving my life twelve years ago and for demystifying mathematics; Charlie Smith, without whom I would never have studied Physics; Herr Lutter for his philosophical weekends at the Möhnesee; Prof. Malte

Faber for being a wonderful teacher and for his help and support; Prof. Sonntag for the famous evenings with all the others in Mozartstr. 8.

And finally I thank my parents for their love and support, my brother for showing up in emergencies, Amai for two wonderful years at Boppstr. 14, the Kischka family for always keeping their door wide open in Heidelberg and Daniel not only for his courage to marry me.